



Copyright Undertaking

This thesis is protected by copyright, with all rights reserved.

By reading and using the thesis, the reader understands and agrees to the following terms:

1. The reader will abide by the rules and legal ordinances governing copyright regarding the use of the thesis.
2. The reader will use the thesis for the purpose of research or private study only and not for distribution or further reproduction or any other purpose.
3. The reader agrees to indemnify and hold the University harmless from and against any loss, damage, cost, liability or expenses arising from copyright infringement or unauthorized usage.

IMPORTANT

If you have reasons to believe that any materials in this thesis are deemed not suitable to be distributed in this form, or a copyright owner having difficulty with the material being included in our database, please contact lbsys@polyu.edu.hk providing details. The Library will look into your claim and consider taking remedial action upon receipt of the written requests.



THE HONG KONG POLYTECHNIC UNIVERISTY
CIVIL AND STRUCTURAL ENGINEERING DEPARTMENT

**MODELING OF UNCERTAINTY IN
BRIDGE-VEHICLE SYSTEM AND
THE INTERACTION FORCE
IDENTIFICATION**

SHAOQING WU

B.Sc, M.Sc.

A thesis submitted in partial fulfillment of the requirements for the

Degree of **Doctor of Philosophy**

Oct, 2010

CERTIFICATE OF ORIGINALITY

I hereby declare that this thesis is my own work and that, to the best of my knowledge and belief, it reproduces no material previously published or written, nor material that has been accepted for the award of my other degree or diploma, except where due acknowledgement has been made in the text.

_____ (Signed)

_____ WU Shaoqing _____ (Name of student)

To My Parents and My Brother

ABSTRACT

Bridge-vehicle interaction problem plays an important role in the bridge design, the bridge condition assessment and the overweight vehicle control. The topics including dynamic analysis of the bridge structure under moving vehicles and the identification of moving vehicle axle loads from the measured bridge responses have drawn much attention in recent years.

Most of the existed approaches to solve the above topics are deterministic in which the uncertainty in the bridge-vehicle system and the loading processes is ignored. Moreover, the road surface roughness is treated as deterministic samples of irregular profile according to its power spectrum density defined in the ISO standard. A few research work has addressed the stochastic analysis of bridge-vehicle interaction problem in which the road surface roughness and the parameters in vehicle system were assumed as Gaussian random variables/processes and the perturbation method was employed to handle the uncertainties involved. Since the randomness in the bridge structure has not been introduced in the bridge-vehicle interaction problem and the perturbation method adopted in the previous research works tends to loss accuracy with the increasing in variation of uncertainty, the methods proposed in this Thesis aim to fulfill these gaps and to provide theoretical studies on the stochastic analysis of the bridge-vehicle interaction problem as well as on the identification of vehicle axle loads from samples of bridge response with uncertainties in both system

parameters and road surface roughness.

The bridge is modeled as a simply supported planar Euler-Bernoulli beam with a vehicle either modeled as multiple forces or a mass-spring system moving on top. The finite element method is adopted to build the bridge-vehicle interaction model in which the system parameters as well as the road surface roughness are assumed as random processes. Firstly, only the randomness in road surface roughness is included and to be assumed as Gaussian random process represented by the Karhunen-Loève Expansion. Based on the formulated model, both the dynamic analysis and the moving force identification are conducted. Secondly, the uncertainty in the material properties of the bridge structure which is assumed to be small and have Gaussian property is further included. A stochastic finite element model is formulated with the Karhunen-Loève Expansion representing the Gaussian random processes in the equation of motion of the system. Based on the model, a general stochastic moving force identification algorithm is proposed to identify the statistics of the vehicle axle loads from samples of bridge response with uncertainty in both the excitations and system parameters. Finally, to model larger variation of uncertainty in the system parameters, the Spectral Stochastic Finite Element Method is adopted with the Karhunen-Loève Expansion and the Polynomial Chaos Expansion representing the Gaussian and non-Gaussian random processes, respectively. The system parameters are assumed as Gaussian random processes and will be further extended to non-Gaussian case which is regarded to be more appropriate. Dynamic

analysis on the bridge-vehicle interaction problem with large variation of uncertainty in both system parameters and excitation forces is conducted. All the methods proposed in this Thesis are verified with numerical examples in which the Monte Carlo Simulation is adopted to obtain the reference solutions. Results show that the proposed methods on the dynamic analysis of the bridge-vehicle interaction problem and on the identification of statistics of moving vehicle axle loads with uncertainties are effective and with good performance in the response statistics prediction even when large variation of uncertainties are existed in both the system parameters and the excitations.

LIST OF PUBLICATIONS

Journal Papers:

Wu, S.Q. and Law, S.S. (2010) “Moving force identification based on stochastic finite element model.” *Engineering Structures*, 32, 1016-1027.

Wu, S.Q. and Law, S.S. (2010) “Dynamic analysis of bridge-vehicle system with uncertainties based on finite element model.” *Probabilistic Engineering Mechanics*, 25, 425-432.

Wu, S.Q. and Law, S.S. “Dynamic analysis of bridge with non-Gaussian uncertainties under a moving vehicle.” *Probabilistic Engineering Mechanics*.
(in press)

Wu, S.Q. and Law, S.S. “Vehicle axle load identification on bridge deck with irregular road surface profile.” *Engineering Structures*. (under re-review)

Wu, S.Q. and Law, S.S. “Statistical moving load identification including uncertainties.” *Journal of Applied Mechanics-ASME*. (under review)

Wu, S.Q. and Law, S.S. “Dynamic analysis of bridge-vehicle interaction with Gaussian system uncertainties.” *Mechanical Systems and Signal Processing*.
(under review)

Conference Papers:

Wu, S.Q. and Law, S.S. (2009) “A stochastic finite element model with non-Gaussian properties for bridge-vehicle interaction problem.”
Proceedings of the International Symposium on Computational Structural

Engineering, 22-24, June, Shanghai, China.

Law, S.S. and Wu, S.Q. (2009) “Moving force identification in a deterministic system with Gaussian random components.” *4th International Conference on Structural Health Monitoring of Intelligent Infrastructure (SHMII-4)*, 22-24, July, Zurich, Switzerland.

Wu, S.Q. and Law, S.S. (2009) “Stochastic bridge-vehicle interaction problem with Gaussian uncertainties.” *The 10th International Conference on Structural Safety and Reliability (ICOSSAR2009)*, 13-17, September, Osaka, Japan.

Law, S.S. and Wu, S.Q. (2009) “Stochastic force identification algorithm for bridge-vehicle interaction problem.” *13th Asia-Pacific Vibration Conference (APVC2009)*, 22-25, November, New Zealand.

Law, S.S. and Wu, S.Q. (2009) “Moving force identification of bridge-vehicle system with Gaussian system parameters and excitations.” *13th Asia-Pacific Vibration Conference (APVC2009)*, 22-25, November, New Zealand.

Wu, S.Q. and Law, S.S. (2010) “Bridge-moving vehicle system with uncertainties.” *The First International Conference on Advances in Interaction & Multiscale Mechanics (AIMM'10)*, May 30-June 3, Jeju, Korea.

ACKNOWLEDGEMENTS

My deepest gratitude goes first and foremost to my supervisor, Prof. S.S. Law, not only for his consistent and illuminating instructions on my research, but also his research attitude, research strategy, creative thinking and high efficiency benefit me a lot through my whole PhD study.

Secondly, I would like to express my heartfelt gratitude to Prof. Z.Y. Shi from Nanjing University of Aeronautics and Astronautics where I got my M.Sc. degree, it is his recommendation that let me to have this great opportunity to study in Hong Kong.

I am very lucky to have Mr. Z.H. Chen, Mr. Z.W. Chen, Mr. J. Li, Mr. W.Y. Liao, Dr. W. Lin and Mr. P. Zhang who are my colleagues as well as my good friends. I would like to express my gratitude to them for the friendship and for their persistent help to me.

Appreciation is extended to the Hong Kong Polytechnic University, who provides me the financial support which makes the study in Hong Kong possible.

Last but not least, I would like to express my gratitude to my family and share my happiness with them. Their love means everything to me.

TABLE OF CONTENTS

CERTIFICATE OF ORIGINALITY	I
ABSTRACT	III
LIST OF PUBLICATIONS	VI
ACKNOWLEDGEMENTS.....	VIII
TABLE OF CONTENTS	IX
NOTATIONS	XVII
LIST OF TABLES	XXIX
LIST OF FIGURES	XXXII
CHAPTER 1	1
INTRODUCTION.....	1
1.1 RESEARCH BACKGROUND.....	1
1.2 RESEARCH OBJECTIVES	9
1.3 OUTLINE OF THE THESIS.....	10
CHAPTER 2	15
LITERATURE REVIEW	15
2.1 DETERMINISTIC ANALYSIS OF BRIDGE-VEHICLE SYSTEM.....	15
2.1.1 <i>Methods Based on Modal Superposition Technique</i>	<i>16</i>

2.1.2	<i>Methods Based on Finite Element</i>	19
2.1.3	<i>Other Research Work</i>	23
2.1.3.1	Response of Bridge with Prestressing Forces	23
2.1.3.2	Response of Bridge with Damage.....	24
2.2	DETERMINISTIC MOVING FORCE IDENTIFICATION.....	25
2.2.1	<i>Weigh-In-Motion Technique</i>	26
2.2.2	<i>Moving Force Identification Technique</i>	27
2.2.3	<i>Model Condensation Technique</i>	36
2.3	STOCHASTIC ANALYSIS OF BRIDGE-VEHICLE SYSTEM.....	42
2.3.1	<i>Source of Randomness</i>	42
2.3.2	<i>Stochastic Methods in Structural Dynamics</i>	43
2.3.2.1	Representation of the Stochastic Process.....	43
2.3.2.2	Stochastic Response Calculation.....	46
2.3.3	<i>Stochastic Finite Element Method</i>	46
2.3.3.1	Discretization of Random Fields.....	47
2.3.3.2	Methods for Evaluating the Stochastic Responses.....	50
2.3.3.3	Estimation of the Response Statistics	56
2.3.4	<i>Stochastic Forward Problem of Bridge-vehicle Interaction</i>	58
CHAPTER 3		64
BEAM-LOAD SYSTEM WITH UNCERTAINTY IN EXCITATION		64
3.1	INTRODUCTION	64
3.2	EQUATION OF MOTION OF BEAM UNDER MOVING FORCES	65

3.3	KARHUNEN-LOÈVE EXPANSION	67
3.3.1	<i>Theory</i>	68
3.3.2	<i>Representation of Stochastic Process Vector</i>	69
3.4	SYSTEM MODELING AND RESPONSE STATISTICS	71
3.5	STOCHASTIC MOVING FORCE IDENTIFICATION.....	73
3.6	NUMERICAL SIMULATION.....	76
3.6.1	<i>Beam-Load Model</i>	77
3.6.1.1	Beam Model I.....	77
3.6.1.2	Force Model I.....	77
3.6.1.3	Force Model II	78
3.6.2	<i>Forward Analysis: Response Statistics</i>	80
3.6.3	<i>Inverse Analysis: Force Identification</i>	83
3.6.3.1	Verification of the Algorithm	83
3.6.3.2	Number of Samples Used	86
3.6.3.3	Comparison with Existing Deterministic Moving Force Identification Method.....	87
3.7	SUMMARY	90
CHAPTER 4		101
BRIDGE-VEHICLE INTERACTION WITH UNCERTAINTY IN EXCITATION.....		101
4.1	INTRODUCTION	101
4.2	MODELING OF THE BRIDGE-VEHICLE SYSTEM.....	103

4.2.1	<i>The Vehicle Model</i>	103
4.2.2	<i>The Coupled Equation of Motion</i>	105
4.3	BRIDGE-VEHICLE INTERACTION WITH ROAD SURFACE ROUGHNESS	106
4.3.1	<i>The Road Surface Roughness</i>	106
4.3.2	<i>Forward Problem</i>	107
4.3.3	<i>Inverse Problem: Moving Force Identification</i>	110
4.4	NUMERICAL SIMULATION.....	113
4.4.1	<i>Bridge-vehicle Model</i>	113
4.4.2	<i>Verification of the Proposed Stochastic Approach</i>	113
4.4.2.1	Gaussian Assumption of the Road Surface Roughness.....	113
4.4.2.2	Forward Problem: The Statistics of Response	115
4.4.2.3	Inverse Problem: Identify the Statistics of the Interaction Forces	116
4.4.3	<i>Number of the Samples Used</i>	118
4.4.4	<i>The Effect of Road Surface Roughness</i>	120
4.5	DISCUSSION ON THE MEASUREMENT NOISE.....	121
4.6	SUMMARY	123
CHAPTER 5		132
STOCHASTIC BEAM-LOAD SYSTEM: THE GAUSSIAN ASSUMPTION		132
5.1	INTRODUCTION	132
5.2	MODELING OF GAUSSIAN UNCERTAINTY IN SYSTEM PARAMETERS.....	134

5.2.1	<i>The Stochastic Finite Element Algorithm</i>	134
5.2.2	<i>Response Statistics</i>	139
5.3	MOVING FORCE IDENTIFICATION WITH GAUSSIAN UNCERTAINTY IN SYSTEM PARAMETERS.....	140
5.3.1	<i>Problem of the First Kind</i>	141
5.3.2	<i>Problem of the Second Kind</i>	143
5.3.3	<i>General Force Identification Algorithm</i>	144
5.3.4	<i>Identification Procedure</i>	147
5.4	NUMERICAL SIMULATION.....	149
5.4.1	<i>Beam-Load Model</i>	149
5.4.2	<i>Forward Analysis</i>	150
5.4.2.1	Verify with Monte Carlo Simulation.....	150
5.4.2.2	Effect of Moving Velocity.....	153
5.4.2.3	Effect of the Level of Randomness in System Parameters	154
5.4.2.4	Effect of the Level of Randomness in Excitation	155
5.4.3	<i>Inverse Analysis</i>	156
5.4.3.1	Effect of the Number of Samples Used.....	159
5.4.3.2	Effect of the Level of Randomness in System Parameters	160
5.4.3.3	Effect of the Level of Randomness in Excitation	162
5.5	DISCUSSIONS.....	163
5.6	SUMMARY	165
CHAPTER 6	180

6.4.3	<i>Non-Gaussian System Parameters: A Reduced PCE Model</i>	207
6.4.3.1	Coefficients in One-dimensional Polynomial Chaos Expansion.....	209
6.4.3.2	Effect of the Level of Randomness in System Parameters	210
6.4.3.3	Effect of the Level of Randomness in Excitation	212
6.5	SUMMARY	213
CHAPTER 7		231
STOCHASTIC BRIDGE-VEHICLE INTERACTION: THE SSFEM MODEL.....		231
7.1	INTRODUCTION	231
7.2	THE COUPLED MODEL WITH UNCERTAINTY IN SYSTEM PARAMETERS	232
7.2.1	<i>Gaussian System Parameters</i>	232
7.2.2	<i>Non-Gaussian System Parameters</i>	235
7.2.3	<i>Response Statistics</i>	236
7.3	NUMERICAL SIMULATION.....	237
7.3.1	<i>Gaussian System Parameters</i>	237
7.3.2	<i>Non-Gaussian System Parameters</i>	239
7.3.2.1	Dynamic Analysis Procedure	239
7.3.2.2	Level of Randomness in System Parameters	241
7.3.2.3	Truncation in Karhunen-Loève Expansion	244
7.3.2.4	Level of the Randomness in Excitation	245
7.4	DISCUSSIONS ON COMPUTATIONAL ASPECTS.....	246

7.5 SUMMARY	249
CHAPTER 8	265
SUMMARY, CONCLUSIONS AND RECOMMENDATIONS.....	265
8.1 SUMMARY	265
8.2 CONCLUSIONS.....	267
8.3 RECOMMENDATIONS	272
REFERENCES.....	275

NOTATIONS

A	Cross-section area
A_F	Amplitude of the PSD of the random part of the moving forces
B	Threshold for the truncation in KLE
\mathbf{B}^e	Stain-displacement matrix of each element
\mathbf{C}	Damping matrix
$\mathbf{C}(x_1, x_2)$	Covariance kernel for a Gaussian random process
$\mathbf{C}^{(k,j)}$	Sub-matrices in the system damping matrix
\mathbf{C}_b	Damping matrix of beam or bridge structure
$\hat{\mathbf{C}}_b$	Condensed damping matrix of beam or bridge structure
\mathbf{C}_i	Deterministic matrix in the expansion of damping matrix
C_{si}	Damping of the suspensions of the vehicle
C_{ti}	Damping of the tires of the vehicle
COV_F	Coefficient of variation of the excitation force
$E(x), E(x, \theta)$	Young's modulus
$\bar{E}(x)$	Mean value of the Young's modulus
$\tilde{E}(x, \theta)$	Random part of the Young's modulus
$E(\bullet)$	Expectation
EI	Flexural rigidity
F	Static Force
$\mathbf{F}(t, \theta)$	Stochastic moving load vector

$\hat{\mathbf{F}}(t, \theta)$	The identified stochastic moving load vector
F_i	The i th moving load
F_{id}	The deterministic part of the i th moving load
F_{ir}	The random part of the i th moving load
\mathbf{F}_m	Force vector on master <i>dofs</i>
\mathbf{F}_s	Force vector on slave <i>dofs</i>
F^{cal}	Calculated force
F^{ref}	Reference force
FE	Relative error between the calculated and reference force vector
$\mathbf{H}(x)$	Shape function of the beam element
\mathbf{H}_b	Location matrix for the moving load
$\hat{\mathbf{H}}_b$	Condensed location matrix for the moving load
\mathbf{H}^e	Shape function matrix of each element
\mathbf{H}_i	Sub-matrix in location matrix for the moving load
\mathbf{H}_m	Location matrix for the moving load on master <i>dofs</i>
\mathbf{H}_s	Location matrix for the moving load on slave <i>dofs</i>
\mathbf{I}	Identity matrix
I_v	Moment of inertia of the vehicle
L	Length of beam or bridge structure
$L(x, \theta)$	Lognormal random process
$L_0(x)$	Mean term of a Lognormal random process
\mathbf{K}	Stiffness matrix

\mathbf{K}_b	Stiffness matrix of beam or bridge structure
$\hat{\mathbf{K}}_b$	Condensed stiffness matrix of beam or bridge structure
\mathbf{K}_i	Deterministic matrix in the expansion of stiffness matrix
$\mathbf{K}^{(k,j)}$	Sub-matrices in the system stiffness matrix
\mathbf{K}_{mm}	Sub-matrix of the stiffness matrix on master <i>dofs</i>
\mathbf{K}_{ms}	Sub-matrix of the stiffness matrix on master and slave <i>dofs</i>
\mathbf{K}_{Rd}	Condensed stiffness matrix with dynamic condensation technique
\mathbf{K}_{RI}	Condensed stiffness matrix with IRS method
$\mathbf{K}_{RI,i}$	Condensed stiffness matrix at the <i>i</i> th step with Iterative IRS method
\mathbf{K}_{Rs}	Condensed stiffness matrix with static condensation technique
\mathbf{K}_{sm}	Sub-matrix of the stiffness matrix on slave and master <i>dofs</i>
\mathbf{K}_{ss}	Sub-matrix of the stiffness matrix on slave <i>dofs</i>
\mathbf{KN}	Covariance kernel of the problem with uncertainty in both system parameters and excitation
\mathbf{KN}_d	Covariance kernel of the Problem of the First Kind
\mathbf{KN}_s	Covariance kernel of the Problem of the Second Kind
K_c	Number of terms in PCE of the damping
K_E	Number of terms in PCE of the Young's modulus
K_F	Number of terms in PCE of the excitation force
K_p	Number of Polynomials required in a reduced PCE
K_R	Number of terms in PCE of the response
K_{si}	Stiffness of the suspensions of the vehicle

K_{ti}	Stiffness of the tires of the vehicle
K_{ρ}	Number of terms in PCE of the mass density
K_Z	Number of terms in PCE of the response of bridge-vehicle system
\mathbf{M}	Mass matrix
$\mathbf{M}^{(k,j)}$	Sub-matrices in the system mass matrix
\mathbf{M}_b	Mass matrix of beam or bridge structure
$\hat{\mathbf{M}}_b$	Condensed mass matrix of beam or bridge structure
\mathbf{M}_i	Deterministic matrix in the expansion of mass matrix
\mathbf{M}_{Rd}	Condensed mass matrix with dynamic condensation technique
\mathbf{M}_{RI}	Condensed mass matrix with IRS method
$\mathbf{M}_{RI,i}$	Condensed mass matrix at the i th step with Iterative IRS method
\mathbf{M}_{Rs}	Condensed mass matrix with static condensation technique
$MEAN_{\mathbf{R}}(t)$	Mean value of response
$MEAN_F(t)$	Mean value of moving loads
$MEAN_p(t)$	Mean value of identified interaction forces
N_d	Number of <i>dofs</i> of the beam with boundary condition
N_F	Number of moving loads
N_k	Number of frequency divisions
N_m	Number of the measurement points
N_T	Number of the time instants
N_v	Dimension of the covariance matrix
N_{θ}	Number of the samples

OD_R	Order of Polynomial Chaos for representing the response
OD_S	Order of Polynomial Chaos for representing the system parameters
$P(D)$	Polynomial operator
$\mathbf{P}(t, \theta)$	Stochastic force vector acting on bridge-vehicle system
$\mathbf{P}^{(k)}$	Vector of the K-L components of the nodal forces
$\hat{\mathbf{P}}^{(j)}(t)$	Vector of the components of the interaction forces in inverse problem
\mathbf{R}	Nodal displacement vector
$\mathbf{R}(t, \theta)$	Random nodal displacement vector in forward problem
$\hat{\mathbf{R}}(t, \theta)$	Random nodal displacement vector in inverse problem
$\mathbf{R}^{(j)}(t)$	Vector of components for the nodal displacement of bridge
$\dot{\mathbf{R}}$	Nodal velocity vector
$\dot{\mathbf{R}}(t, \theta)$	Random nodal velocity vector in forward problem
$\dot{\hat{\mathbf{R}}}(t, \theta)$	Random nodal velocity vector in inverse problem
$\ddot{\mathbf{R}}$	Nodal acceleration vector
$\ddot{\mathbf{R}}(t, \theta)$	Random nodal acceleration vector in forward problem
$\ddot{\hat{\mathbf{R}}}(t, \theta)$	Random nodal acceleration vector in inverse problem
R^{cal}	Calculated response
R^{ref}	Reference response
RE	Relative error between the calculated and reference response vector
S	Axle space of the vehicle
$S_a(f)$	PSD for the road surface roughness
$S_d(f_0)$	Degree of the roughness of the road

$S_{FF}(\omega)$	PSD for the random part of moving force
T	Total time duration
\mathbf{T}	Transformation matrix
\mathbf{T}_s	Transformation matrix for static condensation
\mathbf{T}_d	Transformation matrix for dynamic condensation
$\mathbf{T}_{id}, \mathbf{T}_{IRS}$	Transformation matrix for IRS method
$\mathbf{T}_{IRS,i+1}$	Transformation matrix at the $(i+1)$ th step with Iterative IRS method
$\mathbf{V}(x, \theta)$	Multi-dimensional stochastic process vector
$VAR_{\mathbf{R}}(t)$	Variance of the response
$VAR_F(t)$	Variance of the moving loads
$VAR_p(t)$	Variance of the identified interaction moving forces
$\mathbf{V}\mathbf{V}(t, \theta)$	Vector of a discretized random process
$\mathbf{x}^{(j)}(t), \mathbf{x}^{(j)}(t)$	Vector of the j th K-L components for nodal displacement
Y_1, Y_2	Functions of Gaussian random variables
$\mathbf{Y}(t, \theta)$	Vector of displacement of the vehicle system
$\mathbf{Y}^{(j)}(t)$	Vector of K-L components for displacement of vehicle
$\dot{\mathbf{Y}}(t, \theta)$	Vector of velocity of the vehicle system
$\ddot{\mathbf{Y}}(t, \theta)$	Vector of acceleration of the vehicle system
$\mathbf{Z}(t, \theta)$	Vector of displacement of the bridge-vehicle system
$\mathbf{Z}^{(j)}(t)$	Vector of K-L components for nodal displacement of the bridge-vehicle system
$\dot{\mathbf{Z}}(t, \theta)$	Vector of displacement of the bridge-vehicle system

$\dot{\mathbf{Z}}^{(k)}(t)$	Vector of the corresponding components for nodal velocity of the bridge-vehicle system
$\ddot{\mathbf{Z}}(t, \theta)$	Vector of displacement of the bridge-vehicle system
$\ddot{\mathbf{Z}}^{(k)}(t)$	Vector of the corresponding components for nodal acceleration of the bridge-vehicle system
a	Correlation length
a_1, a_2	Dimension of the vehicle
b_i	Generalized Fourier coefficients
c	Damping
$\bar{c}(x)$	Mean value of the damping
$\tilde{c}(x, \theta)$	Random part of the damping
c_M, c_K	Constants in Rayleigh damping
f	Spatial frequency
f_0	Discontinuity frequency
$\mathbf{f}^{(j)}(t)$	Vector of K-L components of the moving loads
$\hat{\mathbf{f}}^{(j)}(t)$	Vector of components of the moving loads to be identified
g	Acceleration due to gravity
$g(x, \theta)$	A Gaussian random process
$g_i(x)$	The K-L components for $g(x, \theta)$
k_c	Number of K-L components in KLE of the damping retained after truncation
k_E	Number of K-L components in KLE of the Young's modulus retained

	after truncation
k_F	Number of K-L components of the forces retained in forward problem
\hat{k}_F	Number of components of the forces in inverse problem
k_l	Number of terms of the K-L components in a PCE of a Lognormal random process
k_p	Number of K-L components required for a reduced PCE
\hat{k}_p	Number of components of the interaction forces in inverse problem
k_R, k_m	Number of K-L components of the nodal displacement in forward problem
\hat{k}_R	Number of K-L components of the nodal displacement in inverse problem
k_r	Number of K-L components of the road surface roughness retained after truncation
k_s	Total number of K-L components in the KLE of the excitation and system parameters
k_v	Number of K-L components of a random process retained after truncation
k_z	Number of components in the expansion of the nodal displacement of the bridge-vehicle system
k_ρ	Number of K-L components in KLE of the mass density retained after truncation

l	Length of the beam element
l_a	Distance between the two moving forces
m_v	Mass of the vehicle
m_1, m_2	Mass of the bogie
n	Number of time instants
p	Order of Polynomial Chaos
$r(x)$	Road surface profile
$r(x, \theta)$	Road surface roughness
$r^{(j)}(x)$	The j^{th} K-L components in KLE of the road surface roughness
t	Time
$u(x, \theta)$	Random process
$v_i(t, \theta)$	The i th random process in a multi-dimensional vector
$\bar{u}(x), \bar{v}_i(x)$	Expected value of a random process
$\tilde{u}(x, \theta)$	Stochastic part of a random process
$\tilde{v}_i(x, \theta)$	Stochastic part of the i th random process
\mathbf{u}_m	Eigenvectors of the condensed system
v	Speed of the moving load
v_i	Speed of the i th moving load
$w(x, t)$	Deterministic displacement of the beam or bridge structure
$w(x, t, \theta)$	Stochastic displacement of the beam or bridge structure
$\hat{w}(x_i, t_j, \theta_k)$	“Measured” displacement samples under the bridge deck
x, x_i, x_j	Location on the beam or bridge structure

$\hat{x}_1(t), \hat{x}_2(t)$	Position of the vehicular axle
\mathbf{x}	Displacement vector on all the <i>dofs</i>
$\ddot{\mathbf{x}}$	Acceleration vector on all the <i>dofs</i>
\mathbf{x}_{Fd}	The adjustment force vector
\mathbf{x}_m	Displacement vector on master <i>dofs</i>
$\ddot{\mathbf{x}}_m$	Acceleration vector on master <i>dofs</i>
\mathbf{x}_s	Displacement vector on slave <i>dofs</i>
$\ddot{\mathbf{x}}_s$	Acceleration vector on slave <i>dofs</i>
$\mathbf{y}^{(j)}$	Corresponding components of nodal displacement vector in forward problem
$\hat{\mathbf{y}}^{(j)}$	Corresponding components of nodal displacement vector in inverse problem
$\dot{\mathbf{y}}^{(j)}$	Corresponding components of nodal velocity vector in forward problem
$\hat{\dot{\mathbf{y}}}^{(j)}$	Corresponding components of nodal velocity vector in inverse problem
$\ddot{\mathbf{y}}^{(j)}$	Corresponding components of nodal acceleration vector in forward problem
$\hat{\ddot{\mathbf{y}}}^{(j)}$	Corresponding components of nodal acceleration vector in inverse problem
z	Distance from the neutral axis of the beam cross-section to the strain gauge

$\Delta\omega$	Frequency increment
$\Gamma_p(\cdot)$	Polynomial chaos of order p
$\Gamma_{\mathbf{v}\mathbf{v},\mathbf{v}\mathbf{v}}$	Covariance matrix of a discretized random process
$\Phi(\omega_0)$	Amplitude coefficient related to different classes of road
$\Phi_{rr}(\omega)$	PSD of the road surface roughness
Ψ_j	Hermite Polynomials
$\delta(t)$	Dirac delta function
δ_{kl}, δ_{mn}	Kronecker delta
$\varepsilon(x,t,\theta)$	Random strain under the bridge deck
$\hat{\varepsilon}(x_i, t_j, \theta_k)$	Random strain under the bridge deck in inverse problem
ζ	Damping ratio
θ	Random dimension
θ_k	Uniformly distributed phase angle
$\lambda_i, \lambda_j, \lambda_n$	Eigenvalues of the covariance kernel
μ_g	Mean value of $g(x,\theta)$
$\boldsymbol{\mu}_{\mathbf{v}}(t)$	Mean vector of a multi-dimensional stochastic process
$\xi_n(\theta)$	Standard Gaussian random variables
ρ	Mass per unit length
$\bar{\rho}(x)$	Mean value of the mass density
$\tilde{\rho}(x, \theta)$	The random part of the mass density
σ	Standard deviation
σ_g^2	Variance of $g(x,\theta)$

$\varphi_n(x)$	Eigenvectors of the covariance kernel
ω^2	Eigenvalue of the condensed system
$\bar{\omega}$	A specific natural frequency of the dynamic system
ω_0	Reference angular spatial frequency
ω_{\min}	Minimum frequency
ω_{\max}	Maximum frequency

LIST OF TABLES

Table 3.1 - Relative error in the statistics of the mid-span displacement with uncertainty in excitation (Force Model I)	92
Table 3.2 - Relative error in the statistics of the mid-span displacement with different threshold for truncation	92
Table 3.3 - Relative error in the statistics of the mid-span displacement with uncertainty in excitation (Force Model II)	93
Table 3.4 - Relative error in the statistics of the identified forces with different uncertainty (Force Model I)	93
Table 3.5 - Relative error in the statistics of the identified forces with different uncertainty (Force Model II)	94
Table 3.6 - Relative error in the identified forces using different number of response samples (Force Model I)	94
Table 3.7 - Relative error in the identified forces using different number of response samples (Force Model II)	95
Table 3.8 - Relative error in the mean value of the identified moving forces with different approaches (Force Model II)	95
Table 4.1- Parameters of the bridge-vehicle systems	125
Table 4.2 - Relative error in the identified forces from different kinds of response samples	125
Table 4.3 - Relative error in the identified forces from different number of	

response samples.....	126
Table 4.4 - Relative error in the identified forces from different classes of roads	126
Table 5.1 - Relative error of mid-span displacement for different vehicle speed	167
Table 5.2 - Relative error of mid-span displacement for different level of randomness in system parameters.....	167
Table 5.3 - Relative error of mid-span displacement for different level of randomness in excitation forces.....	167
Table 5.4 - Relative error in the identified forces from different number of response samples (F_1 in Force Model I).....	168
Table 5.5 - Relative error in the identified forces from different number of response samples (F_1 in Force Model II).....	168
Table 5.6 - Relative error in the identified force for different level of uncertainty in system parameters (F_1 in Force Model I).....	169
Table 5.7 - Relative error in the identified force for different level of uncertainty in system parameters (F_1 in Force Model II).....	169
Table 5.8 - Relative error in the identified forces for different level of uncertainty in excitation (F_1 in Force Model I).....	170
Table 5.9 - Relative error in the identified forces for different level of uncertainty in excitation (F_1 in Force Model II).....	170
Table 6.1 - Percentage error in the statistics of mid-span displacement with	

different order of Polynomial Chaos used	216
Table 6.2 - Percentage error in the statistics of mid-span displacement with different level of randomness in excitation forces when order of PC=2....	216
Table 6.3 - Percentage error in mid-span displacement statistics due to different level of randomness in system parameters.....	217
Table 6.4 - Percentage error in the calculated response statistics due to different level of randomness in excitation.....	218
Table 6.5 - Percentage error in coefficients calculation of the three methods in one dimensional PCE.....	218
Table 6.6 - Percentage error in mid-span displacement statistics due to different level of PC representation when $COV_F=0\%$	219
Table 6.7 - Percentage error in mid-span displacement statistics due to different level of PC representation when $COV_E=COV_\rho=20\%$	219
Table 7.1 - Percentage error in mid-span displacement statistics due to different level of Gaussian randomness in system parameters	252
Table 7.2 - Percentage error in mid-span displacement statistics due to different level of randomness in excitation with Gaussian system parameters	252
Table 7.3 - Percentage error in mid-span displacement statistics due to different level of non-Gaussian randomness in system parameters.....	253
Table 7.4 - Percentage error in the calculated responses using different threshold for truncation in KLE of road surface roughness.....	254
Table 7.5 - Percentage error in mid-span displacement statistics due to different	

level of randomness in excitation with non-Gaussian system parameters .254

LIST OF FIGURES

Figure 3.1 - Beam-load model	96
Figure 3.2 - Comparison of mid-span responses from the two methods (Force Model I).....	96
Figure 3.3 - Comparison of mid-span responses from the two methods (Force Model II)	97
Figure 3.4 - Mean value of identified forces from 500 samples (Force Model I)	97
Figure 3.5 - Variance of identified forces from 500 samples (Force Model I)	98
Figure 3.6 - Mean value of identified forces from 500 samples (Force Model II)	98
Figure 3.7 - Variance of identified forces from 500 samples (Force Model II) ...	99
Figure 3.8 - Identified force time histories from a deterministic approach (Force Model II)	99
Figure 3.9 - Comparison of the identified force time histories from different approaches (Force Model II).....	100
Figure 4.1 - The bridge-vehicle system.....	127
Figure 4.2 - Comparison of the PDF and CDF between samples from the road surface and the corresponding Gaussian random variable.....	127
Figure 4.3 - Comparison of statistics of mid-span displacement.....	128
Figure 4.4 - Comparison of identified and theoretical mean value of the interaction forces (Class A Road).....	128

Figure 4.5 - Comparison of identified and theoretical variance of the interaction forces (Class <i>A</i> Road).....	129
Figure 4.6 - Typical road surface profiles	130
Figure 4.7 - Comparison of the identified and theoretical mean value of the interaction forces (Class <i>E</i> Road).....	131
Figure 4.8 - Comparison of identified and theoretical variance of the interaction forces (Class <i>E</i> Road).....	131
Figure 5.1 - Kernel for the K-L decomposition	171
Figure 5.2 - Comparison of statistics of mid-span displacement (F_1 in Force Model I).....	171
Figure 5.3 - Comparison of statistics of mid-span displacement (F_1 in Force Model II).....	172
Figure 5.4 - Comparison of statistics of mid-span displacement for $COV_F=0\%$ (Force Model I)	172
Figure 5.5 - Comparison of statistics of mid-span displacement for $COV_F=10\%$ (Force Model I).....	173
Figure 5.6 - Covariance kernel of \mathbf{KN}	173
Figure 5.7 - Comparison of identified and theoretical moving force.....	174
Figure 5.8 - Covariance kernel of \mathbf{KN}_s	174
Figure 5.9 - Error between the calculated and theoretical \mathbf{KN}_s	175
Figure 5.10 - Error between the calculated and theoretical \mathbf{KN}_d	175
Figure 5.11 - Comparison of the first eight eigenvalues of \mathbf{KN}_d	176

Figure 5.12 - Comparison of the first eight K-L components of mid-span displacement.....	177
Figure 5.13 - Comparison of identified and theoretical force statistics (500 samples)	178
Figure 5.14 - Comparison of identified and theoretical force statistics (5 samples)	178
Figure 5.15 - Comparison of identified and theoretical force statistics with $\Phi(\omega_0)=16\times 10^{-6} m^3$ (200 samples)	179
Figure 5.16 - Comparison of identified and theoretical force statistics with $COV_F=15\%$ (200 samples).....	179
Figure 6.1 - Convergence analysis of the MCS in Case 1, when $COV_E=COV_\rho=20\%$ and $t=0.5s$	220
Figure 6.2 - Comparison of calculated variance from SSFEM and MCS in Case 1 when $COV_E=COV_\rho=10\%$	220
Figure 6.3 - Comparison of calculated variance from SSFEM and MCS in Case 1 when $COV_E=COV_\rho=20\%$	221
Figure 6.4 - Convergence analysis of the MCS in Case 2, when $COV_E=COV_\rho=10\%$, $COV_F=62.56\%$ and $t=0.5s$	221
Figure 6.5 - Comparison of calculated statistics from SSFEM and MCS in Case 2, when $COV_E=COV_\rho=10\%$ and $COV_F=62.56\%$	222
Figure 6.6 - Comparison of mean value of mid-span displacement with different order of PC used.....	223

Figure 6.7 - Comparison of variance of mid-span displacement with different order of PC used	224
Figure 6.8 - Comparison of mean value of mid-span displacement with different level of randomness in excitation when $COV_E=COV_\rho=20\%$	225
Figure 6.9 - Comparison of variance of mid-span displacement with different level of randomness in excitation when $COV_E=COV_\rho=20\%$	226
Figure 6.10 - Comparison of mean value of mid-span displacement when $COV_F=0\%$ and different order of PC Used	227
Figure 6.11 - Comparison of variance of mid-span displacement when $COV_F=0\%$ and different order of PC Used	228
Figure 6.12 - Comparison of mean value of mid-span displacement when $COV_E=COV_\rho=20\%$ with different level of randomness in excitation	229
Figure 6.13 - Comparison of variance of mid-span displacement when $COV_E=COV_\rho=20\%$ with different level of randomness in excitation	230
Figure 7.1 - Comparison of statistics of mid-span displacement from SSFEM and MCS with different order of PC when $COV_E=COV_\rho=10\%$	255
Figure 7.2 - Comparison of statistics of mid-span displacement from SSFEM and MCS with different order of PC when $COV_E=COV_\rho=20\%$	255
Figure 7.3 - Comparison of mean values of mid-span displacement from SSFEM and MCS, when $COV_E=COV_\rho=10\%$	256
Figure 7.4 - Comparison of variances of mid-span displacement from SSFEM and MCS, when $COV_E=COV_\rho=10\%$	257

Figure 7.5 - Comparison of response statistics from SSFEM and MCS, when $COV_E=COV_\rho=20\%$, Road C and $B=0.99$	258
Figure 7.6 - Comparison of mean values of mid-span displacement with different order of PC used.....	259
Figure 7.7 - Comparison of variances of mid-span displacement with different order of PC used.....	260
Figure 7.8 - Comparison of statistics of mid-span displacement with different threshold for truncation when $COV_E=COV_\rho=20\%$ and $S_d(f_0)=64\times 10^{-6}$	261
Figure 7.9 - Comparison of mean values of mid-span displacement under different road surface conditions when $COV_E=COV_\rho=20\%$, $B=0.97$ and $OD_s=OD_R=2$	262
Figure 7.10 - Comparison of variances of mid-span displacement under different road surface conditions when $COV_E=COV_\rho=20\%$, $B=0.97$ and $OD_s=OD_R=2$	263
Figure 7.11 - Typical sparsity patterns of the system matrices in SSFEM with different order of PCE when $k_s=9$	264

CHAPTER 1

INTRODUCTION

1.1 Research Background

Bridge plays an important role in a transportation system, and is directly linked to the country's development as well as people's daily living. However, it is subjected to the damaging effects of the daily traffic and freight trains. The importance of investigating the moving loads on top of the bridge deck was first recognized in the 19th century. Following the collapses of some railway bridges in Great Britain, engineers and researchers began to pay more attention to the dynamic behavior of the bridge under moving vehicular loads, and further research on new techniques for the bridge design and bridge condition assessment had been carried out (Cantieni 1983, 1992; Chan 1988, 1990). The structural conditions of the bridge will be affected by the operation loads including the dead load, live load, wind load and seismic load, etc. Among these loads, the moving vehicular axle load plays a vital role in the condition assessment especially for median span bridges.

The dynamic response of a bridge can be significant and Cebon (1987) concluded that the dynamic wheel loads may increase road surface damage by a factor of two to four over that due to static ones. In order to evaluate the influence of a passing vehicle on a bridge deck, the dynamic problem is converted into a

pseudo-static one with a dynamic amplification factor (DAF) in the design codes. However, the DAF may not always reveal the true dynamic behavior of the bridge. The dynamic responses of a bridge structure subject to moving vehicular loads have been studied for decades. Various research works on bridge-vehicle interaction (BVI) problem can be found. These works can be categorized into two kinds according to the technique employed to decompose the equation of motion of the bridge-vehicle system:

- (1) Methods based on modal superposition technique (Green and Cebon 1994; Chatterjee et al. 1994; Wang and Chou 1998; Zhu and Law 2002a, 2003a; Law and Zhu 2003; Sniady 2008; Li et al. 2008).
- (2) Methods based on finite element method (Wang et al. 1992, 1996; Yang and Lin 1995; Henchi et al. 1998; Huang et al. 1998; Lei and Noda 2002; Lee and Yhim 2004, 2005; Nallasivam et al. 2007; Ju and Lin 2007).

In these studies, different vehicle models such as moving force model, moving mass model, quarter car model, half car model and multi-axle three-dimensional vehicle model considering the pitch and roll effect according to American Association of State Highway and Transportation Officials (AASHTO) standard (Standard Specification for Highway Bridges 1989) etc. were used. The corresponding bridge models include beam model (Euler-Bernoulli beam and Timoshenko beam), plate model (single span orthotropic rectangular plate and multi-span continuous plate) and box-girder bridge model etc. There are also other kinds of bridge models such as the prestressed beam (Kim 2004; Kocaturk and

Simsek 2006; Simsek and Kocaturk 2007) and beams with cracks (Mahmond and Abou Zaid 2002; Khiem and Lien 2002; Law and Zhu 2004; Bilello and Bergman 2004; Yang et al. 2008) have been adopted in the bridge-vehicle interaction problems. All these research works on the dynamic analysis of bridge-vehicle interaction problem are very important achievements for considering the dynamic effects rather than static ones.

On the other hand, due to the importance of vehicle axle load information in transportation management and bridge condition assessment, how to acquire vehicle axle load accurately and efficiently is another important topic. Traditional ways to acquire vehicle axle load by stopping and weighing vehicle using weighbridge or loadometers are expensive and subject to bias. Weigh-in-motion (WIM) technique (Moses 1979; Davis and Sommerville 1987; Freund and Bonaquist 1989; Zhi et al. 1999) was developed for the purpose of obtaining vehicle axle loads when vehicle traveling across certain instrumented bridge. However, the WIM systems can only measure the equivalent static loads but not the peak dynamic wheel loads or the time series of these moving axle loads. Since the dynamic vehicular axle load it noted to increase the damage of the pavement, therefore, it should be accurately and efficiently acquired. A kind of identification technique emerged to meet the need of acquiring the time series of the dynamic vehicular axle loads. The main idea of this technique is using the measured bridge responses to identify the parameters of bridge-vehicle system from which the interaction forces can be subsequently identified. This technique is also called the

Moving Force Identification (MFI) technique which can be used to acquire vehicular axle loads, to inspect overweight vehicles, and to further provide data for bridge condition assessment and bridge design. These MFI methods can mainly be divided into two categories:

- (1) Methods based on a continuous bridge model with the modal superposition technique to decouple the equation of motion of the bridge structure with the subsequent solution obtained using an optimization scheme, e.g. Time Domain Method (TDM) (Law et al. 1997), Interpretive Method II (IMII) (Chan et al. 1999), Frequency-Time Domain Method (FTDM) (Law et al. 1999), State Space Method (SSM) (Zhu et al. 2006) and Identification based on genetic algorithm (Jiang et al. 2003, 2004) etc.
- (2) Methods based on discrete bridge model using the finite element method to model the bridge structure, e.g. Interpretive Method I (IMI) (O' Connor and Chan 1988), Optimal State Estimation Approach (OSEA) (Law and Fang 2001), Finite element approach with orthogonal function approximation (Law et al. 2004), Finite element approach with update static component (USC) technique (Pinkaw 2006) and Wavelet Based Method (WBM) (Law et al. 2008) etc.

Although the aforementioned research works include most aspects in the dynamic analysis and moving force identification of the bridge-vehicle interaction (BVI), they are all deterministic methods which treat the parameters in bridge-vehicle system and other important factors such as road surface roughness,

traveling velocity of vehicles, etc, as deterministic. The samples of irregular profile according to its power spectral density defined in the ISO standard (ISO 8606:1995(E) 1995) was often adopted to represent the effect of the road surface roughness in the dynamic analysis of bridge-vehicle interaction problem. In practice, randomness and uncertainties exist in the BVI problem. The excitation forces on the bridge deck can be random due to the irregular road profile. The uncertainty in the traveling velocity and uncertainties existed in the vehicle body. When performing deterministic analysis of the bridge-vehicle interaction problem, different sample of response data will be obtained in different computation due to different samples of road surface roughness is adopted. Therefore, the response statistics have to be included for a full description of the dynamic response of the bridge-vehicle system. Besides, the bridge structure often exhibits an inherent randomness. For example, the material properties in bridge structure such as the Young's modulus, mass density, sectional area, Poisson ratio, etc. are often varying within the system; Moreover, concrete bridges often exhibit a large number of cracks, and the models on the cracks can only approximately simulate the dynamic behavior of bridge with damage; Similar problems can also be found in modeling the effect of prestress in reinforced concrete structures. The conventional deterministic analysis generally represents only an "approximation" of the actual reality due to unavoidable uncertainties in the structural properties as well as in the loading processes. Stochastic analysis should be performed instead for the bridge-vehicle interaction problem to give more reliable results to

engineers.

The developments in stochastic computational mechanics provide methodologies either for the stochastic modeling of dynamic systems or evaluating the response statistics. Both the random excitations and system parameters may be assumed as Gaussian/non-Gaussian processes, and they can be represented by mathematic tools such as the Auto-Regressive Moving Average (ARMA) model (Samaras et al. 1985), Spectral Representation (SR) (Shinozuka and Jan 1972), Wavelet Representation (WR) (Zeldin and Spanos 1996), Karhunen-Loève Expansion (KLE) (Kac and Siegert 1947) and Polynomial Chaos Expansion (PCE) (Wiener 1938) etc. For the dynamic system with random excitations and deterministic system parameters, the equation of motion of the system which is a stochastic differential equation can be transformed into a set of deterministic equations when the random processes involved are represented by these mathematical tools. Numerical methods such as the Newmark- β method can then be employed to solve these equations to evaluate the response statistics. Great effort had been spent on developing techniques to solve the dynamic system with inherent uncertainties based on finite element model. It is commonly known as the Stochastic Finite Element Method (SFEM) in the past few decades. In most stochastic finite element applications, it is necessary to represent a continuous-parameter random field in terms of a vector of random variables. This process is known as discretization of the random field. Existing methods such as the mid-point method (Der Kiureghian and Ke 1988), the spatial averaging method

(Vanmarcke and Grigoriu 1983), the shape function method (Liu et al. 1986) and the series expansion method (Lawrence 1987; Spanos and Ghanem 1989) can be adopted to discretize these continuous random fields. To calculate the statistic of the dynamic response with uncertainties in the system parameters, the Monte Carlo Simulation (MCS) (Shinozuka 1972) which is a very versatile but comparatively time-consuming method, often serves to verify other stochastic methods. One of the alternatives which are widely used for evaluating the stochastic responses is the perturbation method (Hisada and Nakagiri 1981). However, this approach is only justified for small deviations from the center value and it requires simulations to assess the reliability of results. Another approach which is similar to the perturbation method, the Neumann expansion method (Shinozuka and Nomoto 1980), also requires simulations to assess the reliability of the results. The convergence of the Neumann series representing the inverse operator requires the norm of the kernel smaller than one. The Spectral Stochastic Finite Element Method (SSFEM) proposed by Ghanem and Spanos (1991) overcomes these weaknesses. It is a general technique for the solution of complex problems in probabilistic mechanics and is capable of handling variables with a large range of variation. In this method, the KLE and/or PCE are employed to represent the random processes involved in the mathematical model for a structural system. However, it suffers from the curse of exponentially increased dimension in the Polynomial Chaos Expansion for the solution when the required number of the Karhunen-Loève components for both the system parameters and

excitation are large (Stefanou 2009).

The dynamic analysis of a bridge deck under moving vehicles with uncertainties had been carried out by many researchers in recent years based on the analysis methods developed in computational mechanics. Some researchers considered the randomness in the excitation due to the road surface roughness while the system parameters of the bridge and vehicle were treated as deterministic. These works can mainly be classified into two categories including the frequency domain method (Da Silva 2004; Lin 2006) and the time domain method (Schenk and Bergman 2003; Seetapan and Chucheepsakul 2006). Others extended the work by introducing randomness in the vehicle modeling (Muscolino et al. 2002; Chang et al. 2006, 2009) in which Gaussian assumption was made on the system parameters and the perturbation method was employed for the solution. However, when the variation of uncertainties increases, the Gaussian assumption on the system parameters, which has a very small probability to take up a negative value, may lead to inaccurate solution and the perturbation method also tends to become less accurate. A stochastic model of traffic excitation on bridge in which the arrival of vehicles was assumed to follow a Poisson process, was proposed by Chen et al (2009) for the bridge structural condition assessment. However, the uncertainty in the arrival of vehicles will not be discussed in this Thesis.

Research work by employing the finite element method should be conducted thus more complex structure with uncertainties in both excitation and system

parameters can be investigated. Moreover, the uncertainties in the bridge structure, which have been ignored in the aforementioned research works, should also be taken into account. It has already been mentioned that the modal analysis needs the knowledge of model shapes which are difficult to obtain for a complex structure with complex boundary condition in the bridge-vehicle interaction problem. Since the perturbation method can only handle small variation in random system parameters, more powerful methods based on finite element bridge-vehicle model should be introduced.

1.2 Research Objectives

Research work presented in this Thesis aims to perform a theoretical study of the bridge-vehicle interaction problem with uncertainties, to develop new methods on stochastic analysis of finite element model of bridge-vehicle system and to fill the gap of lacking stochastic moving force identification technique considering both randomness in excitations and system parameters. All the research work within this scope will be focused on the finite element bridge-vehicle interaction model which will be achieved with the completion of the following objectives:

- (1) To perform the dynamic analysis of a deterministic bridge-vehicle system with randomness in the excitation forces due to the road surface roughness and to develop a moving force identification technique based on the formulated model in which the mean value and variance of the excitation

forces can be identified from the response samples of the bridge deck.

- (2) To develop a bridge-vehicle interaction model with uncertainties in both system parameters and excitation forces. Based on the formulated model, firstly, the dynamic analysis will be performed and the response statistics of the bridge-vehicle system will be evaluated. Then stochastic moving force identification with uncertainty in both system parameters and excitation will be developed with discussion on the factors which may affect the algorithm.

1.3 Outline of the Thesis

The contents of this Thesis will be divided into eight Chapters. The outline is given as follows:

In Chapter one, research background as well as the research gap of the existing dynamic analysis and moving force identification will be introduced. The research objectives are stated as above. An outline of the Thesis is also given at the end of this Chapter.

In Chapter two, a detail literature review on existing research work related to the following topics will be addressed: deterministic dynamic analysis of bridge-vehicle interaction, deterministic moving force identification techniques, the randomness existing in bridge-vehicle interaction problem, the mathematical tools on representation of random process and the stochastic modeling techniques for engineering structures and the dynamic analysis of bridge-vehicle interaction

with uncertainties.

In Chapter three, the bridge-vehicle system is modeled as a planar simply supported Euler-Bernoulli beam with moving forces on top. In order to introduce uncertainty to the moving forces, the basic theory of Karhunen-Loève Expansion and the representation of multi-dimensional Gaussian random processes using these tools are next addressed. The system modeling with Gaussian uncertainties in the excitation forces as well as the response statistics calculation of the bridge structure are introduced next. Numerical simulations will be conducted to verify the proposed algorithm and different factors which may affect the accuracy of the proposed algorithm will be investigated. Two kinds of force model will be adopted in the numerical simulation of the excitation on the bridge deck:

- (1) In Force Model I, the mean value of each force contains a deterministic component composed of two sine waves with different frequencies and a constant Coefficients of Variation (COV) at each time instance with Gaussian property.
- (2) In Force Model II, the mean value of each force is the same as in Force Model I and the random part of each moving force is assumed as a zero-mean Gaussian random process with a Power Spectral Density (PSD) function according to the ISO standard (ISO 8606:1995(E) 1995).

In Chapter four, the bridge-vehicle system is modeled as a planar simply supported Euler-Bernoulli beam with a four degrees-of-freedom mass-spring system moving on top. The road surface roughness according to the ISO standard

(ISO 8606:1995(E) 1995) is introduced and regarded as the source of randomness in the interaction problem. The mathematical model is formulated and based on which the response statistics of the bridge-vehicle system is evaluated. Similarly, a moving vehicle axle load identification algorithm is proposed to quantify the mean value and variance of the interaction forces which are usually difficult to obtain from direct measurements from the “measured” response samples.

In Chapter five, the uncertainties in the system parameters are included in the bridge-vehicle interaction model. The material properties of the bridge structure are assumed as Gaussian random processes. The bridge-vehicle system is modeled as a planar simply supported Euler-Bernoulli beam with moving forces on top. When the level of randomness in the system parameters is assumed not large, the response of the bridge is approximated by Gaussian random processes. The mathematical model of the bridge-vehicle system is formulated by adopting the finite element method and with the Gaussian random processes represented by the Karhunen-Loève Expansion, and the accuracy of which is verified with the numerical examples. A general moving force identification algorithm based on the formulated model with uncertainties in both system parameters and excitation forces are also proposed in this Chapter.

In Chapter six, the assumption on the small variation of the system parameters is removed, and the bridge-vehicle interaction model with uncertainty in system parameters in the bridge structure is modeled by the Spectral Stochastic Finite Element Method (SSFEM) which is a powerful modeling technique that can

handle large uncertainties in the finite element model of a structure with good accuracy. The bridge-vehicle system is modeled as a planar simply supported Euler-Bernoulli beam with moving forces on top. The system parameters and excitation forces, which are assumed as Gaussian random processes will be represented by the Karhunen-Loève Expansion (KLE). The response of the bridge structure, which may have non-Gaussian properties, will be represented by the Polynomial Chaos Expansion. The accuracy of the model is verified in the numerical simulation with cases of large variation of uncertainties in system parameters. Since the stochastic system parameters with Gaussian assumption will have a small probability to take up negative values, it may lead to inaccurate solution. The non-Gaussian assumption is further adopted and the dynamic analysis of the bridge-vehicle interaction with non-Gaussian system parameters is performed. Due to the curse of exponentially increased dimension for Polynomial Chaos Expansion (PCE) for the solution when the required number of the Karhunen-Loève components for both the system parameters and excitation are large, a reduced Polynomial Chaos Expansion for non-Gaussian random processes is introduced to improve the efficiency of the dynamic analysis of the bridge-vehicle interaction problem with non-Gaussian uncertainty in system parameters. Numerical simulations will be conducted to investigate the accuracy of the proposed models with both the full PCE and reduced PCE, and the results are compared with those from the Monte Carlo Simulation.

In Chapter seven, the dynamic analysis of the bridge-vehicle system with the

bridge modeled as a planar simply support Euler-Bernoulli beam with uncertainties in material properties and a moving vehicle modeled as a four degrees-of-freedom mass-spring system is performed. The road surface roughness is modeled as a Gaussian random process with a Power Spectrum Density (PSD) function defined according to the ISO standard (ISO 8606:1995(E) 1995). The cases with the Gaussian/non-Gaussian assumption for the material properties of the bridge structure are investigated. The mathematical model is formulated with the SSFEM and verified by the Monte Carlo Simulation in the numerical simulations. Different factors such as the order of Polynomial Chaos used and the level of randomness in both system parameters and excitation, etc., which may affect the accuracy of the proposed model, will be investigated.

In Chapter eight, conclusions are drawn from the research work presented in the Thesis. Due to the limitation of the time and the author's knowledge, some recommendations on the future work related to the bridge-vehicle interaction problem with uncertainties are addressed.

CHAPTER 2

LITERATURE REVIEW

2.1 Deterministic Analysis of Bridge-Vehicle System

The dynamic response of a bridge structure subject to moving vehicular loads has been studied for decades. Various research works on bridge-vehicle interaction (BVI) problem can be found.

A general summarization has been included in the monograph written by Fryba (1999). Various types of moving forces includes constant, harmonic, arbitrarily varying in time, moving system with two-degrees-of-freedom, moving multi-axle system and moving random loads. The structure model includes single-/multi-span uniform/non-uniform beam, beam with elastic/non-elastic properties, beam/plate on elastic foundation and beam subject to axial forces. Beams with various boundary conditions subject to a moving load was also studied, and various factors which may influence the dynamic response of structure under moving forces, such as the velocity of the moving forces, the ratio between the weight of vehicle and beam, the initial conditions, the damping of the beam structure and etc. were discussed.

A detailed review of the more recent developments in dynamic analysis of the deterministic bridge-vehicle interaction problem will be listed in this Chapter.

Since different research works have been done on this topic in which similar research was carried out by different scholars, a selected review will be given and the corresponding conclusions will be summarized. These works can mainly be categorized into two categories according to the method adopted to decompose the equation of motion of the bridge-vehicle system.

2.1.1 Methods Based on Modal Superposition Technique

Amongst various methods in the dynamic analysis of the bridge structure under moving vehicle, the modal superposition technique is typically used to decompose the equation of motion of the system in which the response of structure is represented by a set of modal shapes with different amplitudes. The equation of motion of a dynamic system, which is a partial differential equation, is transformed into a set of ordinary differential equations which can be easily solved by numerical methods such as the Newmark- β method. Existing research employing the modal superposition technique will be reviewed.

With the bridge deck modeled as an Euler-Bernoulli beam, Green and Cebon (1994) gave the solution to the dynamic responses of the deck under a “quarter-car” vehicle model in the frequency domain using an iterative procedure. The algorithm was validated by extensive experiments on a typical highway bridge. Modal tests showed that beam and plate models of the bridge dynamics gave reasonable predictions on the measured vibration mode shapes and natural frequencies of the bridge. Results from the vehicle tests indicated that the method

proposed was accurate for predicting the dynamic response of short-span highway bridges under heavy vehicle loads. An analysis method for a beam with non-uniform cross-section and with a time varying concentrated force traveling on the top was proposed by Gutierrez and Laura (1997). The vibrational behavior of an elastic homogeneous isotropic beam with different boundary conditions due to a moving harmonic force was studied by Abu-Hilal and Mohsen (2000). Law and Zhu (2005) investigated the influence of braking on a multi-span non-uniform bridge deck under moving vehicle axle forces. Results showed that vehicle braking generates an equivalent impulsive force covering a wide range of the frequency spectrum. In this case, a large number of vibration modes are required in the computation for a higher accuracy in the dynamic responses of the structure.

With the bridge deck modeled as a Timoshenko beam, the vibration of a continuous bridge deck under a vehicle modeled as a mass-spring system with two-degrees-of-freedom was carried out by Chatterjee et al. (1994). Wang (1997) proposed a modal analysis method to investigate the vibration of a multi-span Timoshenko beam under a moving force. The ratio of the radius of gyration of the cross-section to the span length was defined as a parameter, and the effect of this parameter on the first modal frequency of the beam was studied. Wang and Chou (1998) employed the large deflection theory to derive the equation of motion of the Timoshenko beam due to the couple effect of an external force with the weight of the beam. Results showed that the effect of weight of the beam increases the fundamental natural frequency of the structure. Both the dynamic deflection and

moment of the beam predicted by the theory including the effect of weight of beam are less than those predicted either by the small deflection theory or by the large deflection theory without including the effect of weight of beam. A dynamic analysis of a Timoshenko beam subject to a moving force was also investigated by Sniady (2008) in which a closed form solution was provided.

When the bridge deck is modeled as a plate, Marchesiello et al. (1999) presented an analytical approach to the vehicle-bridge dynamic interaction problem with a seven-degrees-of-freedom vehicle system moving on a multi-span continuous bridge deck modeled as an isotropic plate. Both the flexural and torsional mode shapes were included in the study. An iterative method was adopted to calculate the responses of the bridge and vehicle separately, i.e. the equations of motion of the bridge and vehicle system were not coupled. The theoretical modes, defined by means of the Rayleigh-Ritz approach, had been found to be in good agreement with that from the finite element model. Zhu and Law (2003a) investigated the dynamic behavior of a rectangular orthotropic plate under moving loads. Results showed that the impact factor of the plate increases with the ratio between the flexural and torsional rigidities of the plate, and the equivalent beam model of the bridge deck could give an accurate estimate on the impact factor along the centerline of the deck. But it would underestimate the dynamic response along the edge of the structure. A further study was carried out (Zhu and Law 2002a) on a more complex model with a two-axle three-dimensional vehicle model with seven degrees-of-freedom according to the

H20-44 vehicle design loading (Standard Specification for Highway Bridges 1989) moving on a multi-lane continuous bridge deck. The dynamic behavior of the bridge deck under single and several vehicles moving in different lanes was analyzed using the orthotropic plate theory and modal superposition technique. The impact factor is found varying in an opposite trend with the dynamic responses under the different loading cases in this study.

2.1.2 Methods Based on Finite Element

Finite Element Method (FEM) is a powerful technique originally developed for numerical solution of complex problems in structural mechanics. It is a numerical technique for finding approximate solutions of partial differential equations (PDE) as well as of integral equations. The solution approach is based either on eliminating the differential equation completely (steady state problems), or rendering the PDE into an approximate system of ordinary differential equations, which are then numerically integrated using standard techniques such as Newmark- β method, Runge-Kutta method, etc. In the Finite Element Analysis (FEA) of a structure, shape functions are assumed for specific finite elements to establish a relationship between the nodal displacements and the displacement field. According to the relationships that exist in the displacement and strain, and in the strain and stress, the system stiffness matrix can be obtained from the relationship between the nodal forces and nodal displacements via the minimum potential energy principle. Compared with the modal superposition technique

which needs modal shapes in decomposing the system equation which may be difficult to obtain for complex structures, the finite element method is capable of handling more complex bridge-vehicle models with complex boundary conditions in the dynamic analysis. Since the research work conducted on simple finite element model of the bridge-vehicle system had already been summarized in the monograph by Fryba (1999), the research works on complex models will be presented in the following paragraphs to show the advantage of the FEM.

Wang et al. (1992; 1996) investigated the dynamic loading of girder bridges with different girder number and span length due to several vehicles moving across bridge decks with rough surface. The vehicle was simulated as a nonlinear model with eleven-degrees-of-freedom according to the HS20-44 truck in the AASHTO specifications (Standard Specification for Highway Bridges 1989). The maximum impact factors in different girders of bridges were obtained for different number of loading trucks, road surface roughness, transverse loading positions and the vehicle speeds. Huang et al. (1998) developed a procedure for obtaining the response of thin-walled curved box-girder bridges due to the HS20-44 truck model. The analytical results show that most impact factors of torsion and distortion are much larger than those from vertical bending responses. The impact factors of normal stress at different points in the same cross-section are quite different. Research work on a highway steel bridge with the effect of longitudinal grades under an eleven-degrees-of-freedom HS20-44 truck was also carried out by Huang and Wang (1998). The dynamic responses of three steel multi-girder bridges with

different span lengths due to multiple vehicles moving across rough bridge decks with different vehicle speeds are evaluated. Henchi et al. (1998) proposed an efficient algorithm for the dynamic analysis of a bridge discretized into three-dimensional finite elements with a system of vehicles running on top at a prescribed speed. The vehicular axle loads acting on the bridge deck were represented as nodal forces using shape functions. The coupled equations of motion of the bridge and vehicle model were solved directly without the use of iterative method. Numerical simulation showed that the proposed coupled method was much more efficient than the uncoupled iterative method. It is also declared that there is no limitation on the complexity (number of degrees-of-freedom) of the bridge structure in this method if the stability criterion was satisfied. Lee and Yhim (2004) studied the dynamic responses of single and two span continuous composite plate structures subject to multi-moving loads with the third-order plate theory. Results showed that the maximum deflection of symmetric laminates to dynamic loading was superior to that of the anti-symmetric laminates. However the differences in dynamic resistance for anti-symmetric layup sequences were similar to those of the symmetric cases. The authors (2005) also investigated the dynamic behavior of long-span box-girder bridges subject to moving vehicles with numerical simulation and experimental verification. Similar work was done by Kim et al. (2005) and Li et al. (2008) with numerical simulation of vehicles traveled along a girder bridge. Field test data was used to verify the proposed algorithm. Nallasivam et al. (2007) analyzed the impact effect on curved

box-girder bridges due to moving vehicles. The results highlighted that the impact factors of a curved box-girder bridge corresponding to torsion, distortion and their corresponding bimoments had been observed to be generally very high, while those of the other responses were also relatively higher than that of similar straight box-girder bridges. The analysis of bridge-vehicle dynamic response with the effect of braking and acceleration was studied by Ju and Lin (2007) with a finite element model. Numerical examples indicated that the bridge longitudinal response was more sensitive than the bridge vertical response when the vehicle braking or acceleration was active, especially for higher piers.

There are also other kinds of method based on finite element model specially for interaction problems, such as the “moving element method”, in which the beam model is discretized into elements that ‘flow’ with the moving vehicle. A series of works has been carried out by Yang and co-workers in the 1990s (Yang and Lin 1995; Yang et al. 1995; Yang and Yau 1997) on bridge-vehicle element using the dynamic condensation. A vehicle-bridge interaction (VBI) element firstly introduced by Yang and Wu (2001) was used to solve the bridge-vehicle interaction problem. It is quite versatile to deal with vehicle models of various complexities, ranging from the moving load, moving mass, sprung mass, to suspended rigid bar, and etc.. Pan and Li (2002) used the method to solve the transient response of a vehicle-structure interaction problem in time domain. This method was also employed to model a train traveling along the railway beam (Koh et al. 2003). A car of the moving train was modeled as a mass-spring-dampers

system of three-degrees-of-freedom, and the rail was modeled as an infinite Euler-Bernoulli beam. Thus the ‘element’ would never reach the end of the beam. Contrasting to FEM, the moving vehicle always acts at the same point in the numerical model, thereby eliminating the need for keeping track of the contact point with respect to individual elements. Similar ‘moving element’ method was also proposed by Wu (2005a, 2005b, 2007) in which the method with “moving distributed mass element” was adopted to solve the problem of dynamic analysis on beam, frame and plate structures under moving forces.

2.1.3 Other Research Work

2.1.3.1 Response of Bridge with Prestressing Forces

For an unbonded prestressed bridge, the prestressing force produces an axial force effect as well as a bending moment due to the eccentricity of prestressed tendons. The prestressed bridges are commonly modeled as axial loaded beams though the measured modal frequencies from beams or bridges show an opposite trend to that from the axial loaded beam theory (Saiidi et al. 1994). However, the axial loaded beam model had been adopted in theoretical analyses. Law and Lu (2005) studied the time domain responses of an unbonded prestressed beam modeled as an axial loaded beam on which a prestressed force identification algorithm was also proposed. Kocaturk and Simsek (2006) used Lagrange equations to study the dynamic response of eccentrically prestressed visco-elastic Timoshenko beams under a moving harmonic load, and the same problem was

further studied using higher order shear deformation theory (Simsek and Kocaturk 2006). Although the effect of prestress force has been investigated in recent year for bonded prestress beams (Hamed and Frostig 2006), the dynamic analysis of such bridge model can rarely be found.

2.1.3.2 Response of Bridge with Damage

Research work on dynamic behavior of bridge with damage under moving forces has been carried out by many scholars. Mahmoud and Abou Zaid (2002) proposed a rotational spring model to simulate the effect of transverse cracks in simply supported undamped Euler-Bernoulli beams subject to a moving mass on which the dynamic analysis was performed. The presence of cracks resulted in higher deflections and it altered the beam response patterns. In particular, the largest deflection in a damage beam for a given speed needs longer time to build up, and a discontinuity appears in the slope of the beam-deflected shape at the crack location. Experimental validation of damage beams modeled by rotational spring model under a moving mass was carried out by Bilello and Bergman (2004) in which good agreement with the theoretical predictions was shown. Moreover, the percentage of variation in the beam response due to damage was, in general, larger than those in the structural natural frequencies. Law and Zhu (2004) studied the dynamic behavior of damaged reinforced concrete bridge structures under a moving vehicle modeled as either a moving mass or a moving mass-spring system. The damage function proposed by Abdel Wahab et al. (1999) was adopted in the study which is capable of representing either open or breathing crack model. Both

the numerical simulation and the experimental verification were conducted. Results showed the damage model used was accurate enough to describe the crack damage in the concrete bridge beam. The relative frequency change (RFC) and absolute frequency change (AFC) of the beam varied when the vehicle was moving on the bridge deck. They are sensitive to the weight of vehicle, and the frequency ratio between vehicle and bridge had some effect on the RFC and AFC. It is noted that the RFC would be a useful parameter in damage detection of bridge structure because it is very sensitive to damage. Yang et al. (2008) presented an analytical study on the free and forced vibration of inhomogeneous Euler-Bernoulli beams containing open edge cracks. The rotation spring model was adopted to model the cracks. Factors which may affect the dynamic deflection of the beam including the total number of cracks, slenderness ratio, boundary conditions, moving speed of force, etc. were examined. Results showed that the natural frequencies decreases and the dynamic deflection increases due to the presence of the edge crack and the axial compressive force. The natural frequencies were greatly influenced by the edge cracks while the dynamic deflection was not very sensitive to the presence and the location of crack. Both free vibration and dynamic response were much more affected by the axial compression than by the edge cracks.

2.2 Deterministic Moving Force Identification

The vehicle axle load and the gross weight information are very important

factors for bridge design and bridge condition assessment. Overweight vehicles will cause excessive damage to the road pavement and bridge structure. How to obtain vehicle axle load accurately and efficiently in order to achieve a reliable assessment of bridge condition and effective control of the transportation network becomes a crucial problem and it draws attention of many researchers.

Traditional ways to acquire vehicle axle load by stopping and weighing vehicle using weighbridge or loadometer is expensive and subject to bias. Drivers of overweight vehicles may try to avoid the check points on the road because of the fear of penalty. It seems that an effective way to avoid this is to monitor vehicular weights all the time with some sort of undetectable weigh-in-motion stations.

2.2.1 Weigh-In-Motion Technique

To meet the need of controlling the overweight vehicles, considerable research work and tests have been carried out worldwide since the late 60s and early 70s on equipment and schemes for weighing vehicles at highway speed (Moses 1979; Davis and Sommerville 1987; Freund and Bonaquist 1989; Zhi et al. 1999). Two famous research projects, namely, COST 323 and WAVE, were carried out in Europe (Jacob 1994; Jacob and O'Brien 1996). The Weigh-in-Motion (WIM) systems can mainly be categorized into two types, namely the road-surface system and the under-structure system (Law et al. 1997).

Weigh-in-Motion systems can obtain the vehicle axle loads for bridge and pavement design. However, the above system can only measure the equivalent

static loads but not the peak dynamic wheel loads or the time series of moving axle loads. In fact, the dynamic response of a bridge due to dynamic moving loads can be significant, and Cebon (1987) concluded that the dynamic wheel loads may increase road surface damage by a factor of two to four over that due to static ones. For this reason the studies on dynamic wheel loads and ways to measure them had always been of interest. The dynamic wheel loads have been described in different terminology such as pavement loads, tyre forces, contact forces and interaction forces, etc. Basically, all of them refer to the dynamic variation of the interactive forces exerted from the vehicular axle and acting on the contact surfaces. Three systems had been used to acquire such data: (1) Tyre Pressure Transducer System; (2) Strain-Gauged Axle Housing Transducer System; and (3) Wheel Force Transducer System. Whittemore et al. (1970) and Cantieni (1992) had separately given a summary of the above three systems. These systems were subject to bias because they all used instrumented vehicles to measure dynamic axle loads which prompt the need to develop a system to measure dynamic interaction forces using an unbiased random sample of vehicles.

2.2.2 Moving Force Identification Technique

A method based on force identification provides an effective way to solve the above problem. The main idea of this method is using the measured bridge responses to identify the parameters of a bridge-vehicle system, and subsequently to identify the contact forces. This method is also called the Moving Force

Identification (MFI) technique which can be used to acquire vehicle axle loads, inspect overweight vehicles, and to prepare data for bridge design and bridge condition assessment.

The first MFI method was proposed by O'Connor and Chan (1988) named as the Interpretive Method I (IMI). Consequently, various methods on different bridge-vehicle system were developed to identify the interactions force between bridge and vehicle based on vibration theory and system identification technique. In the literature review on the MFI method, the bridge models including the Euler-Bernoulli beam model, Timoshenko beam model, orthotropic plate model, multi-span plate model etc were adopted. MFI algorithm on prestressed beams can also be found (Law et al. 2008). The vehicle was commonly modeled as moving forces, moving masses or the two-axle vehicle model, etc. These methods can mainly be divided into two categories:

- (1) Methods based on modal superposition technique with a continuous bridge model.

In this kind of method, the modal superposition technique is firstly employed to decouple the equation of motion of the bridge and force model to a set of ordinary differential equations. Then the relationship between the moving forces and bridge responses in each mode can be formulated. Finally, the inverse problem can be solved by least-squares estimation with regularization or other optimization methods. Methods within this kind include:

- Time Domain Method (TDM).

This method was firstly proposed by Law et al. (1997) in which the relationship of moving axle force and modal response is formulated by convolution integral. The discrete form of equation of motion of the system for each vibration mode can be obtained by assuming the time series of moving forces to be step functions in small time intervals. The time varying forces on a simply supported beam can be identified by solving the resulting discrete equations. The application of this method on identifying the moving forces on a multi-span continuous bridge was investigated by Zhu and Law (2000, 2001a, 2002b). The research was also extended to study the possibility of identifying axle loads when applied to real bridge-vehicle system with road surface roughness and incomplete vehicle speed. Experimental tests showed that the method can identify individual axle loads travelling at non-uniform speed with small error (Zhu and Law 2003c). The effect of bearing stiffness on the bridge support was also included in this MFI procedure by Zhu and Law (2006).

- Interpretive Method II (IMII).

This method was firstly proposed by Chan et al. (1999) in which the bridge was modeled as a planar simply supported Euler-Bernoulli beam with a single force moving on top. The bridge responses at various locations, such as the vertical displacement or bending moments, were transformed to modal values. The central different method is used to numerically differentiate the modal displacements to obtain the corresponding modal velocities and modal

accelerations. Then the values of the axle load at any time instance can be obtained by solving the linear equations using least-squares method. The IMII was adopted to identify the moving forces on a multi-span continuous Timoshenko beam with non-uniform cross-section (Zhu and Law 1999) and a generalized orthogonal function approach was also proposed to obtain the derivatives of bridge modal responses from the strain measurements instead of direct differentiation (Zhu and Law 2001b).

- Frequency-Time Domain Method (FTDM).

This method was proposed by Law et al. (1999) in which Fast Fourier Transform (FFT) was performed on the ordinary differential equations after applying the modal superposition technique. A relationship between the moving forces and the bridge responses in frequency domain can be formulated in terms of the Frequency Response Function (FRF). The equations in frequency domain are discretized and least-squares method is applied to solve the equation. Finally the time history of moving forces can be obtained by performing the inverse Fourier transformation. The regularization method (Law et al. 2001) and the SVD technique (Yu and Chan 2003) were adopted in the inverse procedure respectively to improve the accuracy of this method.

- State Space Method (SSM).

This method was firstly proposed by Zhu and Law (2001c) combined with a high-precision integration method. The bridge was modeled as a

non-uniform continuous Euler-Bernoulli beam. Hamilton principle and modal superposition were employed to establish the system model including the mass, damping and stiffness matrices in state space, and then the identification procedure is performed with regularization. Application of this method on a plate model can be found in Zhu et al. (2006) and Law et al. (2007).

- Method of Moments (MOM) based algorithm.

This method was proposed by Yu et al. (2008a, 2008b) in which the moving vehicle loads were described as a combination of whole basis functions, such as the orthogonal Legendre or Fourier series, and the force identification can be transformed into a parameter identification problem.

- Identification based on genetic algorithm.

This method was proposed by Jiang et al (2003, 2004) in which the acceleration signals of a bridge model at selected locations were adopted and the corresponding velocities and displacements were obtained by integration. Pseudo-inverse and singular value decomposition were first employed to arrive at approximations of the moving forces and a genetic algorithm is then used to find the best estimated value of the forces by minimizing the errors between the measured accelerations and the reconstructed ones in each generation.

- (2) Methods based on finite element method (FEM) on discrete bridge model.

The finite element method is adopted to model the bridge structure. A location matrix (or vector for the case with one moving force) is introduced for the

moving forces with which the concentrate forces applied on the bridge deck can be transformed into nodal forces. Based on the formulated finite element model, moving force identification can be conducted in which the least-squares estimation with regularization or other optimization methods are adopted to identify the moving forces. Methods of this kind include:

- Interpretive Method I (IMI).

This method was proposed by O'Connor and Chan (1988). The bridge structure is modeled with an assembly of lumped masses interconnected by massless elastic beam elements, and thus the nodal responses of displacements and bending moments at any time instance can be related to the moving forces. The forces are then identified from the responses (Chan and O'Connor 1990).

- Optimal State Estimation Approach (OSEA).

This method in which a vector was introduced to indicate the location of the moving forces in the finite element model of the bridge deck was firstly proposed by Law and Fang (2001). The bridge-vehicle model is formulated in the state space and the moving forces are identified in the time domain by adopting the dynamic programming technique to overcome the weakness of having large fluctuations in the identified results. The method was later applied in vehicle axle load identification of a three dimensional bridge under a moving truck by Gonzalez et al. (2008). The first-order regularization was adopted instead of the zeroth-order regularization to improve the accuracy of

the identified results from contaminated response data.

- Finite Element approach with orthogonal function approximation.

The method was proposed by Law et al. (2004) in which the same idea of OSEA is employed for the moving force identification. Orthogonal functions were employed to curve fit the strain or displacement signals, and the velocities and accelerations can then be accurately calculated through differentiation. The force identification problem is then transformed into a set of linear equations which is solved with the least-squares method with regularization taking the coefficients as unknowns. The improved reduction system (IRS) scheme (O'Callahan 1989) was employed to reduce the degrees-of-freedom (*dofs*) of the bridge structure. The *dofs* which are measured in field tests were retained as contrast to the use of the selection matrix in OSEA to achieve the same purpose.

- Finite Element approach with update static component (USC) technique.

This method was proposed by Pinkaew and Akarawittayapoom (2003). It is an iterative method based on finite element model in which the moving loads to be identified were decomposed into static and dynamic components. The static component was updated iteratively until convergence is achieved in the identified moving forces (Pinkaew 2006). This method was further verified in experimental tests (Pinkaew and Asnachinda 2007) and the application of which was extended to more complex bridge-vehicle models (Asnachinda et al. 2008). Results show that the method is very accurate even

with relative large level of noise in the measured bridge response.

- Wavelet Based Method.

This method was firstly proposed by Wu and Shi (2006) in which the nodal responses and nodal forces were represented with wavelet basis. By employing a Galerkin procedure, the relationship between the coefficients of responses and the coefficients of moving forces in the wavelet domain is formulated. The wavelet coefficients of moving forces can be identified by solving the set of equations and the time history of forces can be obtained by signal reconstruction. The method was further applied on identifying vehicle axle loads on a prestressed bridge structure by Law et al. (2008).

In the group of moving force identification methods based on modal superposition, the SVD technique was firstly suggested by Yu and Chan (2002; 2003) in solving the linear problem with pseudo-inverse using bending moment of bridge response which greatly improved the accuracy of the TDM and FTDM. Theoretical reviews of four method including IMI, IMII, TDM and FTDM and the corresponding comparative studies including experimental tests have been conducted by Chan et al. (2001a; 2001b). Parameters including the speed of vehicles, sampling frequency, axle-spacing-to-span ratio (ASSR) and the sensitivity to noisy data were studied. Numerical simulations and experiments in laboratory showed that the accuracy of these four methods was independent of sampling frequency and both the IMII and TDM were also independent of the speed of vehicle. However, the accuracy of IMI was significantly affected by the

ASSR and noise level. If the number of bridge modes was equal to the number of sensors, IMII would be good for applications with any ASSR and a low level of noise. TDM and FTDM were suitable for any case studied but time consuming. The potential of the above four identification methods were again studied by Yu and Chan (2007). A comparison between TDM and the finite element approach with orthogonal function approximation was given by Zhu and Law (2002c). Results showed that the latter gave consistently smaller error in the results for all noise levels while the accuracy of TDM was affected by noise to a large extent. The orthogonal function approximation of response signals was shown to be effective in filtering the high-frequency noise components in the responses. It was also emphasized that pre-processing of the measured data to remove the measurement noise should be conducted before the identification. It should be noted that the two kinds of functions which are commonly used in MFI, i.e. the orthogonal functions and cubic spline interpolation, have different performances. As contrast to the orthogonal functions which are capable of smoothing the signal, cubic spline interpolation do not have such benefit. But it is a very accurate method for obtaining the differentiation of the interpolated signal and it can be used in IMII instead of central difference method to achieve better performance. MFI technique based on finite element model is suitable for solving problem in bridge models with complex boundary conditions while the TDM and FTDM are not applicable due to the difficulty to obtain the vibration mode shapes for such structure. Moreover, TDM and FTDM are very time consuming when there are

multiple forces on top of a complex structure. The road surface roughness is a very important factor and it has always been considered in most of the moving force identification procedures in which deterministic samples are adopted to represent the effect of the road surface roughness. The random nature of the road surface roughness will be further discussed in the stochastic analysis of bridge-vehicle interaction problem in this Thesis. It should also be noted that other methods (Thite and Thompson 2003a, 2003b; Nordstrom and Nordberg 2004; Liu and Shepard 2005; Lu and Law 2006; Nordberg and Gustafsson 2006a, 2006b) had been adopted in force identification may also be applicable for the moving force identification problem.

2.2.3 Model Condensation Technique

The structural analysis on large-scale bridge/buildings is computationally expensive or sometimes even impractical with the full degrees-of-freedom model. Similarly in the inverse problems of the force or parameter identification, structural response measured from field test is limited, i.e. to obtain the structural responses at all the degrees-of-freedom (*dofs*) of the structure is impractical due to the limitations of responses and measuring techniques. The model condensation techniques can help to alleviate the problems. Since model condensation techniques play a very important role in structural dynamic analysis and the inverse analysis especially for large-scale structural systems, a brief review on this topic will be given in this Section.

The first model condensation method is called Guyan/Iron method (Guyan 1965; Iron 1965) which is a static condensation method. Considering a system with only static forces \mathbf{F}_m applied on selected *dofs*. Partitioning the stiffness matrix and response vector gives

$$\begin{bmatrix} \mathbf{K}_{mm} & \mathbf{K}_{ms} \\ \mathbf{K}_{sm} & \mathbf{K}_{ss} \end{bmatrix} \begin{Bmatrix} \mathbf{x}_m \\ \mathbf{x}_s \end{Bmatrix} = \begin{Bmatrix} \mathbf{F}_m \\ \mathbf{0} \end{Bmatrix} \quad (2.1)$$

where the subscript ‘*m*’ and ‘*s*’ denote the master (selected) *dofs* and slave (truncated) *dofs*, respectively. From the second equation in Equation (2.1), the relationship between the selected response vector \mathbf{x}_m and the truncated response vector \mathbf{x}_s can be obtained as

$$\mathbf{x}_s = -\mathbf{K}_{ss}^{-1}\mathbf{K}_{sm}\mathbf{x}_m \quad (2.2)$$

The response vector \mathbf{x} can be formulated from the selected response \mathbf{x}_m as

$$\mathbf{x} = \begin{Bmatrix} \mathbf{x}_m \\ \mathbf{x}_s \end{Bmatrix} = \begin{bmatrix} \mathbf{I} \\ -\mathbf{K}_{ss}^{-1}\mathbf{K}_{sm} \end{bmatrix} \mathbf{x}_m = \mathbf{T}_s \mathbf{x}_m \quad (2.3)$$

where $\mathbf{T}_s = \begin{bmatrix} \mathbf{I} \\ -\mathbf{K}_{ss}^{-1}\mathbf{K}_{sm} \end{bmatrix}$ is the static transformation matrix between the full state vector \mathbf{x} and the master coordinates vector \mathbf{x}_m . The condensed mass and stiffness matrix \mathbf{M}_{Rs} , \mathbf{K}_{Rs} , respectively, can be expressed as

$$\mathbf{M}_{Rs} = \mathbf{T}_s^T \mathbf{M} \mathbf{T}_s, \quad \mathbf{K}_{Rs} = \mathbf{T}_s^T \mathbf{K} \mathbf{T}_s \quad (2.4)$$

where \mathbf{M} and \mathbf{K} are respectively the system matrices before reduction. The eigen-solution for the condensed system can be denoted as

$$\left(\mathbf{K}_{Rs} - \omega^2 \mathbf{M}_{Rs} \right) \mathbf{u}_m = 0 \quad (2.5)$$

where ω^2 and \mathbf{u}_m are respectively the eigenvalues and eigenvectors of the condensed system. It is noted that any frequency response functions generated

from the reduced matrices in Equation (2.4) are exact only when frequency is equal to zero. For a dynamic system with an excitation frequency, the neglected inertia effect will become more significant which may cause condensation error in this method. Since improper selection of *dofs* in model condensation may result in singularity of the eigenvalue problem, several selection schemes (Shan and Raymund 1982; Matta 1987) of the master *dofs* were developed to improve the accuracy. These schemes can also be adopted in other model reduction methods reviewed in this Section.

In order to improve the Guyan/Iron method, the dynamic condensation method was developed to include the inertia terms neglected in Equation (2.1) (Kuhar and Stahle 1974; Miller 1980). The equation becomes,

$$\begin{bmatrix} \mathbf{M}_{mm} & \mathbf{M}_{ms} \\ \mathbf{M}_{sm} & \mathbf{M}_{ss} \end{bmatrix} \begin{Bmatrix} \ddot{\mathbf{x}}_m \\ \ddot{\mathbf{x}}_s \end{Bmatrix} + \begin{bmatrix} \mathbf{K}_{mm} & \mathbf{K}_{ms} \\ \mathbf{K}_{sm} & \mathbf{K}_{ss} \end{bmatrix} \begin{Bmatrix} \mathbf{x}_m \\ \mathbf{x}_s \end{Bmatrix} = 0 \quad (2.6)$$

The eigenvalue problem becomes,

$$\left(-\omega^2 \begin{bmatrix} \mathbf{M}_{mm} & \mathbf{M}_{ms} \\ \mathbf{M}_{sm} & \mathbf{M}_{ss} \end{bmatrix} + \begin{bmatrix} \mathbf{K}_{mm} & \mathbf{K}_{ms} \\ \mathbf{K}_{sm} & \mathbf{K}_{ss} \end{bmatrix} \right) \begin{Bmatrix} \mathbf{x}_m \\ \mathbf{x}_s \end{Bmatrix} = 0 \quad (2.7)$$

Thus the truncated response vector \mathbf{x}_s can be obtained in terms of \mathbf{x}_m as

$$\mathbf{x}_s = -[\mathbf{K}_{ss} - \omega^2 \mathbf{M}_{ss}]^{-1} [\mathbf{K}_{sm} - \omega^2 \mathbf{M}_{sm}] \mathbf{x}_m = \mathbf{T}_d \mathbf{x}_m \quad (2.8)$$

where $\mathbf{T}_d = -[\mathbf{K}_{ss} - \omega^2 \mathbf{M}_{ss}]^{-1} [\mathbf{K}_{sm} - \omega^2 \mathbf{M}_{sm}]$ is the dynamic transformation matrix between the full state vector and the master coordinates. It is noted that the eigenvalue ω in \mathbf{T}_d is unknown. This problem could be solved by selecting a system frequency $\bar{\omega}$ beginning with an initial zero value. A new transformation matrix based on the updated eigenvalue is calculated. The process is repeated until

the eigenvalue no longer changes. After obtaining the dynamic transformation matrix, the condensed mass and stiffness matrix \mathbf{M}_{Rd} , \mathbf{K}_{Rd} , respectively, can be expressed as

$$\mathbf{M}_{Rd} = \mathbf{T}_d^T \mathbf{M} \mathbf{T}_d, \quad \mathbf{K}_{Rd} = \mathbf{T}_d^T \mathbf{K} \mathbf{T}_d \quad (2.9)$$

To avoid the matrix inverse in calculating \mathbf{T}_d , using the binomial theorem and neglecting the higher order terms of ω up to ω^2 , \mathbf{T}_d can be obtained as

$$\begin{aligned} \mathbf{T}_d &= -[\mathbf{K}_{ss} - \omega^2 \mathbf{M}_{ss}]^{-1} [\mathbf{K}_{sm} - \omega^2 \mathbf{M}_{sm}] = -\mathbf{K}_{ss}^{-1} [\mathbf{I} - \omega^2 \mathbf{M}_{ss} \mathbf{K}_{ss}^{-1}]^{-1} [\mathbf{K}_{sm} - \omega^2 \mathbf{M}_{sm}] \\ &= -\mathbf{K}_{ss}^{-1} [\mathbf{I} + \omega^2 \mathbf{M}_{ss} \mathbf{K}_{ss}^{-1}] [\mathbf{K}_{sm} - \omega^2 \mathbf{M}_{sm}] = -\mathbf{K}_{ss}^{-1} [\mathbf{K}_{sm} + \omega^2 (\mathbf{M}_{ss} \mathbf{K}_{ss}^{-1} \mathbf{K}_{sm} - \mathbf{M}_{sm})] \end{aligned} \quad (2.10)$$

Substituting Equations (2.8) and (2.10) into Equation (2.7) and neglecting the higher order terms of ω compared to ω^2 , it gives

$$\omega^2 (\mathbf{M}_{mm} - \mathbf{M}_{ms} \mathbf{K}_{ss}^{-1} \mathbf{K}_{sm} - \mathbf{K}_{ms} \mathbf{K}_{ss}^{-1} \mathbf{M}_{ss} \mathbf{K}_{ss}^{-1} \mathbf{K}_{sm}) \mathbf{x}_m = (\mathbf{K}_{mm} - \mathbf{K}_{ms} \mathbf{K}_{ss}^{-1} \mathbf{K}_{sm}) \mathbf{x}_m \quad (2.11)$$

From Equation (2.11), the eigenvalue can be calculated directly without the need of iteration. In fact, the eigenvalue calculated from Equation (2.11) equals to the one calculated from Guyan/Iron method which can be expressed as

$$\omega^2 \mathbf{M}_{Rs} \mathbf{u}_m = \mathbf{K}_{Rs} \mathbf{u}_m \quad (2.12)$$

where \mathbf{M}_{Rs} , \mathbf{K}_{Rs} are the matrices as shown in Equation (2.4). Employing the relationship formulated in Equation (2.12), the dynamic transformation matrix \mathbf{T}_d can be obtained from the following equation,

$$\mathbf{T}_{id} = -\mathbf{K}_{ss}^{-1} [\mathbf{K}_{sm} + (\mathbf{M}_{ss} \mathbf{K}_{ss}^{-1} \mathbf{K}_{sm} - \mathbf{M}_{sm}) \mathbf{M}_{Rs}^{-1} \mathbf{K}_{Rs}] \quad (2.13)$$

where \mathbf{M}_R and \mathbf{K}_R are the system mass and stiffness after reduction. \mathbf{T}_{id} is the

transformation matrix for a new model condensation method called the Improved Reduction System (IRS) method. The formulation including Equations (2.10) to (2.13) was proposed by Gordis (1992).

The same dynamic transformation matrix \mathbf{T}_{id} was also derived by O'Callahan (1989) with a different procedure. The following is a brief introduction. Considering a static force F applied on all the *dofs* of a structure and performing the same partition as in Guyan/Iron method, Equation (2.1) becomes

$$\begin{bmatrix} \mathbf{K}_{mm} & \mathbf{K}_{ms} \\ \mathbf{K}_{sm} & \mathbf{K}_{ss} \end{bmatrix} \begin{Bmatrix} \mathbf{x}_m \\ \mathbf{x}_s \end{Bmatrix} = \begin{Bmatrix} \mathbf{F}_m \\ \mathbf{F}_s \end{Bmatrix} \quad (2.14)$$

where \mathbf{F}_s is the force applied on the slave *dofs*. The truncated set of equations in Equation (2.14) is

$$\mathbf{K}_{sm} \mathbf{x}_m + \mathbf{K}_{ss} \mathbf{x}_s = \mathbf{F}_s \quad (2.15)$$

Solving the Equation (2.15), \mathbf{x}_s can be calculated as

$$\mathbf{x}_s = -\mathbf{K}_{ss}^{-1} \mathbf{K}_{sm} \mathbf{x}_m + \mathbf{K}_{ss}^{-1} \mathbf{F}_s \quad (2.16)$$

Thus the full state vector \mathbf{x} can be expressed as

$$\mathbf{x} = \mathbf{T}_s \mathbf{x}_m + \mathbf{x}_{Fd} \quad (2.17)$$

where \mathbf{T}_s has been shown in Equation (2.3) and \mathbf{x}_{Fd} is the truncated distributed force adjustment defined as

$$\mathbf{x}_{Fd} = \begin{Bmatrix} \mathbf{0} \\ \mathbf{K}_{ss}^{-1} \mathbf{F}_s \end{Bmatrix} = \begin{bmatrix} \mathbf{0} & \mathbf{0} \\ \mathbf{0} & \mathbf{K}_{ss}^{-1} \end{bmatrix} \mathbf{F} = \mathbf{K}_s^{-1} \mathbf{F} \quad (2.18)$$

According to Equations (2.12) and (2.14), the full modal vector \mathbf{u} can be expressed in terms of the selected vector \mathbf{u}_m using the static reduction, i.e.

$\mathbf{u} = \mathbf{T}_s \mathbf{u}_m + \mathbf{x}_{Fd}$ can be obtain as

$$\mathbf{x}_{Fd} = \mathbf{K}_s^{-1} \mathbf{M} \mathbf{T}_s \mathbf{u}_m \omega^2 = \mathbf{K}_{ss}^{-1} \mathbf{M}_{ss} \mathbf{T}_s \mathbf{M}_R^{-1} \mathbf{K}_R \mathbf{u}_m \quad (2.19)$$

Combine Equations (2.18) and (2.19),

$$\mathbf{x} = \left(\mathbf{T}_s + \mathbf{K}_{ss}^{-1} \mathbf{M}_{ss} \mathbf{T}_s \mathbf{M}_R^{-1} \mathbf{K}_R \right) \mathbf{u}_m = \mathbf{T}_{IRS} \mathbf{u}_m \quad (2.20)$$

where

$$\mathbf{T}_{IRS} = -\mathbf{K}_{ss}^{-1} \left[\mathbf{K}_{sm} + \left(\mathbf{M}_{ss} \mathbf{K}_{ss}^{-1} \mathbf{K}_{sm} - \mathbf{M}_{sm} \right) \mathbf{M}_R^{-1} \mathbf{K}_R \right] \quad (2.21)$$

It is noted that \mathbf{T}_{IRS} in Equation (2.21) is identical to \mathbf{T}_{id} shown in Equation (2.13). The mass and stiffness matrices for the reduced system shown in Equation (2.13) or (2.21) have superior performance than that in Guyan/Iron method since the deleted inertia effect has been included. The improved mass and stiffness matrices for the reduced system become

$$\mathbf{M}_{RI} = \mathbf{T}_{IRS}^T \mathbf{M} \mathbf{T}_{IRS}, \quad \mathbf{K}_{RI} = \mathbf{T}_{IRS}^T \mathbf{K} \mathbf{T}_{IRS} \quad (2.22)$$

The IRS method is relatively insensitive to the number and location of the *dofs* comparing to the two methods mentioned above.

The IRS method was further improved and modified to become iterative by other researchers which are called the Iterative IRS method (IIRS). There are two kinds of IIRS method. The first one was proposed by Blair (1991). Since the transformation matrix for IRS utilized the reduced mass and stiffness matrices approximated by the Guyan/Iron method, an improvement can be made by using the newly approximated matrices described in Equation (2.22) and a better transformation matrix can be constructed by iterations on Equation (2.21), that is

$$\mathbf{T}_{IRS,i+1} = -\mathbf{K}_{ss}^{-1} \left[\mathbf{K}_{sm} + \left(\mathbf{M}_{ss} \mathbf{T}_s - \mathbf{M}_{sm} \right) \mathbf{M}_{RI,i}^{-1} \mathbf{K}_{RI,i} \right] \quad (2.23)$$

and Equation (2.22) becomes

$$\mathbf{M}_{RI,i+1} = \mathbf{T}_{IRS,i+1}^T \mathbf{M} \mathbf{T}_{IRS,i+1}, \quad \mathbf{K}_{RI,i+1} = \mathbf{T}_{IRS,i+1}^T \mathbf{K} \mathbf{T}_{IRS,i+1} \quad (2.24)$$

The second kind of IIRS method (Friswell 1995) made further improvement by modifying Equation (2.23) as

$$\mathbf{T}_{IRS,i+1} = -\mathbf{K}_{ss}^{-1} \left[\mathbf{K}_{sm} + (\mathbf{M}_{ss} \mathbf{T}_{IRS,i} - \mathbf{M}_{sm}) \mathbf{M}_{RI,i}^{-1} \mathbf{K}_{RI,i} \right] \quad (2.25)$$

2.3 Stochastic Analysis of Bridge-Vehicle System

2.3.1 Source of Randomness

Although most of the deterministic analysis of bridge-vehicle interaction problem consider the road surface roughness as an uncertain factor, yet it is conventionally treated in a deterministic manner, i.e. the road surface roughness was considered as deterministic samples of irregular profile according to its power spectral density defined in the ISO standard (ISO 8606:1995(E) 1995). The randomness in the excitation forces on the bridge deck may be caused by the road surface roughness, the random velocities of vehicles, the random arrivals of vehicles and uncertainties in the vehicle system. When performing deterministic analysis of a bridge under moving vehicle, different samples of response data will be obtained in different computation due to the different samples of road surface roughness adopted. Thus the response statistics have to be estimated in the dynamic analysis for a full description of the response of the bridge-vehicle system under moving vehicle. Besides, when expressing the problem in a literal sense, the bridge-vehicle system often exhibits an inherent randomness. For example, the values of system parameters in the bridge structure such as the

Young's modules, mass density, sectional area, Poisson ratio and etc. have a distribution. Moreover, concrete bridges in use often contain local damages. Uncertainties are also existed in modeling the prestressing effect and the constraints in bridge structure. The conventional deterministic analysis generally represents only an "approximation" of the actual reality due to these unavoidable uncertainties in the structural properties as well as in the loading processes. Stochastic analysis should be performed instead for the bridge-vehicle interaction problem.

2.3.2 Stochastic Methods in Structural Dynamics

2.3.2.1 Representation of the Stochastic Process

The representation of the stochastic process plays a very important role in stochastic analysis of engineering structure. The uncertainties in engineering structures are often represented by stochastic processes (or variables) which can be represented by mathematic tools. System equations may become much easier to solve with the representation of the stochastic processes involved, e.g. the stochastic system equations will be transformed into a set of deterministic equations. These mathematical tools include: the autoregressive moving average (ARMA) model (Gersch and Yonemoto 1977), filtered (Spanos and Hansen 1981) or Poisson (Grigoriu 1996) white noise model, Spectral Representation (SR) (Shinozuka and Jan 1972), Karhunen-Loève Expansion (KLE) (Kac and Siegert 1947), Polynomial Chaos Expansion (PCE) (Wiener 1938) and Wavelets

Representation (WR) (Spanos and Failla 2004), etc.

Among the various tools aforementioned, the Spectral Representation method appears to be most widely used (Schuëller 1997). In this method, sample functions of the stochastic processes or fields are generated according to prescribed power spectrum density information. For the stationary or homogenous case, the Fast Fourier Transform (FFT) is utilized for improving the computational efficiency. The Spectral Representation generates ergodic sample functions, each of which exactly fulfills the requirements of the target power spectrum. The spectral representation-based algorithm can be extended to non-stationary case with the generation of stochastic waves, and to the incorporation of non-Gaussian stochastic fields by a memoryless nonlinear transformation together with an iterative procedure to match the target spectrum density (Yamazaki and Shinozuka 1988; Deodatis and Micaletti 2001) or via the sampling theorem (Grigoriu 1998).

Karhunen-Loève Expansion is another method that is capable of representing Gaussian (Kac and Siegert 1947) as well as non-Gaussian (Phoon et al. 2002, 2005) stochastic processes (or fields). The most important property of this expansion is that the spatial random fluctuations can be decomposed into a set of deterministic functions in the spatial variables multiplied with random coefficients that are independent of these variables. Thus a large number of correlated random variables can be reduced to a few more important uncorrelated ones. Hence the representation is most suitable for band-limited colored excitations and stochastic finite element representation of random media. The Karhunen-Loève Expansion is

a mean-square convergent representation technique irrespective of the probabilistic structure of the process with a finite variance. The closer a process is to white noise, the more terms are required in its expansion. It might also be utilized to represent the uncorrelated but non-independent random variables in other expansion, e.g. the Polynomial Chaos Expansion, with a new set of independent Gaussian random variables.

Polynomial Chaos Expansion (PCE), which is often regarded as a generalization of the above Karhunen-Loève Expansion, has been proposed for applications where the covariance function is not known *a-priori* (Ghanem and Spanos 1991). For the special case of a Gaussian random process, the PCE coincides with the KLE. The Polynomial Chaos Expansion is adjustable in two ways: increasing the number of random variables involved in the expansion results for a refinement in the random fluctuations, while an increase of the maximum order of the polynomial captures nonlinear (non-Gaussian) behavior of the process.

Similar to the deterministic case, wavelet analysis is often used to avoid the missing of local features in time or space domain in Fourier analysis (Schuëller 2006). The Wavelet Presentation of random process is also studied in stochastic senses (Dijkerman and Mazumdar 1994; Spanos and Failla 2004; Spanos et al. 2005). The “detail capturing” features of wavelets may prove advantageous for system identification and damage detection purposed. However, it is not obvious that wavelets possess overwhelming advantages over traditional methods such as

Spectral Representation or ARMA model, etc. (Schuëller 1997).

2.3.2.2 Stochastic Response Calculation

The evaluation of the stochastic response of structures is the main theme in stochastic mechanics.

Monte Carlo Simulation (MCS) (Shinozuka 1972) is a powerful tool for handling stochastic system even with highly nonlinear and large number of random variables. Traditional MCS is time consuming which limits the application of this ‘universal’ method. With the evolution of digital computers, MCS is increasingly utilized to generate samples of the stochastic response for systems where no analytical solution is available. However, it is most widely used for checking and verifying approximate analytical results on the stochastic response in this research study.

The analytical procedures based on the representation of the stochastic process have been developed to simulate the system with uncertainties and numerical methods can be employed to solve the system equation to obtain the response statistics. These methods with correlation analysis, spectral analysis, wavelet analysis, Karhunen-Loève Expansion and Polynomial Chaos Expansion, etc, have been successfully developed.

2.3.3 Stochastic Finite Element Method

The system of an engineering structure and its environment often exhibits a certain extent of randomness. In the last two decades, many researchers have

interest in the research on structures with uncertainties. The Stochastic Finite Element Method (SFEM) modeled the structure with finite elements with random properties and it is one of most important development widely used in stochastic analysis of engineering structures. Seven monographs on this method are available (Nakagiri and Hisada 1985; Ghanem and Spanos 1991; Qiu and Liu 2003; Kleiber and Hien 1993; Haldar and Mahadevan 2000; Elishakoff and Ren 2003; Qin et al. 2006). These literatures cover various methods for modeling the random fields and solving the stochastic finite element problem.

The issues in SFEM can mainly be distinguished into three categories. The first issue is the discretization of the random field of the structure containing uncertainty in system parameters. The second one addresses the methods for evaluating of the stochastic response of the Finite element model. The third one is the estimation of the response statistics.

2.3.3.1 Discretization of Random Fields

In the dynamic analysis of structures with uncertainties, the material properties are often modeled as spatially correlated continuous stochastic processes (or fields) which are usually characterized in terms of statistics such as the mean values and auto-correlation functions. The stochastic processes (or fields) representing the random material properties may be assumed statistically Gaussian or non-Gaussian. Although the SFEM is based on the discretization of strain or stress field, the SFEM requires a second discretization of the random fields associated with the system parameters, which is not necessarily identical to the

other discretization. It should be noted that different kind of discretization of random fields will lead to different number of random variables needed for representing, thus affecting the response statistics of the structure. The discretization of random fields is very different from the concept of element meshing in deterministic finite element method where different finite element mesh only affects the accuracy of the responses of structure when the number of element not too small. Most of the research work on the SFEM utilizes the discretization of finite element to describe the stochastic field of system parameters. This can facilitate the formulation of SFEM since the system parameters can be assumed to be constant within an element. The solution regarding the response statistics are highly influenced by the discretization used. Research on the effect of mesh size (Mahadevan and Haldar 1991; Li and Der Kiureghian 1993; Liu and Liu 1993) had been conducted and it was suggested that the mesh size should be carefully selected by examining the correlation of the stochastic field of the structure which may be characterized by the correlation distance (Shinozuka and Deodatis 1988; Schuëller and Brenner 1996) or the scale of fluctuation (Vanmarcke 1983; Schuëller and Brenner 1996).

There are several methods available for discretization of a random field and a review of which was given by Li and Kiureghian (1993). A new and efficient discretization based on the principles of optimal linear estimation theory was also proposed. These discretization methods are midpoint method, local averaging method, weighted integral method, shape function method, and series expansion

method, etc.

In the midpoint method (Der Kiureghian and Ke 1988), the field within the domain of an element is described by a single random variable representing the value of the field at the central point of the element. The value within the field of the element is assumed to be a constant.

The local averaging method proposed by Vanmarcke and Grigoriu (1983) described the field within each element in terms of the spatial average of the field throughout the element. This definition would expect a better fit over the midpoint method because of the averaging process.

Takada (1990) and Deodatis (1990) proposed the concept of weighted integral that involved element integration of the stochastic fields and deterministic weighting functions on the basis of a variational theorem when spatially varying material properties were taken into account. The weighted integral method can be used effectively without increasing the number of random variables for the case where a finer discretization is needed in the mid-point method. The midpoint method tends to lead to an over-estimation of the variance of the response and the local average method gives an underestimation, while the weighted integral method leads to the most accurate results.

The shape function method (Liu et al. 1986) described a random field with an element in terms of a set of nodal values and the corresponding shape functions. In this case, the nodal realization of the discretized field is a continuous function which is different from those in the midpoint method and local average method

which are stepwise functions with discontinuities along the element boundaries.

Another method for random field discretization is the series expansion method based on the representation of the stochastic field. This method was introduced by Spanos and Ghanem (1989) by employing the Karhunen-Loève Expansion. The field is thus represented by a finite set of random variables with truncation.

2.3.3.2 Methods for Evaluating the Stochastic Responses

After the discretization of the random field, the methods for evaluating the stochastic response of the finite element model will be reviewed.

Monte Carlo Simulation (MCS) (Shinozuka 1972) is always applicable for solving engineering problems modeled with finite element and with uncertainty in system parameters. It is a versatile method where accurate results including the probability density distribution of random responses can be obtained with sufficient runs. However, the MCS is time consuming and it has been traditionally employed to verify the results from newly developed analytical methods in stochastic computational mechanics. A direct application of the MCS in the finite element analysis of structures with random non-uniformity of material properties can be found in Reusch and Estrin (1998).

The Perturbation Method (PM), which is well-known as one of the effective methods for general nonlinear problems, has also been adopted to estimate the response statistics of a finite element model with uncertainties. It is considered to be one of the most widely used methods due to its analytical tractability and

computational efficiency. Each stochastic quantity of a system is expanded into a series with deviations in the stochastic parameters at their mean values under the assumption of small variation. By comparing the coefficients of different order of perturbations, a set of deterministic equations can be obtained to relate the stochastic excitations and the stochastic responses. The pioneering application of PM in problems of mechanical engineering where the structural shape is uncertain was carried out by Hisada and Nakagiri (1981). Extensive applications using the perturbation-based FEM in the stochastic analysis of structure with uncertainties can be found. A stochastic finite element modeling in linear transient heat transfer problem was proposed by Hien and Kleiber (1997) based on the combination of the second-order perturbation technique and second-moment analysis. A dynamic and reliability analysis of a complex nonlinear structural system subject to random forces using the PM method was proposed by Moon et al. (2004). A reliability analysis on linear structure with parameter uncertainty subject to non-stationary earthquake was carried out using the PM-based stochastic finite element method by Chaudhuri and Chakraborty (2006). Free vibration analysis and reliability analysis of a rotating beam with random properties under a stochastic load modeled as a stationary white noise were investigated by Hosseini and Khadem (2005, 2007) with the second-order perturbation method. The PM based stochastic finite element method was adopted by Onkar et al. (2006) to conduct the buckling analysis of laminated plates with random material properties and by Pandit et al. (2008) to study the deflection statistics of laminated sandwich plates with random

material properties.

For the inverse problem, a model updating method was proposed by Xia and Hao (2003) to detect the structural damage based on the PM-based stochastic finite element model. An improved perturbation method for stochastic finite element model updating was proposed by Hua et al. (2008). In the aforementioned applications, the first- and second-order perturbation method is commonly used under the assumption of small deviations from the center value and only the first two moments are obtained. Though the higher order perturbation can be formulated in a similar way, it is rarely done due to its huge computational efforts and the unavailability of information on higher-order moments of the stochastic input parameters (Elishakoff and Ren 2003).

It is well known that the inverse of an operator in an equation can be expanded in a convergent series (Mikhlin 1957). The adoption of the Taylor series expansion in the inverse of the operator in the system equation to obtain the random fluctuation of the displacement will result in exactly the same equations as those obtained by the perturbation technique (Elishakoff and Ren 2003). The Neumann expansion method for stochastic finite element method was firstly introduced by Shinozuka and Nomoto (1980). Similar to the Perturbation Method, the Neumann expansion method requires simulations in order to assess the reliability of the results and it is also quite difficult to extend it to obtain higher order moments than the first two. The stochastic finite element method with Neumann expansion was employed by Chakraborty and Dey (1998) to analysis a

multi-degrees-of-freedom linear structural system involving uncertain parameters subject to harmonic excitation in the frequency domain. This stochastic finite element method was also employed by Chakraborty and Sarkar (2000) to obtain the solution of a curved beam on uncertain elastic foundation. A comparison among the Neumann expansion based SFEM, the PM based SFEM and the MCS based SFEM was carried out by Lei and Qiu (2000). An improved form of Neumann expansion method was introduced by Ghanem and Spanos (1991) in which the Neumann expansion is conjunction with a Galerkin based finite element method where the Karhunen-Loève expansion is employed to represent random parameters in the random operator. This improvement leads to an explicit expression in the solution process as a multivariate polynomial function of a set of uncorrelated random variables from which the statistical moments of the solution can be obtained. Similar work had been done by Hussein et al. (2008) and Galal et al. (2008) in which the Neumann expansion and the Polynomial Chaos were adopted. The adoption of KLE (or PC) in the Neumann expansion-based SFEM is a useful improvement. However, the convergence of the series to represent the inverse operator requires the norm the kernel $L^{-1}\Pi$ smaller than one, where L and Π are deterministic and random operators in a structural system, respectively.

The Spectral Stochastic Finite Element Method (SSFEM) (Ghanem and Spanos 1991) which is capable of handing complex and general problems in probabilistic mechanics with high level of randomness in both system parameters and excitations was developed to overcome weaknesses of the previous methods.

In this method, the KLE is employed to represent the continuous Gaussian random field of material properties with a countable set of random variables. For the random response solution where the covariance function is not known *a-priori*, the Polynomial Chaos is adopted to represent. The Polynomial Chaos is also commonly adopted in this method to represent non-Gaussian material properties.

Since the SSFEM will be employed in the stochastic analysis of bridge-vehicle system in this Thesis, a detail review on the development and the application studies of SSFEM will be conducted. The monograph on SSFEM by Ghanem and Spanos (1991) was focused on the basis theory of stochastic modeling and analysis of structure with uncertainties in finite element.

An implementation of the SSFEM to fulfill the need of this method when applied to the dynamic analysis of stochastic vibration system was further presented by Ghanem (1999a) where the modeling of uncertainty in system parameters was further extended to non-Gaussian/non-linear cases. The SSFEM was coupled with the element-free Galerkin method by Kim and Inoue (2004) to provide an alternative analysis tool in the problems with random material properties and structures with complex meshing. Since the system matrices in the SSFEM tend to be much larger than those in the deterministic FEM, two approaches including an iterative solution scheme and the method based on hierarchical basis concept were presented by Ghanem and Kruger (1996) to achieve an efficient solution. The proposed algorithms can dramatically reduce the amount of computation in the numerical solution. Similar iterative solution

of a linear model based on SSFEM was also studied by Pellissetti and Ghanem (2000). A substructure coupling technique integrating with the SSFEM based on orthogonal decompositions and projections of stochastic processes was also presented by Sarkar and Ghanem (2003) to improve the efficiency of computation. A model reduction of the stochastic representation for a better computational efficiency of the spectral stochastic Galerkin schemes in the solution of partial differential equations with stochastic coefficients was proposed by Doostan et al. (2007). Various applications can be found to analyze engineering problems with random material properties with SSFEM. Le Maitre et al. (2001a, 2001b) employed the SSFEM as a solver for the fluid flow problem. Similar studies for uncertainty quantification in Computational Fluid Dynamic (CFD) problem was proposed by Knio and Le Maitre (2006). Ngah and Young (2007) applied the SSFEM to predict the performance of a composite structure with variable material constitutive properties. Foo et al. (2007) investigated the solution of riser-sections with uncertain measured pressure loads and/or uncertain material properties with generalized Polynomial Chaos. An efficient solution of a stochastic system modeled with SSFEM (Ghanem et al. 2007) was applied on an embankment dam problem in which the SSFEM solution consisting of high dimensional polynomials in Gaussian independent variables was obtained for the coarse mesh problem. The attained solution was used to define a new basis for solving the fine mesh problem. The idea proposed shows the possibility of application of the SSFEM in the stochastic analysis of uncertain engineering structures even with extremely large

number of degrees-of-freedom.

There are other stochastic finite element methods which provide alternative ways to solve engineering problem with stochastic material proprieties including Stochastic Response Surface Method (SRSM) (Isukapalli et al. 1998; Huang and Kou 2007; Huang et al. 2007), Stochastic Reduced Basis Method (SRBM) (Nair and Keane 2002; Mohan et al. 2008) and methods based on variational principles (Ren et al. 1997; Lei and Qiu, 2000; Asokan and Zabararas 2006), etc.

2.3.3.3 Estimation of the Response Statistics

When the stochastic system equation is solved numerically, the estimation of response statistics is the last step. It is very important for the perturbation method and Neumann expansion method since the results from which can not be directly used for reliability analysis. The estimation approaches can be divided into three categories including the statistical approach, the non-statistical approach and the hybrid approach (Schuëller 1997).

Statistical approaches are based on a finite number of deterministic analyses using samples of the system parameters according to their original probability density functions. The Monte Carlo Simulation is categorized as one of these approaches, which transforms the basic stochastic fields associated with the system parameters into those of the system response fields by using many samples. Other sample techniques such as Latin Hypercube Sampling (McKay et al. 1979), etc. can be employed to generate the field of random parameters to achieve higher efficiency. The updated Latin hypercube sampling which is regarded as one of the

most important efficient sampling technique was first proposed by Florian (1992). It was an extension of the work of McKay et al. (1979). Further improvements had also been made by Huntington et al. (1998).

Non-statistical approaches refer to those methods directly estimates the response function of the random variables or discretized stochastic fields. The Perturbation Method, Neumann expansion method and the SSFEM are belonging to this type. The response statistics of the first two methods require simulation of random variables to assess the reliability of the results. However, the results of SSFEM can be directly used for response statistics since the set of random variables are orthogonal and the moments of responses can be directly obtained by the deterministic coefficients calculated from the eigenvalue analyses of the covariance kernel.

The response surface method (Faravelli 1989, 1990) is one of the hybrid methods which were firstly approximated with the aid of the non-statistical approaches, and then the response statistics are computed by substituting digitally generated stochastic fields into the above response surface. Statistical approaches such as the Monte Carlo Simulation requires an enormous amount of computation effort. More efficient methods have been proposed to reduce the sample size including the efficient sampling techniques such as important sampling, Latin hypercube sampling, etc. which are also denoted as “variance reduction techniques” as well as response surface method. The response surface method (Huang and Kou 2007) has been intensively adopted to solve problems where the

physical properties exhibit spatial random variation. Although most of the relevant literatures used the above sampling techniques and the response surface method, these techniques are limited to problems involving a small number of random variables. Application of the above techniques to SFEM is not straightforward, primarily due to the large number of correlated random variables, thus the techniques such as the KLE are employed to discretize the continuous stochastic field to reduce the number of random variables. Also a combination of statistical approach and non-statistical approach was proposed to improve the efficiency of calculation. Yamazaki et al. (1988) proposed a method which combined the Neumann expansion and Monte Carlo simulation. A combination of the SSFEM and Monte Carlo Simulation was also proposed by Huang et al. (2007).

2.3.4 Stochastic Forward Problem of Bridge-vehicle Interaction

The development in stochastic computational mechanics provided a foundation for solving stochastic bridge-vehicle interaction problem. Research work on the dynamic response of a bridge deck under random moving force excitations has been carried out by many researchers.

Some researchers only considered the randomness in the excitation due to the road surface roughness and the system parameters in both bridge and vehicle model were treated as deterministic. A general study on the stochastic analysis of a

simply supported beam with a random force moving on top with constant velocity was carried out by Fryba (1999). Research work addressed on this aspect can mainly be classified into the following categories:

- Method based on MCS.

In this method, the dynamic response of a bridge-vehicle system is directly evaluated with MCS. The Monte Carlo Simulation was employed by Sasidhar and Talukdar (2003) to study the non-stationary response of a simply supported girder bridge induced by the vehicle travelling at variable speed with the road surface roughness assumed as random process. O'Brien et al. (2006) studied the bridge roughness index (BRI) as an indicator of bridge dynamic amplification using Monte Carlo Simulation. Results showed that there is a clear correlation between the BRI and the dynamic amplifier factor (DAF).

- Frequency domain method.

In this method, the response of a bridge-vehicle system is evaluated in frequency domain. Lin (2006) developed a spectral approach in which the random forces were assumed as a series of sinusoidal waves and the variation of bridge deflections due to a moving vehicle was evaluated. A closed-form solution on the variances of the bridge deflections in frequency domain was also presented. For the dynamic analysis of the bridge-vehicle system, the representation of the vehicle effect is not accurate since the effect of inertia has been ignored. Li et al. (2002) investigated the vibration analysis of a coupled bridge-vehicle system in which the vehicle was modeled as a moving oscillator. Da Silva (2004) used

quarter vehicle model with one axle and two degrees-of-freedom to investigate the dynamic performance of highway bridge decks with irregular pavement surface via spectral density analysis in frequency domain. Results showed that the effect due to interaction of the vehicles with an irregular pavement surface was much more significant than that produced by the load mobility alone. These dynamical effects increased drastically with the decrease of the pavement surface quality. The pseudo excitation method combined with moving element method was employed by Lu et al. (2009) to study non-stationary random vibrations of a bridge-vehicle system.

- Time domain method.

In this method, the response of a bridge-vehicle system is evaluated in time domain. The random vibration of a simply supported Euler-Bernoulli beam subject to random loads moving with time-varying velocity was studied by Zibdeh (1995). Similar study on laminated composite beam was investigated by Zibdeh and Abu-Hilal (2003). A uniform Euler-Bernoulli beam with different boundary conditions subject to a random moving concentrated force was investigated by Abu-Hilal (2003). Results showed that the fixed-fixed and the pinned-fixed beams behaved, in general, similar to pinned-pinned beam. Closed form solutions for the mean and variance of the responses for an Euler-Bernoulli, Rayleigh and Timoshenko beam models under a random moving load with constant covariance were obtained using correlation analysis by Zibdeh et al. (2004). Results showed that Timoshenko model has the largest dynamic effect among the three models.

Dynamic behavior of multi-girder bridges under heavy trucks was investigated by Liu et al. (2002) based on the correlated road surface roughness where the spatial coherence function is approximately taken as a constant. Schenk and Bergman (2003) investigated the second moment characteristics of a linear system under a moving concentrate load in which the surface roughness was modeled as spatial Gaussian and stationary colored noise. Seetapan et al. (2006) studied the dynamic response of a two-span beam subject to a two degrees-of-freedom vehicle in time domain. The road surface roughness was modeled by filtered white noise, and the equation of the coupled vehicle-bridge system was formulated in state space. Statistical moments of the state vectors were obtained by solving the first-order Lyapunov equation. Reliability analysis of bridge-vehicle interaction was also evaluated by Xiang et al. (2007) with a time domain transfer matrix method.

Others extended the work by introducing randomness in the system modeling in which Gaussian assumption was made on the system parameters.

Fryba et al. (1993) performed the stochastic finite element analysis with the first order perturbation method, and the first order second moment method was adopted to evaluate the variance of the deflection and bending moment of a beam on foundations with uncertain damping and stiffness under a moving force. The effects of the number of finite elements, vehicle speed, etc. were investigated and different correlation functions such as the exponential covariance, cosine covariance were tested. The dynamic analysis of an Euler-Bernoulli beam excited by a moving oscillator with random mass, velocity and acceleration was

investigated by Muscolino et al. (2002) with the improved perturbation approach. Chang et al. (2006, 2009) studied the dynamic response of an Euler-Bernoulli beam subject to a moving oscillator/half-car model with uncertain parameters such as random mass, stiffness, damping, velocity as well as acceleration. Modal analysis was used to obtain governing equations of motion with time-dependent random coefficients. The improved perturbation technique was adopted to evaluate the statistical characteristics of deflection of the beam and the method proposed was verified by Monte Carlo Simulation. The reliability analysis for a bridge-vehicle system with uncertainties in excitation forces, material properties of bridge and the irregular profile was performed by Cho et al. (2010) with an improved response surface method.

There are situations which may need to model the uncertainty in system parameters with large variations. Research (Da Silva 2004) showed that the effects due to interaction of the vehicles with an irregular pavement surface, in some cases, were even larger than those due to the static presence of the vehicles. When the quality of pavement surface is poor, large uncertainties due to road surface roughness need to be taken into account. The perturbation based SFEM is suitable for handling the case with small uncertainty. However, when the system response at a certain time instance has strong nonlinear behavior with respect to the system parameters, the lower-order approximation of perturbation may fail to estimate the response statistics (Schuëller 1997). A more effective method should be adopted for the stochastic analysis of bridge-vehicle interaction problem with large

uncertainties.

The stochastic aspects in moving force identification of bridge-vehicle system have not been investigated by researchers. The research work in this Thesis aims to fill this gap with new methods proposed for the stochastic dynamic analysis of bridge-vehicle system with uncertainties and new techniques developed for the stochastic moving vehicle load identification and for the quantification of the randomness in the excitations.

CHAPTER 3

BEAM-LOAD SYSTEM WITH UNCERTAINTY IN EXCITATION

3.1 Introduction

Existing approaches of moving force identification treat the beam-load system as deterministic in which the identified results do not have any statistical prediction them. In fact, uncertainties exist in both the interaction forces and structural responses, and their existence erodes the accuracy of the identified moving loads. In this Chapter, a new method will be proposed to evaluate the dynamic response of bridge structure under random moving forces which are assumed as Gaussian random. The Karhunen-Loève Expansion will be adopted to represent these random processes. A new model will be formulated for the dynamic analysis of bridge-vehicle interaction problem with randomness in excitation based on which a stochastic moving force identification technique is presented with the statistics of the moving force time histories identified from samples of the structural responses. Numerical simulations with two forces moving over a simply supported beam will be conducted to verify the proposed forward analysis method as well as the stochastic moving force identification algorithm with the Monte Carlo Simulation.

The beam-load model formulated with the finite element method is given in Section 3.2. Basic theory of the Karhunen-Loève Expansion as well as its application to represent a multi-dimensional Gaussian random process vector will be addressed in Section 3.3. The model formulated by using KLE is developed and the forward analysis as well as the response statistics of the beam will be conducted in Section 3.4. The stochastic moving force identification with uncertainties based on this model will be proposed in Section 3.5. Numerical simulation will be conducted in Section 3.6 which includes the verification of the forward analysis, the proposed identification algorithm and a comparison between the proposed stochastic moving force identification with an existing deterministic method. A summary will be given at the end of this Chapter.

3.2 Equation of Motion of Beam under Moving Forces

The structure is modeled as a planar simply supported beam with multiple moving loads on top as shown in Figure 3.1. The equation of motion can be expressed as

$$\rho A \frac{\partial^2 w(x,t)}{\partial t^2} + c \frac{\partial w(x,t)}{\partial t} + EI \frac{\partial^4 w(x,t)}{\partial x^4} = \sum_{i=1}^{N_F} F_i(t) \delta(x - v_i t), (i = 1, 2, \dots, N_F) \quad (3.1)$$

where A is the cross-sectional area, ρ is the mass per unit length. c and EI are the damping and the flexural rigidity of the beam, respectively. $w(x,t)$ is the displacement of the beam. v_i is the speed of the i^{th} moving load $F_i(t)$. $\delta(t)$ is the Dirac delta function. N_F is the number of moving loads.

Employing the Hermitian cubic interpolation shape functions and with the assumption of Rayleigh damping, the equation of motion of the structure can be rewritten as

$$\mathbf{M}_b \ddot{\mathbf{R}} + \mathbf{C}_b \dot{\mathbf{R}} + \mathbf{K}_b \mathbf{R} = \mathbf{H}_b \mathbf{F} \quad (3.2)$$

where \mathbf{M}_b , \mathbf{C}_b and \mathbf{K}_b are the deterministic mass, damping and stiffness matrices of the beam structure, \mathbf{R} , $\dot{\mathbf{R}}$ and $\ddot{\mathbf{R}}$ are the deterministic nodal displacement, velocity and acceleration response vectors respectively and $\mathbf{H}_b \mathbf{F}$ is the equivalent nodal load vector of the moving forces with

$$\mathbf{H}_b = \left\{ \begin{array}{cccccccc} 0 & \cdots & 0 & \cdots & 0 & \cdots & \mathbf{H}_1 & \cdots & 0 \\ 0 & \cdots & 0 & \cdots & \mathbf{H}_2 & \cdots & 0 & \cdots & 0 \\ 0 & \cdots & 0 \\ 0 & \cdots & \mathbf{H}_{N_F} & \cdots & 0 & \cdots & 0 & \cdots & 0 \end{array} \right\}_{N_d \times N_F} \quad (3.3)$$

where N_d is the number of degree-of-freedom of the beam structure after considering the boundary condition. The shape function \mathbf{H}_i can be written for this structure in the global coordinate as

$$\mathbf{H}_i = \left\{ \begin{array}{l} 1 - 3 \left(\frac{x_j(t) - (i-1)l}{l} \right)^2 + 2 \left(\frac{x_j(t) - (i-1)l}{l} \right)^3 \\ (x_j(t) - (i-1)l) \left(\frac{x_j(t) - (i-1)l}{l} - 1 \right)^2 \\ 3 \left(\frac{x_j(t) - (i-1)l}{l} \right)^2 - 2 \left(\frac{x_j(t) - (i-1)l}{l} \right)^3 \\ (x_j(t) - (i-1)l) \left(\left(\frac{x_j(t) - (i-1)l}{l} \right)^2 - \left(\frac{x_j(t) - (i-1)l}{l} \right) \right) \end{array} \right\}^T \quad (3.4)$$

where $x_j(t)$ is the location of the j^{th} force on the i^{th} element at time t with $(i-1)l \leq x_j(t) < il$ and l is the length of the beam element.

The nodal responses of the bridge model under the moving forces can be

obtained directly by solving Equation (3.3). The displacement of the bridge at position x and time t can then be expressed as:

$$w(x, t) = \mathbf{H}(x)\mathbf{R}(t) \quad (3.5)$$

where $\mathbf{H}(x) = \{0 \cdots \mathbf{H}(x)_i^T \ 0 \cdots 0\}$ and $\mathbf{H}(x)_i^T$ is the shape function of the beam structure. $\mathbf{H}(x)$ is a $1 \times N_d$ vector with zero entries except at the i^{th} beam element on which the force is located.

3.3 Karhunen-Loève Expansion

The Karhunen-Loève Expansion (KLE), which is also known as “Proper Orthogonal Decomposition” (POD) or “Principal Component Analysis” (PCA) is a powerful and elegant method for data analysis aiming at a low-dimensional approximation of a high-dimensional process. The equivalence of the above three techniques was investigated by Liang et al. (2002) and Wu et al. (2003). This kind of expansion minimizes the mean-squares error by representing the random field in finite number of terms (Schenk and Schuëller 2005). A mathematical background of KLE with a discussion on the properties was provided by Hall et al. (2006).

The KLE has already been widely adopted in image processing and data compression, and a review of the application of KLE in structural analysis is given in this Section. The application of KLE in structural analysis mainly includes the deterministic modal analysis and stochastic process representation. A technical research report was presented by Newman (1996a; 1996b) on the model reduction

technique with a dynamic system by adopting the KLE. The “modal shape” obtained from the POD was used in a Galerkin process to obtain lower dimensional models for structural analysis by Azeez and Vakakis (2001). The application of KLE in deterministic modal analysis was also extended to non-linear systems. An overview on the modal analysis of a nonlinear mechanical system with POD was provided by Kerschen et al. (2005). The KLE was adopted to create low-dimensional, reduced order model for a group of linear coupled oscillators with strongly nonlinear end attachments by Ma et al. (2008). The stochastic analysis of a structural system has also been performed based on the K-L representation of both Gaussian (Kac and Siegert 1947) and non-Gaussian (Phoon et al. 2002, 2005) stochastic processes. The stochastic analysis of a dynamic system with nonlinear physical properties and non-stationary Gaussian random excitation was studied by Pradlwarter et al. (2003) and Schenk et al. (2004; 2005) in which the KLE was adopted to represent the random processes involved.

The basic theory of KLE and its representation of a Gaussian random process will be introduced below.

3.3.1 Theory

The Karhunen-Loève Expansion of a random process $u(x,\theta)$ is based on its covariance function $C(x_1,x_2)$ which is bounded, symmetric and positive definite with the following spectral decomposition

$$\mathbf{C}(x_1, x_2) = \sum_{n=0}^{\infty} \lambda_n \varphi_n(x_1) \varphi_n(x_2) \quad (3.6)$$

where λ_n and $\varphi_n(x)$ are the eigenvalue and eigenvector of the covariance kernel, respectively. They can be proved to be the solution of the following integral equation (Ghanem and Spanos 1991)

$$\int \mathbf{C}(x_1, x_2) \varphi_n(x_1) dx_1 = \lambda_n \varphi_n(x_2) \quad (3.7)$$

Due to the symmetry and the positive definiteness of the covariance kernel, the eigenfunctions are orthogonal and they form a complete set representing the covariance function. The eigenvectors can be normalized according to the following

$$\int \varphi_n(x) \varphi_m(x) dx = \delta_{nm} \quad (3.8)$$

where δ_{nm} is the Kronecker delta. The random process $u(x, \theta)$ can then be written as

$$u(x, \theta) = \bar{u}(x) + \tilde{u}(x, \theta) = \bar{u}(x) + \sum_{n=1}^{\infty} \xi_n(\theta) \sqrt{\lambda_n} \varphi_n(x) \quad (3.9)$$

where $\bar{u}(x)$ denotes the expected value of $u(x, \theta)$ and $\xi_n(\theta)$ is a set of uncorrelated random variables. An explicit expression for $\xi_n(\theta)$ can also be expressed as

$$\xi_n(\theta) = \frac{1}{\sqrt{\lambda_n}} \int \tilde{u}(x, \theta) \varphi_n(x) dx \quad (3.10)$$

When $u(x, \theta)$ is a Gaussian random process, $\xi_n(\theta)$ will be a group of standard Gaussian random variables have the following properties,

$$E(\xi_n(\theta)) = 0, \quad E(\xi_k(\theta) \xi_l(\theta)) = \delta_{kl} \quad (3.11)$$

where $E(\cdot)$ denotes the expectation.

3.3.2 Representation of Stochastic Process Vector

A m -dimensional stochastic process vector $\mathbf{V}(t, \theta)$ can be defined as

$$\mathbf{V}(t, \theta) = \{\mathbf{v}_1(t, \theta) \quad \mathbf{v}_2(t, \theta) \quad \cdots \quad \mathbf{v}_m(t, \theta)\}^T \quad (3.12)$$

The mean and random component of the i^{th} element of $\mathbf{V}(t, \theta)$ denoted as $\bar{\mathbf{v}}_i(t)$ and $\tilde{\mathbf{v}}_i(t, \theta)$ respectively can be expressed as

$$\bar{\mathbf{v}}_i(t) = E(\mathbf{v}_i(t, \theta)), \quad (i = 1, \dots, m) \quad (3.13)$$

$$\tilde{\mathbf{v}}_i(t, \theta) = \mathbf{v}_i(t, \theta) - \bar{\mathbf{v}}_i(t), \quad (i = 1, \dots, m) \quad (3.14)$$

where $E(\bullet)$ denotes the expectation.

The stochastic process vector $\mathbf{V}(t, \theta)$ can be discretized at equal time step intervals Δt , and the number of time instants is $n = T/\Delta t + 1$, where T is the total time duration. The Karhunen-Loève (K-L) Expansion of the discrete vector of stochastic processes can be obtained by reshaping the discretized vector process into a one-dimensional process $\mathbf{V}\mathbf{V}$ as

$$\mathbf{V}\mathbf{V}(t, \theta) = \{\mathbf{v}_1(t_1, \theta) \cdots \mathbf{v}_1(t_n, \theta) \quad \mathbf{v}_2(t_1, \theta) \cdots \mathbf{v}_2(t_n, \theta) \cdots \mathbf{v}_m(t_1, \theta) \cdots \mathbf{v}_m(t_n, \theta)\}^T \quad (3.15)$$

with the covariance matrix $\mathbf{\Gamma}_{\mathbf{V}\mathbf{V}, \mathbf{V}\mathbf{V}}$ defined by

$$\mathbf{\Gamma}_{\mathbf{V}\mathbf{V}, \mathbf{V}\mathbf{V}}(i, j) = E\{(\mathbf{v}_i(t, \theta) - \bar{\mathbf{v}}_i(t))(\mathbf{v}_j(t, \theta) - \bar{\mathbf{v}}_j(t))\}, \quad (i, j = 1, \dots, m) \quad (3.16)$$

which can also be written in the following matrix form (Schenk and Schuëller 2005) as

$$\mathbf{\Gamma}_{\mathbf{V}\mathbf{V}, \mathbf{V}\mathbf{V}} = \begin{bmatrix} \mathbf{\Gamma}_{\mathbf{v}_1, \mathbf{v}_1} & \cdots & \mathbf{\Gamma}_{\mathbf{v}_1, \mathbf{v}_m} \\ \vdots & \ddots & \vdots \\ \mathbf{\Gamma}_{\mathbf{v}_m, \mathbf{v}_1} & \cdots & \mathbf{\Gamma}_{\mathbf{v}_m, \mathbf{v}_m} \end{bmatrix}_{N_v \times N_v} \quad (3.17)$$

where $N_v = m \times n$ and the corresponding KLE is defined in the following eigenvalue problem as

$$\mathbf{\Gamma}_{\mathbf{V}\mathbf{V}, \mathbf{V}\mathbf{V}} \boldsymbol{\varphi}_j - \lambda_j \boldsymbol{\varphi}_j = 0 \quad (3.18)$$

After the truncation at the k_v th order according to Equation (3.9), the K-L representation of $\mathbf{V}\mathbf{V}$ is then denoted by

$$\mathbf{V}\mathbf{V}(t, \theta) = \boldsymbol{\mu}_{\mathbf{V}\mathbf{V}}(t) + \sum_{j=1}^{k_v} \xi_j(\theta) \sqrt{\lambda_j} \boldsymbol{\varphi}_j(t) = \boldsymbol{\mu}_{\mathbf{V}\mathbf{V}}(t) + \sum_{j=1}^{k_v} \xi_j(\theta) \mathbf{X}^{(j)}(t) \quad (3.19)$$

where $\boldsymbol{\mu}_{\mathbf{V}\mathbf{V}}(t)$ is the mean vector and $\mathbf{X}^{(j)}$ are the Karhunen-Loève vectors and $\mathbf{X}^{(j)} = \{\mathbf{x}_1^{(j)} \quad \mathbf{x}_2^{(j)} \quad \dots \quad \mathbf{x}_m^{(j)}\}^T$ has a dimension of $N_v \times 1$. Thus the random component of the $\tilde{\mathbf{v}}_i(t, \theta)$ can be expressed as

$$\tilde{\mathbf{v}}_i(t, \theta) = \sum_{j=1}^{k_v} \xi_j(\theta) \mathbf{x}_i^{(j)}(t) \quad (3.20)$$

where $\mathbf{x}_i^{(j)}(t)$ is of size $1 \times n$ representing the j th K-L components of the i th term in $\mathbf{V}(t, \theta)$, and they can be extracted from the Karhunen-Loève vectors $\mathbf{X}^{(j)}(t)$ according to Equations (3.15) to (3.20). Subsequently $\mathbf{V}(t, \theta)$ becomes

$$\mathbf{V}(t, \theta) = \boldsymbol{\mu}_{\mathbf{V}}(t) + \sum_{j=1}^{k_v} \xi_j(\theta) \mathbf{x}^{(j)}(t) = \sum_{j=0}^{k_v} \xi_j(\theta) \mathbf{x}^{(j)}(t) \quad (3.21)$$

with the mean vector $\boldsymbol{\mu}_{\mathbf{V}}(t)$, $\xi_0(\theta)=1$, $\mathbf{x}^{(0)} = \{\bar{\mathbf{v}}_1 \quad \bar{\mathbf{v}}_2 \quad \dots \quad \bar{\mathbf{v}}_m\}^T$, and

$$\mathbf{x}^{(j)}(t) = \{\mathbf{x}_1^{(j)} \quad \mathbf{x}_2^{(j)} \quad \dots \quad \mathbf{x}_m^{(j)}\}^T.$$

3.4 System Modeling and Response Statistics

In the dynamic analysis of a bridge structure under stochastic moving forces, the random excitation force vector $\mathbf{F}(t, \theta)$ which is assumed as a multi-dimensional Gaussian random process can be firstly represented by its K-L components $\mathbf{f}^{(j)}(t)$ multiplied by the corresponding random coefficients $\xi_j(\theta)$ which are standard Gaussian random variables according to Equation (3.21) as

$$\mathbf{F}(t, \theta) = \sum_{j=0}^{k_F} \xi_j(\theta) \mathbf{f}^{(j)}(t) \quad (3.22)$$

where k_F is the number of K-L components retained after truncation.

Based on the superposition of the linear system and the representation of the stochastic moving forces as a sum of independent vectors of the corresponding K-L components, the stochastic structural nodal displacement, velocity and acceleration vectors denoted as $\mathbf{R}(t, \theta)$, $\dot{\mathbf{R}}(t, \theta)$ and $\ddot{\mathbf{R}}(t, \theta)$ respectively can be expressed as

$$\mathbf{R}(t, \theta) = \sum_{j=0}^{k_R} \xi_j(\theta) \mathbf{y}^{(j)}(t) \quad (3.23)$$

$$\dot{\mathbf{R}}(t, \theta) = \sum_{j=0}^{k_R} \xi_j(\theta) \dot{\mathbf{y}}^{(j)}(t) \quad (3.24)$$

$$\ddot{\mathbf{R}}(t, \theta) = \sum_{j=0}^{k_R} \xi_j(\theta) \ddot{\mathbf{y}}^{(j)}(t) \quad (3.25)$$

where $\mathbf{y}^{(j)}$, $\dot{\mathbf{y}}^{(j)}$ and $\ddot{\mathbf{y}}^{(j)}$ are the corresponding deterministic components. It should be noted that though the expansion for the stochastic nodal response vector have the same forms as those for the excitation forces, these deterministic components in the response vectors calculated from the corresponding K-L components of the excitation forces can not be considered as K-L components, and the number of terms in these expansions equals to the number of the K-L components in the KLE of the stochastic forces, i.e. $k_R=k_F$.

Substituting Equations (3.22) to (3.25) into Equation (3.2) and taking the inner product of both side of the equation with $\check{\zeta}_k(\theta)$ and employing the orthogonal property as shown in Equation (3.11), we have

$$\mathbf{M}_b \ddot{\mathbf{y}}^{(k)}(t) + \mathbf{C}_b \dot{\mathbf{y}}^{(k)}(t) + \mathbf{K}_b \mathbf{y}^{(k)}(t) = \mathbf{H}_b \mathbf{f}^{(k)}(t), \quad (k=0, \dots, k_R) \quad (3.26)$$

Equation (3.26) can be solved by Newmark- β method and the deterministic coefficients $\mathbf{y}^{(j)}$, $\dot{\mathbf{y}}^{(j)}$ and $\ddot{\mathbf{y}}^{(j)}$ can be obtained. The mean and variance of the random nodal displacements of the bridge structure can be evaluated as

$$MEAN_{\mathbf{R}}(t) = \mathbf{y}^{(0)}(t), \quad VAR_{\mathbf{R}}(t) = \sum_{j=1}^{k_R} (\mathbf{y}^{(j)}(t))^2 \quad (3.27)$$

where the subscript “ \mathbf{R} ” denotes the random nodal displacement vector. The mean and variance of displacement of the beam at position x and time t can be obtained according to Equation (3.5) as

$$MEAN_w(x, t) = \mathbf{H}(x) \mathbf{y}^{(0)}(t), \quad VAR_w(x, t) = \sum_{j=1}^{k_R} (\mathbf{H}(x) \mathbf{y}^{(j)}(t))^2 \quad (3.28)$$

where the subscript “ w ” denotes the random displacement under the bridge deck. The statistics of the velocity and acceleration of the bridge structure at any position can be obtained in a similar way by replacing the $\mathbf{y}^{(j)}$ in Equation (3.28) with $\dot{\mathbf{y}}^{(j)}$ and $\ddot{\mathbf{y}}^{(j)}$, respectively.

3.5 Stochastic Moving Force Identification

In the stochastic moving force identification procedure, a set of nodal response samples, e.g. the nodal displacement samples, will form a discretized multi-dimensional random process vector with Gaussian properties denoted as $\hat{\mathbf{R}}(t, \theta)$. According to Equation (3.21), the random nodal displacement vector of the bridge structure can be represented by its K-L components $\hat{\mathbf{y}}^{(j)}(t)$ as

$$\hat{\mathbf{R}}(t, \theta) = \sum_{j=0}^{\hat{k}_R} \xi_j(\theta) \hat{\mathbf{y}}^{(j)}(t) \quad (3.29)$$

where \hat{k}_R is the number of K-L components of the nodal response samples after truncation and $\xi_j(\theta)$ are standard Gaussian random variables having the orthogonal properties described in Equation (3.11). Noted that the K-L components of the nodal displacement denoted as $\hat{\mathbf{y}}^{(j)}(t)$ are different from the components for the nodal displacement in the forward analysis denoted as $\mathbf{y}^{(j)}(t)$. The random nodal velocity vectors and acceleration vectors will respectively take the forms as

$$\dot{\hat{\mathbf{R}}}(t, \theta) = \sum_{j=0}^{\hat{k}_R} \xi_j(\theta) \dot{\hat{\mathbf{y}}^{(j)}}(t) \quad (3.30)$$

$$\ddot{\hat{\mathbf{R}}}(t, \theta) = \sum_{j=0}^{\hat{k}_R} \xi_j(\theta) \ddot{\hat{\mathbf{y}}^{(j)}}(t) \quad (3.31)$$

where $\dot{\hat{\mathbf{y}}^{(j)}}(t)$ and $\ddot{\hat{\mathbf{y}}^{(j)}}(t)$ are the first and second derivatives of $\hat{\mathbf{y}}^{(j)}(t)$ with respect to time t , respectively.

It is noted that the covariance matrix of the stochastic excitation forces to be identified is not known *a-prior*, and therefore the KLE of the excitation forces can not be performed. However, based on the superposition of the linear system and the representation of the stochastic nodal response vector as a sum of independent vectors of the corresponding K-L components, the random excitation $\hat{\mathbf{F}}(t, \theta)$ can be represented as

$$\hat{\mathbf{F}}(t, \theta) = \sum_{j=0}^{\hat{k}_F} \xi_j(\theta) \hat{\mathbf{f}}^{(j)}(t) \quad (3.32)$$

where $\hat{\mathbf{f}}^{(j)}(t)$ is the deterministic coefficient vector corresponding to $\hat{\mathbf{y}}^{(j)}(t)$ and \hat{k}_F is the number of components for the stochastic moving forces to be identified with $\hat{k}_F = \hat{k}_R$. It should be noted that Equation (3.32) is not a KLE of the excitation forces vector and $\hat{\mathbf{f}}^{(j)}(t)$ is not the vector of K-L components from

the eigenvalue analysis of the covariance kernel of the stochastic excitation forces but it represents the corresponding terms related to the K-L components of the random nodal displacement in the inverse problem.

Since only the degrees-of-freedom (*dofs*) with measured data are included in the nodal response vector $\hat{\mathbf{R}}(t, \theta)$ in the force identification procedure, a model condensation technique should be adopted to reduce the bridge model with full *dofs* to match the *dofs* of measured data. Substituting Equations (3.29) to (3.32) into the condensed equation of motion of the system and taking the inner product of both side of the equations with $\xi_k(\theta)$ and employing the orthogonal property as shown in Equation (3.11),

$$\hat{\mathbf{M}}_b \ddot{\hat{\mathbf{y}}^{(k)}}(t) + \hat{\mathbf{C}}_b \dot{\hat{\mathbf{y}}^{(k)}}(t) + \hat{\mathbf{K}}_b \hat{\mathbf{y}}^{(k)}(t) = \hat{\mathbf{H}}_b \hat{\mathbf{f}}^{(k)}(t), \quad (k = 0, \dots, \hat{k}_F) \quad (3.33)$$

where $\hat{\mathbf{M}}_b$, $\hat{\mathbf{C}}_b$, $\hat{\mathbf{K}}_b$ and $\hat{\mathbf{H}}_b$ are the mass, damping, stiffness and location matrices of the bridge deck in the inverse problem after condensation respectively. In this Thesis, the Improved Reduced System (IRS) reduction scheme (O'Callahan 1989) is adopted to condense the unmeasured degrees-of-freedom of the bridge structure. All the measured *dofs* are denoted as the master *dofs* and the remaining *dofs* are called the slave *dofs*. The mass, damping, stiffness and location matrices can be partitioned according to the master and slave *dofs* as

$$\mathbf{M}_b = \begin{bmatrix} \mathbf{M}_{mm} & \mathbf{M}_{ms} \\ \mathbf{M}_{sm} & \mathbf{M}_{ss} \end{bmatrix}, \quad \mathbf{C}_b = \begin{bmatrix} \mathbf{C}_{mm} & \mathbf{C}_{ms} \\ \mathbf{C}_{sm} & \mathbf{C}_{ss} \end{bmatrix}$$

$$\mathbf{K}_b = \begin{bmatrix} \mathbf{K}_{mm} & \mathbf{K}_{ms} \\ \mathbf{K}_{sm} & \mathbf{K}_{ss} \end{bmatrix}, \quad \mathbf{H}_b = \begin{bmatrix} \mathbf{H}_m \\ \mathbf{H}_s \end{bmatrix}^T \quad (3.34)$$

where the subscript 'm' and 's' denote the master *dofs* and slave *dofs*,

respectively.

The transformation matrix \mathbf{T} in IRS is defined as

$$\mathbf{T} = \mathbf{T}_s + \mathbf{T}_i \quad (3.35)$$

where

$$\mathbf{T}_s = \begin{bmatrix} \mathbf{I} \\ -\mathbf{K}_{ss}^{-1}\mathbf{K}_{sm} \end{bmatrix}, \quad \mathbf{T}_i = \begin{bmatrix} 0 \\ \mathbf{K}_{ss}^{-1}(\mathbf{M}_{sm} - \mathbf{M}_{ss}\mathbf{K}_{ss}^{-1}\mathbf{K}_{sm})(\mathbf{T}_s^T\mathbf{M}_b\mathbf{T}_s)^{-1}(\mathbf{T}_s^T\mathbf{K}_b\mathbf{T}_s) \end{bmatrix}.$$

The condensed matrices in Equation (3.33) can be obtained as

$$\begin{aligned} \hat{\mathbf{M}}_b &= \mathbf{T}^T\mathbf{M}_b\mathbf{T}, & \hat{\mathbf{C}}_b &= \mathbf{T}^T\mathbf{C}_b\mathbf{T} \\ \hat{\mathbf{K}}_b &= \mathbf{T}^T\mathbf{K}_b\mathbf{T} & \hat{\mathbf{H}}_b &= \mathbf{T}^T\mathbf{H}_b \end{aligned} \quad (3.36)$$

The components of the stochastic moving loads can be identified from the corresponding K-L components of the stochastic nodal responses according to Equation (3.33) by using the least-squares method as

$$\hat{\mathbf{f}}^{(k)}(t) = \left(\hat{\mathbf{H}}_b^T\hat{\mathbf{H}}_b\right)^{-1}\hat{\mathbf{H}}_b^T\mathbf{U}^{(k)}(t) \quad (3.37)$$

where $\mathbf{U}^{(k)}(t) = \hat{\mathbf{M}}_b\ddot{\mathbf{y}}^{(k)}(t) + \hat{\mathbf{C}}_b\dot{\mathbf{y}}^{(k)}(t) + \hat{\mathbf{K}}_b\mathbf{y}^{(k)}(t)$.

The mean value and variance of the identified forces can be expressed as

$$MEAN_F(t) = \hat{\mathbf{f}}^{(0)}(t), \quad VAR_F(t) = \sum_{j=1}^{\hat{k}_F} \left(\hat{\mathbf{f}}^{(j)}(t)\right)^2 \quad (3.38)$$

where the subscript ‘‘F’’ denotes the identified random moving forces.

3.6 Numerical Simulation

In this Section, the beam-load model will be introduced followed by the proposed method for the forward analysis of a bridge structure under random moving forces. The stochastic moving force identification algorithm based on the

proposed model will be verified by the Monte Carlo Simulation (MCS) with numerical examples. The beam model is divided into eight planar Euler-Bernoulli finite elements each with of 5 m length. The sampling rate for all the simulations is 200 Hz .

The relative errors between the statistics of calculated response and the reference response from the MCS denoted as RE in forward problem is defined as

$$RE = \frac{\|R^{cal} - R^{ref}\|}{\|R^{ref}\|} \times 100\% \quad (3.39)$$

The relative errors between the statistics of the identified moving forces and the reference forces denoted as FE , in inverse problem is defined as

$$FE = \frac{\|F^{cal} - F^{ref}\|_2}{\|F^{ref}\|_2} \times 100\% \quad (3.40)$$

3.6.1 Beam-Load Model

3.6.1.1 Beam Model I

Beam model I for the numerical simulation will have the following properties: Length of the beam $L=40$ m ; Cross-sectional area $A=4.8$ m^2 ; Second moment of inertia of cross-section $I=2.5498$ m^4 ; Damping ratio $\zeta=0.02$ for all modes; Elastic modulus E and mass density ρ of material are 5×10^{10} N/m^2 and 2.5×10^3 kg/m^3 respectively. The first three natural frequencies of the beam are 3.2, 12.8 and 28.8 Hz and Rayleigh damping is assumed for the beam structure.

3.6.1.2 Force Model I

In Force Model I, the mean values of the two random time-varying moving forces are

$$F_{1d}=20000(1+0.1\sin(10\pi t)+0.05\sin(40\pi t)) \quad (3.41)$$

$$F_{2d}=20000(1-0.1\sin(10\pi t)+0.05\sin(40\pi t)) \quad (3.42)$$

where the subscript ‘*d*’ denotes the deterministic part. The randomness in the moving forces with Gaussian property is defined with a specific value of Coefficient Of Variation (COV_F) at each time instance. This model is a non-stationary Gaussian white noise model in which the covariance kernel has a very small correlation length.

3.6.1.3 Force Model II

This force model is a stationary Gaussian random process in which the covariance kernel has a given correlation length. In Force Model II, the mean values of the two random time-varying moving forces are the same as those for Force Model I but with different properties of randomness as described below.

The random part of each moving force is assumed as a zero-mean Gaussian random process with a Power Spectrum Density (PSD) function $S_{FF}(\omega)$ as

$$S_{FF}(\omega) = A_F \Phi_{rr}(\omega) \quad (3.43)$$

where A_F is a constant and $\Phi_{rr}(\omega)$ is the PSD of the surface roughness of road pavement according to the ISO specification (ISO 8606:1995(E), 1995) as

$$\Phi_{rr}(\omega) = \Phi(\omega_0) \left[\frac{\omega}{\omega_0} \right]^{-2} \quad (3.44)$$

where $\Phi(\omega_0)$ is an amplitude coefficient associated with the travel path surface

roughness and ω_0 is the reference angular spatial frequency. According to the theory of the Spectral Representation (Shinozuka and Deodatis 1991) for a stationary Gaussian random process, the surface profile $r(x)$ can be simulated by the following series,

$$r(x) = \sum_{k=1}^{N_k} A_{rk} \cos(\omega_k x + \varphi_k) \quad (3.45)$$

where

$$A_{rk} = \sqrt{2\Delta\omega\Phi_{rr}(\omega_k)} \quad (3.46)$$

$$\omega_k = \omega_{\min} + \Delta\omega(k-1) \quad (3.47)$$

$$N_k = (\omega_{\max} - \omega_{\min})/\Delta\omega \quad (3.48)$$

In Equations (3.45) to (3.48), A_{rk} is the amplitude of the harmonics. φ_k is a random phase angle uniformly distributed in the interval $[0, 2\pi]$. $\Delta\omega$ is the frequency increment and N_k is the total number of frequency divisions in the interval $[\omega_{\min}, \omega_{\max}]$. ω_{\min} , ω_{\max} are the minimum and maximum frequencies respectively in the spectrum defined. According to Equation (3.45), the random parts of the two moving forces, F_{1r} and F_{2r} , can be represented as

$$F_{1r} = \sqrt{A_F} \sum_{k=1}^{N_k} A_{rk} \cos(\omega_k vt + \varphi_k) \quad (3.49)$$

$$F_{2r} = \sqrt{A_F} \sum_{k=1}^{N_k} A_{rk} [\cos \omega_k v(t - l_a/v) + \varphi_k] \quad (3.50)$$

where l_a is the distance between the two forces and v is the velocity. The subscript ‘ r ’ denotes the random part. Samples of the random moving forces with Gaussian properties can be generated according to Equations (3.41), (3.42), (3.49) and (3.50).

The Coefficient Of Variation (COV_F) of the moving forces is defined as

$$COV_F = E \left(\frac{\sum_i \sqrt{VAR_{F_i}(t)}}{\sum_i MEAN_{F_i}(t)} \right) \quad (3.51)$$

where $E(\bullet)$ denotes the expectation.

The parameters for the random part of the two moving forces used in the numerical simulation are: $A_F=2 \times 10^5$, $\omega_0=1 \text{ rad/s}$, $\omega_{\min}=0.1 \text{ rad/s}$, $\omega_{\max}=10 \text{ rad/s}$, $\Delta\omega=2\pi/2L=0.0785 \text{ rad/s}$ (Henchi et al. 1998), $l_d=4 \text{ m}$, $v=40 \text{ m/s}$. Set $\Phi(\omega_0)=1 \times 10^{-6}$, 4×10^{-6} , 16×10^{-6} , 64×10^{-6} and $256 \times 10^{-6} \text{ m}^3$ to represent different levels of randomness of the excitation forces. The corresponding COV_F are equal to 0.0382, 0.0778, 0.1517, 0.3073 and 0.6256 respectively according to Equations (3.44) to (3.51).

3.6.2 Forward Analysis: Response Statistics

In the forward problem of the present dynamic analysis of a beam structure under two random moving forces with Gaussian property, both kinds of force model will be adopted in the proposed K-L method and the accuracy of the proposed method will be verified with the Monte Carlo Simulation.

Ten thousand samples of random moving forces are generated within the population from which the covariance kernel shown in Equation (3.17) is obtained. The K-L components of the random moving forces as shown in Equation (3.22) can be obtained by performing the eigenvalue analysis on the kernel. A threshold B on the eigenvalues λ_j of the K-L component is selected and

the K-L component will be truncated when its eigenvalue is smaller than B . For each of the K-L components of the moving loads in Equation (3.26), the Newmark- β method is employed to calculate the corresponding components of the nodal responses at each time step.

For the case with Force Model I, the accuracy of the proposed K-L method at different levels of uncertainty in excitation with $B=10^0$ is investigated. Results from the Monte Carlo Simulation with 10000 runs are taken as reference. The percentage errors in the mean value and variance of the mid-span displacements calculated from both methods according to Equation (3.39) are shown in Table 3.1. A comparison of the mid-span displacement for the case with $COV_F=10\%$ is plotted in Figure 3.2.

For the case with Force Model II, an extra study is carried out on the selection of the threshold value B for the truncation of the K-L component. The criterion for selecting the threshold is to use as few K-L components as possible in the forward analysis while maintaining sufficient accuracy. Threshold values equal to 10^0 , 10^5 , 10^6 , 10^7 and 10^8 are studied and the number of the K-L components left after truncation, the time cost for the response calculation and the relative error of the statistics between the calculated response from the K-L method and the Monte Carlo Simulation are compared in Table 3.2. The mean value of the response is noted not to be affected by the truncation while the calculated variance of the response maintains a good accuracy for $B \leq 10^7$. Therefore $B=10^7$ is suggested as the threshold for truncation in this case. The K-L

components with eigenvalues λ_j smaller than 10^7 are truncated and the number of K-L components used in the response calculation is 19 which is much less than the total number of the K-L components in the expansion noted as 442. It is also noted from Table 3.2 that the time cost for calculations with different trial threshold values for truncation is similar. This is because most of the time is spent on the eigenvalue analysis of the covariance kernel in the response calculation. The mean and variance of 10000 samples of the mid-span displacement calculated from the Monte Carlo Simulation is taken as reference. The mean and variance of the mid-span displacement calculated from the proposed K-L method are compared with the reference ones from MCS in Figure 3.2 with good agreements. However, the time required for the response calculation using the proposed K-L methods is 31.96 s which is much less than 243.39 s required by the MCS running on a computer with Intel(R) Core(TM) Duo CPU 2.66Hz and 4GB RAM.

The accuracy of the proposed method at different levels of randomness in the interaction forces is further investigated. The relative errors of the mean value and variance of the seven nodal displacements along the beam at equal spacing calculated from both the K-L methods and MCS at different levels of uncertainty according to Equation (3.39) are shown in Table 3.3. Results from both methods on two force models show very similar accuracy at different levels of uncertainty. The relative error in both the mean value and variance of the response decreases slightly with reduction in the COV_F of the interaction forces. The accuracy of the proposed method in the forward analysis is not sensitive to the level of randomness

in the excitation forces.

3.6.3 Inverse Analysis: Force Identification

3.6.3.1 Verification of the Algorithm

In the inverse force identification procedure, a set of 500 samples of seven displacements evenly distributed underneath the beam structure are generated for the moving force identification according to Equation (3.23) in which the Gaussian random variables are generated using the Latin Hypercube sampling technique and the deterministic coefficients are obtained in the forward analysis. There are 16 degrees-of-freedom (*dofs*) in the planar beam structure and the Improved Reduced System (IRS) (O’Callahan 1989) scheme is employed to condense the structural system to only seven *dofs*. The computation procedure for the moving force identification is given as follows:

- a) The averaging process is performed according Equation (3.13) on the 500 sets of seven nodal displacements. The covariance kernel of the displacement samples can then be calculated according to the theory described in Section 3.3.2. The eigenvalue analysis on the kernel is performed to obtain the K-L components of the random nodal displacement, and the cubic spline interpretation will be adopted to each K-L component of displacement. The first and second derivatives representing corresponding components of the velocities and accelerations can then be derived according to Equations (3.30) and (3.31).

- b) The system matrices of the beam structure, \mathbf{M}_b , \mathbf{C}_b , \mathbf{K}_b , and the location matrix \mathbf{H}_b in Equation (3.2) are formulated with the finite element method, and the IRS scheme is adopted for the model condensation.
- c) The corresponding components of the interaction forces can be calculated according to Equation (3.37) based on the K-L components of the nodal responses and their derivatives. The statistics of the identified forces can be evaluated according to Equation (3.38).

The statistics of the moving forces for reference are calculated from the two force models introduced in Sections 3.6.1.2 and 3.6.1.3, respectively. Due to the relatively large error in the identified forces when the moving loads enter and leave the beam as noted in Figures 3.4 to 3.7, the relative error FE calculated for the whole time history is relatively large. Therefore only data within 0.1s-0.9s for the first axle force and 0.2s-1.0s for the second axle force will be adopted in the following error analysis.

For the case with Force Model I, the errors in the mean value and variance of the interaction forces identified from the 500 response samples according to Equation (3.40) are shown in Table 3.4. A comparison of the mean value and variance of the identified random moving forces from the two methods for the case of $COV_F=10\%$ are plotted in Figures 3.4 and 3.5, respectively. Results show that the mean value of the identified random moving forces is very accurate, while large error exists in the variance. The error in the variance of the identified forces is noted to be almost independent of the COV of the interaction forces.

For the case with Force Model II, a comparison of the statistics between the identified and the reference forces for the case of $\Phi(\omega_0) = 16 \times 10^{-6} m^3$ are plotted in Figures 3.6 and 3.7. The errors in the mean value and variance of the interaction forces identified from the set of 500 response samples according to Equation (3.40) with different level of randomness are shown in Table 3.5. Results show that both the mean value and variance of the random moving forces are accurately identified. It is also revealed that the proposed stochastic force identification algorithm has a good accuracy for different level of randomness even when the COV_F is quite large (e.g. $COV_F = 0.6256$) and the relative error in the identified statistics of the moving forces are not sensitive to the level of randomness.

For the two force models adopted, the mean value of random moving force can be accurately identified. However, the variance of the random moving forces is accurately identified for the case of Force Model II comparing with the variance with large error in the identification for the case of Force Model I. This large error exists in the procedure of obtaining the corresponding components of nodal velocity and nodal acceleration from the K-L components of nodal displacement with the cubic spline interpolation. Since the white noise model is adopted in Force Model I, the two adjacent time instances of the time history of response of structure are independent with each other. This property also exhibits by the K-L components of the nodal displacement. Therefore the differentiation process to find the first and second derivatives will not be accurate due to the discontinuity of signal in the adjacent time instances. For the case of Force

Model II, the correlation length in the defined covariance kernel of the Gaussian random forces is larger than zero. Thus the K-L components of nodal displacement will be smooth between two adjacent time instances. The corresponding derivatives can therefore be accurately calculated with the cubic spline interpolation technique and the variance of moving forces can finally be effectively identified.

3.6.3.2 Number of Samples Used

Results in Table 3.5 are promising, but the number of response samples required is quite large that might not be acceptable in engineering practice. The effect of reducing the number of response samples on the identification accuracy should be further investigated.

When the number of response samples decreases, the statistics of the responses may not be accurately represented by the limit number of samples, and the variance of the identified excitation forces may become inaccurate. Moreover, the variance of the identified forces will become unstable, i.e. identification based on a small and different group of response samples will lead to different results. The better the samples representing the statistics of the whole population, the more accurate variance can be identified. The relative error between the identified and the reference forces from different number of response samples is shown in Tables 3.6 and 3.7 for the case of Force Model I and Force Model II, respectively.

Results show that the relative errors in the mean value of the identified moving forces are quite small and they increase slightly with a decrease in the

sample number down to 10. The error in the variance of the identified moving forces increases with decreasing sample number. For the case of Force Model I, since the error in the differentiation of the K-L component of the nodal displacement is included, the relative errors in the variance of the identified excitation forces are very large especially when the number of samples becomes small. For the case of Force Model II, when the number of response samples used in the identification is smaller than 100, a relative large error in the variance occurs. The identified results become unstable as noted in Table 3.7 where the relative error for the case from 20 samples is larger than that for the case from 10 samples. This is true only when the group of 10 samples used in the identification can better represent the statistics of the response than the group of 20 samples used. The decrease in the number of response samples used in the identification will give rise to an inaccuracy in the variance of the identified forces and even in the identified mean force time histories when the COV_F is relatively large (e.g. larger than 0.5). The accuracy of the identified mean value will be further discussed in next Section and in Table 3.8 for the case of Force Model II.

3.6.3.3 Comparison with Existing Deterministic Moving Force Identification Method

The proposed method is used to study the same beam structure as in Law et al. (2004) but treating the excitation as a population including uncertainty. A comparison of the identified time history of the moving forces between the stochastic moving force identification technique and the deterministic one (Law et

al. 2004) from only one sample of bridge response will be conducted in this Section.

To clearly demonstrate the advantage of the stochastic force identification method with large uncertainties, the Force Model II with a high level of randomness in the excitation forces with $\Phi(\omega_0) = 64 \times 10^{-6} \text{ m}^3$ is adopted. The identified moving forces in the deterministic approach with only one response sample are compared with the reference forces in Figure 3.8. It should be noted that when only one response sample generated in the forward problem is used, different moving forces will be identified from response samples with different randomness included. The uncertainty in the response sample is propagated into the identified forces in the moving force identification. The percentage error in the identified moving forces by adopting the deterministic approach (Law et al. 2004) is $FE = 37.16\%$ according to Equation (3.40) which is very large. A comparison between the relative errors in the mean values of the identified moving forces from different number of samples is given in Table 3.8 where the case of “1 sample” denotes results from the deterministic moving force identification technique. Results in Table 3.8 show that the relative error in the identified forces increase significantly with increasing level of randomness. The deterministic approach almost fail to identify the moving forces when COV_F is large, e.g. larger than 0.5.

The identified results using the stochastic force identification method from both 10 and 100 samples are compared with those from the deterministic

approach in Figure 3.9 and Table 3.8. When 10 samples are used, the accuracy of the identified forces is significantly improved when the randomness in excitation forces is large, e.g. in the case when $\Phi(\omega_0)=4\times 10^{-6}$, 16×10^{-6} and $64\times 10^{-6} m^3$. For the case where the randomness in the excitation force is very small, e.g. when $\Phi(\omega_0)=1\times 10^{-6} m^3$, the accuracy of the identified forces is similar to that from the deterministic approach. This is because when the randomness in the responses is small, the averaging effect in the proposed approach is not so notable. For the case when the level of randomness is relatively high, e.g. $\Phi(\omega_0)=256\times 10^{-6} m^3$, large relative error is found because only 10 samples can not effectively eliminate the effect of uncertainties in the responses in this case. 100 samples may be noted to be sufficient and the relative error calculated from Equation (3.40) is $FE=5.41\%$ which is small. Results in the case when $\Phi(\omega_0)=256\times 10^{-6} m^3$ show that the uncertainties in the structural responses can be separated from the deterministic component through the averaging procedure. The identified time histories of the moving forces are very accurate when 100 samples are adopted compared with the erroneous results from only one sample. It is noted that when a relative large number of response samples, e.g. 100 samples, is used in the proposed method, the mean value of the identified moving forces is very accurate even with a high level of randomness in the response. The accuracy of the identified results is relatively not sensitive to the level of randomness. It may be concluded that the proposed moving force identification algorithm based on the uncertainty model could lead to more accurate identified results compared with

the existing deterministic method.

3.7 Summary

In this Chapter, both the dynamic analysis and the moving force identification with a beam-load model are performed. The bridge structure is modeled as a simply supported planar Euler-Bernoulli beam with random moving forces on top. These random moving forces are assumed as Gaussian random process. The Karhunen-Loève Expansion is adopted to represent both the random excitation forces and the structural response. The mathematical model for the beam-load system with random moving excitation forces is formulated based on which the forward analysis and the stochastic moving force identification technique are proposed. Two force models on the random excitations are adopted in the numerical simulation in which the proposed stochastic method is verified with MCS and the following conclusions are drawn.

The proposed method is found very accurate in the forward problem of response prediction with different levels of uncertainty and results are not sensitive to the level of randomness in the excitation forces. In the inverse force identification problem, the statistics of the random moving forces can be accurately identified from a set of samples of the structural response. The accuracy of identification is significantly improved with a small number of measured responses samples by the stochastic force identification approach when compared to that obtained from an existing deterministic method based on one sample of

measured response. The uncertainties in the measured responses can be largely removed from the mean values of the identified moving forces in the identification process when a relative large number of response samples are used. The mean value of the identified moving forces are very accurate even when the level of randomness in the response is high, and the accuracy of the identified results is relatively not sensitive to the level of randomness.

The method proposed in this Chapter can be extended to engineering application of a bridge-vehicle interaction problem in which the uncertainty in the excitation forces can be regarded as the uncertainty arising from the road surface roughness whereas the uncertainties in the system parameters of the bridge structure are neglected. This extension will be described in next Chapter. The proposed method is general to account for the errors caused by the surface roughness in the identification procedure. A significant advantage of the proposed approach is that it can identify mean force time histories which are free of most of the effect of random errors arising from the environmental factors while the propagation of these random errors in the identification procedure is noted in the variance of identified value of each time instance in the time duration studied.

Table 3.1 - Relative error in the statistics of the mid-span displacement with uncertainty in excitation (Force Model I)

<i>RE</i> (%)	<i>COV_F</i>			
	1%	2%	5%	10%
Mean Value	0.01%	0.01%	0.04%	0.06%
Variance	3.43%	3.63%	3.48%	4.94%

Table 3.2 - Relative error in the statistics of the mid-span displacement with different threshold for truncation

	Threshold <i>B</i> for truncation					
	10^0	10^5	10^6	10^7	10^8	
Number of K-L components	136	129	58	19	6	
Time Cost (s)	38.95	37.93	33.62	31.96	31.16	
<i>RE</i> (%)	Mean Value	0.33%	0.33%	0.33%	0.33%	0.33%
	Variance	1.62%	1.67%	1.98%	2.29%	20.08%

Table 3.3 - Relative error in the statistics of the mid-span displacement with uncertainty in excitation (Force Model II)

<i>RE</i> (%)	Different level of randomness $\Phi(\omega_0)$ ($10^{-6} m^3$)				
	1	4	16	64	256
Mean value	0.03%	0.12%	0.15%	0.16%	0.49%
Variance	0.89%	1.57%	1.66%	1.76%	1.93%

Table 3.4 - Relative error in the statistics of the identified forces with different uncertainty (Force Model I)

<i>FE</i> (%)	<i>COV_F</i>				
	1%	2%	5%	10%	
Force (deterministic)	11.35%	11.42%	11.54%	12.04%	
500 samples	Mean value	3.58%	3.58%	3.58%	3.58%
	Variance	39.73%	40.03%	39.90%	39.97%

Table 3.5 - Relative error in the statistics of the identified forces with different uncertainty (Force Model II)

<i>FE</i> (%)	Different level of randomness $\Phi(\omega_0)$ (10^{-6} m^3)				
	1	4	16	64	256
Mean value	3.58%	3.58%	3.59%	3.60%	3.62%
Variance	6.91%	6.96%	8.59%	5.80%	6.29%

Table 3.6 - Relative error in the identified forces using different number of response samples (Force Model I)

<i>FE</i> (%)	Number of response samples used					
	10	20	50	100	200	500
Mean value	4.27%	4.13%	3.76%	3.74%	3.67%	3.58%
Variance	*64.75%	*48.50%	42.92%	41.79%	40.19%	39.97%

*-denotes the results become unstable.

Table 3.7 - Relative error in the identified forces using different number of response samples (Force Model II)

<i>FE</i> (%)	Number of response samples used					
	10	20	50	100	200	500
Mean value	5.03%	4.88%	5.34%	3.72%	3.69%	3.59%
Variance	*29.22%	*34.58%	21.28%	14.58%	10.92%	8.59%

* denotes the results become unstable.

Table 3.8 - Relative error in the mean value of the identified moving forces with different approaches (Force Model II)

<i>FE</i> (%)	Different level of randomness $\Phi(\omega_0)$ (10^{-6} m^3)				
	1	4	16	64	256
Deterministic method (1 sample)	3.94%	10.01%	13.01%	37.16%	69.38%
Stochastic method (10 samples)	3.92%	3.89%	5.94%	9.90%	31.31%
Stochastic method (100 samples)	3.58%	3.79%	4.37%	4.32%	5.41%

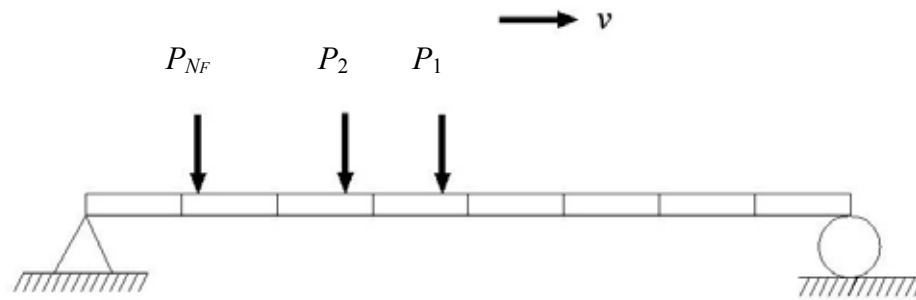


Figure 3.1 - Beam-load model

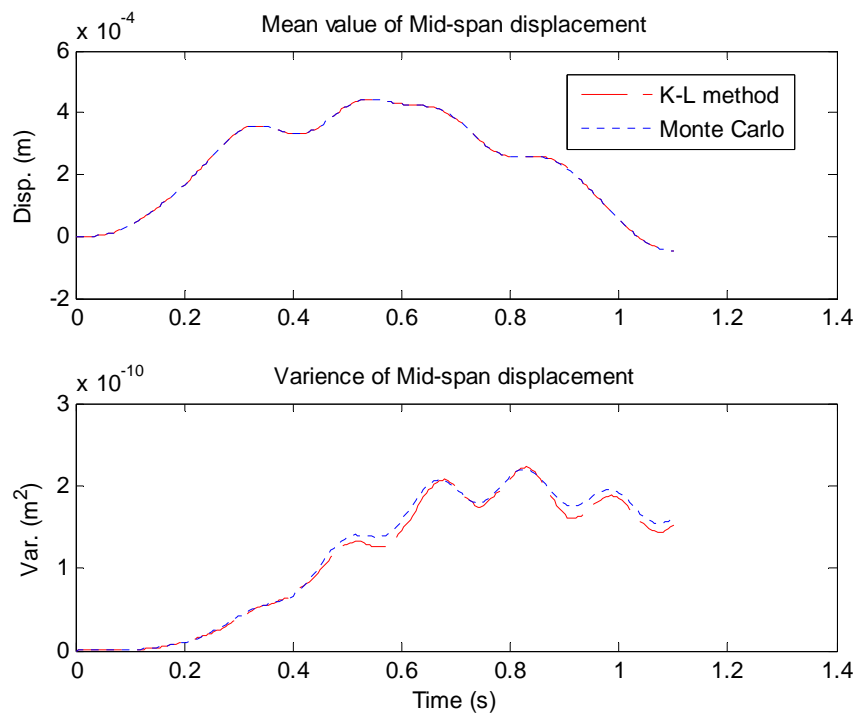


Figure 3.2 - Comparison of mid-span responses from the two methods (Force Model I)

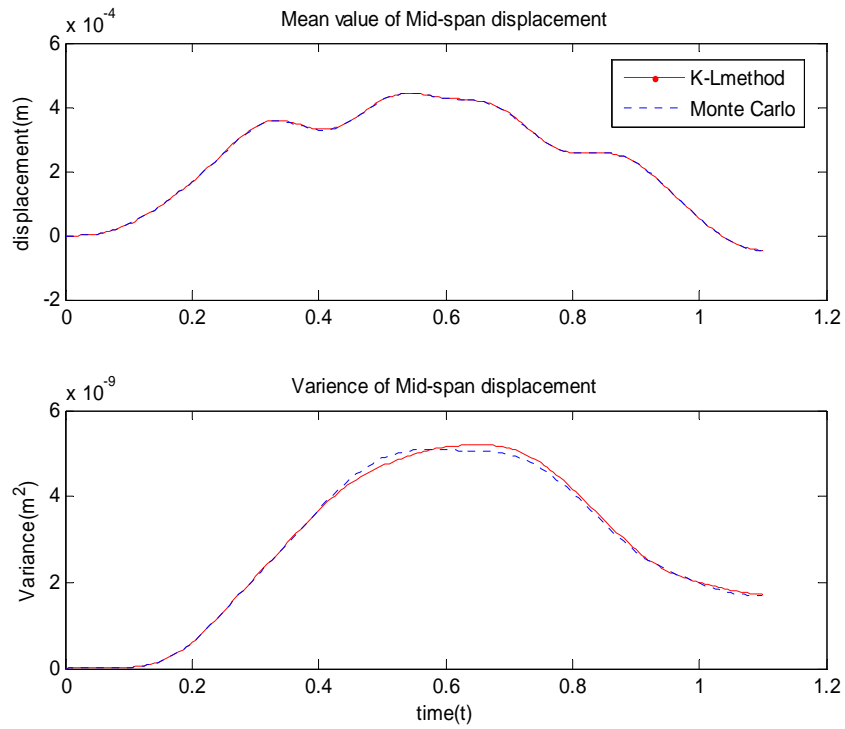


Figure 3.3 - Comparison of mid-span responses from the two methods (Force Model II)

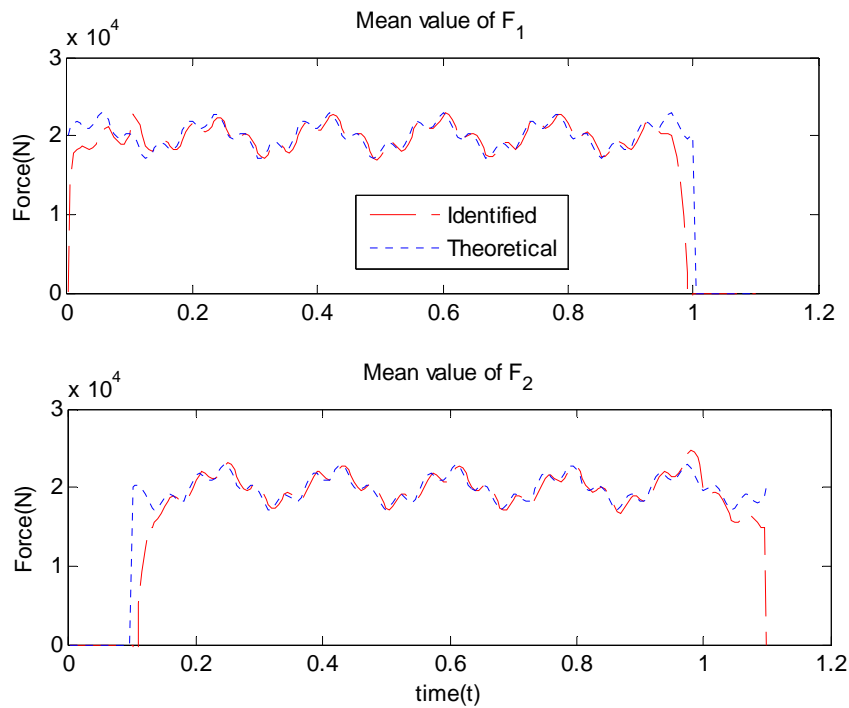


Figure 3.4 - Mean value of identified forces from 500 samples (Force Model I)

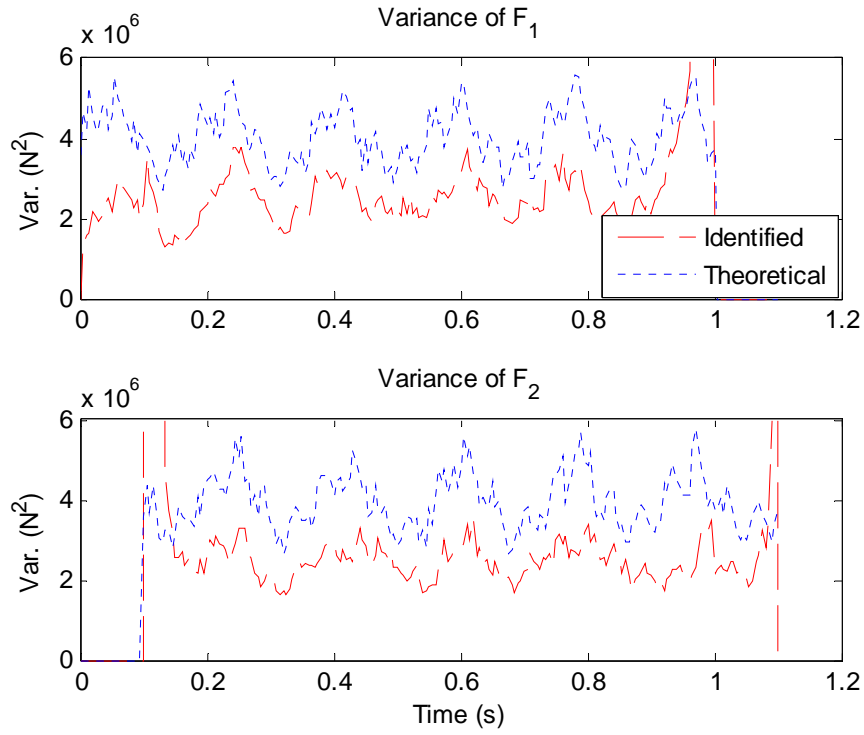


Figure 3.5 - Variance of identified forces from 500 samples (Force Model I)

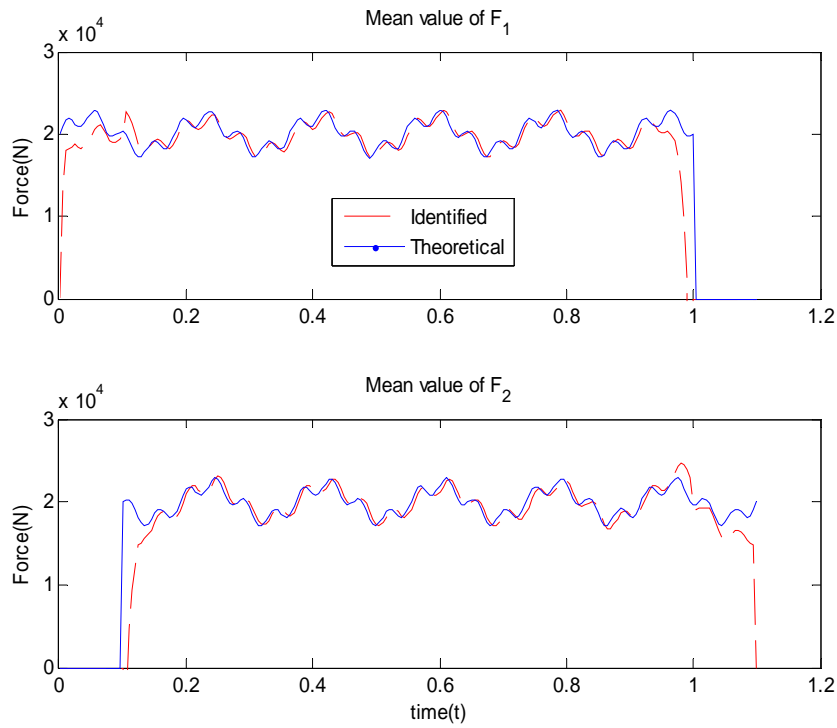


Figure 3.6 - Mean value of identified forces from 500 samples (Force Model II)

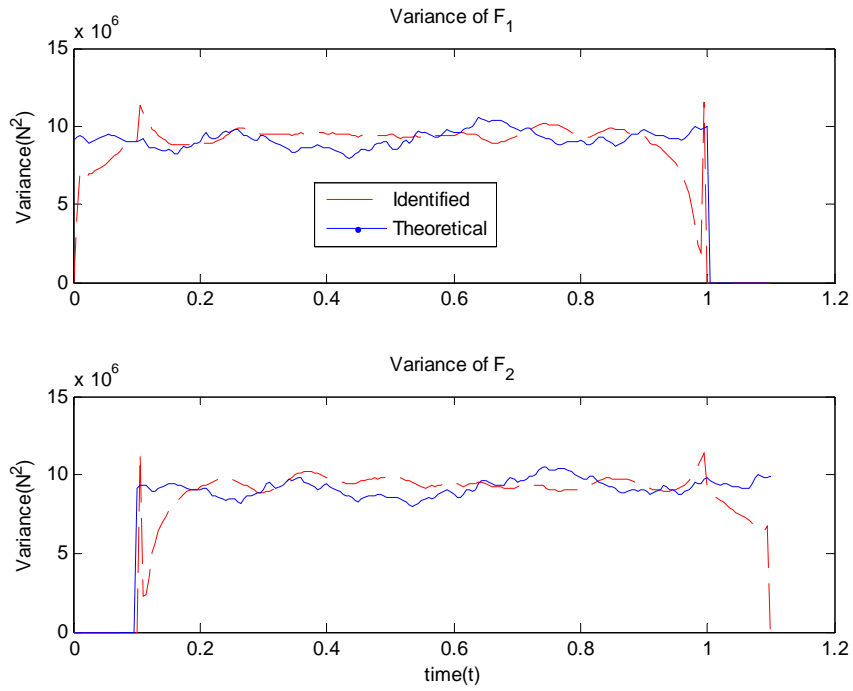


Figure 3.7 - Variance of identified forces from 500 samples (Force Model II)

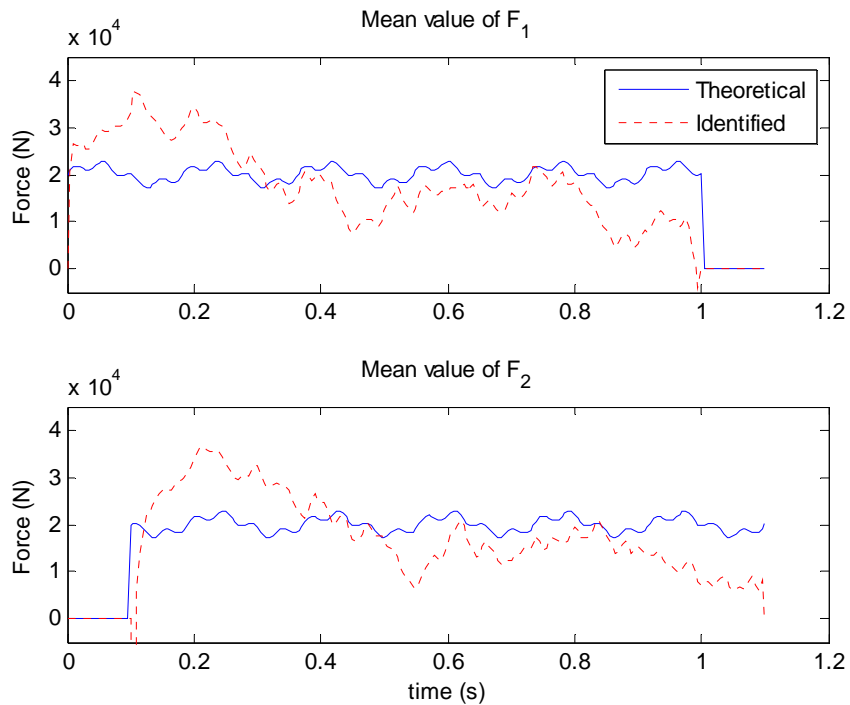


Figure 3.8 - Identified force time histories from a deterministic approach (Force Model II)

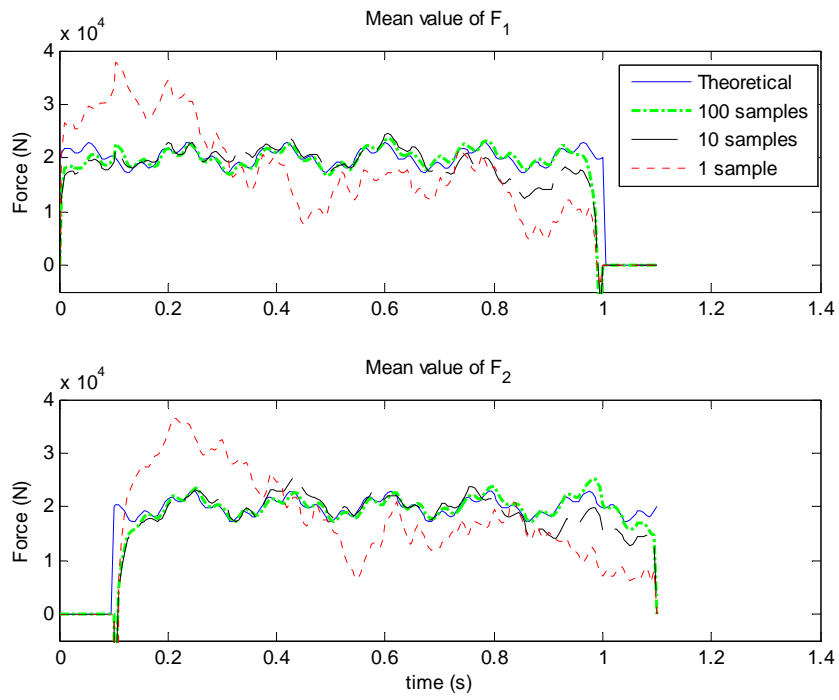


Figure 3.9 - Comparison of the identified force time histories from different approaches (Force Model II)

CHAPTER 4

BRIDGE-VEHICLE INTERACTION WITH UNCERTAINTY IN EXCITATION

4.1 Introduction

The beam-load model in Chapter THREE provides a theoretical background to investigate the problem of bridge-vehicle interaction problem. The disadvantage of adopting the moving forces to simulate the vehicle axle loads is that inertia effect of the moving force model can not be appropriately modeled. Moving mass model is one alternative which, however, tend to introduce too much rigidity into the vehicle model. The mass-spring systems such as the quarter car model (Schenk et al. 2002; Xiang et al. 2007), half car model (Law et al. 2004; Pinaew 2006), tractor-trailer model (Mulcahy 1983; Law and Zhu 2005), three dimensional vehicle model (Liu et al. 2002; Kim et al. 2005), etc., which are capable of modeling more complex and practical vehicle axle loads, have been widely adopted in the bridge-vehicle interaction problem. By modeling the vehicle with mass-spring system, the road surface roughness which is one of the most important factors can be introduced in the bridge-vehicle interaction problem. Da Silva (2004) concluded that the effects due to the interaction of the vehicles with an irregular pavement surface are much more important than those

produced by the load mobility alone and these effects are even larger than those due to the static presence of the vehicles in some cases.

In this Chapter, a new bridge-vehicle interaction model will be introduced in which the bridge is modeled as a simply supported planar Euler-Bernoulli beam with a vehicle moving on top modeled by a four degrees-of-freedom mass-spring system. The road surface roughness is assumed as Gaussian random process and it will be represented by the Karhunen-Loève Expansion. By representing the Gaussian random process involved, the equation of motion of the bridge-vehicle system becomes a set of ordinary differential equations which can be easily solved by any numerical methods such as the Newmark- β method and the response statistics of the bridge can be evaluated. Based on the model formulated, a stochastic force identification algorithm is proposed in which the statistics of the moving interaction forces can be accurately identified from a set of random samples of responses of the bridge deck. Numerical simulations are conducted in which the Gaussian assumption for the road surface roughness, the response statistics calculation and the new stochastic force identification technique based on the proposed stochastic bridge-vehicle model are verified.

The outline of this Chapter is as follows: the equation of motion of the bridge-vehicle system will be introduced in Section 4.2. The formulations of a bridge-vehicle system with the road surface roughness modeled as a Gaussian random process is given in Section 4.3 with discussions on the response statistics. Numerical simulations are conducted in Section 4.4 with the verification of the

proposed technique and studies on the effect of different influencing factors in practice which may affect the accuracy of the proposed analysis approach. A discussion on the possibility of adopting the contaminated response data for random interaction forces identification is presented in Section 4.5. A summary is given in Section 4.6.

4.2 Modeling of the Bridge-Vehicle System

4.2.1 The Vehicle Model

A vehicle with four degrees-of-freedom moving at a uniform speed v over a simply-supported beam-like bridge deck is shown in Figure 4.1. The equation of motion of the vehicle is derived using the Lagrange formulation as follows (Law et al. 2004):

$$\begin{bmatrix} \mathbf{M}_{V1} & 0 \\ 0 & \mathbf{M}_{V2} \end{bmatrix} \ddot{\mathbf{Y}} + \begin{bmatrix} \mathbf{C}_{V11} & \mathbf{C}_{V12} \\ \mathbf{C}_{V21} & \mathbf{C}_{V22} \end{bmatrix} \dot{\mathbf{Y}} + \begin{bmatrix} \mathbf{K}_{V11} & \mathbf{K}_{V12} \\ \mathbf{K}_{V21} & \mathbf{K}_{V22} \end{bmatrix} \mathbf{Y} = -\begin{Bmatrix} 0 \\ \mathbf{F}(t, \theta) \end{Bmatrix} + \begin{Bmatrix} 0 \\ \mathbf{F}_0 \end{Bmatrix} \quad (4.1)$$

where $\mathbf{Y} = \{y_V \theta_V y_1 y_2\}^T$ is the vector of displacement of the vehicle in which y_V and θ_V are the displacement and rotation of the vehicle body; y_1 and y_2 are the displacements of m_1 and m_2 , respectively. $\dot{\mathbf{Y}}$ and $\ddot{\mathbf{Y}}$ are the first two derivatives of \mathbf{Y} which represent the vector of the velocity and acceleration of the vehicle, respectively. \mathbf{M}_{V1} , \mathbf{M}_{V2} , \mathbf{C}_{V11} , \mathbf{C}_{V12} , \mathbf{C}_{V21} , \mathbf{C}_{V22} , \mathbf{K}_{V11} , \mathbf{K}_{V12} , \mathbf{K}_{V21} , \mathbf{K}_{V22} are the sub-matrices of mass, damping and stiffness matrices for the vehicle, respectively, which are given as follows.

$$\mathbf{M}_{V1} = \begin{bmatrix} m_v & 0 \\ 0 & I_v \end{bmatrix}; \quad \mathbf{M}_{V2} = \begin{bmatrix} m_1 & 0 \\ 0 & m_2 \end{bmatrix};$$

$$\begin{aligned}
\mathbf{C}_{V11} &= \begin{bmatrix} C_{s1} + C_{s2} & (-C_{s1}a_1 + C_{s2}a_2)S \\ (-C_{s1}a_1 + C_{s2}a_2)S & (C_{s1}a_1^2 + C_{s2}a_2^2)S^2 \end{bmatrix}; \\
\mathbf{C}_{V12} &= \begin{bmatrix} -C_{s1} & -C_{s2} \\ C_{s1}a_1S & -C_{s2}a_2S \end{bmatrix}; \quad \mathbf{C}_{V21} = \begin{bmatrix} -C_{s1} & C_{s1}a_1S \\ -C_{s2} & -C_{s2}a_2S \end{bmatrix}; \\
\mathbf{C}_{V22} &= \begin{bmatrix} C_{s1} & 0 \\ 0 & C_{s2} \end{bmatrix}; \quad \mathbf{K}_{V11} = \begin{bmatrix} K_{s1} + K_{s2} & (-K_{s1}a_1 + K_{s2}a_2)S \\ (-K_{s1}a_1 + K_{s2}a_2)S & (K_{s1}a_1^2 + K_{s2}a_2^2)S^2 \end{bmatrix}; \\
\mathbf{K}_{V12} &= \begin{bmatrix} -K_{s1} & -K_{s2} \\ K_{s1}a_1S & -K_{s2}a_2S \end{bmatrix}; \quad \mathbf{K}_{V21} = \begin{bmatrix} -K_{s1} & K_{s1}a_1S \\ -K_{s2} & -K_{s2}a_2S \end{bmatrix}; \\
\mathbf{K}_{V22} &= \begin{bmatrix} K_{s1} & 0 \\ 0 & K_{s2} \end{bmatrix}; \quad \mathbf{F}(t, \theta) = \begin{Bmatrix} F_1(t, \theta) \\ F_2(t, \theta) \end{Bmatrix}; \quad \mathbf{F}_0 = \begin{Bmatrix} (m_1 + a_2m_v)g \\ (m_2 + a_1m_v)g \end{Bmatrix}
\end{aligned}$$

where S is the axle spacing, $\{K_{si}, C_{si}, (i=1,2)\}$ are the stiffness and the damping of the two suspensions, m_v, I_v are the mass and the moment of inertia of the vehicle, m_1, m_2 are the masses of the bogie. a_1 and a_2 denote the dimensions of the vehicle as shown in Figure 4.1. \mathbf{F}_0 is the static load vector due to vehicle. $\mathbf{F}(t, \theta) = \{\mathbf{F}_1(t, \theta), \dots, \mathbf{F}_{NF}(t, \theta)\}^T$ is the vehicle-bridge interaction force vector with $N_F=2$, and

$$\begin{cases} F_1(t, \theta) = (m_1 + a_2m_v)g + K_{t1}(y_1 - w(\hat{x}_1(t), t, \theta) - r(\hat{x}_1(t), \theta)) \\ \quad + C_{t1}(\dot{y}_1 + \dot{w}(\hat{x}_1(t), t, \theta) + w'(\hat{x}_1(t), t, \theta)\dot{\hat{x}}_1(t) - r'(\hat{x}_1(t), \theta)\dot{\hat{x}}_1(t)) \\ F_2(t, \theta) = (m_2 + a_1m_v)g + K_{t2}(y_2 - w(\hat{x}_2(t), t, \theta) - r(\hat{x}_2(t), \theta)) \\ \quad + C_{t2}(\dot{y}_2 + \dot{w}(\hat{x}_2(t), t, \theta) + w'(\hat{x}_2(t), t, \theta)\dot{\hat{x}}_2(t) - r'(\hat{x}_2(t), \theta)\dot{\hat{x}}_2(t)) \end{cases} \quad (4.2)$$

where θ denotes the random dimension; $K_{t1}, K_{t2}, C_{t1}, C_{t2}$ are the stiffness and damping of the two tires, respectively; $r(x, \theta)$ is the road surface roughness at the location of tires which is assumed as a Gaussian random process; The mathematic model for the road surface roughness will be given in Section 4.3.1. $\hat{x}_1(t)$ and $\hat{x}_2(t)$ are the position of the front axle and rear axle respectively at time t , and g is the acceleration of gravity. $w(\hat{x}_i(t), t, \theta)$ is the stochastic vertical dynamic deflection of the bridge deck at the contact position of the i^{th} moving load at time t .

The over-dot ($\dot{\cdot}$) denotes the differentiation with respect to time t and the right prime ($'$) denotes the differentiation with respect to local coordinate x .

4.2.2 The Coupled Equation of Motion

Substituting Equation (4.2) into Equations (3.1) and (4.1), the combined equation of motion of the bridge-vehicle system can be obtained as

$$\mathbf{M}(t)\ddot{\mathbf{Z}}(t, \theta) + \mathbf{C}(t)\dot{\mathbf{Z}}(t, \theta) + \mathbf{K}(t)\mathbf{Z}(t, \theta) = \mathbf{P}(t, \theta) \quad (4.3)$$

where $\mathbf{Z}(t, \theta) = \{\mathbf{R}(t, \theta) \ \mathbf{Y}(t, \theta)\}^T$ is the vector of stochastic displacement of the bridge-vehicle system, similarly, $\dot{\mathbf{Z}}(t, \theta) = \{\dot{\mathbf{R}}(t, \theta) \ \dot{\mathbf{Y}}(t, \theta)\}^T$ and $\ddot{\mathbf{Z}}(t, \theta) = \{\ddot{\mathbf{R}}(t, \theta) \ \ddot{\mathbf{Y}}(t, \theta)\}^T$ are the vectors of stochastic velocity and acceleration, respectively; θ denotes the random dimension. $\mathbf{M}(t)$, $\mathbf{C}(t)$, $\mathbf{K}(t)$ are the time-varying matrices of the bridge-vehicle system. $\mathbf{P}(t, \theta)$ is the stochastic force vector acting on the system. Details of these matrices are shown as follows:

$$\mathbf{M}(t) = \begin{bmatrix} \mathbf{M}_b & 0 & \mathbf{H}_b \mathbf{M}_{V2} \\ 0 & \mathbf{M}_{V1} & 0 \\ 0 & 0 & \mathbf{M}_{V2} \end{bmatrix}; \quad \mathbf{C}(t) = \begin{bmatrix} \mathbf{C}_b & \mathbf{H}_b \mathbf{C}_{V21} & \mathbf{H}_b \mathbf{C}_{V22} \\ 0 & \mathbf{C}_{V11} & \mathbf{C}_{V12} \\ \mathbf{C}_t \mathbf{H}_b^T & \mathbf{C}_{V21} & \mathbf{C}_{V22} + \mathbf{C}_t \end{bmatrix};$$

$$\mathbf{K}(t) = \begin{bmatrix} \mathbf{K}_b & \mathbf{H}_b \mathbf{K}_{V21} & \mathbf{H}_b \mathbf{K}_{V22} \\ 0 & \mathbf{K}_{V11} & \mathbf{K}_{V12} \\ \mathbf{K}_t \mathbf{H}_b^T & \mathbf{K}_{V21} & \mathbf{K}_{V22} + \mathbf{K}_t \end{bmatrix}; \quad \mathbf{P}(t, \theta) = \begin{Bmatrix} \mathbf{H}_b \mathbf{F}_0 \\ 0 \\ 0 \\ \mathbf{f}(t, \theta) \end{Bmatrix};$$

$$\mathbf{f}(t, \theta) = \begin{Bmatrix} C_{t1} r'(\hat{x}_1(t), \theta) \dot{\hat{x}}_1(t) + K_{t1} r(\hat{x}_1(t), \theta) \\ C_{t2} r'(\hat{x}_2(t), \theta) \dot{\hat{x}}_2(t) + K_{t2} r(\hat{x}_2(t), \theta) \end{Bmatrix};$$

where $\mathbf{C}_t = \text{diag}(C_{t1}, C_{t2})$; $\mathbf{K}_t = \text{diag}(K_{t1}, K_{t2})$, and

$$\mathbf{H}'_b = \left\{ \begin{array}{ccccccc} 0 & \dots & 0 & \dots & \frac{\partial \mathbf{H}_1(x)}{\partial x} \Big|_{x=\hat{x}_1(t)} \dot{\hat{x}}_1(t) & \dots & 0 \\ 0 & \dots & 0 & \dots & 0 & \dots & 0 \\ 0 & \dots & 0 & \dots & 0 & \dots & 0 \\ 0 & \dots & \frac{\partial \mathbf{H}_{NF}(x)}{\partial x} \Big|_{x=\hat{x}_{NF}(t)} \dot{\hat{x}}_{NF}(t) & \dots & 0 & \dots & 0 \end{array} \right\}$$

Equation (4.3) is a set of stochastic ordinary differential equations which can not be directly solved by the Newmark- β method. The stochastic displacement of the bridge at position x and time t can be expressed as:

$$w(x, t, \theta) = \mathbf{H}(x)\mathbf{R}(t, \theta) \quad (4.4)$$

It is noted that Equation (4.4) is similar to Equation (3.5) except that the randomness has been included.

4.3 Bridge-Vehicle Interaction with Road Surface Roughness

4.3.1 The Road Surface Roughness

In ISO-8606 specification (ISO 8606:1995(E) 1995), the road surface roughness is related to the velocity of vehicle by a formula between the velocity power spectral density (PSD) and the displacement PSD. The general form of the displacement PSD of the road surface roughness is given as:

$$S_d(f) = S_d(f_0)(f/f_0)^{-\alpha} \quad (4.5)$$

where f_0 is the discontinuity frequency equal to $1/2\pi$ (cycle/m) and f is the spatial frequency in cycle/m. $S_d(f)$ is the Power Spectral Density (PSD) in $m^3/cycles$. $S_d(f_0)$ is the roughness coefficient in $m^3/cycles$. Equation (4.5) gives an estimate on the degree of roughness of the road by the $S_d(f_0)$ value. This classification is made by

assuming a constant vehicle velocity PSD and taking $\alpha=2$.

Based on this ISO specification, the road surface roughness in the time domain can be simulated by applying the inverse fast Fourier transformation on $S_d(f_0)$ as follows (Henchi et al. 1998)

$$r_k(x) = \sum_{k=1}^N \left(4S_d(f_0) \left(\frac{2\pi k}{L_c f_0} \right)^{-2} \frac{2\pi}{L_c} \right)^{1/2} \cos \left(\frac{2\pi k f_0}{L_c} x + \theta_k \right) \quad (4.6)$$

where L_c is, in general, twice the length of the bridge. θ_k is a set of independent random angle uniformly distributed between 0 and 2π . According to Equation (4.6), the samples of the road surface roughness $r_k(x)$ can be generated.

4.3.2 Forward Problem

In this Section, the irregular profiles of the road surface are assumed as samples from a Gaussian random process with a PSD defined in Section 4.3.1. According to the theory of the Karhunen-Loève Expansion introduced in Section 3.3, the road surface roughness can be represented by its K-L components as

$$r(x, \theta) = \sum_{j=1}^{k_r} \xi_j(\theta) r^{(j)}(x) \quad (4.7)$$

where $\xi_j(\theta)$ are the standard Gaussian random variables with the orthogonal properties shown in Equation (3.11); θ denotes the random dimension; $r^{(j)}(x)$ is the j^{th} K-L components of the road surface roughness. k_r is the number of the K-L components of the road surface roughness after truncation. The first derivative of $r(x, \theta)$ with respect to location x is given as

$$r'(x, \theta) = \sum_{j=1}^{k_r} \xi_j(\theta) r'^{(j)}(x) \quad (4.8)$$

The random interaction forces $\mathbf{f}(t, \theta)$ due to the road surface roughness acting on the bridge-vehicle system are obtained as

$$\mathbf{f}(t, \theta) = \sum_{j=1}^{k_r} \mathbf{f}^{(j)}(t) \xi_j(\theta) \quad (4.9)$$

$$\text{where } \mathbf{f}^{(j)}(t) = \begin{Bmatrix} C_{t1} r'^{(j)}(\hat{x}_1(t)) \dot{\hat{x}}_1(t) + K_{t1} r'^{(j)}(\hat{x}_1(t)) \\ C_{t2} r'^{(j)}(\hat{x}_2(t)) \dot{\hat{x}}_2(t) + K_{t2} r'^{(j)}(\hat{x}_2(t)) \end{Bmatrix}$$

Based on the superposition principle of the linear system and the representation of the random excitation forces as a sum of independent components according to Equation (4.9), the stochastic nodal displacement vector of the bridge and vehicle denoted as $\mathbf{R}(t, \theta)$ and $\mathbf{Y}(t, \theta)$, respectively, can be expanded with the following forms,

$$\mathbf{R}(t, \theta) = \sum_{j=0}^{k_z} \xi_j(\theta) \mathbf{R}^{(j)}(t) \quad (4.10)$$

$$\mathbf{Y}(t, \theta) = \sum_{j=0}^{k_z} \xi_j(\theta) \mathbf{Y}^{(j)}(t) \quad (4.11)$$

Combining Equations (4.10) and (4.11),

$$\mathbf{Z}(t, \theta) = \sum_{j=0}^{k_z} \xi_j(\theta) \mathbf{Z}^{(j)}(t) \quad (4.12)$$

where $\mathbf{Z}^{(j)}(t) = \{\mathbf{R}^{(j)}(t) \ \mathbf{Y}^{(j)}(t)\}^T$ and $k_z = k_r$. k_z is the number of the corresponding components of the stochastic nodal displacement vector of the bridge-vehicle system; $\mathbf{R}^{(j)}(t)$, $\mathbf{Y}^{(j)}(t)$ and $\mathbf{Z}^{(j)}(t)$ are vectors of the deterministic component of the nodal displacement of the bridge, vehicle and the whole coupled system, respectively. It is noted that the corresponding expansion for the nodal responses

of the bridge-vehicle system contains the *zero*th component ($j=0$) which represents the nodal responses due to deterministic moving vehicle axle loads.

Taking the derivatives with respect to time t in Equation (4.12), the corresponding component vectors for the nodal velocity and nodal acceleration in the bridge-vehicle system respectively can be represented as,

$$\dot{\mathbf{Z}}(t, \theta) = \sum_{j=0}^{k_Z} \xi_j(\theta) \dot{\mathbf{Z}}^{(j)}(t) \quad (4.13)$$

$$\ddot{\mathbf{Z}}(t, \theta) = \sum_{j=0}^{k_Z} \xi_j(\theta) \ddot{\mathbf{Z}}^{(j)}(t) \quad (4.14)$$

Substituting Equations (4.9) and (4.12) to (4.14) into Equation (4.3) and taking the inner product of both side of the equations with $\xi_k(\theta)$, and employing the orthogonal property demonstrated in Equation (3.11), Equation (4.3) can be rewritten as

$$\mathbf{M}(t)\ddot{\mathbf{Z}}^{(k)}(t) + \mathbf{C}(t)\dot{\mathbf{Z}}^{(k)}(t) + \mathbf{K}(t)\mathbf{Z}^{(k)}(t) = \mathbf{P}^{(k)}(t), \quad (k=0, \dots, k_Z) \quad (4.15)$$

where $\mathbf{P}^{(0)} = \{\mathbf{H}_b \mathbf{F}_0 \ 0 \ 0\}^T$ and $\mathbf{P}^{(k)} = \{0 \ 0 \ \mathbf{f}^{(k)}(t)\}^T$, $k=1, \dots, k_Z$.

Compared with Equation (4.3), Equation (4.15) is a set of deterministic ordinary differential equations which can be solved by any numerical methods such as the Newmark- β method. The first two statistics of the displacements of the vehicle can be evaluated as

$$MEAN_{\mathbf{Z}}(t) = \mathbf{Z}^{(0)}(t), \quad VAR_{\mathbf{Z}}(t) = \sum_{j=1}^{k_Z} \left(\mathbf{Z}^{(j)}(t) \right)^2 \quad (4.16)$$

where the subscript “ \mathbf{Z} ” denotes the nodal displacement vector for the bridge-vehicle system. The mean value and variance of the nodal displacement under the bridge deck at position x and time t can be obtained according to

Equation (4.4) as

$$MEAN_w(x, t) = \mathbf{H}(x)\mathbf{R}^{(0)}(t), \quad VAR_w(x, t) = \sum_{j=1}^{k_r} (\mathbf{H}(x)\mathbf{R}^{(j)}(t))^2 \quad (4.17)$$

where the subscript “w” denotes the random displacement under the bridge deck..

4.3.3 Inverse Problem: Moving Force Identification

An inverse procedure can be formulated based on the bridge-vehicle interaction model formulated in the forward problem. The response statistics of the interaction forces between the bridge and vehicle can be identified indirectly from samples of the “measured” responses of the bridge. Any kind of responses of the bridge structure, e.g. displacement, strain, velocity and acceleration, can be adopted in the force identification. Though in practice, the strain and acceleration signals are more frequently used, the displacement signals are however adopted in this study. It should be noted that the displacements of bridge $w(x, t, \theta)$ can be obtained according to the following relationship from the strain $\varepsilon(x, t, \theta)$,

$$\varepsilon(x, t, \theta) = -z \frac{\partial^2 w(x, t, \theta)}{\partial x^2} \quad (4.18)$$

where z represents the distance from the neutral axis of the beam cross-section to the strain gauge.

Suppose that a set of displacements $\hat{w}(x_i, t_j, \theta_k)$ (or strains $\hat{\varepsilon}(x_i, t_j, \theta_k)$) is measured from the bridge, where $i=1, \dots, N_m, j=1, \dots, N_T, k=1, \dots, N_\theta$. N_m, N_T and N_θ are the number of the measurement points, time instants and samples,

respectively. The nodal displacement vector of the bridge $\hat{\mathbf{R}}(t, \theta)$ can be obtained from Equation (4.4) (or together with Equation (4.18) in case the strains are used). Assuming the responses along the random dimension θ at each node and each time instance are Gaussian distributed, samples of the nodal displacements vector of the bridge $\hat{\mathbf{R}}(t, \theta)$ can be represented by a small number of its K-L components according to the theory introduced in Section 3.3.2 as

$$\hat{\mathbf{R}}(t, \theta) = \sum_{j=0}^{\hat{k}_R} \xi_j(\theta) \hat{\mathbf{R}}^{(j)}(t) \quad (4.19)$$

where \hat{k}_R is the number of K-L components of the stochastic nodal displacement after truncation.

The corresponding components for the vectors of the stochastic nodal velocities $\dot{\hat{\mathbf{R}}}^{(j)}(t)$ and nodal accelerations $\ddot{\hat{\mathbf{R}}}^{(j)}(t)$ of the bridge model are obtained from the K-L components of nodal displacement $\hat{\mathbf{R}}^{(j)}(t)$ by differentiation using the cubic spline interpolation technique as

$$\dot{\hat{\mathbf{R}}}(t, \theta) = \sum_{j=0}^{\hat{k}_R} \xi_j(\theta) \dot{\hat{\mathbf{R}}}^{(j)}(t) \quad (4.20)$$

$$\ddot{\hat{\mathbf{R}}}(t, \theta) = \sum_{j=0}^{\hat{k}_R} \xi_j(\theta) \ddot{\hat{\mathbf{R}}}^{(j)}(t) \quad (4.21)$$

Due to the superposition principle of the linear system and the orthogonal property of the K-L components, the random excitation force $\hat{\mathbf{P}}(t, \theta)$ can also be represented as

$$\hat{\mathbf{P}}(t, \theta) = \sum_{j=0}^{\hat{k}_p} \xi_j(\theta) \hat{\mathbf{P}}^{(j)}(t) \quad (4.22)$$

where $\hat{\mathbf{P}}^{(j)}(t)$ are the corresponding components of the random interaction forces to be identified and $\hat{k}_p = \hat{k}_R$. It should be noted that both the components and the number of these components for both the bridge responses and the interaction forces in inverse problem are different from those in the forward problem. The number of the K-L components in forward problem, which is truncated when the eigenvalue λ_i in Equation (3.9) is much smaller than the rest, is dependent on the properties of the random process to be represented, i.e. the closer the random process to white noise, the more terms are required in its expansion.

Substituting Equations (4.19) to (4.22) into the equation of motion of the condensed bridge structure in the inverse problem and taking the inner product of both sides of the equation with $\zeta_k(\theta)$, and then employing the orthogonal property demonstrated in Equation (3.11), we have

$$\hat{\mathbf{M}}_b \ddot{\hat{\mathbf{R}}}^{(k)}(t) + \hat{\mathbf{C}}_b \dot{\hat{\mathbf{R}}}^{(k)}(t) + \hat{\mathbf{K}}_b \hat{\mathbf{R}}^{(k)}(t) = \hat{\mathbf{H}}_b \hat{\mathbf{P}}^{(k)}(t), \quad k=0, \dots, \hat{k}_p \quad (4.23)$$

where $\hat{\mathbf{M}}_b$, $\hat{\mathbf{C}}_b$, $\hat{\mathbf{K}}_b$ and $\hat{\mathbf{H}}_b$ are the mass, damping, stiffness and location matrices respectively of the condensed bridge structure in the inverse problem. In this study, the Improved Reduced System (IRS) reduction scheme (O' Callahan 1989) is adopted and the expressions of these condensed matrices have been shown in Equation (3.36).

From Equation (4.23), the corresponding components in the expansion of the random interaction forces $\hat{\mathbf{P}}^{(k)}(t)$ can be identified using the least-squares method as

$$\hat{\mathbf{P}}^{(k)}(t) = \left(\hat{\mathbf{H}}_b^T \hat{\mathbf{H}}_b \right)^{-1} \hat{\mathbf{H}}_b^T \mathbf{U}^{(k)}(t) \quad (4.24)$$

where $\mathbf{U}^{(k)}(t) = \hat{\mathbf{M}}_b \ddot{\hat{\mathbf{R}}^{(k)}}(t) + \hat{\mathbf{C}}_b \dot{\hat{\mathbf{R}}^{(k)}}(t) + \hat{\mathbf{K}}_b \hat{\mathbf{R}}^{(k)}(t)$.

The response statistics of the identified random interaction forces are obtained as

$$MEAN_{\mathbf{P}}(t) = \hat{\mathbf{P}}^{(0)}(t), \quad VAR_{\mathbf{P}}(t) = \sum_{j=1}^{\hat{k}_p} \left(\hat{\mathbf{P}}^{(j)}(t) \right)^2 \quad (4.25)$$

where the subscript ‘‘P’’ denotes the random interaction force vector.

4.4 Numerical Simulation

4.4.1 Bridge-vehicle Model

The parameters of the bridge-vehicle model for the numerical simulation are shown in Table 4.1. The traveling velocity of vehicle is 20 *m/s*. The bridge model is divided into eight Euler-Bernoulli finite elements each of 3.75 *m* length. The first five natural frequencies are 3.9 ,15.6 ,35.1 ,62.5 and 97.6 *Hz*. The sampling rate for all the simulations is 200 *Hz* which can capture the response of the first five natural modes of the beam. The bridge responses used for moving force identification are obtained from the forward analysis either using the K-L method from Equation (4.15) or using the Monte Carlo Simulation (MCS).

4.4.2 Verification of the Proposed Stochastic Approach

4.4.2.1 Gaussian Assumption of the Road Surface Roughness

It is not easy to obtain the distribution of the set of samples $r_k(x)$ theoretically from Equation (4.6) where a Gaussian assumption may not be

appropriate. A theoretical background of the correctness of Gaussian assumption to the road surface roughness was provided in the work by Shinozuka and Deodatis (1991). However, in this Section, a numerical study is provided to demonstrate the appropriateness of the Gaussian assumption to the road surface roughness. The Class A road with $S_d(f_0) = 6 \times 10^{-6} \text{ m}^3/\text{cycles}$ is assumed in the following studies except in Section 4.4.4 where different classes of road profiles will be investigated.

Ten thousand samples of the irregular road surface profile are generated to represent the random process $r(x, \theta)$. The uniformly distributed random angle θ_k is represented by a random number between zero to one with the command ‘*rand*’ in MATLAB. The values at an arbitrary position denoted as x_1 on the road surface profile along the random dimension forms a set of samples from the population of the corresponding random variable $r(x_1, \theta)$. The statistics of the random variable $r(x_1, \theta)$ are compared with the corresponding Gaussian random variable with the same mean value and standard deviation. Comparisons between these two kinds of random variables at the 1/4 span, mid-span and 3/4 span are shown in Figure 4.2 in which the Probability Density Function (PDF) and the Cumulative Density Function (CDF) of the generated samples are denoted by the dash lines and those from the corresponding Gaussian variables are represented by solid lines. Results show that the PDF and the CDF for the road surface roughness are very close to those for the corresponding Gaussian random variables. The assumption of the Gaussian random process for the road surface

roughness is thus demonstrated to be appropriate.

4.4.2.2 Forward Problem: The Statistics of Response

The statistics of the bridge response calculated from the algorithm proposed in Section 4.3.2 will be compared with results from the MCS. Ten thousand samples of the irregular road surface profile generated according Equation (4.6) is adopted for both methods.

In the K-L method proposed in Section 4.3.2, 10000 samples of the random excitation forces $\mathbf{f}(t, \theta)$ are obtained from samples of the irregular road surface profile. The KLE is applied to $\mathbf{f}(t, \theta)$ according to the theory introduced in Section 3.3.2. The K-L components when the eigenvalue λ_i in Equation (3.9) is less than unity, which are much smaller than the rest, are truncated. A total number of 106 K-L components is retained after truncation to represent 10000 samples of random forces. For each of the K-L components of the random interaction forces in Equation (4.9), Newmark- β method is employed to calculate the corresponding components of the stochastic nodal displacement, velocity and acceleration vectors denoted by $\mathbf{Z}^{(k)}(t)$, $\dot{\mathbf{Z}}^{(k)}(t)$ and $\ddot{\mathbf{Z}}^{(k)}(t)$ respectively at each time step. A total of 500 samples of seven displacements evenly distributed under the bridge deck are generated by using Latin Hypercube Sampling (LHS) technique for comparison of the statistics of response with the MCS.

In the MCS, samples of bridge response are obtained from the deterministic time response analysis according to Equation (4.3) by neglecting the random dimension. A comparison of the statistics of the mid-span displacement under the

bridge deck from the two methods is shown in Figure 4.3. The relative errors between the mean value and variance from the two methods according to Equation (3.39) are 0.04% and 2.13%, respectively. Results from the two methods are in good agreement which indicates that the proposed method is accurate and the Gaussian assumption for the road surface roughness is appropriate for the study. Compared with the MCS, the proposed K-L method is much faster. The time required in the calculation of the response statistics using the K-L method is 173.14 *s* compared with 1769.43 *s* required by the Monte Carlo Simulation for 10000 runs on a computer with Inter(R) Core(TM)2 Duo CPU 2.66 *Hz* with 4GB RAM.

4.4.2.3 Inverse Problem: Identify the Statistics of the Interaction Forces

In the force identification, two sets of 500 samples of seven evenly distributed displacements of the bridge deck are adopted with one from the MCS and another from the KLE of the random nodal displacements in which the samples of standard Gaussian random variables are generated with the LHS. The Improved Reduced System (IRS) reduction scheme (O’Callahan 1989) is employed in the identification procedure to reduce the system matrices \mathbf{M}_b , \mathbf{C}_b , \mathbf{K}_b as well as the location matrix \mathbf{H}_b from 16 degrees-of-freedom (*dofs*) to only seven translational *dofs*. When the eigenvalue λ_i in the KLE is less than 10^{-20} , the corresponding K-L components of the random nodal displacements vector $\hat{\mathbf{R}}(t, \theta)$ are truncated. A total of 111 number of K-L components after truncation

is retained in this case. The cubic spline interpolation technique is employed to calculate the corresponding components in the nodal velocities and accelerations vectors of the bridge structure by Equations (4.20) and (4.21) from the K-L components of the nodal displacement vector in Equation (4.19). The corresponding components of the interaction forces can be obtained from least-squares estimation according to Equation (4.24). The mean value and variance of the interaction forces can be obtained according to Equation (4.25). The theoretical statistics of the interaction forces serve as reference are calculated from 10000 samples of the bridge displacements and their derivatives obtained from the MCS in the forward analysis.

A comparison of mean value and variance of the theoretical and the identified interaction forces is shown in Figures 4.4 and 4.5, respectively. Due to the relatively large error in the identified interaction forces when the vehicle axle loads enter and leave the bridge span (e.g. see Figure 4.4), the relative error FE calculated for the whole time history will be relatively large. Since the error is stable in the remaining period of the time history, only the data from 0.05s-1.45s after entry of the first axle for the front axle force and 0.25s-1.65s after the entry of the rear axle for the rear axle force will be included in the error analysis of this study. The relative errors in the mean value and variance between the theoretical and identified interaction forces according to Equation (3.40) are listed in Table 4.2. Results show good agreement of the identified statistics of the interaction forces from the two methods. For the K-L method proposed in Section 4.3.3, the

identified statistics of the interaction forces using the two kinds of samples are very closed to each other which indicates the displacement samples calculated from the MCS approximately form a discretized Gaussian random process, i.e. the random response of the bridge deck in this case can be assumed as Gaussian distributed.

The mean values of the identified interaction forces are noted to have small fluctuations and they are close to the equivalent static axle loads. This fluctuation arises from the vibration of vehicular system acting on the bridge deck and the effect of the road surface roughness. The former would be dependent on the stiffness combination of the vehicle and bridge systems, but it would be in general much smaller than that due to the road surface roughness. The stochastic modeling of the road surface roughness in this paper results in the fact that the “dynamic” components due to road surface roughness in the existing deterministic analysis method become “stochastic” components and are represented in the variance of the identified forces. Therefore, only the fluctuations due to the vehicular system have been included in the mean values of the identified interaction forces which are shown to be relatively small.

4.4.3 Number of the Samples Used

In practical application of the algorithm, the number of samples of the responses used in the identification is a very important factor to be considered. It is obvious that 500 samples of the response signals are too many to obtain in the

field test, while for a stochastic identification algorithm without the assumption of the ergodicity in the response samples, using a small number of displacement samples in the force identification may fail to represent the statistics of the random process leading to poor results in the variance of the identified interaction forces.

The influence of the number of samples used on the accuracy of the identified force statistics is investigated with results shown in Table 4.3. Samples of the bridge displacements are generated from the forward analysis with Monte Carlo Simulation. The error in the mean value increases slightly with a decrease in the sample number while error in the variance increases slightly with decreasing sample number down to 50 and it goes up dramatically with further decrease in the sample number. When the sample number is less than 20, poor results are obtained due to the failure of representing the statistics of the whole population and the variance of the identified moving forces become unstable, i.e. different groups of samples will result in different variance of the identified force. In the following study, 50 samples of the displacement from the forward analysis with MCS will be adopted in the force identification.

It is noted that samples of the bridge displacement from the same population may require the same vehicle to run over the bridge for many times which may not be feasible for all the situations in practice. The possibility of getting more samples from a set of over-provided sensors has been considered. But the measured data from one measurement contains only one sample information of the road roughness. Since all sensors are dependent, therefore the different combinations of responses from the sensor set may not be able to provide more

statistical information. The problem on how to get the required number of measurement samples in an efficient way would need to be solved in future.

4.4.4 The Effect of Road Surface Roughness

In previous Sections of the numerical simulations in this Chapter, Class *A* road with $S_d(f_0) = 6 \times 10^{-6} \text{ m}^3/\text{cycles}$ has been adopted. A further study will be conducted to investigate the application of the proposed identification algorithm with different classes of road profiles in this Section. The road classifications according to the ISO specification is based on the value of roughness coefficient $S_d(f_0)$. Five classes of road representing different qualities of the road surface are studied. They are classified as *A*=very good, *B*=good, *C*=average, *D*=poor, *E*=very poor with the value of roughness coefficient $S_d(f_0)$ equals to 6×10^{-6} , 16×10^{-6} , 64×10^{-6} , 256×10^{-6} and $1024 \times 10^{-6} \text{ m}^3/\text{cycles}$, respectively. Typical irregular pavement profiles are shown in Figure 4.6.

The relative errors between the reference and identified interaction forces with different classes of road are listed in Table 4.4. Results show that the relative error in the mean value increases slightly with the decrease of the quality of the road surface, while the relative error in the variance is not sensitive to the road class. When the quality of the road surface decreases, the coefficient of variation (COV) of the bridge response due to vehicle excitations will increase. The accuracy of the mean value of the identified interaction forces is slightly affected by the quality of the road surface. The identified and reference mean value and variance of the interaction forces from the Class *E* road are compared

in Figures 4.7 and 4.8. The reference values are obtained from the MCS in which 10000 samples of bridge displacement are adopted to identify the corresponding samples of the interaction forces. It can be seen that though the shape of the variance of the identified interaction forces in the case with Class *E* road shown in Figure 4.8 is different from that with Class *A* road shown in Figure 4.5, the relative error shown in Table 4.4 is not sensitive to different classes of road. The maximum Coefficient Of Variation (COV) of the time-varying forces calculated as the ratio of the identified time-varying standard deviation to the identified time-varying mean value of the moving force is 0.8748. This is very large indicating that the proposed algorithm can identify the moving forces with quite large COV and this property makes the proposed method very attractive for engineering application.

4.5 Discussion on the Measurement Noise

In practical engineering application, the response data is polluted by measurement noise. It should be noted that the noise effect on the “measured” displacement responses has not been included in this stochastic moving force identification algorithm. The mean value of the interaction force can be accurately identified from the contaminated data because the noise effect can be mostly removed by the averaging procedure on the response samples. Any noise removal procedures can be applied before the force identification procedure to improve the accuracy in the variance of the identified random interaction forces.

It is noted that the randomness in the response signals, e.g. strains or accelerations due to road surface roughness may also be removed by the noise removal procedure. Fortunately, the difference between the randomness in the response signals caused by road surface roughness and the measurement noise is judged from whether they are derived from the system equation of motion, i.e. the random part of the acceleration due to the road surface roughness can be obtained from differentiation of the random part of displacement. This property does not hold for the random part due to the noise pollution. To deal with the noise polluted data, both the strain and acceleration data of the bridge deck can be measured, and the noise removal procedure on the strain data can be implemented by referring to the acceleration data as follows: firstly, calculate the displacement signals based on the strain signals with noise removed. Then the differentiation on the displacement signals is performed to obtain the calculated accelerations signals. Finally, the calculated acceleration signals are compared with the measured acceleration signals. If good agreement is achieved, it indicates that the randomness in the strain signals due to measurement noise are removed while the randomness in the strain signals due to random excitations remains. Otherwise, the parameters for the noise removal filter should be reset for another trial.

The proposed strategy described above may be effective to handle the noisy data to achieve an accurate variance of the identified interaction forces. However, the noise removal technique discussed here is beyond the scope of this study.

4.6 Summary

A new strategy on the bridge-vehicle interaction problem is formulated in which both the irregular road surface profile and the system responses are assumed as Gaussian random processes which can be represented by the Karhunen-Loève Expansion. By representing the Gaussian random process involved, the equation of motion of the bridge-vehicle system becomes a set of deterministic equations which can be easily solved by any numerical methods such as the Newmark- β method. A stochastic force identification algorithm is proposed based on this model in which statistics of the moving interaction forces are accurately identified from a set of samples of the random responses of the bridge deck.

The numerical simulations have been conducted to achieve the following purposes. The Gaussian assumption for the road surface roughness is demonstrated to be correct. The response statistics calculated from the proposed method compared with those from the Monte Carlo Simulation are found to be accurate. The stochastic moving force identification algorithm adopted to identify the statistics of the interaction forces between the bridge and the moving vehicle is found to be effective.

To consider practical engineering application, the effect of the number of response samples used and the effect of the different road surface roughness on the accuracy of the proposed stochastic force identification algorithm are investigated. It is recommended that 50 response samples may be suitable for a

satisfactory identification of the variance of the moving vehicle axle forces. Results also show that the proposed force identification algorithm can identify the moving forces with COV at any time instance as large as 0.8, and the relative error in the variance of the identified forces is not sensitive to the road class.

To conduct the research work a step further in the following Chapters, the inherent randomness in the material properties of the bridge structures will be included. New techniques will be employed to formulate the bridge-vehicle interaction model with uncertainties in both excitations and system parameters. Base on this new model, the dynamic analysis as well as the stochastic moving force identification technique will be proposed.

Table 4.1- Parameters of the bridge-vehicle systems

Bridge	Vehicle	
$L=30\ m$	$I_v=1.47\times 10^5\ kgm^2$	$m_v=17735\ kg$
$EI=2.5\times 10^{10}\ Nm^2$	$a_1=0.519$	$a_2=0.481$
$\rho A=5.0\times 10^3\ kg/m$	$m_1=1500\ kg$	$m_2=1000\ kg$
$z=1.0\ m$	$k_{s1}=2.47\times 10^6\ N/m$	$k_{s2}=4.23\times 10^6\ N/m$
$f_1=1.03\ Hz$	$k_{t1}=3.74\times 10^6\ N/m$	$k_{t2}=4.60\times 10^6\ N/m$
$f_2=4.75\ Hz$	$c_{s1}=3.00\times 10^4\ N/m/s$	$c_{s2}=4.00\times 10^4\ N/m/s$
$f_3=10.11\ Hz$	$c_{t1}=3.90\times 10^3\ N/m/s$	$c_{t2}=4.30\times 10^3\ N/m/s$
$\zeta=0.02$ for all mode	$S=4.27\ m$	

Table 4.2 - Relative error in the identified forces from different kinds of response samples

<i>FE (%)</i>	Mean Value		Variance	
	K-L Samples	MC Samples	K-L Samples	MC Samples
Front Axle	3.61	3.68	9.51	8.62
Rear Axle	3.26	3.32	15.97	13.86

Table 4.3 - Relative error in the identified forces from different number of response samples

<i>FE (%)</i>	Mean Value						Variance					
Number of Samples	10	20	50	100	200	500	10	20	50	100	200	500
Front Axle	3.79	3.66	3.58	3.65	3.65	3.68	45.1	36.8	17.8	13.0	11.0	8.62
Rear Axle	3.41	3.32	3.19	3.29	3.21	3.32	42.06	31.6	24.1	21.6	17.2	13.9

Table 4.4 - Relative error in the identified forces from different classes of roads

<i>FE (%)</i>	Mean Value					Variance				
Road Class	<i>A</i>	<i>B</i>	<i>C</i>	<i>D</i>	<i>E</i>	<i>A</i>	<i>B</i>	<i>C</i>	<i>D</i>	<i>E</i>
Front Axle	3.58	3.62	3.93	5.37	9.29	17.8	17.9	17.7	17.9	17.8
Rear Axle	3.19	3.19	3.24	3.84	5.88	24.1	24.6	24.3	24.6	24.5

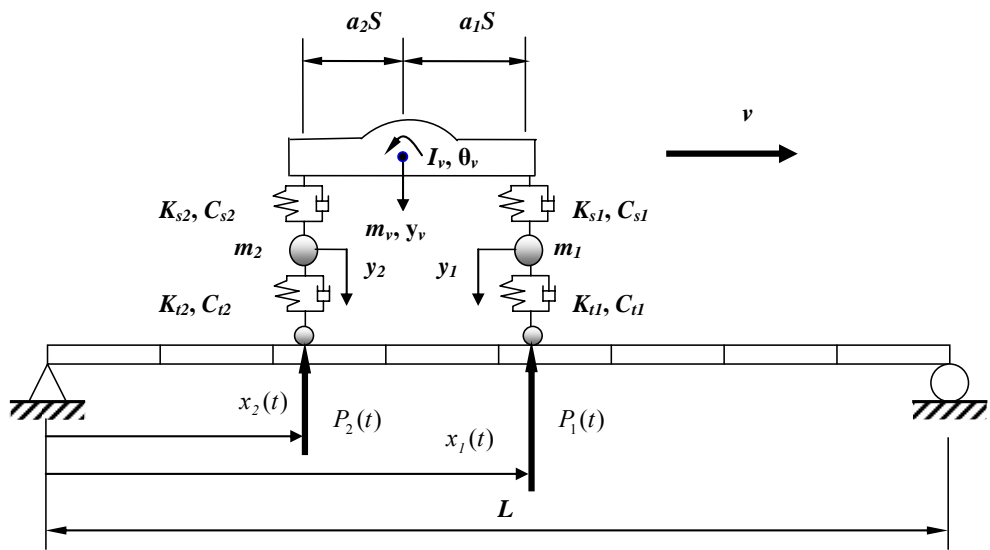


Figure 4.1 - The bridge-vehicle system

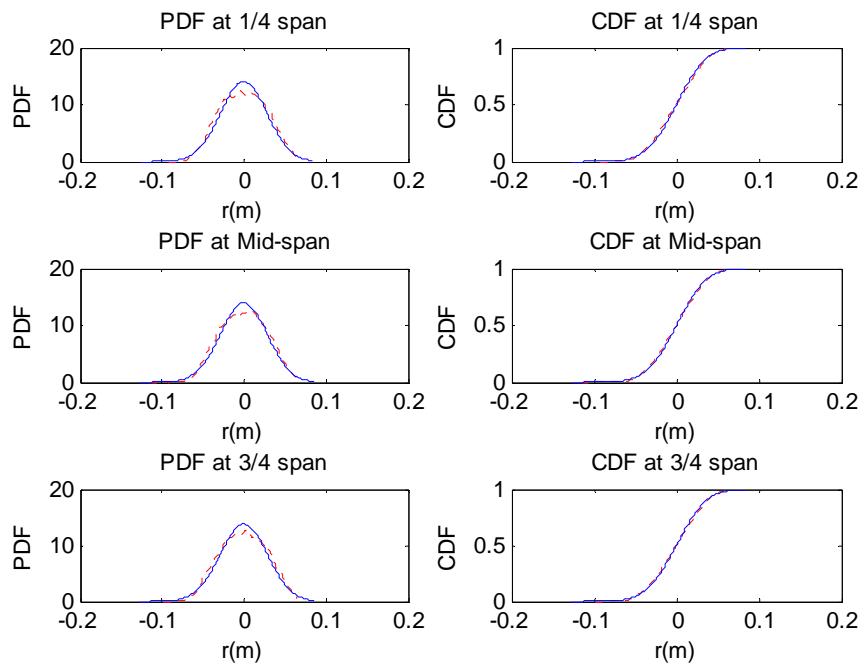


Figure 4.2 - Comparison of the PDF and CDF between samples from the road surface and the corresponding Gaussian random variable

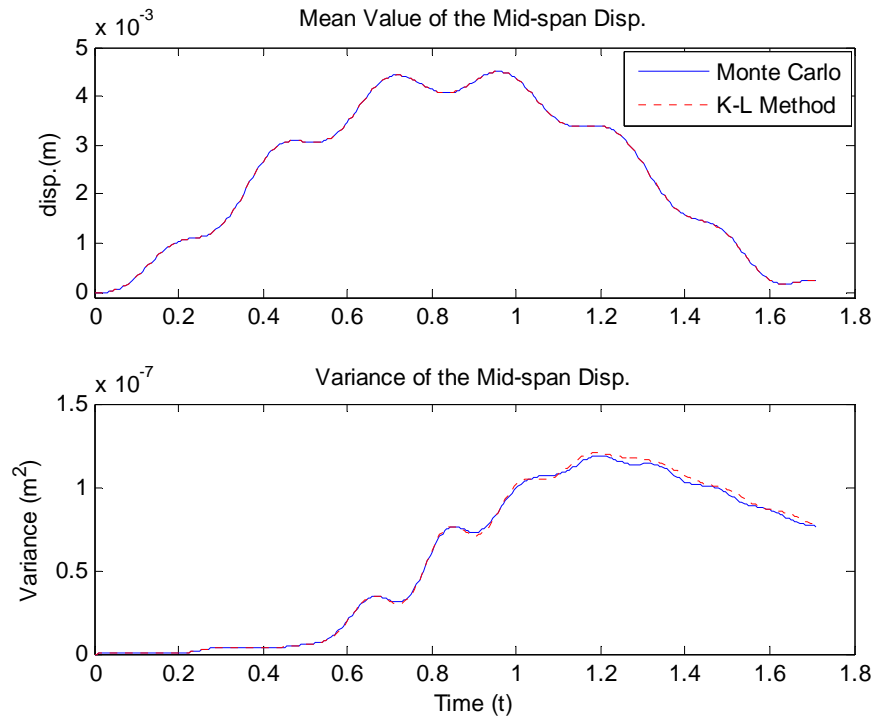


Figure 4.3 - Comparison of statistics of mid-span displacement

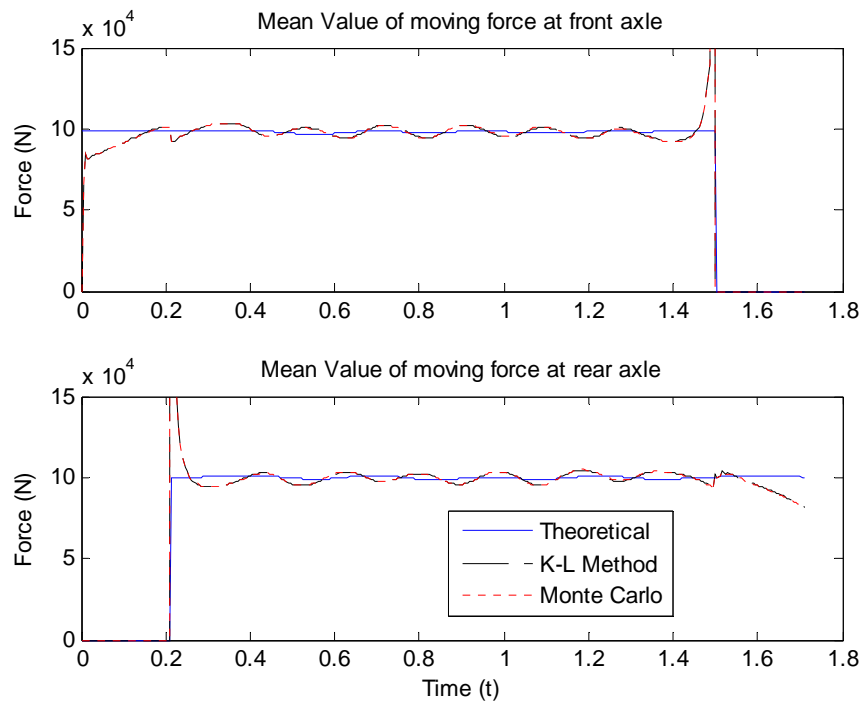


Figure 4.4 - Comparison of identified and theoretical mean value of the interaction forces (Class A Road)

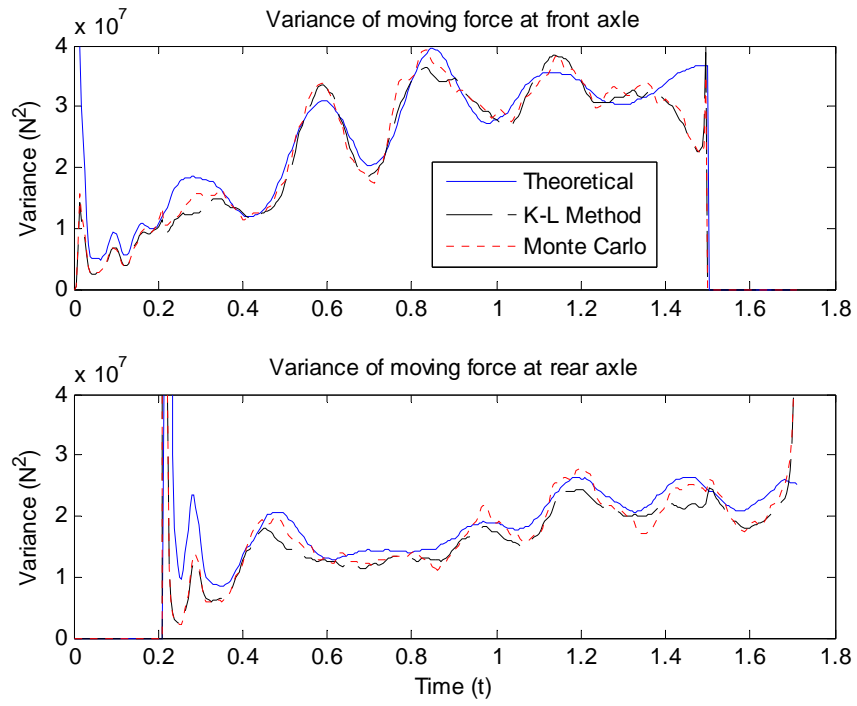


Figure 4.5 - Comparison of identified and theoretical variance of the interaction forces (Class A Road)

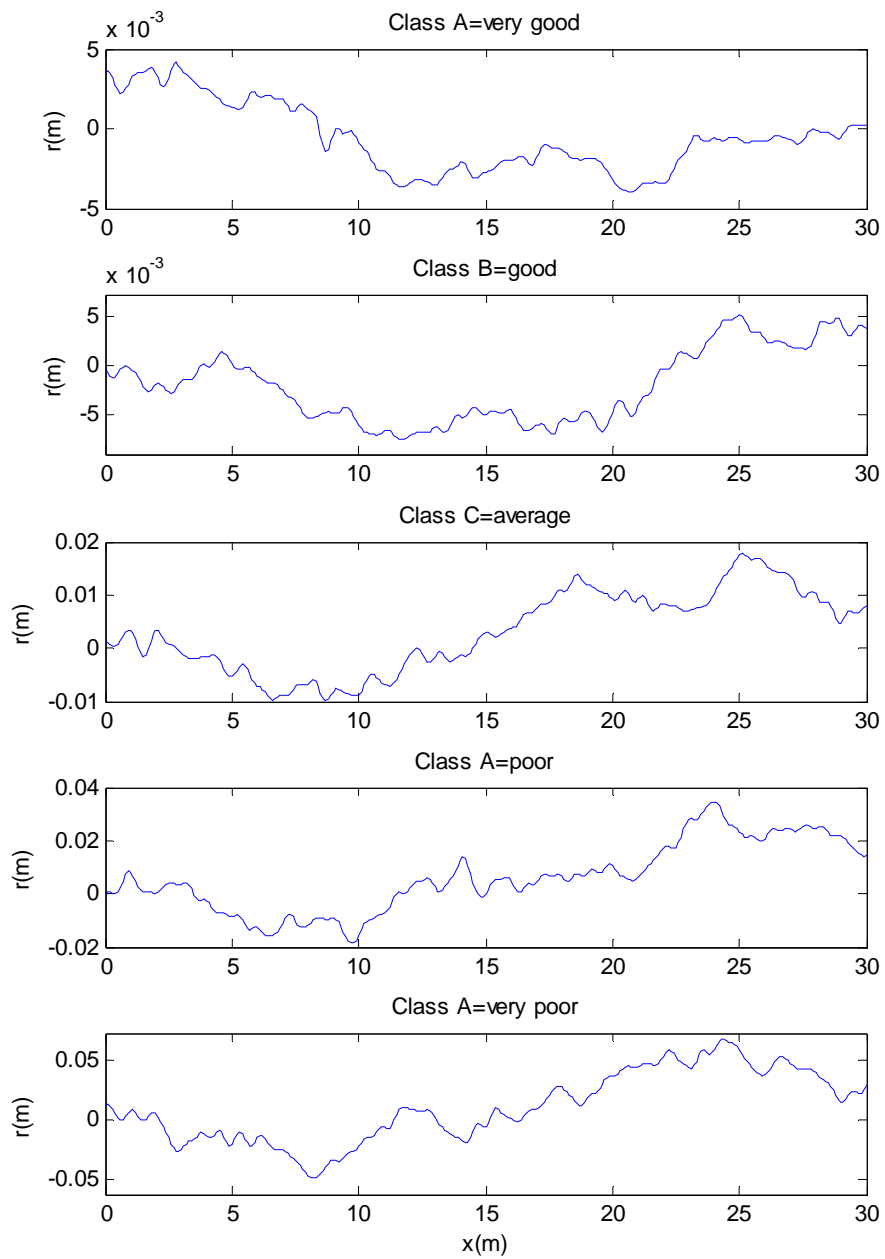


Figure 4.6 - Typical road surface profiles

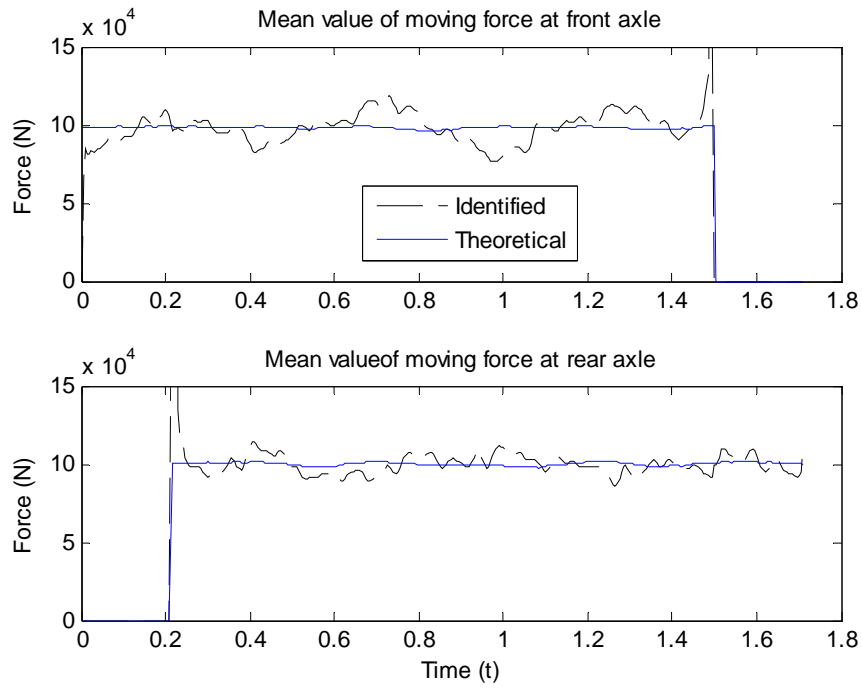


Figure 4.7 - Comparison of the identified and theoretical mean value of the interaction forces (Class E Road)

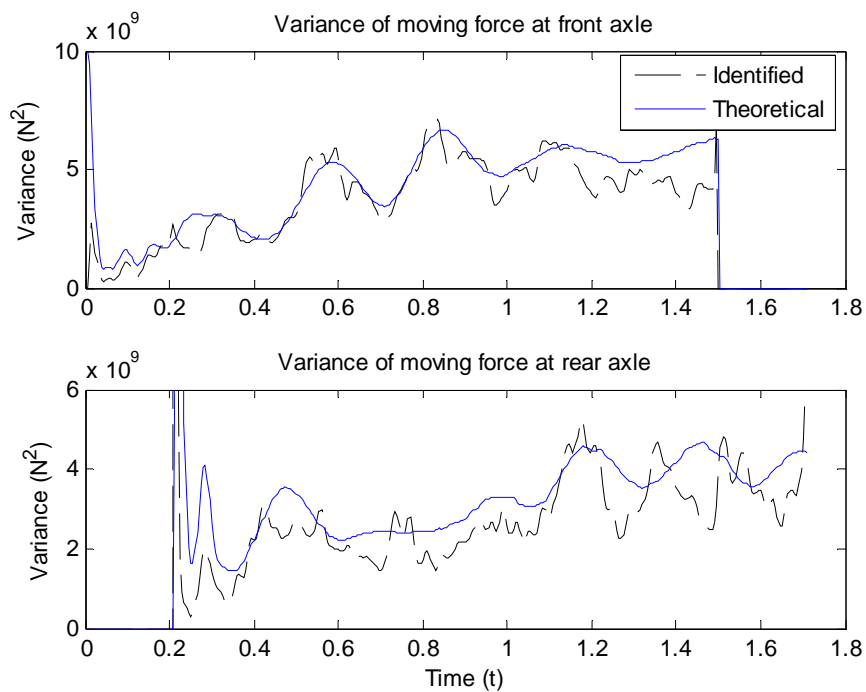


Figure 4.8 - Comparison of identified and theoretical variance of the interaction forces (Class E Road)

CHAPTER 5

STOCHASTIC BEAM-LOAD SYSTEM: THE GAUSSIAN ASSUMPTION

5.1 Introduction

A bridge-vehicle interaction model has been proposed in Chapter FOUR in which the randomness in the excitation due to road surface roughness is included. Since the bridge-vehicle system has an inherent randomness in the material properties of the bridge structure, from this Chapter, it will be included in the bridge-vehicle interaction problem to provide a practical estimation of the response statistics of the bridge-vehicle system. Though there are other sources of randomness, e.g. the velocity of vehicle, etc. which can also be modeled as a random variable or random process. However, these factors will not be discussed in this Chapter.

Methods for introducing randomness in the material properties of a structure in engineering problems have been reviewed in Chapter two. In last two Chapters, the Karhunen-Loève Expansion (KLE) was adopted to represent both the random excitation force and random response of the bridge structure which are assumed as Gaussian random processes. When the material properties of a bridge structure are assumed as Gaussian random processes, they can also be represented by the

KLE. It should be noted that the random response of a dynamic system with Gaussian randomness in both the system parameter and excitation tends to be non-Gaussian. However, the random response is assumed with Gaussian property in this Chapter under the assumption of small randomness in system parameters. The random response assumed with Gaussian property and it can be represented by a set of deterministic coefficients multiplying with the corresponding standard Gaussian random variables. This is a simplification of the traditional solution to the problem in the Spectral Stochastic Finite Element Method (SSFEM) (Ghanem and Spanos 1991). The algorithm proposed in this Chapter based on the Gaussian assumption of the random response may be more economical for solving the stochastic bridge-vehicle interaction problem with uncertainty in system parameters compared with SSFEM, though with a disadvantage of a lower accuracy when the randomness in system parameter becomes large.

A stochastic finite element model is proposed in this Chapter for a bridge-vehicle system with inherent randomness and stochastic loading. The algorithm based on the proposed model can handle random excitation forces with large uncertainties but with relatively small uncertainties in the system parameters. The bridge is modeled as a simply supported Euler-Bernoulli beam with Gaussian random elastic modulus and mass density of material and Gaussian random moving forces on top. The equation of motion of the bridge-vehicle system with Gaussian uncertainties is presented with the adoption of the Karhunen-Loève Expansion, and the response statistics are obtained by solving the system equation

of motion using the Newmark- β method. A statistical relationship between the random moving forces and the random structural responses is derived. Based on the stochastic finite element model, a general stochastic moving force identification algorithm is then formulated. Numerical simulations are given to verify the beam-load model in the forward analysis and the proposed stochastic moving force identification algorithm with quantifications on the errors occur at different stages of the identification process. Case studies on different factors which may affect the accuracy of the formulated model and the proposed force identification algorithm are also presented.

The stochastic system modeling with Gaussian uncertainties using KLE is introduced in Section 5.2 and the general force identification algorithm based on the formulated stochastic finite element model will be developed in Section 5.3. Numerical simulation on the verification of both the formulated model and the application of this stochastic moving force identification algorithm is presented in Section 5.4. Discussions on the algorithms proposed in the Chapter will be addressed in Section 5.5. A summary is given in Section 5.6.

5.2 Modeling of Gaussian Uncertainty in System Parameters

5.2.1 The Stochastic Finite Element Algorithm

The mass density $\rho(x, \theta)$, Young's modulus $E(x, \theta)$ and damping $c(x, \theta)$ of a beam structure are assumed as Gaussian random processes with the mean value

$\bar{\rho}(x), \bar{E}(x), \bar{c}(x)$ and standard deviation $\sigma_\rho, \sigma_E, \sigma_c$, respectively. The random components of these random processes are denoted as $\tilde{\rho}(x, \theta), \tilde{E}(x, \theta)$ and $\tilde{c}(x, \theta)$, respectively. The equation of motion of the beam structure with random material properties and random excitations can be written as

$$\begin{aligned} \rho(x, \theta)A \frac{\partial^2}{\partial t^2} w(x, t, \theta) + c(x, \theta) \frac{\partial}{\partial t} w(x, t, \theta) \\ + E(x, \theta)I \frac{\partial^4}{\partial x^4} w(x, t, \theta) = \sum_{i=1}^{N_E} F_i(t, \theta) \delta(x - v_i t) \end{aligned} \quad (5.1)$$

It is noted that Equation (5.1) is similar as Equation (3.1) but with the randomness in material properties included. Employing the Hermitian cubic interpolation shape functions and with the assumption of Rayleigh damping, Equation (5.1) will take the following form

$$\mathbf{M}(\theta)\ddot{\mathbf{R}}(t, \theta) + \mathbf{C}(\theta)\dot{\mathbf{R}}(t, \theta) + \mathbf{K}(\theta)\mathbf{R}(t, \theta) = \mathbf{H}_b \mathbf{F}(t, \theta) \quad (5.2)$$

where $\mathbf{R}(t, \theta), \dot{\mathbf{R}}(t, \theta)$ and $\ddot{\mathbf{R}}(t, \theta)$ are the random nodal displacement, velocity and acceleration vectors of the beam structure, respectively with $\mathbf{M}(\theta), \mathbf{C}(\theta), \mathbf{K}(\theta)$ are the stochastic mass, damping and stiffness matrices of the beam structure, respectively; $\mathbf{M}(\theta) = \mathbf{M}_b + \tilde{\mathbf{M}}(\theta)$, $\mathbf{C}(\theta) = \mathbf{C}_b + \tilde{\mathbf{C}}(\theta)$, $\mathbf{K}(\theta) = \mathbf{K}_b + \tilde{\mathbf{K}}(\theta)$. $\tilde{\mathbf{M}}(\theta), \tilde{\mathbf{C}}(\theta)$ and $\tilde{\mathbf{K}}(\theta)$ are the random components of the system mass, damping and stiffness matrices, respectively, and they can be obtained by assembling the corresponding elemental matrices as

$$\tilde{\mathbf{M}}^e = \int_l \mathbf{H}^{eT} \tilde{\rho}(x, \theta) A \mathbf{H}^e dl, \quad \tilde{\mathbf{K}}^e = \int_l \mathbf{B}^{eT} \tilde{E}(x, \theta) I \mathbf{B}^e dl \quad (5.3)$$

where \mathbf{H}^e and \mathbf{B}^e are respectively the shape function matrix and strain-displacement matrix of each element. l is the length of each element.

Rayleigh damping is assumed with the equation,

$$\mathbf{C}(\theta) = c_M \mathbf{M}(\theta) + c_K \mathbf{K}(\theta) \quad (5.4)$$

where c_M and c_K are constants.

The KLE can be employed to represent the Gaussian random processes according to Equation (3.9). Taking the Young's modulus for example

$$E(x, \theta) = \bar{E}(x) + \sum_{i_1=1}^{k_E} \xi_{i_1}(\theta) \sqrt{\lambda_{i_1}} \varphi_{i_1}(x) \quad (5.5)$$

where k_E is the number of components in the KLE for the Young's modulus after truncation. The elemental stiffness matrix becomes

$$\tilde{\mathbf{K}}^e(\theta) = \sum_{i_1=1}^{k_E} \xi_{i_1}(\theta) \int_l \sqrt{\lambda_{i_1}} \varphi_{i_1}(x) \mathbf{B}^e \mathbf{B}^{eT} dl = \sum_{i_1=1}^{k_E} \xi_{i_1}(\theta) \mathbf{K}_{i_1}^e \quad (5.6)$$

and the system stiffness matrix $\mathbf{K}(\theta)$ can be expressed as

$$\mathbf{K}(\theta) = \mathbf{K}_b + \sum_{i_1=1}^{k_E} \xi_{i_1}(\theta) \mathbf{K}_{i_1} \quad (5.7)$$

where \mathbf{K}_{i_1} can be assembled from $\mathbf{K}_{i_1}^e$. Let $\mathbf{K}_0 = \mathbf{K}_b$, we have

$$\mathbf{K}(\theta) = \sum_{i_1=0}^{k_E} \xi_{i_1}(\theta) \mathbf{K}_{i_1} \quad (5.8)$$

Similarly the system mass matrix can be expressed as

$$\mathbf{M}(\theta) = \sum_{i_2=0}^{k_p} \xi_{i_2}(\theta) \mathbf{M}_{i_2} \quad (5.9)$$

Since the Rayleigh damping matrix is the linear combination of the system mass and stiffness matrices according to Equation (5.4), the damping matrix can be written as

$$\mathbf{C}(\theta) = \sum_{i_3=0}^{k_c} \xi_{i_3}(\theta) \mathbf{C}_{i_3} \quad (5.10)$$

where k_ρ and k_c are the number of the components in the KLE for mass density and damping after truncation, respectively, and $k_c=k_\rho+k_E$.

The random excitation force vector $\mathbf{F}(t,\theta)$ can be expressed by its K-L components according to Equation (3.21) as

$$\mathbf{F}(t,\theta) = \sum_{j_1=0}^{k_F} \xi_{j_1}(\theta) \mathbf{f}^{(j_1)}(t) \quad (5.11)$$

where $\mathbf{f}^{(j_1)}(t)$ are the K-L components for the random moving forces and k_F is the number of K-L components retained after truncation.

Since the covariance matrix of the response in Equation (3.17) is not known *a-priori*, the KLE can not be performed according to Equation (3.21) for the nodal displacement vector $\mathbf{R}(t,\theta)$. However, it is assumed that the randomness in system parameters in this Chapter is small and the structural response can be approximated to have Gaussian property. The response will therefore take the following form as

$$\mathbf{R}(t,\theta) = \sum_{j=0}^{k_R} \xi_j(\theta) \mathbf{y}^{(j)}(t) \quad (5.12)$$

where k_R is the number of corresponding components $\mathbf{y}^{(j)}(t)$ which is determined by the number of K-L components for both the excitation forces and system parameters as $k_R=k_\rho+k_E+k_F$

Similarly, the nodal velocity vector and nodal acceleration vector will respectively take the following forms,

$$\dot{\mathbf{R}}(t,\theta) = \sum_{j=0}^{k_R} \xi_j(\theta) \dot{\mathbf{y}}^{(j)}(t) \quad (5.13)$$

$$\ddot{\mathbf{R}}(t, \theta) = \sum_{j=0}^{k_R} \xi_j(\theta) \ddot{\mathbf{y}}^{(j)}(t) \quad (5.14)$$

where $\dot{\mathbf{y}}^{(j)}$ and $\ddot{\mathbf{y}}^{(j)}$ are the first and second derivatives of $\mathbf{y}^{(j)}(t)$ with respect to time t , respectively.

By substituting Equations (5.8) to (5.14) into Equation (5.2) and taking the inner product on both sides of the equation with $\xi_k(\theta)$ and employing the orthogonal property shown in Equation (3.11), we have

$$\begin{aligned} \sum_{j=0}^{k_R} \sum_{i_2=0}^{k_\rho} \langle \xi_{i_2}(\theta) \xi_j(\theta) \xi_k(\theta) \rangle \mathbf{M}_{i_2} \ddot{\mathbf{y}}^{(j)}(t) + \sum_{j=0}^{k_R} \sum_{i_3=0}^{k_c} \langle \xi_{i_3}(\theta) \xi_j(\theta) \xi_k(\theta) \rangle \mathbf{C}_{i_3} \dot{\mathbf{y}}^{(j)}(t) \\ + \sum_{j=0}^{k_R} \sum_{i_1=0}^{k_E} \langle \xi_{i_1}(\theta) \xi_j(\theta) \xi_k(\theta) \rangle \mathbf{K}_{i_1} \mathbf{y}^{(j)}(t) = \mathbf{H}_b \mathbf{f}^{(k)}(t) \end{aligned} \quad (5.15)$$

$$\text{Let } \mathbf{M}^{(k,j)} = \sum_{i_2=1}^{k_\rho} \langle \xi_{i_2}(\theta) \xi_j(\theta) \xi_k(\theta) \rangle \mathbf{M}_{i_2},$$

$$\mathbf{C}^{(k,j)} = \sum_{i_3=0}^{k_c} \langle \xi_{i_3}(\theta) \xi_j(\theta) \xi_k(\theta) \rangle \mathbf{C}_{i_3} \quad \text{and} \quad \mathbf{K}^{(k,j)} = \sum_{i_1=0}^{k_E} \langle \xi_{i_1}(\theta) \xi_j(\theta) \xi_k(\theta) \rangle \mathbf{K}_{i_1}.$$

Rewriting Equation (5.15) in matrix form,

$$\begin{aligned} \begin{bmatrix} \mathbf{M}^{(0,0)} & \mathbf{M}^{(0,1)} & \dots & \mathbf{M}^{(0,k_m)} \\ \mathbf{M}^{(1,0)} & \mathbf{M}^{(1,1)} & \dots & \mathbf{M}^{(1,k_m)} \\ \vdots & \vdots & \ddots & \vdots \\ \mathbf{M}^{(k_m,0)} & \mathbf{M}^{(k_m,1)} & \dots & \mathbf{M}^{(k_m,k_m)} \end{bmatrix} \begin{bmatrix} \ddot{\mathbf{y}}^{(0)}(t) \\ \ddot{\mathbf{y}}^{(1)}(t) \\ \vdots \\ \ddot{\mathbf{y}}^{(k_m)}(t) \end{bmatrix} + \begin{bmatrix} \mathbf{C}^{(0,0)} & \mathbf{C}^{(0,1)} & \dots & \mathbf{C}^{(0,k_m)} \\ \mathbf{C}^{(1,0)} & \mathbf{C}^{(1,1)} & \dots & \mathbf{C}^{(1,k_m)} \\ \vdots & \vdots & \ddots & \vdots \\ \mathbf{C}^{(k_m,0)} & \mathbf{C}^{(k_m,1)} & \dots & \mathbf{C}^{(k_m,k_m)} \end{bmatrix} \begin{bmatrix} \dot{\mathbf{y}}^{(0)}(t) \\ \dot{\mathbf{y}}^{(1)}(t) \\ \vdots \\ \dot{\mathbf{y}}^{(k_m)}(t) \end{bmatrix} \\ + \begin{bmatrix} \mathbf{K}^{(0,0)} & \mathbf{K}^{(0,1)} & \dots & \mathbf{K}^{(0,k_m)} \\ \mathbf{K}^{(1,0)} & \mathbf{K}^{(1,1)} & \dots & \mathbf{K}^{(1,k_m)} \\ \vdots & \vdots & \ddots & \vdots \\ \mathbf{K}^{(k_m,0)} & \mathbf{K}^{(k_m,1)} & \dots & \mathbf{K}^{(k_m,k_m)} \end{bmatrix} \begin{bmatrix} \mathbf{y}^{(0)}(t) \\ \mathbf{y}^{(1)}(t) \\ \vdots \\ \mathbf{y}^{(k_m)}(t) \end{bmatrix} = \begin{bmatrix} \mathbf{H}_b & 0 & \dots & 0 \\ 0 & \mathbf{H}_b & \dots & 0 \\ \vdots & \vdots & \ddots & \vdots \\ 0 & 0 & \dots & \mathbf{H}_b \end{bmatrix} \begin{bmatrix} \mathbf{f}^{(0)}(t) \\ \mathbf{f}^{(1)}(t) \\ \vdots \\ \mathbf{f}^{(k_m)}(t) \end{bmatrix} \end{aligned} \quad (5.16)$$

where $k_m = k_R$ and $\langle \xi_i(\theta) \xi_j(\theta) \xi_k(\theta) \rangle$ are constants which can be calculated analytically (Ghanem and Spanos 1991).

5.2.2 Response Statistics

The nodal response vectors of the beam structure can be obtained according to Equations (5.12) to (5.14) once the deterministic components $\mathbf{y}^{(j)}(t)$, $\dot{\mathbf{y}}^{(j)}(t)$ and $\ddot{\mathbf{y}}^{(j)}(t)$ are calculated by solving Equation (5.16) using the Newmark- β method. The mean and the variance of the nodal displacements can then be evaluated as

$$MEAN_{\mathbf{R}}(t) = \mathbf{y}^{(0)}(t), \quad VAR_{\mathbf{R}}(t) = \sum_{j=1}^{k_m} (\mathbf{y}^{(j)}(t))^2 \quad (5.17)$$

where the subscript “R” denotes the random displacement vector. The random displacement of the bridge at position x and time t can be derived as

$$w(x, t, \theta) = \mathbf{H}(x) \sum_{j=0}^{k_m} \xi_j(\theta) \mathbf{y}^{(j)}(t) = \sum_{j=0}^{k_m} \xi_j(\theta) (\mathbf{H}(x) \mathbf{y}^{(j)}(t)) \quad (5.18)$$

Thus the mean and variance of displacement at position x and time t can be obtained as

$$MEAN_w(x, t) = \mathbf{H}(x) \mathbf{y}^{(0)}(t), \quad VAR_w(x, t) = \sum_{j=1}^{k_m} (\mathbf{H}(x) \mathbf{y}^{(j)}(t))^2 \quad (5.19)$$

where the subscript “w” denotes the random displacement of the beam structure.

Substituting the first and second derivatives $\dot{\mathbf{y}}^{(j)}$ and $\ddot{\mathbf{y}}^{(j)}$ of the components $\mathbf{y}^{(j)}$ in Equation (5.19), the mean and variance of random velocity and acceleration at position x and time t can be obtained. Samples of the random displacements can be easily generated according to Equation (5.12) with any available sampling techniques, e.g. Latin Hypercube Sampling (LHS) (Florian 1992) to simulate the Gaussian random variables $\xi_j(\theta)$. The probabilistic density

function of the displacement of the beam structure at position x and time t can also be obtained according to Equation (5.18) after the components $\mathbf{y}^{(j)}$ are calculated.

5.3 Moving Force Identification with Gaussian Uncertainty in System Parameters

To identify the statistics of the moving forces applied on the beam structure from samples of the responses, the KLE can be applied to represent the ‘measured’ response, e.g. displacement, to obtain the K-L components denoted as $\hat{\mathbf{y}}^{(j)}(t)$ according to Equation (3.21). It is important to note that the K-L components of the “measured” responses $\hat{\mathbf{y}}^{(j)}(t)$ in the inverse procedure are different from those denoted as $\mathbf{y}^{(j)}(t)$ calculated in the forward problem from Equation (5.16). The identification of forces may not be so ‘simple’ as that in the case of a deterministic system, i.e. the statistics of excitation forces can not be identified by applying a general inverse method, e.g. with a least-squares estimation, to solve Equation (5.16) from the K-L components of response $\hat{\mathbf{y}}^{(j)}(t)$. This is because of the existence of non-zeros in the $(j,0)$ and $(0,j)$ sub-blocks in the system matrix in Equation (5.16).

Before the stochastic moving force identification algorithm is proposed, two kinds of problem will be firstly addressed. The first kind of problem refers to a deterministic system under Gaussian random excitations. The second one refers to a system with Gaussian uncertainties under deterministic excitations. With the

assumption of small uncertainties in the system parameters and according to the Problem of the Second Kind defined in Section 5.3.2, the stochastic moving force identification problem based on the stochastic finite element model with the KLE representing uncertainties in both the system parameters and excitations formulated can be transformed into the Problem of the First Kind as defined in Section 5.3.1. As demonstrated in Chapter 3, similar stochastic moving force identification problem had already been solved. The solution of the Problem of the First Kind will also be briefly addressed in Section 5.3.1 according Equations (5.27) and (5.28).

5.3.1 Problem of the First Kind

In this kind of problem, the non-diagonal blocks in Equation (5.16) are all zero. The system equation can be expressed as

$$\mathbf{M}_d \ddot{\mathbf{y}}^{(k)}(t) + \mathbf{C}_d \dot{\mathbf{y}}^{(k)}(t) + \mathbf{K}_d \mathbf{y}^{(k)}(t) = \mathbf{H}_b(x) \mathbf{f}^{(k)}(t), \quad (j = 0, \dots, k_m) \quad (5.20)$$

In the moving force identification problem, the measured responses, e.g. displacement, will form a population with a mean value and variance. Performing the Karhunen-Loève Expansion on the displacements vector according to Equation (3.21) will lead to

$$\hat{\mathbf{R}}(t, \theta) = \sum_{j=0}^{\hat{k}_R} \xi_j(\theta) \hat{\mathbf{y}}^{(j)}(t) \quad (5.21)$$

It is noted that the K-L components $\hat{\mathbf{y}}^{(j)}(t)$ from the ‘measured’ responses in the inverse problem are different from $\mathbf{y}^{(j)}(t)$ obtained in the forward problem from Equation (5.16), i.e. the ‘energy’ in each component has been redistributed in the

inverse analysis. However the following equalities representing the mean value and variance of responses still hold because they are from the same population of response samples.

$$\hat{\mathbf{y}}^{(0)}(t) = \mathbf{y}^{(0)}(t) \quad (5.22a)$$

$$\sum_{j=1}^{\infty} (\hat{\mathbf{y}}^{(j)})^2 = \sum_{j=1}^{\infty} (\mathbf{y}^{(j)})^2 \quad (5.22b)$$

For a second-order linear differential equation which has the form denoted by Equation (5.16), a polynomial operator $P(D)$ (Borrelli and Coleman 1987) can be introduced to establish the relationship between each K-L components of the excitation forces and responses for both the forward and inverse problems as

$$P(D)[\mathbf{y}^{(j)}(t)] = \mathbf{f}^{(j)}(t) \quad (5.23a)$$

$$P(D)[\hat{\mathbf{y}}^{(j)}(t)] = \hat{\mathbf{f}}^{(j)}(t) \quad (5.23b)$$

where $P(D) = M_d D^2 + C_d D + K_d$ and D is a differential operator which has the action $D : y \rightarrow Dy \equiv \dot{y}$. Repeat application of the operator one more time produces the derivative \ddot{y} and this operator is denoted by D^2 . The operator $P(D)$ is a linear operator with the following property (Borrelli and Coleman 1987),

$$P(D)[c_1 \mathbf{y}^{(1)} + c_2 \mathbf{y}^{(2)} + \dots + c_n \mathbf{y}^{(n)}] = c_1 P(D)[\mathbf{y}^{(1)}] + c_2 P(D)[\mathbf{y}^{(2)}] + \dots + c_n P(D)[\mathbf{y}^{(n)}] \quad (5.24)$$

where $c_i, i=1, \dots, n$. are constants.

The following equality can be obtained from Equations (5.22a) and (5.23) as

$$\hat{\mathbf{f}}^{(0)}(t) = \mathbf{f}^{(0)}(t) \quad (5.25)$$

Equation (5.25) shows that the mean value of the identified moving forces is

equal to the mean value of the excitation force samples in the forward problem which are known. In Chapter 3, numerical simulation shows that the variance of the identified moving forces and the variance of true excitation forces are equal as shown in Equation (5.26) despite the fact that ‘energy’ in each component of the identified set of forces has been redistributed, i.e. $\hat{\mathbf{y}}^{(i)}(t) \neq \mathbf{y}^{(i)}(t), j > 0$.

$$\sum_{j=1}^{\infty} (\hat{\mathbf{f}}^{(j)})^2 = \sum_{j=1}^{\infty} (\mathbf{f}^{(j)})^2 \quad (5.26)$$

Therefore the relationship between the K-L components of responses and excitation forces in the inverse problem can be expressed in the same form of Equation (5.20) as

$$\mathbf{M}_d \ddot{\hat{\mathbf{y}}^{(j)}}(t) + \mathbf{C}_d \dot{\hat{\mathbf{y}}^{(j)}}(t) + \mathbf{K}_d \hat{\mathbf{y}}^{(j)}(t) = \mathbf{H}_b(\mathbf{x}) \hat{\mathbf{f}}^{(j)}(t), \quad (j = 0, \dots, \hat{k}_F) \quad (5.27)$$

It is noted that Equation (5.27) is similar to Equation (3.33), and the definitions of the matrices and variables in Equation (5.27) can refer to Section 3.5. The mean value and variance of the identified forces can be obtained as

$$MEAN_F = \hat{\mathbf{f}}^{(0)}(t), \quad VAR_F(t) = \sum_{j=1}^{\hat{k}_F} (\hat{\mathbf{f}}^{(j)}(t))^2 \quad (5.28)$$

where the subscript ‘ F ’ denotes the random moving force vector.

5.3.2 Problem of the Second Kind

If a system with Gaussian uncertainties is subject to deterministic moving forces, the terms in the force vector on the right-hand-side of Equation (5.16) are all equal to zero except $\mathbf{f}^{(0)}(t)$ which represents the deterministic forces. Only the diagonal blocks and the $(i, 0)$ and $(0, i)$ blocks of the mass, stiffness and damping

matrices in Equation (5.16) are non-zero. The system equation of motion of this kind of problem can then be rewritten as

First Row of the Equation of Motion:

$$\begin{aligned} & \mathbf{M}^{(0,0)}\ddot{\mathbf{y}}^{(0)}(t) + \mathbf{C}^{(0,0)}\dot{\mathbf{y}}^{(0)}(t) + \mathbf{K}^{(0,0)}\mathbf{y}^{(0)}(t) \\ &= \mathbf{H}_b(x)\mathbf{f}^{(0)}(t) - \left(\sum_{j=1}^{k_m} \mathbf{M}^{(0,j)}\ddot{\mathbf{y}}^{(j)}(t) + \sum_{j=1}^{k_m} \mathbf{C}^{(0,j)}\dot{\mathbf{y}}^{(j)}(t) + \sum_{j=1}^{k_m} \mathbf{K}^{(0,j)}\mathbf{y}^{(j)}(t) \right) \end{aligned} \quad (5.29a)$$

Other Rows of the Equation of Motion:

$$\begin{aligned} & \mathbf{M}^{(k,k)}\ddot{\mathbf{y}}^{(k)}(t) + \mathbf{C}^{(k,k)}\dot{\mathbf{y}}^{(k)}(t) + \mathbf{K}^{(k,k)}\mathbf{y}^{(k)}(t) \\ &= -\left(\mathbf{M}^{(k,0)}\ddot{\mathbf{y}}^{(0)}(t) + \mathbf{C}^{(k,0)}\dot{\mathbf{y}}^{(0)}(t) + \mathbf{K}^{(k,0)}\mathbf{y}^{(0)}(t) \right), \quad (k=1, \dots, k_m) \end{aligned} \quad (5.29b)$$

Noting that for the model formulated in Equation (5.16), each diagonal block of system matrices $\mathbf{M}^{(k,k)}$, $\mathbf{C}^{(k,k)}$, $\mathbf{K}^{(k,k)}$, ($k= 0,1, \dots, k_m$) are equal to the deterministic system matrix \mathbf{M}_d , \mathbf{C}_d , \mathbf{K}_d respectively, and thus the left-hand-side of Equation (5.29) is the same as the corresponding part in Equation (5.20). The terms on the right-hand-side of Equation (5.29) except $\mathbf{f}^{(0)}(t)$ can be regarded as the effect due to uncertainty in system parameters on the randomness of the structural responses.

5.3.3 General Force Identification Algorithm

When Gaussian uncertainty in both excitation and system parameters is considered, the system equation of motion can be expressed as Equation (5.16). The first row of the system equation of motion can be written similar to Equation (5.29a). Other rows can be expressed as

$$\begin{aligned}
& \mathbf{M}^{(k,k)}\ddot{\mathbf{y}}^{(k)}(t) + \mathbf{C}^{(k,k)}\dot{\mathbf{y}}^{(k)}(t) + \mathbf{K}^{(k,k)}\mathbf{y}^{(k)}(t) \\
& = \mathbf{H}_b(x)\mathbf{f}^{(k)}(t) - \left(\mathbf{M}^{(k,0)}\ddot{\mathbf{y}}^{(0)}(t) + \mathbf{C}^{(k,0)}\dot{\mathbf{y}}^{(0)}(t) + \mathbf{K}^{(k,0)}\mathbf{y}^{(0)}(t) \right), \quad (k=1, \dots, k_m)
\end{aligned} \tag{5.30}$$

When the uncertainty in system parameters is included in the moving force identification, the linear relationship between the K-L components of the excitation forces and responses for a deterministic system as demonstrated in Equation (5.20) does not hold. In order to take advantage of the linear characteristic in the case of the deterministic system, we need to transform Equations (5.29a) and (5.30) to the form as shown in Equation (5.20) such that the stochastic moving force identification can be performed following the procedure as described for the Problem of First Kind in Section 5.3.1.

It should be noted that equality shown in Equation (5.22a) on the mean values of the random response of the beam structure still holds. Noting that the summation terms on the right-hand-side of Equation (5.29a) are the higher order terms which are much smaller compared to the corresponding terms on the left-hand-side of Equation (5.29a) when the uncertainty in system parameters is small, therefore, they can be ignored. The deterministic component of the excitation forces $\mathbf{f}^{(0)}(t)$ can be identified from Equation (5.29a) with an under-estimation. If the uncertainty in system parameters is not very large, the deterministic force components $\mathbf{f}^{(0)}(t)$ can be accurately identified.

Let $\mathbf{y}_d^{(j)}, \dot{\mathbf{y}}_d^{(j)}, \ddot{\mathbf{y}}_d^{(j)}$ and $\mathbf{y}_s^{(j)}, \dot{\mathbf{y}}_s^{(j)}, \ddot{\mathbf{y}}_s^{(j)}$ denote the sets of K-L components of the responses obtained in the forward problem from Equation (5.16) for the First and

Second Kind of problem, respectively. In the moving force identification procedure for a system with both Gaussian excitation and Gaussian system parameters, the ‘excitations’ due to uncertainty in system parameters are known *a priori*, and $\mathbf{y}_s^{(j)}, \dot{\mathbf{y}}_s^{(j)}, \ddot{\mathbf{y}}_s^{(j)}$ can be evaluated from Equation (5.29b). The equation for the random K-L components can be rewritten according to Equations (5.29b) and (5.30) as

$$\mathbf{M}_b \ddot{\mathbf{y}}_d^{(j)}(t) + \mathbf{C}_b \dot{\mathbf{y}}_d^{(j)}(t) + \mathbf{K}_b \mathbf{y}_d^{(j)}(t) = \mathbf{H}_b(x) \mathbf{f}^{(j)}(t) \quad (5.31)$$

where $\mathbf{y}_d^{(j)}(t) = \mathbf{y}^{(j)}(t) - \mathbf{y}_s^{(j)}(t)$, $\dot{\mathbf{y}}_d^{(j)}(t) = \dot{\mathbf{y}}^{(j)}(t) - \dot{\mathbf{y}}_s^{(j)}(t)$, $\ddot{\mathbf{y}}_d^{(j)}(t) = \ddot{\mathbf{y}}^{(j)}(t) - \ddot{\mathbf{y}}_s^{(j)}(t)$.

$\mathbf{y}^{(j)}(t)$, $\dot{\mathbf{y}}^{(j)}(t)$ and $\ddot{\mathbf{y}}^{(j)}(t)$ are the K-L components of the responses obtained in the forward problem from Equation (5.31) which has the same form as Equation (5.20). However, $\mathbf{y}^{(j)}(t)$, $\dot{\mathbf{y}}^{(j)}(t)$ and $\ddot{\mathbf{y}}^{(j)}(t)$ which are related to the forward problem responses are not available in the inverse procedure. We know from Equation (5.22b) that the K-L components of response $\hat{\mathbf{y}}^{(j)}(t)$ from the “measured” samples in the inverse problem and that in the forward problem $\mathbf{y}^{(j)}(t)$ are obtained from the same covariance kernel denoted as \mathbf{KN} . The covariance kernel for $\hat{\mathbf{y}}_d^{(j)}(t)$ and $\mathbf{y}_d^{(j)}(t)$ is denoted as \mathbf{KN}_d and that for the covariance kernel for $\hat{\mathbf{y}}_s^{(j)}(t)$ and $\mathbf{y}_s^{(j)}(t)$ is denoted as \mathbf{KN}_s . These three Kernels will have the following relationship according to Equations (3.17) and (5.17) as

$$\mathbf{KN} = \mathbf{KN}_d + \mathbf{KN}_s + 2 \sum_{j=1}^{k_R} \mathbf{Y}_d^{(j)} \mathbf{Y}_s^{(j)T} \quad (5.32)$$

where $\mathbf{Y}_d^{(j)}$ and $\mathbf{Y}_s^{(j)}$ are the vectors of kernel \mathbf{KN}_d and \mathbf{KN}_s assembled from $\mathbf{y}_d^{(j)}$ and $\mathbf{y}_s^{(j)}$, respectively. The relationships between $\mathbf{Y}_d^{(j)}$ and $\mathbf{y}_d^{(j)}$ and between $\mathbf{Y}_s^{(j)}$ and $\mathbf{y}_s^{(j)}$ respectively are the same as that exhibited between $\mathbf{X}^{(j)}$ and $\mathbf{x}^{(j)}$ as shown

in Section 3.3.2.

For Problem of the First Kind, the second and third terms on the right-hand-side of Equation (5.32) are equal to zero. For the problem of second kind, the first and third terms on the right-hand-side of Equation (5.32) are equal to zero. When the responses signals are contaminated with noise, $\mathbf{Y}_d^{(j)}$ mainly consists of components with high frequency while $\mathbf{Y}_s^{(j)}$ is traditionally varying slowly with time for a general discretization of random field of the system parameters, and thus the third term $2\sum_{j=1}^{k_R} \mathbf{Y}_d^{(j)} \mathbf{Y}_s^{(j)T}$ in Equation (5.32) is usually small compared to other terms due to a low correlation between $\mathbf{Y}_d^{(j)}$ and $\mathbf{Y}_s^{(j)}$. The significance of these three Kernels on the accuracy of the identified results will be further discussed in the numerical simulations. To maintain the symmetric characteristic of the third term in Equation (5.32), the equation is refined to have the following expression as

$$\mathbf{KN} = \mathbf{KN}_d + \mathbf{KN}_s + \sum_{j=1}^{k_R} \mathbf{Y}_d^{(j)} \mathbf{Y}_s^{(j)T} + \sum_{j=1}^{k_R} \mathbf{Y}_s^{(j)} \mathbf{Y}_d^{(j)T} \quad (5.33)$$

5.3.4 Identification Procedure

The moving force identification can then be performed according to Equations (5.31) and (5.32) with the stochastic model of the beam-load system in Equation (5.16) according to the following procedure:

Step 1 The response samples used for the stochastic moving force identification can either be obtained from the field tests or from the numerical

simulation of the forward analysis. It is noted that the response samples measured from field test on a bridge each time under the “same condition” are in fact different due to the existence of many random factors and these samples are assumed to be from the whole population of a random process. For the response samples obtained from numerical simulation, they are generated according to Equations (5.12) to (5.14) with sampling technique to obtain samples for the standard Gaussian random variables involved. The obtained response samples will form a population of a random process. The procedure of calculating \mathbf{KN} as shown in Equation (5.32) according to Section 3.3.2 is: Firstly, the mean value and random component of the response samples from measurement or numerical simulation are calculated according to Equations (3.13) and (3.14) respectively, and then the random component of the response vector will be reshaped according Equation (3.15). Finally, the covariance kernel for the response samples denoted as \mathbf{KN} can be calculated according to Equation (3.16).

Step 2 Employ the deterministic moving force identification method (Law et al. 2004) together with the Improved Reduced System (IRS) reduction scheme (O’ Callahan 1989) to obtain the mean value of moving forces. It is noted that when uncertainty in both system parameters and excitation is considered, the higher order (summation) terms in Equation (5.30a) are ignored under the assumption of small variation of the randomness in

system parameter in the deterministic force identification algorithm.

Step 3 When the system parameters are assumed to be known, the mean values of the moving forces identified in **Step 1** can be adopted to calculate the corresponding components of response $\mathbf{y}_s^{(j)}$, $\dot{\mathbf{y}}_s^{(j)}$, $\ddot{\mathbf{y}}_s^{(j)}$ due to the ‘system’ uncertainties according to Equation (5.29b). \mathbf{KN}_s in Equation (5.32) can be obtained from these components.

Step 4 Assuming the third term in Equation (5.32) is small compared to \mathbf{KN}_d and it can be ignored, then \mathbf{KN}_d can be obtained from $\mathbf{KN}_d = \mathbf{KN} - \mathbf{KN}_s$. The K-L components $\hat{\mathbf{y}}_d^{(j)}$ in the inverse problem can be calculated by performing the eigenvalue analysis on \mathbf{KN}_d and the variance of moving forces can be identified in the same way as that in a deterministic system as shown in Section 5.3.1. Cubic spline interpretation is applied to each component $\hat{\mathbf{y}}_d^{(j)}$ to obtain the first and second order derivatives which are the corresponding components for velocity and acceleration. The corresponding components of the interaction forces can be obtained from Equation (5.27) using a general inverse procedure such as the least-squares estimation adopted in this study, and the statistics of the identified forces can then be obtained according to Equation (5.28).

5.4 Numerical Simulation

5.4.1 Beam-Load Model

This beam model adopted in this study is the same as Beam Model I in

Section 3.6.1.1 except the system parameters in beam structure are assumed as Gaussian random processes. The elastic modulus E and the mass density ρ are assumed with mean value $5 \times 10^{10} \text{ N/m}^2$ and $2.5 \times 10^3 \text{ kg/m}^3$, respectively, and they have the spatial correlation represented by an exponential auto-covariance function as:

$$\mathbf{C}(x_1, x_2) = \sigma^2 \exp\left(-\frac{|x_1 - x_2|}{a}\right) \quad (5.34)$$

where σ is the standard deviation of system parameters E or ρ , a and $|x_1 - x_2|$ are the correlation length and the positive dislocation of two points in a spatial domain of interest which are set to 1.0 and 5m, respectively, for both parameters in this study. Both the random elastic modulus E and mass density ρ are assumed with the same spatial correlation and the same Coefficient Of Variation (COV), i.e. $COV_E = COV_\rho$. This selection is arbitrary as the same analysis is applicable for the case when the randomness in E or ρ is totally different.

The force models introduced in Sections 3.6.1.2 and 3.6.1.3 will be adopted in this study. The one moving force model (F_1 in Force Model I and II) will be adopted in both the forward and inverse analysis. The two-force model (Force Model I) will also be adopted in the forward analysis. The velocity of the moving forces is 40 m/s except in Section 5.4.2.2 where the factor of moving velocity is specifically investigated.

5.4.2 Forward Analysis

5.4.2.1 Verify with Monte Carlo Simulation

Ten thousand samples of the random excitation forces will be adopted in both the proposed method and Monte Carlo Simulation to calculate the response statistics. In the proposed method, the covariance kernel of the excitation forces in Equation (3.17) is obtained from samples according to Section 3.3.2. The K-L components for the forces can be obtained by performing the eigenvalue analysis on the derived kernel. The first k_F K-L components with relative large eigenvalues λ_j are retained according to the criterion as $\sum_{j=1}^{k_F} \lambda_j / \sum \lambda_j \geq 0.99$. The covariance kernels of the system parameters are defined according to Equation (5.34), and the case with the coefficient of variation equals to 5% is shown in Figure 5.1. Employing the eigenvalue analysis on the covariance kernel of system parameters, nine K-L components are adopted to represent the fluctuation of each random field in the structural model with eight beam elements. Based on the model formulated, the components $\mathbf{y}^{(j)}(t)$, $\dot{\mathbf{y}}^{(j)}(t)$ and $\ddot{\mathbf{y}}^{(j)}(t)$ of the responses can be obtained by solving Equation (5.16) with the Newmark- β method. The response statistics of the displacements of the beam model can then be evaluated according to Equation (5.19).

When one random moving force is applied on the beam structure, i.e. the single moving force model (F_1 in Force Model I and II) is adopted. The number of K-L components for the F_1 in Force Model I remained after truncation is 190 while the number of K-L components for the F_1 in Force Model II is 1. It is noted that the closer the random process to white noise, the more K-L components are required in the representation. It is noted that the computational efficiency can be

greatly improved by adopting a Gaussian moving force model with a specific correlation length since the system matrices in Equation (5.16) will be much smaller. The statistics of the random displacements of beam under the moving force are obtained from Equation (5.19) with verification by MCS. Comparisons of the mean value and variance of the mid-span displacement of the beam obtained from both methods with $COV_F=10\%$ and $COV_E=COV_\rho=5\%$ for the case with F_1 in Force Model I is shown in Figure 5.2. Comparisons of the mean value and variance of the mid-span displacement of the beam obtained from both methods with $\Phi(\omega_0)=16\times 10^{-6} m^3$ and $COV_E=COV_\rho=5\%$ for the case with F_1 in Force Model II is shown in Figure 5.3. Results from these two methods are in good agreement. The relative error RE according to Equation (3.39) for the mean value and variance in the case with F_1 in Force Model I is 0.08% and 7.39%, respectively. The relative error RE for the mean value and variance in the case with F_1 in Force Model II are 0.08% and 3.87%, respectively.

When two random moving forces are applied on the beam structure, i.e. the two moving force model (Force Model I) is adopted, and the number of K-L components for the excitation force remained after truncation is 199. Both the cases for the beam under deterministic excitation forces (F_1 and F_2 with $COV_F=0\%$) and random excitation forces (F_1 and F_2 with $COV_F=10\%$) are studied. It is noted that the former one is a special case in which only the first term $\mathbf{f}^{(0)}(t)$ in the force vector in Equation (5.16) is non-zero. The mean and variance of the mid-span displacement of the beam calculated from the proposed

method are compared with those from the MCS in Figures 5.4 and 5.5, respectively. Results show that the response statistics from the two methods are in good agreement. However, the proposed method is much faster with the computation time required for the proposed method at 41.33 *s* compared with 1772.59 *s* required by the MCS for 10000 runs on a computer with Pentium(R) DCPU 3.00Hz with 2GB RAM. Within the time required in the proposed method, only 700 runs for the MCS can be conducted. The resulting percentage errors in the mean value and variance of the mid-span displacement of bridge are respectively 0.169% and 7.27% compared with the corresponding errors using the proposed method of 0.034% and 4.34% respectively when $COV_E=COV_\rho=5\%$ and $COV_F=10\%$.

The above study on the verification of the forward analysis shows similar performance of the algorithm with the three kinds of force models proposed. In the following study on the factors which may affect the accuracy of the proposed method, the Force Model I with two moving forces shown in Section 5.4.1.2 will be adopted.

5.4.2.2 Effect of Moving Velocity

The robustness of the proposed method is further investigated with different velocity for the two moving forces. The coefficient of variation of random system parameters is set at 5%, i.e. $COV_E=COV_\rho=5\%$. The mid-span displacement calculated from the proposed method are compared with those from MCS with 10000 samples in Table 5.1 for both the case with deterministic

excitation forces (F_1 and F_2 with $COV_F=0\%$) and random excitation forces (F_1 and F_2 with $COV_F=10\%$) under different velocities. The relative errors are calculated according to Equation (3.39). Results from two methods are shown in good agreement especially for the mean value. It may be concluded that the accuracy of the proposed algorithm is insensitive to the velocity of the moving forces. In the sub-Sections 5.4.2.3 and 5.4.2.4, a moving velocity of 40 m/s for the two moving forces will be adopted.

5.4.2.3 Effect of the Level of Randomness in System Parameters

The accuracy of the proposed method with different levels of uncertainty in system parameters is studied in this sub-Section. Again MCS with 10000 samples is used to obtain the reference sets of results which are regarded to be “accurate”. The random system with both deterministic excitation forces (F_1 and F_2 with $COV_F=0\%$) and random excitation forces (F_1 and F_2 with $COV_F=10\%$) is investigated. Different coefficients of variation for the elastic modulus E and mass density ρ with values equal to 1%, 2%, 5% and 10%, respectively, are adopted and the statistics of the mid-span displacement are calculated using both methods. The relative difference of the mid-span displacement between the results from the proposed method and MCS according to Equation (3.39) is shown in Table 5.2. Results from the proposed method agree well with those from the MCS. There is very small difference for the calculated mean values and the relative difference increases slightly with the randomness of system parameters. The calculated variance is accurate when the coefficient of variations

of the system parameters is small, e.g. smaller than 5%. When the level of randomness in system parameters increases, relative large error emerged as shown in Table 5.2 for $COV_E=COV_\rho=10\%$ which indicates the Gaussian assumption for the response in this case is inappropriate and the non-Gaussian assumption should be adopted for the random response of the beam.

5.4.2.4 Effect of the Level of Randomness in Excitation

The coefficient of variation of the system parameters is maintained at $COV_E=COV_\rho=5\%$ and the accuracy of the proposed method with different levels of randomness in excitation is studied in this sub-Section. Since the randomness in the excitation forces in bridge-vehicle interaction problem tends to be large due to the road surface roughness of the bad road condition (Da Silva 2004), the coefficient of variation of the forces in this study are set to 5%, 10%, 20%, 50% and 80%. The “reference” mid-span displacements calculated from MCS are compared with those from the proposed method under random forces with different levels of randomness in Table 5.3 according to the relative difference computed from Equation (3.39). For both the calculated mean and variance, results from the two methods are similar indicating that large uncertainties in excitation forces can be modeled satisfactorily by employing the KLE in the proposed method. The relative difference in the mean value increases slightly with an increase in the randomness of the excitation forces while the relative error in the variance decreases slightly. The latter indicates that the error in the proposed algorithm is mainly influenced by the COV of the system parameters.

When the randomness in the excitation forces is large, the influence from COV of the system model will become less significant, and results from the proposed method will become more accurate.

5.4.3 Inverse Analysis

In the numerical simulations for the inverse analysis, two kinds of single moving force model (F_1 in Force Model I and II) are adopted. To demonstrate the feasibility of the moving force identification algorithm proposed, F_1 in Force Model I will be firstly adopted to study the error occurs at each stage of the inverse procedure following the identification steps in Section 5.3.4. Different factors which may affect the accuracy of the proposed algorithm will be further investigated for the case with two kinds of single moving force model.

In *Step 1*, 500 sample sets of seven nodal displacements evenly distributed along the structure are obtained from simulation using the proposed method in the forward analysis as described in Section 5.2.1 which is noted as the K-L method. The Latin Hypercube Sampling (LHS) is adopted to generate the corresponding samples of the standard Gaussian random variables in Equation (5.18). The covariance kernel of the response \mathbf{KN} is shown in Figure 5.6.

In *Step 2*, a comparison is given in Figure 5.7 between the mean value of the identified moving force and the theoretical one obtained from sample sets of the random force used in the forward analysis. Result shows that the averaging of response samples removes the effect of randomness in the responses and greatly

improves the accuracy in the force identification. The relative error $RE=3.37\%$ is very small.

In **Step 3**, substitute the mean value of the identified moving force into Equation (5.29) and use Newmark- β method to solve the differential equations. The components $y_s^{(j)}$ are calculated and the covariance kernel \mathbf{KN}_s subsequently obtained is shown in Figure 5.8. The relative error between the calculated and theoretical covariance kernel \mathbf{KN}_s is shown in Figure 5.9. The theoretical covariance kernel is calculated using the true mean value instead of the mean value of the identified moving force. The corresponding relative error $RE=2.47\%$ is quite small indicating that the error arising from the identification of the mean value of force has little effect on the eigenvalues of kernel \mathbf{KN}_s .

In **Step 4**, calculate \mathbf{KN}_d according to Equation (5.32) using \mathbf{KN} minus \mathbf{KN}_s . The relative error between the calculated and theoretical covariance kernel \mathbf{KN}_d which is the third term in Equation (5.32) is shown in Figure 5.10. The theoretical covariance kernel is obtained using the K-L components of response in the forward problem from Equation (5.16) by setting $COV_E=COV_p=0\%$. The corresponding $RE=10.51\%$ is relatively small. In the KLE of \mathbf{KN}_d , the eigenvalues and eigenvectors forming the K-L components of responses $\hat{\mathbf{y}}_d^{(j)}$ will directly affect the statistics of the identified moving force. Therefore it is important to show how significant the effect on the eigensolutions of \mathbf{KN}_d when the third term in Equation (5.32) is ignored. A comparison of the first eight eigenvalues for the calculated and theoretical covariance kernel \mathbf{KN}_d is shown in

Figure 5.11. The comparison of the first eight K-L components of the mid-span displacement of the beam structure calculated from the theoretical and calculated \mathbf{KN}_d is shown in Figure 5.12. Results show that eliminating $2 \sum_{j=1}^{k_R} \mathbf{Y}_d^{(j)} \mathbf{Y}_s^{(j)T}$ in Equation (5.32) will only affect several order of the eigensolutions of \mathbf{KN}_d , e.g. the 3rd, 4th and 5th orders. Most eigensolutions remain the same as the theoretical ones especially for the first two orders which correspond to the two largest eigenvalues. The comparison of the identified and theoretical statistics of moving force is shown in Figure 5.13 with the relative error for the mean value and variance equal to 3.44% and 52.37% respectively.

In the proposed algorithm, the mean value of the identified moving force, which may be the most important statistic of the moving force, is accurately identified. It is noted that the error for the variance of moving force is quite large because the assumption of the third term in Equation (5.32) is small compared the \mathbf{KN}_d may not valid when randomness in excitation in small. This is the first type of error. Since the variance of the identified moving force is the summation from all the identified corresponding components of the moving force as demonstrated in Equation (5.31), small fluctuations in each K-L component of displacement will be enlarged in the identification and will cause an overestimation on the variance of the moving force. This is noted as the second type of error. The third type of error lies with the cubic spline interpolation in the computation for the velocities and accelerations from the K-L components of displacement which have relatively high frequency fluctuations. This type of

error is only significant for the case with F_1 in Force Model I which will lead to an underestimation of the variance of moving force and it can be eliminated by adopting other force models with larger correlation length for the Gaussian random process such as F_1 in Force Model II. Further studies will be provided to study the performance of the proposed force identification algorithm with discussions on different factors which may affect the accuracy.

5.4.3.1 Effect of the Number of Samples Used

The number of samples of displacement used in the simulation will affect the accuracy of the identification algorithm because the response statistics of the beam structure is required to identify the statistics of the moving force. If a relatively small number of displacement samples are adopted in the moving force identification, they may fail to represent the statistics of the whole population with the randomness carrying into the identification results, i.e. different statistics of force will be obtained from using different groups of small number of samples.

The influence of the number of samples on the accuracy of the identified force statistics is studied with results for the two kinds of single moving force model shown in Table 5.4 and Table 5.5. Results show that the error in the mean value increases slightly with a decrease in the sample number. When the number of response samples is small, the mean value of the identified moving force may become unstable. The relative error in the variance of identified F_1 in Force Model I is quite large since the third kind of error described in the paragraph

above Section 5.4.3.1 is included. The relative error in the variance of identified F_1 in Force Model II is relatively small which increases slightly with decreasing sample number down to 100 and it goes up sharply with further decrease in the sample number. When the sample number is less than 100, different groups of samples may result in different variance of the identified force. Such instability of result is noted for the cases of 10 samples and 20 samples in Table 5.4.

A comparison of the identified and theoretical variance for the moving force (F_1 in Force Model I) with 500 response samples when $COV_E=COV_\rho=5\%$ and $COV_F=10\%$ is shown in Figure 5.13. Although the relative error in the variance identification from a small number of sample is large, the variance of moving force can still be estimated with a relative error equals to 134.4% together with the mean value and the latter is very accurate corresponding to the theoretical moving force using five samples for F_1 in Force Model I $COV_E=COV_\rho=5\%$ and $COV_F=10\%$ as shown in Figure 5.14. A Comparison of the identified and theoretical variance for the moving force (F_1 in Force Model II) with 200 response samples when $COV_E=COV_\rho=5\%$ and $\Phi(\omega_0)=16\times 10^{-6} m^3$ is shown in Figure 5.15., the variance of the identified moving force is shown to be accurate.

Whether the samples used can truly represent the statistics of its population will be the most important factor for the variance identification of moving forces. In the following case study, 200 samples of displacement will be used to maintain a good representation of the response statistics.

5.4.3.2 Effect of the Level of Randomness in System Parameters

Before the result of this study is presented, it is noted from Equation (5.32) that the third term on the right-hand-side which causes error in the identification algorithm will decrease when either the level of randomness in system parameters or in excitation decreases. The kernel \mathbf{KN}_s can be calculated from the assumed level of randomness of system parameters and it is then removed from \mathbf{KN} before the force identification using \mathbf{KN}_d according to Equation (5.32) at the beginning of *Step 4*. The following discussions refer to a comparison of the values of \mathbf{KN}_d and the third term in Equation (5.32) which will be the key point on the accuracy of the statistics of the identified force, particularly with the variance.

The identified results when $COV_F=10\%$ for F_1 in Force Model I and $\Phi(\omega_0)=16\times 10^{-6} m^3$ for F_1 in Force Model II with different levels of randomness in system parameters are shown in Tables 5.6 and 5.7, respectively. The error in the mean value of the identified moving force decreases just slightly with the decrease of the level of randomness in system parameters. Error in the variance of the identified moving forces increases with an increase in the level of randomness in system parameters for both force models. The error in variance for identified F_1 in Force Model II is small and it is almost half of that for F_1 in Force Model I when the randomness in system parameters is small. With the increasing of the level of randomness in system parameters, e.g. when COV_E and COV_ρ are larger than 5%, the assumption of a small third term in Equation (5.32) compared to \mathbf{KN}_d may not be true when $COV_F=10\%$, and the identification error

becomes large for both force models. It is noted that the error in the variance for the case $COV_E=COV_\rho=2\%$ is smaller than that for the case of $COV_E=COV_\rho=1\%$ in Table 5.6. This can be explained as follows: when the level of randomness in system parameters decreases, the second type of error defined in the paragraph above Section 5.4.3.1 causing an overestimated variance will decrease. The cubic spline interpolation procedure which would cause an underestimated variance noted as the third type of error in the identification becomes the main source of error. This phenomenon can not be found in Table 5.7 for the case with F_1 in Force Model II since the third type of error is very small and it can be ignored.

5.4.3.3 Effect of the Level of Randomness in Excitation

Another study on the influence of level of randomness in excitation on the accuracy of identified force statistics when $COV_E=COV_\rho=5\%$ for the two kinds of force model are shown in Tables 5.8 and 5.9. Results show that error in the mean value of the identified moving force decreases just slightly with the decrease in the level of randomness in excitation. Error in the variance increases when the level of randomness in excitation decreases. According to Equation (5.32), both \mathbf{KN}_d and the third term decrease when COV_F decreases. Results show that when COV_F becomes small, the third term in Equation (5.32) can not be assumed to be small compared to \mathbf{KN}_d , and thus the identification error becomes large. On the other hand, when COV_F is large, the third term in Equation (5.32) becomes small compared with \mathbf{KN}_d , and the variance can then be accurately identified. When COV_F is large, the error in variance of the

identified moving force will not decrease with an increasing COV_F . A comparison of the identified and theoretical statistics of moving force F_1 in Force Model I using 200 samples with $COV_E=COV_\rho=5\%$ and $COV_F=15\%$ is shown in Figure 5.16. Results show that when KN_d is relatively large compared with the third term in Equation (5.32), all the statistics including mean value and variance of the moving force can be accurately identified. It should be noted that in bridge-vehicle interaction problem with uncertainty in system parameters, the randomness in excitation forces due to road surface roughness will be large compared with the randomness in system parameters. The proposed stochastic moving force identification technique in this Chapter will be suitable for identifying the statistics of the interaction forces. As shown in Table 5.9, except for the case when $\Phi(\omega_0)=1\times 10^{-6} m^3$ for F_1 in Force Model II where the roughness of the path surface is very small, both the mean value and variance of the moving force can be accurately identified.

5.5 Discussions

The proposed method has been shown much more efficient than the Monte Carlo simulation in the forward analysis. The required number of K-L components that represent the random process is a very important index affecting the computation efficiency of the proposed method, and it will be affected by the selected covariance kernel. A covariance kernel that needs the minimum number of terms in its representation should be selected especially for system with a

larger number of degrees-of-freedom. Attention is drawn to Equation (3.17) where the covariance matrix tends to become very large when the number of the components in vector $\mathbf{V}(t,\theta)$ or the number of time instances increases leading to long computation time with the eigenvalue analysis. A high sampling rate of data is therefore not recommended in the stochastic analysis as a result of the above argument. A Galerkin type procedure (Ghanem and Spanos 1991) can also be employed for solving the Fredholm equation shown in Equation (3.7) to improve the computational efficiency of the eigenvalue problem. However, the method used in this Chapter is chosen as an alternative.

The numerical studies in Section 5.4.3 refer to the inverse identification of a single moving force crossing a beam structure. According to the equation of motion of the beam-load model in Equation (5.16) that more forces can be easily included in the identification, the coupling of these moving forces may be difficult to separate. The mean values of these identified moving forces may not be as accurate as that for a single moving force, and this will lead to further degradation of the variance. To identify multiple forces, the inverse procedure with a least-squares solution of Equation (5.27) adopted in this Chapter may not give results as good as for the case of a single moving force. Further research should be carried out to improve the proposed method by giving estimation on the third term in Equation (5.32) rather than ignore this term.

By eliminating the location matrix $\mathbf{H}_b(x)$ in the equation of motion of the stochastic system, the algorithm can give promising results not limited to the

stochastic moving force identification but to any force identification problem in a dynamic system with relatively small uncertainty in system parameters.

5.6 Summary

A new approach for the dynamic analysis of a beam-load system considering uncertainties in both the system parameter and excitation is presented. The material properties such as the mass density, elastic modulus and damping of the beam structure as well as the random moving forces on top are assumed as Gaussian random processes, The Karhunen-Loève expansion is employed to represent these Gaussian random processes in the stochastic modeling. The response of beam is assumed with Gaussian distribution under the assumption of the small randomness in the system parameters. The formulated mathematical model for the stochastic beam-load system is solved by Newmark- β method. With reference to the stochastic finite element model and the force identification algorithm developed for a deterministic system with Gaussian random excitation, a general algorithm that includes both the Gaussian system parameters and excitations in the inverse problem is also developed. Numerical simulations are conducted to verify the proposed model in the forward analysis and in stochastic moving force identification. Different factors which may affect the accuracy of the proposed model and algorithm are investigated.

In the forward analysis, results show that the proposed method has high computational efficiency, insensitive to moving velocity of the forces and good

accuracy for the practical case with relatively small uncertainty in system parameters but large randomness in excitation.

In the inverse analysis, the errors in the mean value of the identified force increase slightly with a decrease in the number of sample of “measured” responses. Whether or not the samples used can truly represent the statistics of its population will be the most important requirement for an accurate identification of the variance of the moving force. A method to determine the threshold number of sample is proposed to maintain a good representation of the response statistics of the moving force. The effect of level of randomness depends on the relationship between the values of the covariance kernel for the case of a deterministic system under random excitation (\mathbf{KN}_d) and the third term in Equation (5.32) which is the key to good accuracy in the statistics of the identified force particularly the variance. When the covariance kernel is relatively large compared to the error term (the third term) in Equation (5.32), all the statistics including the mean value and variance of the moving force can be accurately identified.

For the case with large uncertainties in the system parameters, higher order polynomial chaos expansion may be adopted to represent the random response in the proposed model at the expense of exponentially increased computational cost which will be introduced in next Chapter.

Table 5.1 - Relative error of mid-span displacement for different vehicle speed

Vehicle Speed (m/s)	$COV_E = COV_\rho = 5\%$					$COV_F = 10\%$				
	10	20	30	40	50	10	20	30	40	50
Mean Value	0.003	0.009	0.005	0.055	0.055	0.100	0.080	0.027	0.034	0.022
Variance	1.633	1.649	1.310	1.455	1.675	4.628	5.133	5.812	4.344	5.862

Table 5.2 - Relative error of mid-span displacement for different level of randomness in system parameters

RE (%)	$(COV_F = 0\%)$				$(COV_F = 10\%)$			
	$COV_E = COV_\rho$	1%	2%	5%	10%	1%	2%	5%
Mean Value	0.002	0.008	0.055	0.089	0.032	0.041	0.034	0.099
Variance	0.621	1.293	1.455	6.624	3.697	4.169	4.344	5.826

Table 5.3 - Relative error of mid-span displacement for different level of randomness in excitation forces

RE (%)	$COV_E = COV_\rho = 5\%$				
COV_F	5%	10%	20%	50%	80%
Mean Value	0.020	0.032	0.061	0.153	0.251
Variance	4.821	4.344	2.550	2.117	1.810

Table 5.4 - Relative error in the identified forces from different number of response samples (F_1 in Force Model I)

FE (%)	Number of response samples							
	5	10	20	50	100	150	200	500
Mean value	8.31	5.76	4.48	3.95	3.48	3.49	3.40	3.37
Variance	134.4	108.7	138.1	91.00	74.86	66.84	55.28	52.37

Table 5.5 - Relative error in the identified forces from different number of response samples (F_1 in Force Model II)

FE (%)	Number of response samples							
	5	10	20	50	100	150	200	500
Mean value	10.30	11.93	4.88	3.95	3.48	3.45	3.45	3.45
Variance	-	-	63.92	27.92	18.84	21.00	18.63	19.80

'-' denotes extremely large value.

Table 5.6 - Relative error in the identified force for different level of uncertainty in system parameters (F_1 in Force Model I)

FE (%)		COV_E and COV_ρ				
		1%	2%	5%	7%	10%
200 samples	Mean value	3.34	3.34	3.40	3.43	3.56
$COV_F=10\%$	Variance	43.85	36.13	55.28	119.8	232.5

Table 5.7 - Relative error in the identified force for different level of uncertainty in system parameters (F_1 in Force Model II)

FE (%)		COV_E and COV_ρ				
		1%	2%	5%	7%	10%
200 samples	Mean value	3.50	3.50	3.44	3.41	3.38
$\Phi(\omega_0)=16 \times 10^{-6}$	Variance	20.13	20.91	19.34	73.41	236.7

Table 5.8 - Relative error in the identified forces for different level of uncertainty in excitation (F_1 in Force Model I)

FE (%)		COV_F					
		1%	2%	5%	10%	15%	20%
200 samples $COV_E=5\%$ $COV_\rho=5\%$	Mean value	3.37	3.38	3.37	3.40	3.45	3.45
	Variance	-	-	272.1	55.28	30.40	31.81

'-' denotes extremely large value.

Table 5.9 - Relative error in the identified forces for different level of uncertainty in excitation (F_1 in Force Model II)

FE (%)		$\Phi(\omega_0)$ (10^{-6})				
		1	4	16	64	256
200 samples $COV_E=5\%$ $COV_\rho=5\%$	Mean value	3.45	3.44	3.44	3.46	3.43
	Variance	47.41	27.16	18.00	18.73	19.75

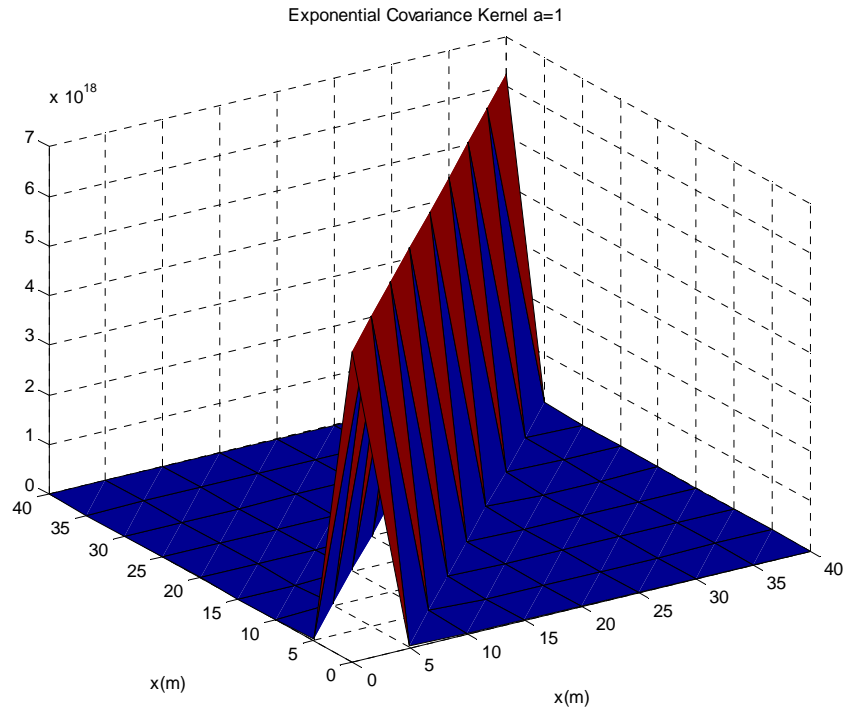


Figure 5.1 - Kernel for the K-L decomposition

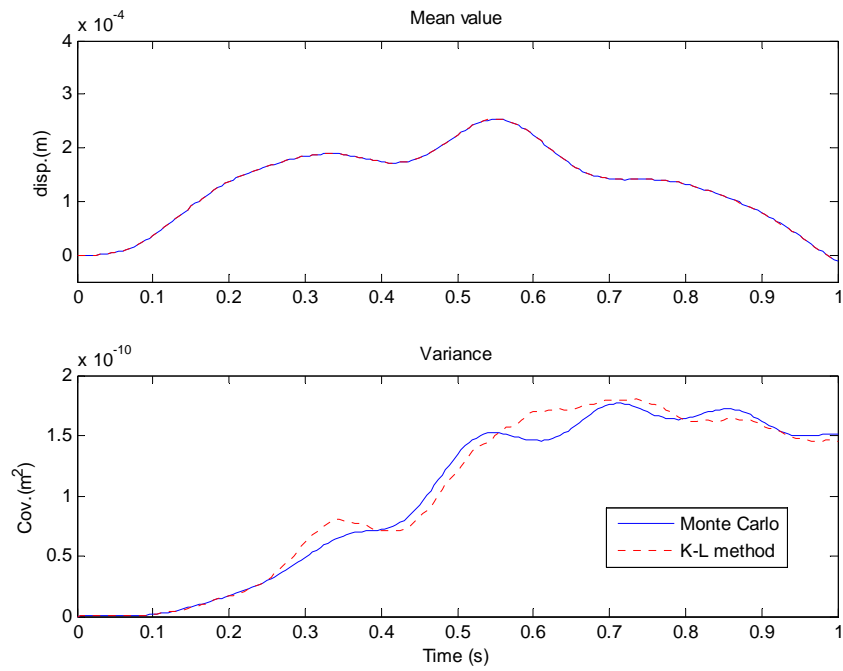


Figure 5.2 - Comparison of statistics of mid-span displacement (F_1 in Force Model I)

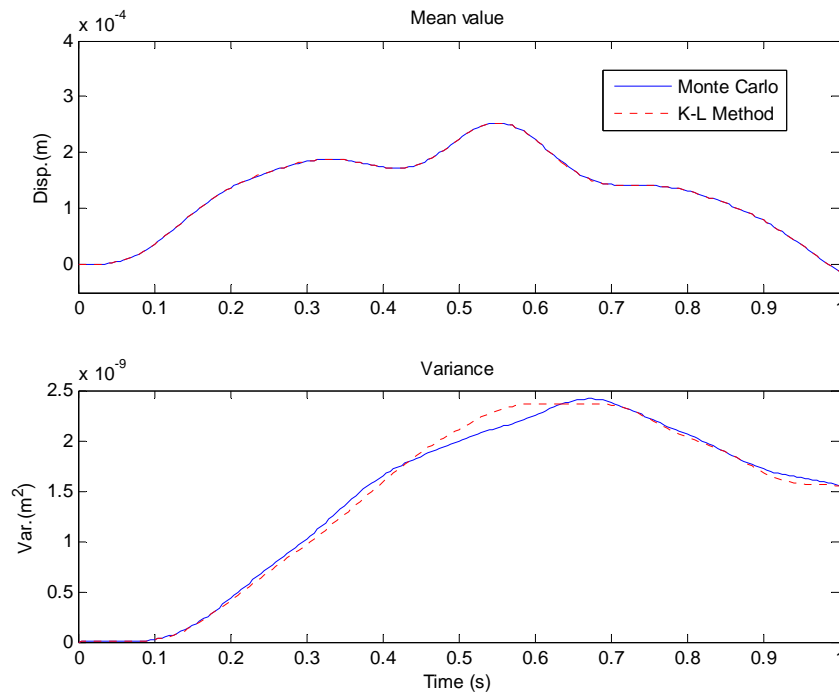


Figure 5.3 - Comparison of statistics of mid-span displacement (F_1 in Force Model II)

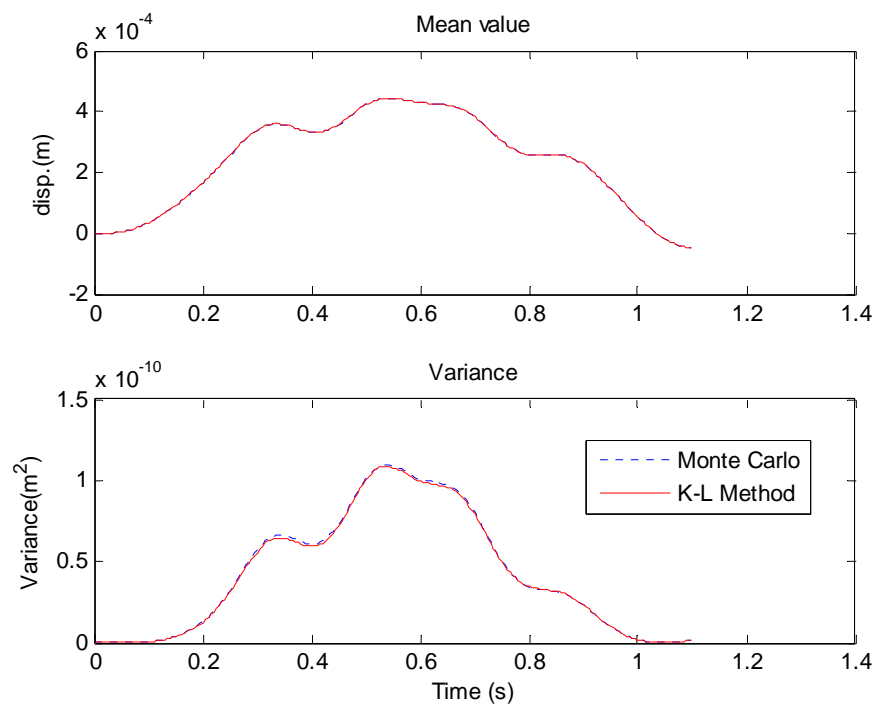


Figure 5.4 - Comparison of statistics of mid-span displacement for $COV_F=0\%$ (Force Model I)

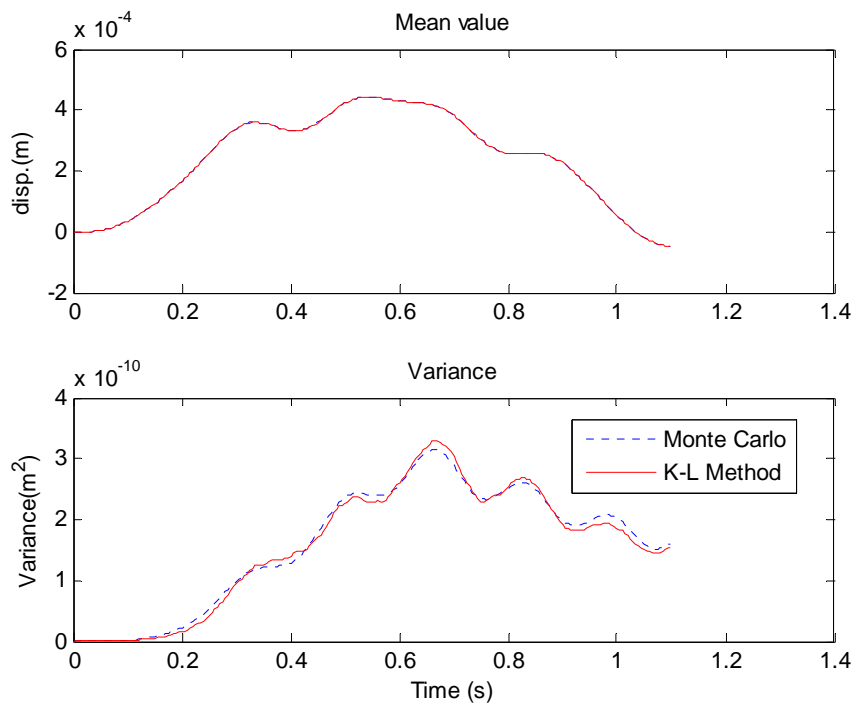


Figure 5.5 - Comparison of statistics of mid-span displacement for $COV_F=10\%$ (Force Model I)

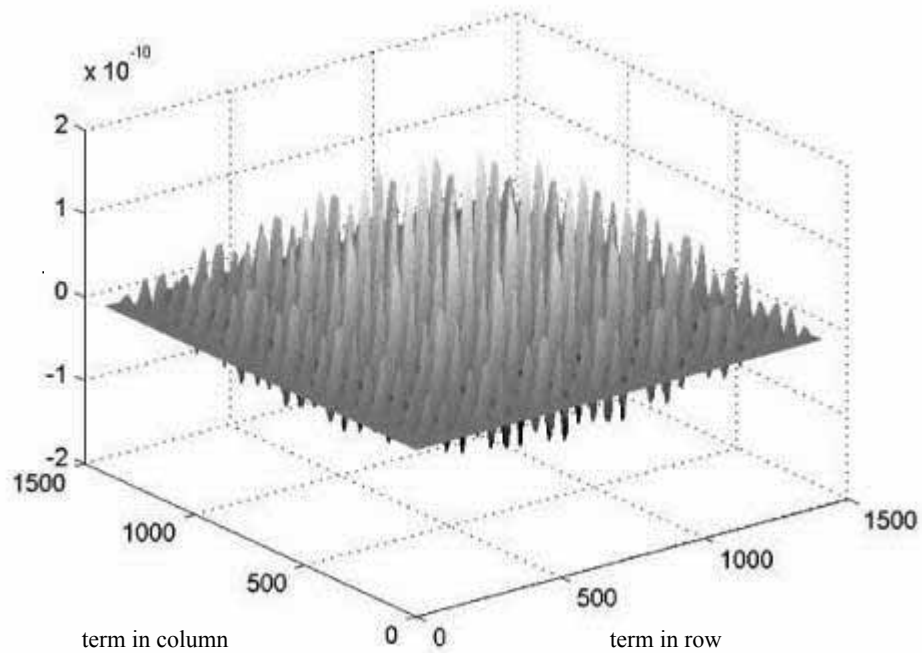


Figure 5.6 - Covariance kernel of KN

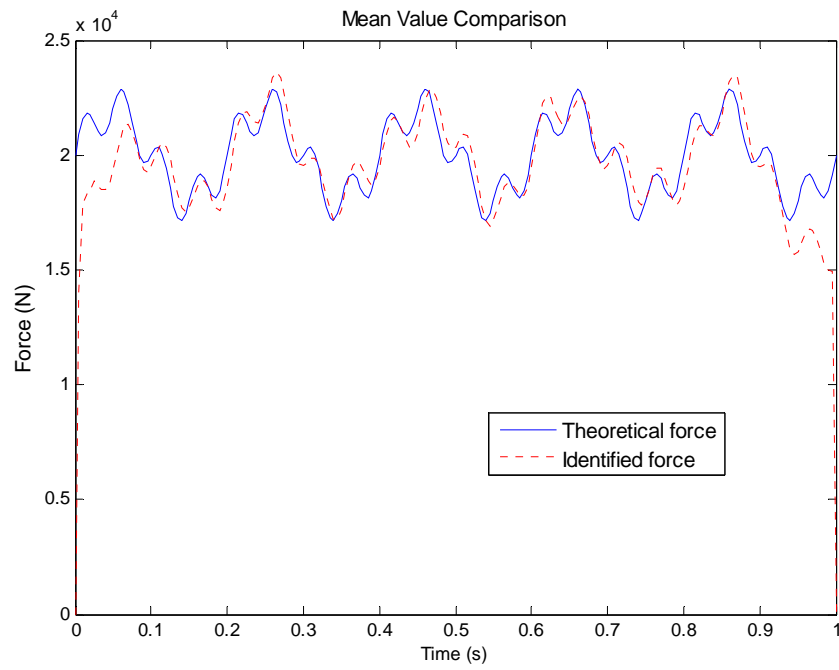


Figure 5.7 - Comparison of identified and theoretical moving force

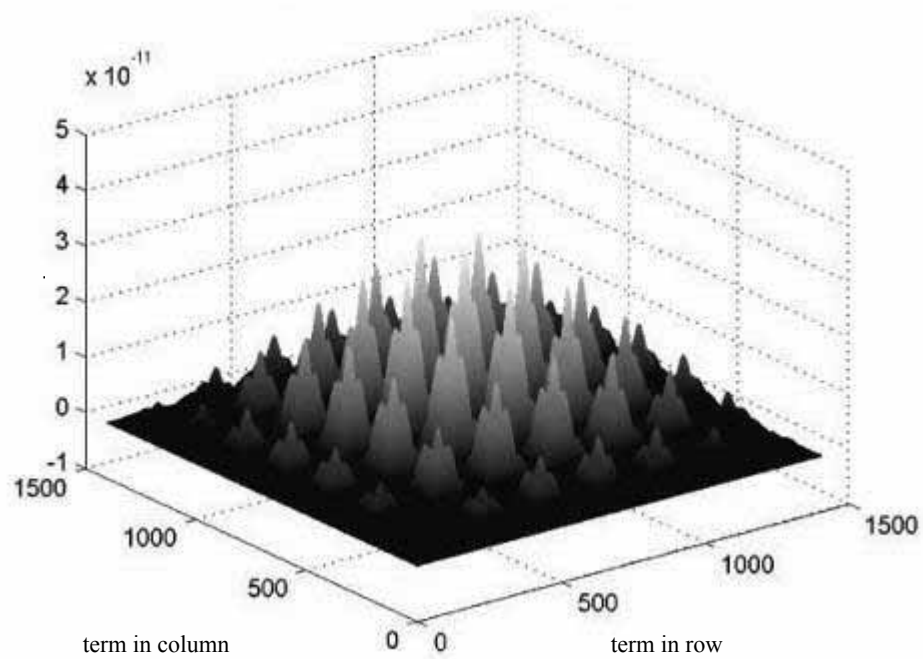


Figure 5.8 - Covariance kernel of \mathbf{KN}_s

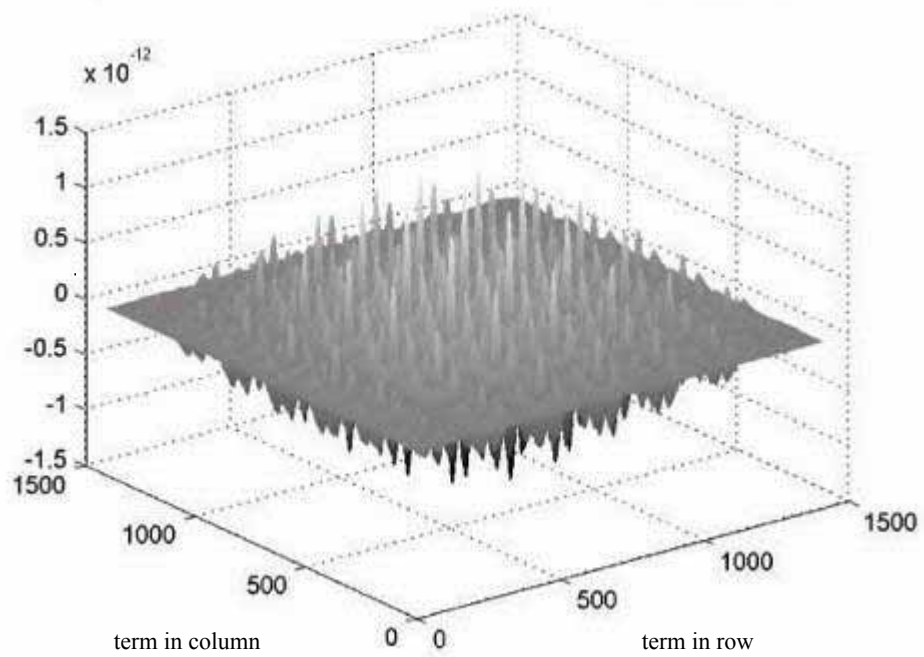


Figure 5.9 - Error between the calculated and theoretical KN_s

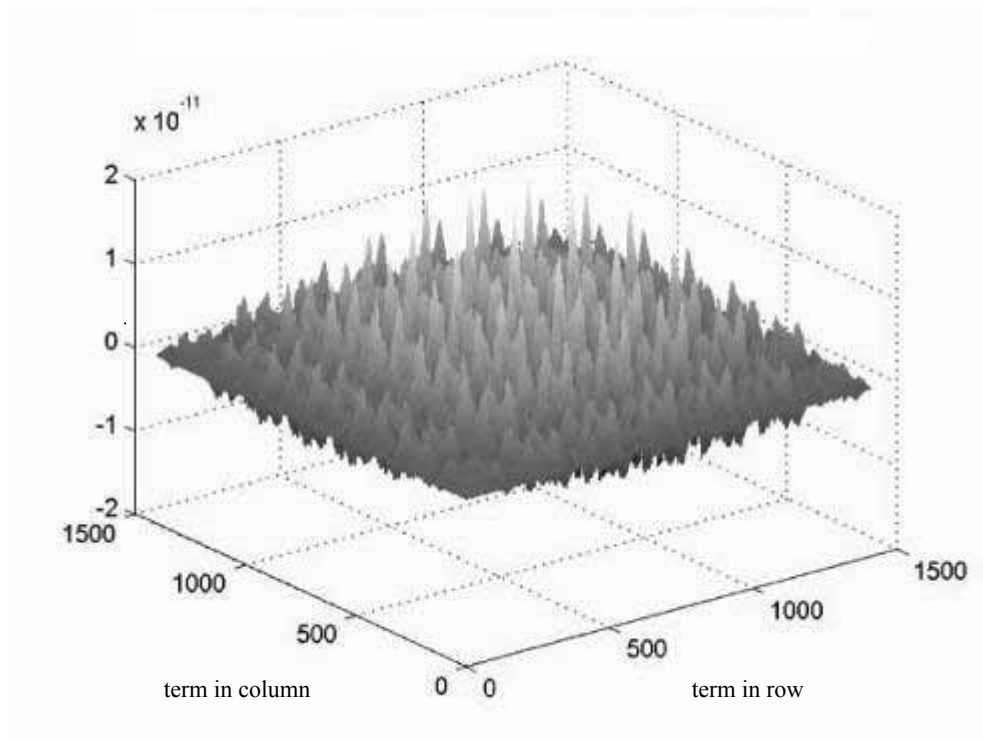


Figure 5.10 - Error between the calculated and theoretical KN_d

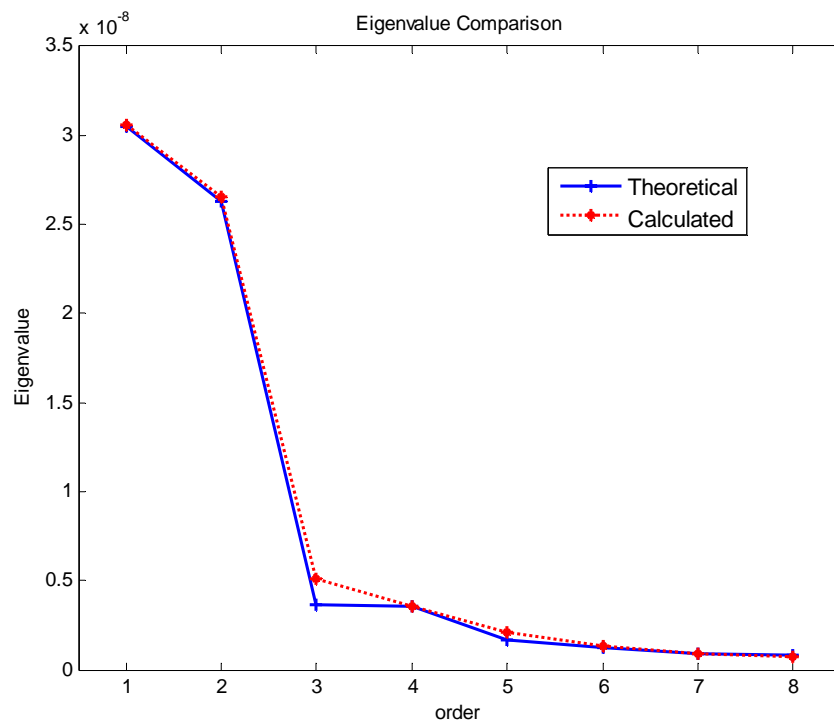


Figure 5.11 - Comparison of the first eight eigenvalues of \mathbf{KN}_d

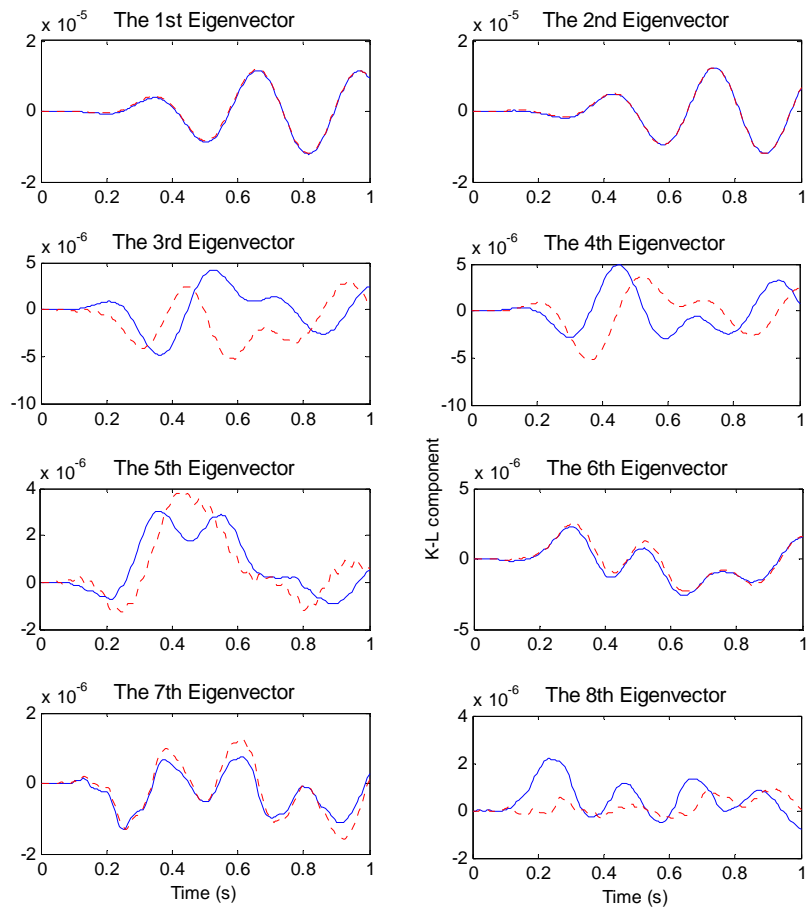


Figure 5.12 - Comparison of the first eight K-L components of mid-span displacement

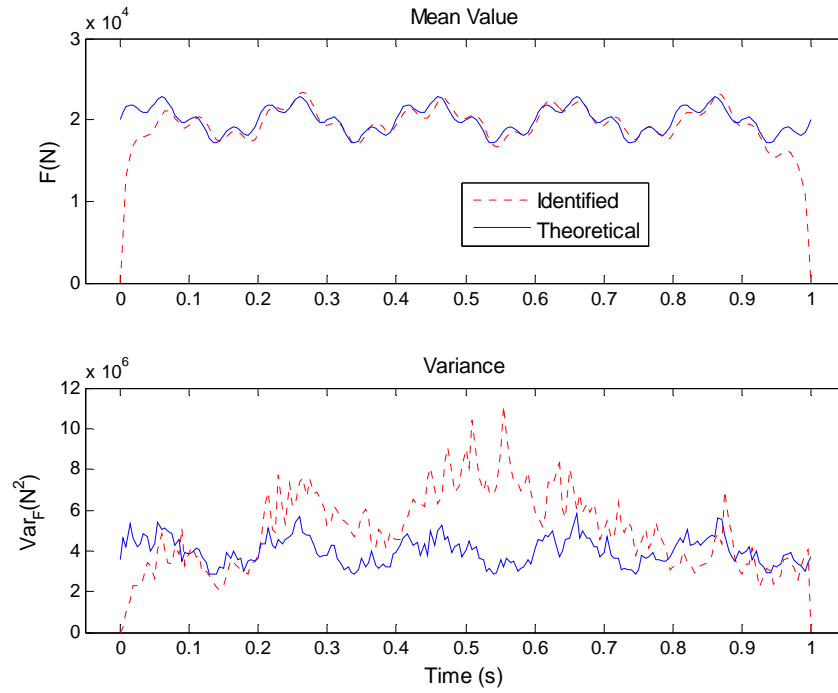


Figure 5.13 - Comparison of identified and theoretical force statistics (500 samples)

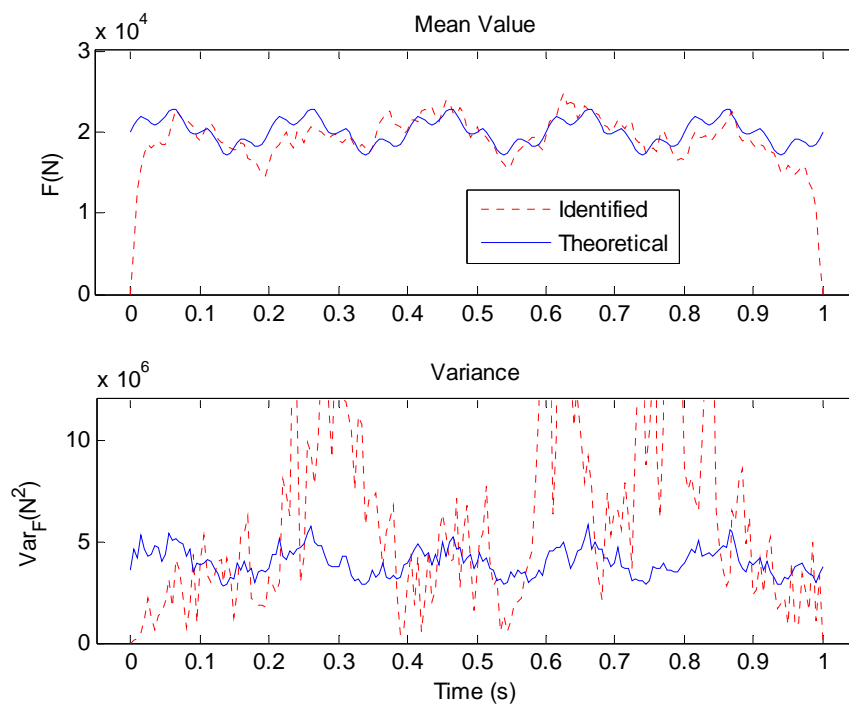


Figure 5.14 - Comparison of identified and theoretical force statistics (5 samples)

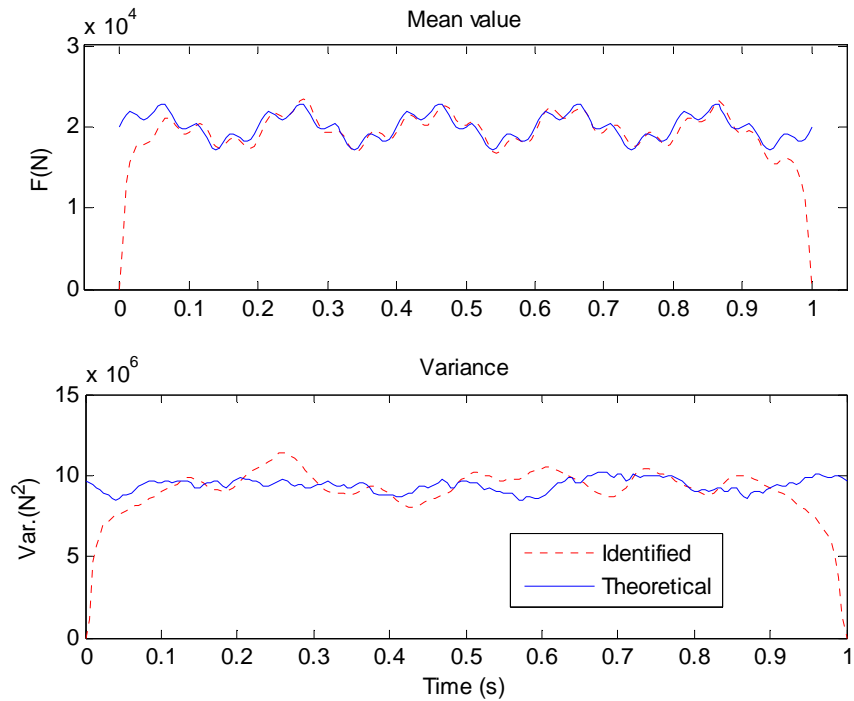


Figure 5.15 - Comparison of identified and theoretical force statistics with $\Phi(\omega_0)=16 \times 10^{-6} m^3$ (200 samples)

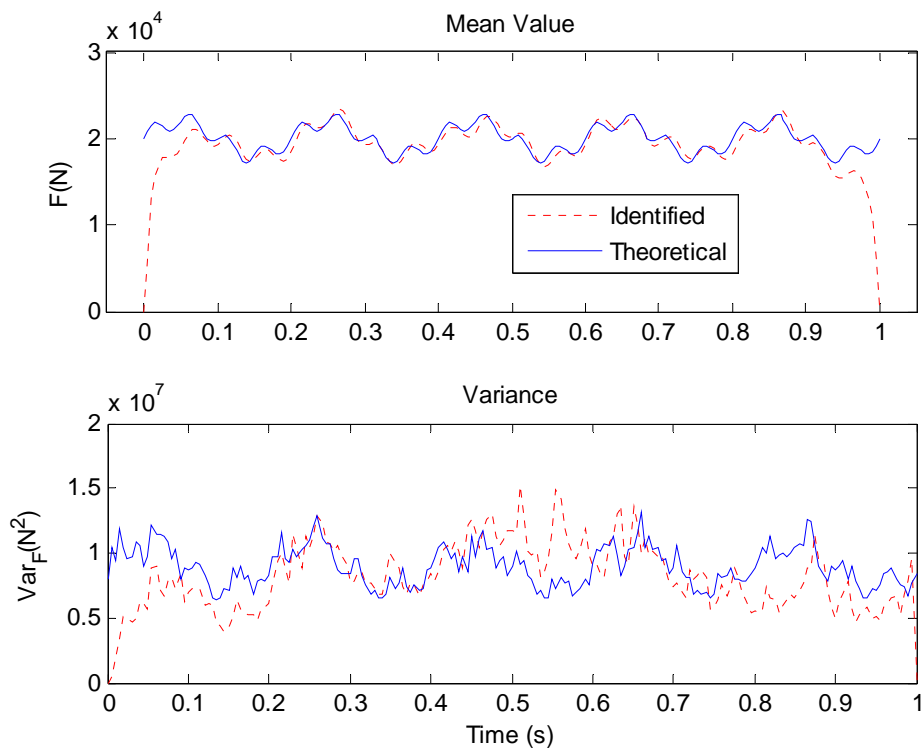


Figure 5.16 - Comparison of identified and theoretical force statistics with $COV_F=15\%$ (200 samples)

CHAPTER 6

STOCHASTIC BEAM-LOAD SYSTEM: THE SSFEM MODEL

6.1 Introduction

In Chapter FIVE, a Gaussian assumption was made for the random response based on which an “economic” stochastic finite element model is proposed for the problem of a beam under stochastic moving loads with relatively small uncertainty in the physical parameters of the beam. Numerical results show the proposed model is accurate and efficient. However, when the level of randomness in system parameter increases, the proposed model will become inaccurate and the Polynomial Chaos should be adopted to represent the response of the beam structure which may have non-Gaussian properties. This method is noted as the Spectral Stochastic Finite Element Method (SSFEM) proposed by Ghanem and Spanos (1991). A detail review of the applications of SSFEM on various engineering problems has been conducted in Section 2.3.3.2. In this Chapter, the dynamic response calculation of a beam structure with both inherent randomness and stochastic loading moving on top will be conducted with the SSFEM to model the uncertainties. The algorithm proposed in this Chapter can solve the problem of the beam-load system with large uncertainties in both system

parameters and excitation forces. The random moving forces and system parameters are assumed to have Gaussian/non-Gaussian properties and they will be represented by the Karhunen-Loève Expansion (KLE)/Polynomial Chaos Expansion (PCE). The stochastic response of the beam structure with non-Gaussian properties will be represented by the Polynomial Chaos Expansion. The formulated model will be verified in numerical simulations with the Monte Carlo Simulation. Different levels of randomness for both the excitation forces and system parameters as well as the order of Polynomial Chaos used which may affect the accuracy of the proposed algorithm will be investigated.

The outline of this Chapter is: a review on the basic theory and applications on representing the random processes with the Polynomial Chaos will be given in Section 6.2. The modeling of the beam-load system with uncertainties is proposed in Section 6.3 in which the SSFEM is adopted. The system parameters are firstly assumed as Gaussian random processes with prescribed covariance kernels and then will be assumed to have non-Gaussian property for further study. Numerical simulations are conducted in Section 6.4 to verify the algorithm proposed and to investigate different factors which may affect the accuracy. A summary will be given in Section 6.5 with some conclusions.

6.2. Polynomial Chaos

Wiener's polynomial chaos (Wiener 1938) is fundamentally a framework for separating the stochastic components of system response from the

deterministic components. It derives from the Cameron-Martin theorem (Cameron and Martin 1947) which establishes that a random process with finite second order moments can be decomposed into an infinite, convergent series of polynomials of random variables. The Hermite orthogonal polynomial is the first such series which is known to be the optimum basis for Gaussian distributions because the weighting function of the Hermite polynomials is the same as their probability density function. Treatment of other important distributions, e.g. uniform, Poisson distribution, etc. is achieved via the Askey scheme discussed by Xiu and Karniadakis (2002) in which each distribution type is related to a specific group of orthogonal polynomials to achieve the convergence properties.

The basic theory of adopting the Polynomial Chaos to represent a random process will be introduced in the following.

Any element $u(\theta)$ from a square integrable space admits the following representation,

$$\begin{aligned}
 u(\theta) = & a_0 \Gamma_0 + \sum_{i_1=1}^{\infty} a_{i_1} \Gamma_1(\xi_{i_1}(\theta)) + \sum_{i_1=1}^{\infty} \sum_{i_2=1}^{i_1} a_{i_1 i_2} \Gamma_2(\xi_{i_1}(\theta), \xi_{i_2}(\theta)) \\
 & + \sum_{i_1=1}^{\infty} \sum_{i_2=1}^{i_1} \sum_{i_3=1}^{i_2} a_{i_1 i_2 i_3} \Gamma_3(\xi_{i_1}(\theta), \xi_{i_2}(\theta), \xi_{i_3}(\theta)) + \dots \quad (6.1)
 \end{aligned}$$

where $\Gamma_p(\bullet)$ are the polynomial chaoses of order p , $a_{i_1, i_2, i_3, \dots}$ are deterministic coefficients. The expansion is convergent in the mean-square sense. The polynomial chaoses of order greater than one have zero mean. Polynomials of different order are orthogonal to each other, and so are the polynomials within the same order. It has been proved that Equation (6.1) can be rewritten in the following

form (Ghanem and Spanos 1991),

$$u(\theta) = \sum_{i=0}^{\infty} b_i \Psi_i(\xi(\theta)) \quad (6.2)$$

where b_i are the generalized Fourier coefficients and $\Psi_i(\xi(\theta))$ are the Hermite Polynomials of $\xi_i(\theta)$ with $\xi_i(\theta)$ defined as the standard Gaussian random variables.

There is a one-to-one correspondence between the functions $\Psi(\cdot)$ and $\Gamma(\cdot)$. For example, the term $a_0\Gamma_0$ in Equation (6.1) is the same as $b_0\Psi_0$ in Equation (6.2). For the finite dimensional polynomial chaos, the upper limit on the summations in Equation (6.2) is replaced by a number equal to the dimension of the polynomials involved, when $i_1=2$, $a_1\Gamma_0(\xi_1(\theta))$ and $a_2\Gamma_0(\xi_2(\theta))$ in Equation (6.1) are identical with the term $b_1\Psi_1(\xi_1(\theta))$ and $b_1\Psi_2(\xi_2(\theta))$ in Equation (6.2) respectively. The series in Equation (6.1) can be refined along the random dimension θ either by adding more random variables $\{\xi_i(\theta)\}$ or by increasing the maximum order of polynomials including in the PCE. The first refinement takes into account higher frequency random fluctuations of the underlying stochastic process, while the second refinement captures strong nonlinear dependence of the solution process of this stochastic process (Ghanem 1999b).

The polynomials $\{\Psi_i(\xi(\theta))\}$ are orthogonal satisfying the relationship

$$\langle \Psi_i \Psi_j \rangle = \langle \Psi_i^2 \rangle \delta_{ij} \quad (6.3)$$

where $\langle \cdot \rangle$ denotes the inner product and δ_{ij} is the Kronecker delta. The value of $\langle \Psi_i^2 \rangle$ can be calculated analytically (Ghanem and Spanos 1991).

The generalized Fourier coefficients b_i in Equation (6.2) can be evaluated from

$$b_i = \frac{\langle u(\theta)\Psi_i[\xi(\theta)] \rangle}{\langle \Psi_i[\xi(\theta)]\Psi_i[\xi(\theta)] \rangle} \quad (6.4)$$

To evaluate the coefficients b_i in a PCE of a random process, several numerical methods had been proposed. One of the simple and direct way by adopting MCS to simulate the polynomials of $\xi_i(\theta)$ in Equation (6.4) was introduced by Field et al. (2002). This method needs numerous samples for the standard Gaussian random variables to achieve accurate results. Other sampling techniques such as the important sampling, the LHS and etc. can also be utilized instead of the MCS to improve the computational efficiency. The numerical integration method proposed by Field et al. (2002) is an alternative which also has good performance. The method proposed by Choi et al. (2004) using Latin Hypercube Sampling and Fitting Regression model shows both high efficiency and good accuracy.

The PCE has been extended to represent more complex random processes with non-Gaussian non-stationary properties. A representation of lognormal stochastic process via Polynomial Chaos was proposed by Ghanem (1999c) which is useful in the context of the SSFEM as well as for the analytical investigation of the mathematical properties of lognormal processes. Sakamoto and Ghanem (2002a; 2002b) proposed a method to simulate non-Gaussian non-stationary random processes/fields according to the prescribed marginal PDF and correlation function with the expansion of the non-Gaussian process at discrete points using PCE. On the other hand, the Polynomial Chaos is also adopted to provide mathematical models for the experimental data. Research

works on the identification of the probabilistic models of the random coefficients in stochastic boundary value problems from experimental data were carried out by Desceliers et al. (2006) in which the maximum likelihood estimation is adopted to identify the unknown field projected on the Polynomial Chaos basis. Das et al. (2009) proposed two different computational techniques to estimate the probability model of a finite dimensional approximation of the underlying non-Gaussian and non-stationary stochastic process which is assumed to be completely characterized by experimental measurements taken simultaneously over space and time.

A study on the accuracy of adopting the Polynomial Chaos to represent the non-Gaussian random variables/processes was conducted by Field and Grigoriu (2004) which demonstrated that the accuracy of the PCE improves in some cases as additional terms are retained but not in all cases and the PCE for certain processes may become computational demanding or even prohibitive because of the large number of coefficients that need to be calculated. The “stochastic arithmetic” on Polynomial Chaos and the functions of Polynomial Chaos are often required to be evaluated in problems of computational mechanics, e.g. the inner product of the Polynomial Chaos in SSFEM. An overview on the techniques to solve the numerical challenges in using the Polynomial Chaos to represent stochastic processes was presented by Debusschere et al. (2004) in which several methods were proposed for performing arithmetic on the evaluation of polynomial and non-polynomial functions of variables represented

by PCE.

6.3 System Modeling with Uncertainty

6.3.1 Gaussian System Parameters

6.3.1.1 Representing the Inputs and Outputs

When the system parameters are assumed as Gaussian random processes, they can be represented by the KLE according to Equations (5.8) to (5.10). As the covariance matrix of the response in Equation (3.17) is not known *a-priori*, the nodal displacement vector $\mathbf{R}(t, \theta)$ which may have non-Gaussian property will be expanded by the Polynomial Chaos in this Chapter according to Equation (6.2) as

$$\mathbf{R}(t, \theta) = \sum_{j=0}^{K_R} \Psi_j(\theta) \mathbf{y}^{(j)}(t) \quad (6.5)$$

where $\Psi_j(\theta)$ is the j^{th} order of Polynomial Chaos and $\mathbf{y}^{(j)}(t)$ in Equation (6.5) is the deterministic coefficient corresponding to $\Psi_j(\theta)$. K_R is the dimension of the Polynomial Chaos Expansion which can be calculated as (Ghanem and Spanos 1991),

$$K_R + 1 = \frac{(k_s + p)!}{k_s! p!} \quad (6.6)$$

where k_s is the number of K-L components required in the representation of the response which depends on the number of K-L components adopted in the representation of both the excitation forces and system parameters, e.g. if the randomness in Young's modulus, mass density and excitation forces are

independent, then $k_s = k_E + k_\rho + k_F$. k_E , k_ρ , k_F are the number of K-L components in the KLE of the Gaussian distributed Young's modulus, mass density and the excitation forces as shown in Equations (5.8), (5.9) and (5.11), respectively. p is the order of the Polynomial Chaos.

Therefore, the random velocity and acceleration vectors will take the following form as

$$\dot{\mathbf{R}}(t, \theta) = \sum_{j=0}^{K_R} \Psi_j(\theta) \dot{\mathbf{y}}^{(j)}(t) \quad (6.7)$$

$$\ddot{\mathbf{R}}(t, \theta) = \sum_{j=0}^{K_R} \Psi_j(\theta) \ddot{\mathbf{y}}^{(j)}(t) \quad (6.8)$$

where $\dot{\mathbf{y}}^{(j)}$ and $\ddot{\mathbf{y}}^{(j)}$ are the first and second derivatives of coefficients $\mathbf{y}^{(j)}$ in Equation (6.5).

The KLE of the excitation forces in Equation (5.11) can then be projected on the basis of the Polynomial Chaos and will take the form as

$$\mathbf{F}(t, \theta) = \sum_{j_2=0}^{K_R} \Psi_{j_2}(\theta) \mathbf{F}^{(j_2)}(t) \quad (6.9)$$

where $\{\overbrace{\mathbf{F}^{(0)}(t) \dots \mathbf{F}^{(K_R)}(t)}^{K_R}\}^T = \{\mathbf{f}^{(0)}(t) \quad \overbrace{0 \dots 0}^{(k_E+k_\rho)} \quad \overbrace{\mathbf{f}^{(1)}(t) \dots \mathbf{f}^{(k_F)}(t)}^{k_r} \quad \overbrace{0 \dots 0}^{(K_R-k_r-1)}\}^T$.

6.3.1.2 Formulation of the System

Substituting Equations (5.8) to (5.10), (6.5), and (6.7) to (6.9) into Equation (5.2) and taking the inner product on both sides of the equation with $\Psi_k(\theta)$ and employing the orthogonal property in Equation (6.3), we have

$$\sum_{j=0}^{K_R} \sum_{i_2=0}^{k_\rho} \langle \xi_{i_2}(\theta) \Psi_j(\theta) \Psi_k(\theta) \rangle \mathbf{M}_{i_2} \dot{\mathbf{y}}^{(j)}(t) + \sum_{j=0}^{K_R} \sum_{i_3=0}^{k_c} \langle \xi_{i_3}(\theta) \Psi_j(\theta) \Psi_k(\theta) \rangle \mathbf{C}_{i_3} \dot{\mathbf{y}}^{(j)}(t)$$

$$+ \sum_{j=0}^{K_R} \sum_{i_1=0}^{k_E} \langle \xi_{i_1}(\theta) \Psi_j(\theta) \Psi_k(\theta) \rangle \mathbf{K}_{i_1} \mathbf{y}^{(j)}(t) = \mathbf{H}_b \langle \Psi_k^2 \rangle \mathbf{F}^{(k)}(t) \quad (6.10)$$

$$\text{Let } \mathbf{M}^{(k,j)} = \sum_{i_2=0}^{k_D} \frac{\langle \xi_{i_2}(\theta) \Psi_j(\theta) \Psi_k(\theta) \rangle}{\langle \Psi_k^2 \rangle} \mathbf{M}_{i_2},$$

$$\mathbf{C}^{(k,j)} = \sum_{i_3=0}^{k_C} \frac{\langle \xi_{i_3}(\theta) \Psi_j(\theta) \Psi_k(\theta) \rangle}{\langle \Psi_k^2 \rangle} \mathbf{C}_{i_3} \text{ and } \mathbf{K}^{(k,j)} = \sum_{i_1=0}^{k_E} \frac{\langle \xi_{i_1}(\theta) \Psi_j(\theta) \Psi_k(\theta) \rangle}{\langle \Psi_k^2 \rangle} \mathbf{K}_{i_1}.$$

Rewrite Equation (6.10) in matrix form, we have

$$\begin{aligned} & \begin{bmatrix} \mathbf{M}^{(0,0)} & \mathbf{M}^{(0,1)} & \dots & \mathbf{M}^{(0,K_R)} \\ \mathbf{M}^{(1,0)} & \mathbf{M}^{(1,1)} & \dots & \mathbf{M}^{(1,K_R)} \\ \vdots & \vdots & \ddots & \vdots \\ \mathbf{M}^{(K_R,0)} & \mathbf{M}^{(K_R,1)} & \dots & \mathbf{M}^{(K_R,K_R)} \end{bmatrix} \begin{bmatrix} \ddot{\mathbf{y}}^{(0)}(t) \\ \ddot{\mathbf{y}}^{(1)}(t) \\ \vdots \\ \ddot{\mathbf{y}}^{(K_R)}(t) \end{bmatrix} + \begin{bmatrix} \mathbf{C}^{(0,0)} & \mathbf{C}^{(0,1)} & \dots & \mathbf{C}^{(0,K_R)} \\ \mathbf{C}^{(1,0)} & \mathbf{C}^{(1,1)} & \dots & \mathbf{C}^{(1,K_R)} \\ \vdots & \vdots & \ddots & \vdots \\ \mathbf{C}^{(K_R,0)} & \mathbf{C}^{(K_R,1)} & \dots & \mathbf{C}^{(K_R,K_R)} \end{bmatrix} \begin{bmatrix} \dot{\mathbf{y}}^{(0)}(t) \\ \dot{\mathbf{y}}^{(1)}(t) \\ \vdots \\ \dot{\mathbf{y}}^{(K_R)}(t) \end{bmatrix} \\ & + \begin{bmatrix} \mathbf{K}^{(0,0)} & \mathbf{K}^{(0,1)} & \dots & \mathbf{K}^{(0,K_R)} \\ \mathbf{K}^{(1,0)} & \mathbf{K}^{(1,1)} & \dots & \mathbf{K}^{(1,K_R)} \\ \vdots & \vdots & \ddots & \vdots \\ \mathbf{K}^{(K_R,0)} & \mathbf{K}^{(K_R,1)} & \dots & \mathbf{K}^{(K_R,K_R)} \end{bmatrix} \begin{bmatrix} \mathbf{y}^{(0)}(t) \\ \mathbf{y}^{(1)}(t) \\ \vdots \\ \mathbf{y}^{(K_R)}(t) \end{bmatrix} = \begin{bmatrix} \mathbf{H}_b & \mathbf{0} & \dots & \mathbf{0} \\ \mathbf{0} & \mathbf{H}_b & \dots & \mathbf{0} \\ \vdots & \vdots & \ddots & \vdots \\ \mathbf{0} & \mathbf{0} & \dots & \mathbf{H}_b \end{bmatrix} \begin{bmatrix} \mathbf{F}^{(0)}(t) \\ \mathbf{F}^{(1)}(t) \\ \vdots \\ \mathbf{F}^{(K_R)}(t) \end{bmatrix} \end{aligned} \quad (6.11)$$

where the values of the inner product of polynomial chaos $\langle \cdot \rangle$ are constants and they can be obtained analytically (Ghanem and Spanos 1991). It should be noted that the sparsity patterns of the system matrices \mathbf{M} , \mathbf{C} and \mathbf{K} respectively are determined from the value of inner product of polynomial chaos $\langle \cdot \rangle$.

6.3.2 Non-Gaussian System Parameters

6.3.2.1 A Full PCE Model

Since the Gaussian assumption on the material properties of engineering structures has a very small probability that will take up negative values, the non-Gaussian assumption is more appropriate. Using the KLE to represent these random physical parameters which are assumed as non-Gaussian random

processes, may require an iterative procedure (Phoon et al. 2005). In this study, the PCE is adopted as an alternative. Taking the Young's modulus for example

$$E(x, \theta) = \sum_{i_1=0}^{K_E} \Psi_{i_1}(\theta) E^{(i_1)}(x) \quad (6.12)$$

where K_E is the number of Polynomial Chaoses used to represent the Young's modulus after truncation which can be calculated from

$$K_E + 1 = \frac{(k_E + p)!}{k_E! p!} \quad (6.13)$$

where k_E is the number of terms in the KLE as shown in Equation (5.5), p is the order of the Polynomial Chaos and $E^{(i_1)}$ are the deterministic coefficients of Young's modulus corresponding to $\Psi_{i_1}(\theta)$ in the PCE. Thus the random components of the stiffness matrix for each element $\tilde{\mathbf{K}}^e$ can be obtained as

$$\tilde{\mathbf{K}}^e = \sum_{i_1=1}^{K_E} \Psi_{i_1}(\theta) \int_l E^{(i_1)}(x) \mathbf{I} \mathbf{B}^{eT} \mathbf{B}^e dl = \sum_{i_1=1}^{K_E} \Psi_{i_1}(\theta) \mathbf{K}_{i_1}^e \quad (6.14)$$

where I is the moment of inertia of the beam structure and l is the length of beam element. $\mathbf{K}_{i_1}^e$ is the deterministic matrix for each element corresponding to $\Psi_{i_1}(\theta)$ and $\mathbf{K}_{i_1}^e = \int_l E^{(i_1)}(x) \mathbf{I} \mathbf{B}^{eT} \mathbf{B}^e dl$. The stochastic stiffness matrix of the beam structure \mathbf{K}_b can be expressed as

$$\mathbf{K}_b = \mathbf{K}_d + \sum_{i_1=1}^{K_E} \Psi_{i_1}(\theta) \mathbf{K}_{i_1} \quad (6.15)$$

where \mathbf{K}_{i_1} is the deterministic matrix for the beam model corresponding to $\Psi_{i_1}(\theta)$ which can be assembled from $\mathbf{K}_{i_1}^e$. \mathbf{K}_d denotes the deterministic component of the stiffness matrix \mathbf{K}_b . Let $\mathbf{K}_0 = \mathbf{K}_d$, we have

$$\mathbf{K}_b = \sum_{i_1=0}^{K_E} \Psi_{i_1}(\theta) \mathbf{K}_{i_1} \quad (6.16)$$

Similarly the stochastic mass matrix of the beam structure can be expressed as

$$\mathbf{M}_b = \sum_{i_2=0}^{K_\rho} \Psi_{i_2}(\theta) \mathbf{M}_{i_2} \quad (6.17)$$

where K_ρ is the number of Polynomial Chaos used to represent the mass density after truncation which can be similarly calculated according to Equation (6.13) by replacing k_E with k_ρ which denotes the number of terms used in the KLE for the mass density. Since the Rayleigh damping matrix assumed in this study is a linear combination of the system mass matrix and system stiffness matrix according to Equation (5.4), the system damping matrix can also be written as

$$\mathbf{C}_b = \sum_{i_3=0}^{K_c} \Psi_{i_3}(\theta) \mathbf{C}_{i_3} \quad (6.18)$$

where K_c is the number of Polynomial Chaos used to represent the damping after truncation and $K_c + 1 = \frac{(k_E + k_\rho + p)!}{(k_E + k_\rho)! p!}$.

As noted in Equation (5.11), the excitation forces with Gaussian properties can be represented by KLE and projected on the Polynomial Chaos basis for the response representation according to Equation (6.9). When the excitation forces are assumed as non-Gaussian random processes, they can be represented by Polynomial Chaos as

$$\mathbf{F}(t, \theta) = \sum_{j_2=0}^{K_F} \Psi_{j_2}(\theta) \mathbf{f}^{(j_2)}(t) \quad (6.19)$$

where K_F is the number of Polynomial Chaoes retained after truncation in the representation of the excitation forces, which can be calculated as

$$K_F + 1 = \frac{(k_F + p)!}{k_F! p!} \quad (6.20)$$

where k_F is the number of terms in the KLE of the excitation forces. Again Equation (6.19) can be projected on the Polynomial Chaos adopted to represent the response of beam structure as

$$\mathbf{F}(t, \theta) = \sum_{j_2=0}^{K_R} \Psi_{j_2}(\theta) \mathbf{F}^{(j_2)}(t) \quad (6.21)$$

where $\{\overbrace{\mathbf{F}^{(0)}(t) \dots \mathbf{F}^{(K_R)}(t)}^{K_R}\}^T = \{\mathbf{f}^{(0)}(t) \quad \overbrace{0 \dots 0}^{(K_E+K_\rho)} \quad \mathbf{f}^{(1)}(t) \dots \mathbf{f}^{(K_F)}(t) \quad \overbrace{0 \dots 0}^{(K_R-K_E-K_\rho-K_F-1)}\}^T$.

Substituting Equations (6.5), (6.7), (6.8), (6.16) to (6.18) and (6.21) into Equation (5.2) and taking the inner product on both sides of the equation with $\Psi_k(\theta)$ and employing the orthogonal property in Equation (6.3), we have

$$\begin{aligned} & \sum_{j=0}^{K_R} \sum_{i_2=0}^{K_\rho} \langle \Psi_{i_2}(\theta) \Psi_j(\theta) \Psi_k(\theta) \rangle \mathbf{M}_{i_2} \ddot{\mathbf{y}}^{(j)}(t) + \sum_{j=0}^{K_R} \sum_{i_3=0}^{K_c} \langle \Psi_{i_3}(\theta) \Psi_j(\theta) \Psi_k(\theta) \rangle \mathbf{C}_{i_3} \dot{\mathbf{y}}^{(j)}(t) \\ & + \sum_{j=0}^{K_R} \sum_{i_1=0}^{K_E} \langle \Psi_{i_1}(\theta) \Psi_j(\theta) \Psi_k(\theta) \rangle \mathbf{K}_{i_1} \mathbf{y}^{(j)}(t) = \mathbf{H}_b \langle \Psi_k^2 \rangle \mathbf{F}^{(k)}(t) \quad (6.22) \end{aligned}$$

$$\text{Let } \mathbf{M}^{(k,j)} = \sum_{i_2=0}^{K_\rho} \frac{\langle \Psi_{i_2}(\theta) \Psi_j(\theta) \Psi_k(\theta) \rangle}{\langle \Psi_k^2 \rangle} \mathbf{M}_{i_2},$$

$$\mathbf{C}^{(k,j)} = \sum_{i_3=0}^{K_c} \frac{\langle \Psi_{i_3}(\theta) \Psi_j(\theta) \Psi_k(\theta) \rangle}{\langle \Psi_k^2 \rangle} \mathbf{C}_{i_3} \quad \text{and} \quad \mathbf{K}^{(k,j)} = \sum_{i_1=0}^{K_E} \frac{\langle \Psi_{i_1}(\theta) \Psi_j(\theta) \Psi_k(\theta) \rangle}{\langle \Psi_k^2 \rangle} \mathbf{K}_{i_1}.$$

Equation (6.22) has the same matrix form as shown in Equation (6.11). The values of the inner product of polynomial chaos $\langle \bullet \rangle$ are constants and they can be obtained analytically (Ghanem and Spanos 1991).

6.3.2.2 A Reduced PCE Model

The KLE of a non-Gaussian process results in a set of deterministic

coefficients multiplying the corresponding uncorrelated non-Gaussian random variables $\{\xi_i(\theta)\}$ which are not independent with each other. In the PCE of a non-Gaussian process, these uncorrelated non-Gaussian random variables are projected on the Polynomial Chaos basis. The dimension of PCE in the representation of the stochastic response of a beam structure is determined by the number of K-L components in the KLE of the excitation forces and system parameters as well as the order of Polynomial Chaos adopted according to Equation (6.6). When a large number of K-L components is required to represent the excitation forces, an extremely large number of Polynomial Chaos may be required in the PCE of non-Gaussian random responses which makes the problem unsolvable due to the limit capability of computer. In the PCE for a random process, the number of K-L components adopted is usually not larger than twenty (Eiermann et al. 2007). This drawback limits the application of the SSFEM in the case with relatively simple excitation forces.

For the case when a larger number of K-L components is required, an alternative way is proposed in this sub-Section by eliminating the correlation terms with an assumption of the uncorrelated non-Gaussian random variables to be independent. This treatment may lead to inaccurate results when the level of randomness in system parameters becomes large. However, since the sensitivities of the retained Polynomial Chaos in the reduced PCE are larger than the eliminated ones and the Polynomial Chaos is a mean-square convergent series for a random process with finite second order moments, by increasing the number of

terms adopted in the KLE, the reduced PCE can have the performance as good as that in a full PCE as introduced in Section 6.3.2.1. Increasing the number of K-L components in the KLE of the non-Gaussian system parameters can be achieved by refining the distance between the two points in a spatial domain of interest. These additional terms from the refining procedure are regarded as compensation to the covariance kernel of the non-Gaussian random processes to be represented. Though the number of the KLE increase, the total number of Polynomial Chaos adopted under the assumption of independent $\{\xi_i(\theta)\}$ will be much smaller than that in a full PCE where the number of K-L components is usually smaller than twenty due to the curse of dimensionality (Stefanou 2009).

According to the assumption of independent $\{\xi_i(\theta)\}$, after the decomposition of a non-Gaussian random process $u(x,t,\theta)$ along the dimension x and t using the finite element method and KLE respectively, each uncorrelated random variable $\xi_i(\theta)$, which is assumed as mutually independent in the reduce PCE model, can be expanded by a one-dimensional Polynomial Chaos as demonstrated in Equation (6.2). The relationship between the number of K-L components k_p and the number of Polynomials K_p required for a reduced PCE of order p becomes

$$K_p = k_p \times p \quad (6.23)$$

The dimension of PCE under this independent assumption is significantly reduced as shown in Equation (6.23) which may allow this modified stochastic finite element algorithm to solve the problem where a large number of K-L components are required in the PCE of the excitation force or the system

parameters with a trade off in accuracy.

According to the reduced PCE for the non-Gaussian random process, the system matrices can be expressed as follows

$$\mathbf{K} = \sum_{i_1=0}^{k_E} \xi_{i_1}(\theta) \mathbf{K}_{i_1} = \sum_{i_1=0}^{k_E} \left(\sum_{k_1=0}^{p_1} \Psi_{i_1, k_1}(\theta) c_{1, k_1}^{(i_1)} \right) \mathbf{K}_{i_1} = \sum_{i=0}^{K_E} \Psi_i(\theta) \mathbf{K}'_i \quad (6.24)$$

$$\mathbf{M} = \sum_{i_2=0}^{k_\rho} \xi_{i_2}(\theta) \mathbf{M}_{i_2} = \sum_{i_2=0}^{k_\rho} \left(\sum_{k_2=0}^{p_2} \Psi_{i_2, k_2}(\theta) c_{2, k_2}^{(i_2)} \right) \mathbf{M}_{i_2} = \sum_{i=0}^{K_\rho} \Psi_i(\theta) \mathbf{M}'_i \quad (6.25)$$

$$\mathbf{C} = \sum_{i_3=0}^{k_c} \xi_{i_3}(\theta) \mathbf{C}_{i_3} = \sum_{i_3=0}^{k_c} \left(\sum_{k_3=0}^{p_3} \Psi_{i_3, k_3}(\theta) c_{3, k_3}^{(i_3)} \right) \mathbf{C}_{i_3} = \sum_{i=0}^{K_c} \Psi_i(\theta) \mathbf{C}'_i \quad (6.26)$$

where p_1, p_2 and p_3 are the order of Polynomial Chaos adopted and $p_3 = \max(p_1, p_2)$, k_E, k_ρ and k_c are the number of the K-L components adopted, K_E, K_ρ and K_c are the number of terms of the Polynomial Chaos in the reduced PCE for the Young's modulus, mass density and damping, respectively. The relationship between the number of K-L components k_p and the number of Polynomials K_p required for a reduced PCE of order p has been defined in Equation (6.23), and

$$\mathbf{K}'_i = c_{1, k_1}^{(i_1)} \mathbf{K}_{i_1}, \quad \mathbf{M}'_i = c_{2, k_2}^{(i_2)} \mathbf{M}_{i_2}, \quad \mathbf{C}'_i = c_{3, k_3}^{(i_3)} \mathbf{C}_{i_3} \quad (6.27)$$

where $c_{1, k_1}^{(i_1)}$, $c_{2, k_2}^{(i_2)}$ and $c_{3, k_3}^{(i_3)}$ are deterministic coefficients corresponding to i_i^{th} ($i=1,2,3$) K-L component and k_i^{th} ($i=1,2,3$) order of Polynomial Chaos for the Young's modulus, mass density and damping, respectively.

The random excitation forces can similarly be expanded as

$$\begin{aligned} \mathbf{F}(t, \theta) &= \sum_{j_1=0}^{k_F} \xi_{j_1}(\theta) \mathbf{f}^{(j_1)}(t) = \sum_{j_1=0}^{k_F} \left(\sum_{k_4=0}^{p_4} \Psi_{j_1, k_4}(\theta) c'_{j_1, k_4} \right) \mathbf{f}^{(j_1)}(t) \\ &= \sum_{j=0}^{K_F} \Psi_j(\theta) \mathbf{F}'^{(j)}(t) \end{aligned} \quad (6.28)$$

where $\mathbf{F}'^{(j)}(t) = c'_{j_1, k_4} \mathbf{f}^{(j_1)}(t)$ is the deterministic coefficient corresponding to

$\Psi_j(\theta)$; k_F , p_4 and K_F are the number of K-L components, the order of Polynomial Chaos and the dimension of the reduced PCE for the excitation force vector, respectively.

The nodal displacement vector with non-Gaussian property can be represented by the reduced PCE after truncation,

$$\begin{aligned}\mathbf{R}(t, \theta) &= \sum_{j_2=0}^{k_R} \xi_{j_2}(\theta) \mathbf{y}^{(j_2)}(t) = \sum_{j_2=0}^{k_R} \left(\sum_{k_5=0}^{p_5} \Psi_{j_2, k_5}(\theta) c'_{j_2, k_5} \right) \mathbf{y}^{(j_2)}(t) \\ &= \sum_{j=0}^{K_R} \Psi_j(\theta) \mathbf{y}'^{(j)}(t)\end{aligned}\quad (6.29)$$

where K_R is the dimension of the reduced PCE which is related to the order of the Polynomial Chaos p_5 and the number of terms used in the KLE k_R as demonstrated in Equation (6.23). In Equation (6.29), $k_R = k_E + k_\rho + k_F$, $\mathbf{y}'^{(j)}(t) = c'_{j_2, k_5} \mathbf{y}^{(j_2)}(t)$.

Taking the first and second derivatives of Equation (6.29) with respect to t , the velocity and acceleration vectors can be obtained respectively as

$$\dot{\mathbf{R}}(t, \theta) = \sum_{j=0}^{K_R} \Psi_j(\theta) \dot{\mathbf{y}}'^{(j)}(t) \quad (6.30)$$

$$\ddot{\mathbf{R}}(t, \theta) = \sum_{j=0}^{K_R} \Psi_j(\theta) \ddot{\mathbf{y}}'^{(j)}(t) \quad (6.31)$$

where $\dot{\mathbf{y}}^{(j)}(t) = c'_{j_2, k_5} \dot{\mathbf{y}}^{(j_2)}(t)$ and $\ddot{\mathbf{y}}^{(j)}(t) = c'_{j_2, k_5} \ddot{\mathbf{y}}^{(j_2)}(t)$.

Substituting Equations (6.24) to (6.26) and (6.28) to (6.31) into Equation (5.2), taking inner product of both side of Equation (5.2) with $\Psi_k(\theta)$ and employing the orthogonal property of Polynomial Chaos introduced in Equation (6.3), a equation with the same form as Equation (6.22) can be obtained as

$$\sum_{j=0}^{K_R} \sum_{i=0}^{K_p} \langle \Psi_i(\theta) \Psi_j(\theta) \Psi_k(\theta) \rangle \mathbf{M}'_i \ddot{\mathbf{y}}'^{(j)}(t) + \sum_{j=0}^{K_R} \sum_{i=0}^{K_c} \langle \Psi_i(\theta) \Psi_j(\theta) \Psi_k(\theta) \rangle \mathbf{C}'_i \dot{\mathbf{y}}'^{(j)}(t)$$

$$+ \sum_{j=0}^{K_R} \sum_{i=0}^{K_E} \langle \Psi_i(\theta) \Psi_j(\theta) \Psi_k(\theta) \rangle \mathbf{K}'_i \mathbf{y}'^{(j)}(t) = \mathbf{H}_b \langle \Psi_k^2 \rangle \mathbf{F}'^{(k)}(t) \quad (6.32)$$

6.3.3 Response Statistics

Equations (6.11), (6.22) and (6.32) can be solved by employing the Newmark- β method, respectively, to obtain the deterministic coefficients in the Polynomial Chaos Expansion for the responses, and the response statistics of the nodal displacements can be evaluated as

$$MEAN_R(t) = \mathbf{y}^{(0)}(t), \quad VAR_R(t) = \sum_{j=1}^{K_R} \left(\mathbf{y}^{(j)}(t) \right)^2 \langle \Psi_j^2 \rangle \quad (6.33)$$

where the subscript “R” denotes the random nodal displacement vector of the bridge structure. The random displacement of the bridge at position x and time t can be derived according to Equations (4.4) and (6.5) as

$$w(x, t, \theta) = \mathbf{H}(x) \sum_{j=0}^{K_R} \Psi_j(\theta) \mathbf{y}^{(j)}(t) = \sum_{j=0}^{K_R} \Psi_j(\theta) \left(\mathbf{H}(x) \mathbf{y}^{(j)}(t) \right) \quad (6.34)$$

The mean and variance of displacement at position x and time t can be obtained as

$$MEAN_w(x, t) = \mathbf{H}(x) \mathbf{y}^{(0)}(t), \quad VAR_w(x, t) = \sum_{j=1}^{K_R} \left(\mathbf{H}(x) \mathbf{y}^{(j)}(t) \right)^2 \langle \Psi_j^2 \rangle \quad (6.35)$$

where the subscript “w” denotes the random displacement of the bridge.

6.4 Numerical Simulation

To demonstrate the effectiveness of the application of SSFEM for a beam under moving loads including uncertainty, numerical examples are given in this

Section to verify the algorithm proposed in this Chapter. The system parameters of the beam structure are assumed as Gaussian random processes. Since the Gaussian assumption still has a very small probability that will take up negative values, the log-normal distributed system parameters are further adopted in the numerical example. The reduced PCE proposed to solve the problem of a beam under moving loads with uncertainty where an extremely large number of K-L components is usually required in the random response representation, will also be verified. Results from the MCS are regarded as reference to compare with those calculated from the proposed algorithm. The sampling rate in all the numerical simulation is 200 *Hz*. The beam structure is divided into eight beam elements with uncertain system parameters. The velocities of the moving forces are 40 *m/s*.

6.4.1 Gaussian System Parameter

The beam model shown in Section 5.4.1 and the Force Model II introduced in Section 3.6.1.3 are adopted in this study. Two cases will be studied in the following sub-Sections. In Case 1, only the uncertainties in the system parameters are included, and the effect of different coefficient of variation for the system parameters and different order of the Polynomial Chaos Expansion for the nodal response will be studied. A combination of the level of uncertainty in system parameters and the order of the Polynomial Chaos with acceptable relative error will be identified. In Case 2, both the uncertainties in system

parameters and excitation forces will be considered. The accuracy of the SSFEM under different COV_F will be investigated for a specified level of the uncertainty in system parameters.

6.4.1.1 Case 1: Deterministic Excitation and Gaussian Material Property

The two deterministic moving forces have been defined according to Equations (3.41) and (3.42). Since the covariance kernels for the system parameters have been defined according to Equation (5.34) for given value of σ , the K-L components representing the system parameters can be obtained by performing eigenvalue analysis on the defined kernels. In the present case of a beam with eight elements, nine K-L components are used to represent the random system parameters with the spatial correlation defined in Equation (5.34). According to Equation (6.6), the numbers of terms in PCE for the random response when the order of Polynomial Chaos equals to 1, 2, and 3 are 10, 55 and 220 respectively. By solving Equation (6.11) using the Newmark- β method, the deterministic coefficients in the PCE of the random nodal response can be calculated. The response statistics can then be evaluated according to Equation (6.35).

A convergence study on the statistics of the mid-span displacement of the beam structure from the Monte Carlo Simulation is conducted. Results from 50000 runs of MCS are obtained as converged and they are used as reference values. The percentage error according to Equation (3.39) for different runs of

MCS when $COV_E=COV_\rho=20\%$ and $t=0.5s$, is shown in Figure 6.1. Results show that the percentage error for variance is larger than that for the mean value and both statistics of the mid-span displacement have small error after 5000 simulations. Hence, results from 10000 Monte Carlo Simulations is taken as reference for comparison with those from the SSFEM.

A study on the effectiveness of the SSFEM at different level of uncertainty in system parameters with different order of Polynomial Chaos is given. The relative errors between the statistics of the mid-span displacement from the SSFEM and MCS are shown in Table 6.1. Results show that the calculated mean values of the mid-span displacement from SSFEM are very accurate. The relative error in the mean values slightly increases with an increase in the coefficient of variation of the system parameters. However, for a fixed level of uncertainty in system parameters, an increase in the order of PC will give a slightly reduced relative error. The maximum COV of the system parameters adopted is 20% in this study. Numerical simulations with larger COV of the system parameters, e.g. $COV_E=COV_\rho=30\%$, will encounter difficulties with the MCS with the Gaussian assumption on the system parameters, because samples of the system parameters will have negative values that will cause divergence in the calculated response statistics in MCS.

The accuracy of variances of the mid-span displacement from SSFEM is dramatically affected by the order of PC adopted. When the uncertainty in system parameters are very small with $COV_E=COV_\rho=5\%$, satisfactory results can be

obtained with different order of PC. However, the use of higher order PC can not improve the accuracy. When the level of randomness in system parameters is at 10% or higher, the use of first order PC will result in large error in the variance calculation. When $COV_E=COV_\rho=20\%$, the third order PC is required to achieve a good accuracy. The variances of the mid-span displacement calculated from SSFEM with different order PC when $COV_E=COV_\rho=10\%$ and $COV_E=COV_\rho=20\%$ are compared with those from MCS in Figure 6.2 and 6.3, respectively.

It is concluded that for the case with very low level of uncertainty in system parameters, e.g. COV smaller than 5%, first order PC is suggested in this study. That is to say, when the uncertainty in system parameters is small, the Gaussian assumption would be appropriate for the random responses. An increase in the order of PC can not improve the accuracy which may be due to the limitation of the PC approximations (Field and Grigoriu 2004) not able to improve the accuracy with additional terms. Second order PC is sufficient to maintain good accuracy in this problem for the case with $COV_E=COV_\rho=10\%$.

6.4.1.2 Case 2: Gaussian Excitation and Material Property

When both the randomness in system parameters and excitation forces are considered, the covariance kernel for the system parameters is also defined the same as for Case 1 above and the Force Model II described in Section 3.6.1.3 is adopted. The level of uncertainty in system parameters with $COV_E=COV_\rho=10\%$ is studied in this case and the second order PC which is proved to be sufficient to

maintain good accuracy is adopted. Samples of the random moving forces are generated according to Equations (3.49) and (3.50). The covariance kernel of the random forces is calculated from these samples according to Equation (3.17), and eigenvalue analysis is then performed on the kernel to give the corresponding K-L components. The first k_F K-L components with larger eigenvalue λ_j are retained according to the criterion as $\sum_{j=1}^{k_F} \lambda_j / \sum \lambda_j \geq B$. It should be noted that more K-L components will be retained when B is close to unity, e.g. when $B=0.99$, the number of retained K-L components k_F is equal to 53 for different COV_F . In this study, B is set to 0.95 which lead to $k_F=16$ according to the criterion. The computational cost is dramatically decreased compared with the case when $B=0.99$ while maintaining good accuracy. Taking nine K-L components to represent the random fields of system parameters, the numbers of terms in PCE required for the response with second order PC is 351.

The random moving forces with different COV_F are applied on the beam structure. A study of convergence similar as that in Case 1 is conducted. The percentage error for different number of iterations in MCS according to Equation (3.39) when $COV_E=COV_p=10\%$, $COV_F=62.56\%$ and $t=0.5s$, is shown in Figure 6.4 where results from 50000 runs of MCS are regarded as reference. Similar trend can be observed as in the convergence analysis in Case 1 and the results from 10000 runs of Monte Carlo Simulations are adopted as reference solution for the error analysis of results from SSFEM. A comparison of the statistics of the mid-span displacement from the SSFEM and the MCS with different COV_F is

shown in Table 6.2. A comparison of the mid-span displacement for the case with $COV_E=COV_\rho=10\%$ and $COV_F=62.56\%$ is shown in Figure 6.5. Results show that for both the mean value and variance of the mid-span displacement, very small difference exists in the results from the two methods under different COV_F . The relative error increases slightly with increasing COV_F . It can be concluded that when the order of PC in PCE is sufficient to represent the uncertainty in system parameters, the proposed algorithm for a beam-load system with uncertainty using SSFEM can maintain a good accuracy even when large uncertainties exist in the moving forces.

6.4.2 Non-Gaussian System Parameters: A Full PCE Model

6.4.2.1 The Lognormal Distributed System Parameters

The Young's modulus E and the mass density ρ of the beam structure are assumed as lognormal random processes with mean value $2.5 \times 10^{10} \text{ m/s}^2$ and $2.5 \times 10^3 \text{ kg/m}^3$ respectively and the Coefficients Of Variation (COV) denoted as COV_ρ and COV_E , respectively. A lognormal random process $L(x, \theta)$ projected on the Polynomial Chaos basis will take the following form (Ghanem 1999c):

$$L(x, \theta) = L_0(x) \left(1 + \sum_{i=1}^{k_l} \xi_i(\theta) g_i(x) + \sum_{i=1}^{k_l} \sum_{j=1}^{k_l} \frac{(\xi_i(\theta)\xi_j(\theta) - \delta_{ij})}{\langle (\xi_i(\theta)\xi_j(\theta) - \delta_{ij})^2 \rangle} g_i(x) g_j(x) + \dots \right) \quad (6.36)$$

where δ_{ij} is the Kronecker delta and $L_0(x)$ refers to the mean of the lognormal process calculated as

$$L_0(x) = e^{\left(\mu_g + \frac{1}{2}\sigma_g^2\right)} \quad (6.37)$$

where μ_g and σ_g^2 are the mean and variance of the corresponding Gaussian random process $g(x, \theta)$, respectively, and

$$\mu_g = \ln(\mu_L) - \frac{1}{2}\sigma_g^2, \quad \sigma_g^2 = \ln\left[\left(\frac{\sigma_L}{\mu_L}\right)^2 + 1\right] \quad (6.38)$$

where μ_L and σ_L^2 are the mean and variance of the lognormal random process.

$g(x, \theta)$ has the following relationship with $L(x, \theta)$,

$$L(x, \theta) = e^{g(x, \theta)} \quad (6.39)$$

$g_i(x)$ and $\zeta_i(\theta)$ are the K-L components and the corresponding standard Gaussian random variables in the KLE of $g(x, \theta)$, respectively. k_l is the number of terms in the KLE retained after truncation. The Gaussian random process $g(x, \theta)$ is assumed to have the spatial correlation represented by an exponential auto-covariance function as

$$C(x_1, x_2) = \sigma_g^2 \exp\left(-\frac{|x_1 - x_2|}{a}\right) \quad (6.40)$$

where a and $|x_1 - x_2|$ are the correlation length and the distance of two points in a spatial domain of interest, respectively. Both the Young's modulus E and mass density ρ are assumed with the same spatial correlation and the same level of Coefficient Of Variation (COV) in this study, i.e. $COV_E = COV_\rho$. This selection is arbitrary as the same analysis is applicable for the case when the levels of randomness in E and ρ are totally different.

6.4.2.2 Case 3: Deterministic Excitation and Non-Gaussian Material Property

Only the uncertainties in material properties are included in this sub-Section to investigate the accuracy of the modeling of the randomness in system parameters with PCE. The two deterministic moving forces applied on the beam structure are shown in Equations (3.41) and (3.42). The material properties which are assumed as lognormal random processes will be represented by the PCE according to the theory described in Section 6.4.2.1 with the following steps:

- (1) The mean values and variances of the corresponding Gaussian random processes denoted as μ_g and σ_g^2 are calculated from μ_L and σ_L^2 of the lognormal distributed material properties according to Equation (6.38).
- (2) The covariance kernels for these Gaussian random processes are defined according to Equation (6.40).
- (3) The KLE are adopted to calculate the K-L components $g_i(x)$ for the corresponding Gaussian random processes and the PCE for the lognormal distributed system parameters can be performed according to Equation (6.36).

In this study, nine K-L components will be adopted for the corresponding Gaussian random processes. Since the deterministic matrices \mathbf{K}_{i_1} , \mathbf{M}_{i_2} , \mathbf{C}_{i_3} in Equations (6.16) to (6.18) respectively can be obtained from the corresponding deterministic components in PCE of the material properties, the deterministic coefficients for the random response are obtained from Equation (6.22) and the response statistics can be evaluated according to Equation (6.35).

Since the order of Polynomial Chaos (PC) adopted will affect the accuracy

in the uncertainty modeling of the system parameters, a study on the different order of PC for the different level of randomness in system parameters is conducted and the statistics of the mid-span displacement of the beam structure calculated from the proposed method are compared with the results from MCS. The cases of different level of randomness in system parameters with $COV_E=COV_\rho=5\%$, 10%, 20%, 30%, 40% and 50% are chosen. Four combinations on the order of PC are adopted including: (1) $OD_S=1$, $OD_R=3$; (2) $OD_S=2$, $OD_R=2$; (3) $OD_S=2$, $OD_R=3$; (4) $OD_S=3$, $OD_R=3$, where OD_S and OD_R are the order of PC for representing the system parameters and the response, respectively. In MCS, 10000 samples of the lognormal distributed system parameters are generated according to Equation (6.36) in which $k_f=9$, $OD_S=3$, to calculate samples of the beam response with deterministic analysis. The first two statistics of the mid-span displacement of the beam are calculated from both the SSFEM with different combinations of the order of PC and MCS, and they are compared in Figures 6.6 and 6.7 respectively, with the percentage errors shown in Table 6.3 calculated according to Equation (3.39).

Results show that when the randomness in system parameters is smaller than 10%, the calculated response statistics at mid-span of the beam are very accurate for all the combinations. When the randomness in system parameters is larger than 20%, large errors exist in the variance of the calculated response for Combination #1. This is because when $OD_S=1$, the PCE is equivalent to KLE and the lognormal distributed material properties are approximated by the Gaussian

random processes with the same mean value and variance and this approximation will cause large error when the randomness in system parameters is large. By increasing the order of PC adopted, accurate results are obtained. The calculated mean values are more accurate than the corresponding variances. The relative errors in the calculated statistics of the mid-span response increase with the level of the randomness in system parameters and decrease with the order of PC adopted. It should be noted that when the level of randomness in system parameters are small, an increase in the order of PC may not improve the accuracy of the results but with more computational efforts. Therefore, the choice of a proper order of PC in the PCE is very important. When the randomness in system parameters is not very large, e.g. smaller than 30%, the order of PC with $OD_S=2$ and $OD_R=2$ can give acceptable results on both the mean value and variance.

6.4.2.3 Case 4: Gaussian Excitation and Non-Gaussian Material Property

The Force Model II introduced in Section 3.6.1.3 will be adopted as the random excitation. The order of PC with $OD_S=2$ and $OD_R=2$ is selected to investigate the effect of the level of the randomness in excitation on the accuracy of the proposed algorithm when $COV_E=COV_p=20\%$. Different level of randomness in excitation as defined in Section 3.6.1.3 with COV_F equal to 0.0382, 0.0778, 0.1517, 0.3073 and 0.6256 respectively, will be adopted and the criterion

in the KLE of the excitation forces is defined as $\sum_{j=1}^{k_f} \lambda_j / \sum \lambda_j \geq 0.99$.

The first two statistics of the mid-span displacement of the beam calculated from the SSFEM and MCS are compared in Figures 6.8 and 6.9 respectively with different level of randomness in excitation and the percentage errors calculated according to Equation (3.39) are shown in Table 6.4.

Results show that the calculated statistics of the mid-span displacement are very accurate. The percentage error in the mean value increases slightly with a increase in the level of randomness in excitation and the errors in the calculated variance slightly decrease with the level of randomness in excitation as noted in Table 6.4. This is because for the calculated mean value of the response, the error in the averaging procedure on the samples of the excitation forces may increase with the level of randomness and it will propagate into the mean value of the calculated response. The errors in the calculated variance are mainly coming from the errors in the modeling of randomness in system parameters since the modeling of Gaussian excitation forces by adopting KLE is very accurate as shown in Section 3.6.2; When the level of randomness in the excitation forces increases, the errors from the system modeling will become insignificant and the errors in the calculated statistics of the response will decrease.

6.4.3 Non-Gaussian System Parameters: A Reduced PCE Model

To verify the application of the reduced PCE model on the problem of a

beam under moving forces with uncertainty, the two moving forces have mean values defined in Equations (3.41) and (3.42), and the lognormal distributed randomness with a specific value of Coefficient Of Variation (COV_F) at each time instance, are adopted. It should be noted that this stochastic force model represents an extreme case in which a large number of K-L components are required in KLE of the random processes. The reduced PCE model is used to handle the problem where the traditional full PCE model will at the expense of a proper accuracy.

Both the system parameters and the excitation forces are assumed as lognormal random processes in this sub-Section. 500 samples of a lognormal distributed variable at each time instance of the excitation forces (or at specified location for material properties) are obtained from its corresponding Gaussian random distribution with the corresponding samples generated from LHS according the relationship shown in Equation (6.39). With the first two statistics of the lognormal random processes, the covariance kernel for the KLE can be obtained from the generated samples according to the theory introduced in Section 3.3.2. The first k_v K-L components are retained according the criterion defined as $\sum_{j=1}^{k_v} \lambda_j / \sum \lambda_j \geq 0.99$, where λ_j is eigenvalues in the eigenvalue analysis of the kernel.

The covariance kernel of the corresponding Gaussian random processes for the system parameters has been defined in Equation (5.34). A positive dislocation of two points in a spatial domain of interest is set to $0.5m$ and a is set as unity for

both the Young's modulus E and mass density ρ in the following study. It should be noted that the covariance kernel for the two system parameters can be totally different. However, the same value of $|x_1 - x_2|$ and a are assumed in this study. The sampling rate for all the simulations is 200Hz . The proposed algorithm is verified with the Monte Carlo Simulation on 10000 samples.

6.4.3.1 Coefficients in One-dimensional Polynomial Chaos

Expansion

Before a detailed investigation of the proposed reduced PCE model is conducted, a comparison of the different methods to calculate the coefficients in the representation of non-Gaussian random variable with one-dimensional Polynomial Chaos will be given and one of these methods will be adopted to calculate the coefficients in the one-dimensional PCE in the reduced PCE model.

Two functions of the standard Gaussian random variable ξ with a zero mean value and unit standard deviation are shown as

$$Y_1 = 2 + \xi + (\xi^2 - 1) + 4(\xi^3 - 3\xi) \quad (6.41)$$

$$Y_2 = e^\xi \quad (6.42)$$

Different methods are adopted to calculate the coefficients in the one-dimensional PCE of the two functions with the order up to four. The percentage errors and the time required in the calculated coefficients in PCE for different order of PC according to Equation (3.39) by using MCS method (Field 2002) with 10000 samples, the Latin Hypercube Sampling (LHS) method (Reagan et al. 2005) with 300 samples, and Fitting Regression Model (FRM)

method (Choi et al. 2004) using 300 samples respectively are shown in Table 6.5. The programme runs on a computer with Intel Core(TM)2, Quad CPU 2.40Hz and 8GB RAM.

Results show that using the fitting regression model method has both high efficiency and accuracy comparing with the other two methods especially for those random variables which can be approximated as Polynomial functions of Gaussian random variables, and this method will be adopted in the following study to calculate the coefficients in the one-dimensional PCE in the reduced PCE model.

6.4.3.2 Effect of the Level of Randomness in System Parameters

To verify the proposed non-Gaussian model on the material properties with the reduced PCE, different levels of randomness in system parameters, i.e. different COV_ρ and COV_E are investigated. To highlight the effect of the level of randomness in system parameters on the accuracy of the non-Gaussian model, the two excitation forces are assumed as deterministic ($COV_F=0\%$) in this sub-Section with values defined in Equations (3.41) and (3.42). Different orders of Polynomial Chaos are adopted to represent the lognormal random processes of system parameters. The effect of the order of Polynomial Chaos on the accuracy of the non-Gaussian model will also be investigated.

The mean value and variance of the mid-span displacement of the beam structure calculated by using the proposed algorithm with a reduce PCE model with different order of PC and the MCS are compared in Figure 6.10 and Figure

6.11, respectively. The percentage errors of the results compared with those from the MCS are listed in Table 6.6.

Results show that the calculated mean values for all the cases are very accurate and the relative error increases slightly with the increase of level of randomness in system parameters. The order of PC adopted has little effect on the accuracy of calculated mean value in general. For the variance of the mid-span displacement, the use of a low order of PC such as an order equals to 2, can achieve an accurate variance of the mid-span displacement as noted in Table 6.6 when the COV_E and COV_ρ are small, e.g. smaller than 0.2,. However, the result can be improved when the 3rd and 4th order PC is used, and the results from a 4th-order representation is better than that from a 3rd-order representation. When the COV_E and COV_ρ are larger than 0.2, large errors exist in the calculated variance when only a 2nd-order PCE is adopted. Another phenomenon noted in Table 6.6 is that for a very large COV_E and COV_ρ , e.g. larger than 0.4, the results from a 3rd-order representation is better than that from a 4-order representation. This phenomenon can be explained as follows: the error in the coefficient calculation from the one-dimensional polynomial chaos expansion will be propagated into every K-L components via the covariance kernel, e.g. the error in the calculated coefficients in the one-dimensional PCE will be amplified by the K-L components of the random processes from the covariance kernel and it will cause larger errors in the coefficients in the reduced PCE model. When more coefficients in the one-dimensional PCE are included in the calculation with

higher order polynomial chaos, the computation error will be amplified and accumulated affecting the accuracy of the calculated response statistics.

6.4.3.3 Effect of the Level of Randomness in Excitation

Investigation on the effect of the level of randomness in excitation is similarly conducted with $COV_\rho=COV_E=20\%$ in this Section. Different levels of randomness of the lognormal distributed excitation forces are used with different order polynomial chaos for representing.

The mean value and variance of the mid-span displacement of the beam structure calculated by using the proposed method with different order of PCE and the MCS are compared in Figure 6.12 and Figure 6.13, respectively. The percentage errors of the results compared to those from the MCS are listed in Table 6.7.

Results show that the order of Polynomial Chaos will generally not affect the accuracy of the mean value of the mid-span displacement. When the COV_F are equal or larger than 0.2, a relative large error exists in the calculated variance which means a 2nd-order representation is not sufficient. When the COV_F becomes large, e.g. equals 0.4 or 0.5, a 3-order representation has better performance than a 4-order representation. The reason for this phenomenon has been explained in the last paragraph in Section 6.4.3.2.

It may be concluded that when a system with the coefficients of variation of both the system parameters and excitation forces smaller than 0.2, a 2nd-order representation of the polynomial chaos should be sufficient to obtain accurate

response statistics of the system. In other cases with larger coefficients of variation, a 3rd-order representation of polynomial chaos is recommended. When the coefficients of variation of the excitation forces reach a large value of 0.5, the response statistics of the proposed non-Gaussian model still maintain a good accuracy when the coefficients of variation of system parameters are not large.

6.5 Summary

A new method for the dynamic analysis of a beam with large uncertainty in system parameters under stochastic moving loads is proposed in this Chapter. The Spectral Stochastic Finite Element Method (SSFEM) proposed by Ghanem and Spanos (1991) is adopted to model the bridge structure with random physical parameters. The Karhunen-Loève Expansion/Polynomial Chaos Expansion is adopted to represent both the system parameters and the moving forces which are assumed as Gaussian/non-Gaussian random processes, and the Polynomial Chaos Expansion is adopted to represent the random responses with non-Gaussian properties. A reduced PCE model is also proposed to solve the cases where a large number of K-L components are required in PCE of random processes involved in the equation of motion of the system. The mathematical model formulated is solved by Newmark- β method and the statistics of response evaluated are compared with those from the Monte Carlo Simulation. Different levels of uncertainties in the system parameters and excitation forces are studied with the following conclusions:

- (1) The calculated mean values from SSFEM in all cases are very accurate. The relative error compared to the results from MCS slightly increases with the level of uncertainty in system parameters and the order of PC adopted will not affect the accuracy of the calculated mean values.
- (2) For the case with Gaussian system parameters, when the uncertainty in system parameters is very small, e.g. smaller than 5%, the Gaussian assumption for the response of beam structure is appropriate. An assumption of non-Gaussian uncertainties for the response cannot improve the accuracy of the calculated variance. When the level of randomness in system parameters increases, the Gaussian assumption for the response, i.e. the adoption of the first order PC to represent the response, will result in large error in the variance estimation. Hence a higher order PC must be adopted to represent the random response with high non-Gaussian property, to get accurate results especially in the variance. When the level of randomness in system parameters is high, e.g. COV larger than 0.3, the Gaussian assumption for the system parameters will include negative values and it will cause divergence in the calculated response statistics in MCS. When the order of PC is sufficient to approximate the uncertainty in system parameters, both the mean value and variance of the mid-span displacement calculated from SSFEM are very accurate even with very large uncertainties in the moving excitation forces. The errors in the calculated mean value and variance increase slightly with an increase in the level of uncertainties in the excitation

forces.

- (3) For the case of non-Gaussian system parameters with a full PCE model, appropriate orders of PC adopted for representing both the non-Gaussian system parameters and the response should be selected to improve the computational efficiency while maintaining the accuracy of the proposed algorithm. When the COV of the system parameters is smaller than 10%, the non-Gaussian system parameters may be approximated with a Gaussian distribution with the same mean value and variance. Higher order PC must be adopted to represent the non-Gaussian randomness when the COV of system parameters increases.
- (4) In the case of non-Gaussian system parameters with a reduced PCE model, when the coefficients of variation of both the system parameters and excitation forces is smaller than 0.2, a 2nd-order representation of the Polynomial Chaos is sufficient to obtain accurate response statistics of the beam structure. In other cases with larger coefficients of variations, a 3rd-order representation of polynomial chaos is recommended.

Table 6.1 - Percentage error in the statistics of mid-span displacement with different order of Polynomial Chaos used

<i>RE (%)</i>		Mean Value			Variance		
Order of PC		1	2	3	1	2	3
$COV_E=COV_\rho$	5%	1.48×10^{-3}	2.95×10^{-4}	2.94×10^{-4}	0.72	1.05	1.13
	10%	0.02	1.52×10^{-3}	1.14×10^{-3}	5.95	0.48	0.93
	15%	0.13	0.01	3.66×10^{-3}	15.8	3.09	0.43
	20%	0.48	0.09	0.03	31.0	10.9	2.50

Table 6.2 - Percentage error in the statistics of mid-span displacement with different level of randomness in excitation forces when order of PC=2

<i>RE (%)</i>	$COV_E=COV_\rho=10\%$				
COV_F	3.82%	7.78%	15.71%	30.73%	62.56%
Mean Value	0.05	0.08	0.18	0.36	0.92
Variance	1.27	1.59	1.87	2.04	2.20

Table 6.3 - Percentage error in mid-span displacement statistics due to different level of randomness in system parameters

$COV_F=0\%$		Order of PC							
		Combination#1		Combination#2		Combination#3		Combination#4	
	$COV_E=COV_\rho$	OD _S	OD _R						
		1	3	2	2	2	3	3	3
Mean Value	5%	0.01	0.01	0.01	0.01	0.01	0.01	0.01	0.01
	10%	0.02	0.01	0.01	0.01	0.01	0.01	0.01	0.01
	20%	0.09	0.03	0.03	0.03	0.03	0.03	0.03	0.03
	30%	0.51	0.08	0.06	0.06	0.06	0.06	0.06	0.06
	40%	2.04	0.24	0.17	0.17	0.17	0.17	0.17	0.17
	50%	7.39	0.57	0.39	0.39	0.39	0.39	0.39	0.39
Variance	5%	0.16	0.03	0.01	0.01	0.01	0.01	0.01	0.01
	10%	2.44	0.65	0.28	0.28	0.28	0.28	0.28	0.28
	20%	10.77	3.23	1.53	1.53	1.53	1.53	1.53	1.53
	30%	30.84	8.00	3.94	3.94	3.94	3.94	3.94	3.94
	40%	82.42	15.13	7.91	7.91	7.91	7.91	7.91	7.91
	50%	261.02	24.45	13.96	13.96	13.96	13.96	13.96	13.96

Table 6.4 - Percentage error in the calculated response statistics due to different level of randomness in excitation

$COV_E = COV_\rho = 20\%$	COV_F				
	3.82%	7.78%	15.17%	30.73%	62.56%
Mean value	0.07	0.07	0.17	0.46	0.83
Variance	2.15	2.44	2.72	1.83	1.60

Table 6.5 - Percentage error in coefficients calculation of the three methods in one dimensional PCE

Functions	Y_1			Y_2			
	Methods	MCS	LHS	RFM	MCS	LHS	RFM
b_0		0.07	0.14	0	0.01	0.06	0.03
b_1		0.04	0.98	0	0	0.29	0.29
b_2		0.09	1.84	0	0.05	0.61	0.24
b_3		0.23	2.75	0	0.08	0.80	0.67
b_4		0.02	2.81	0	0.08	0.80	0.25
Time (s)		35.34	0.17	0.14	33.07	0.14	0.11

Table 6.6 - Percentage error in mid-span displacement statistics due to different level of PC representation when $COV_F=0\%$

$COV_F=0\%$		$COV_E=COV_\rho$					
Order of PC		5%	10%	20%	30%	40%	50%
Mean Value	2	0.01	0.02	0.03	0.06	0.31	0.84
	3	0.01	0.02	0.06	0.20	0.56	1.34
	4	0.01	0.02	0.06	0.22	0.68	1.85
Variance	2	0.63	1.51	2.58	8.31	14.85	21.66
	3	0.06	0.14	1.51	3.27	4.77	5.00
	4	0.08	0.11	1.36	2.88	3.01	8.11

Table 6.7 - Percentage error in mid-span displacement statistics due to different level of PC representation when $COV_E=COV_\rho=20\%$

$COV_E=COV_\rho=20\%$		COV_F				
Order of PC		10%	20%	30%	40%	50%
Mean Value	2	1.81	1.90	1.99	2.11	2.24
	3	1.79	1.83	1.84	1.87	1.91
	4	1.79	1.83	1.83	1.80	1.88
Variance	2	4.23	11.2	14.0	17.8	23.1
	3	3.35	4.44	3.93	4.83	5.21
	4	3.59	6.90	3.82	12.5	16.2

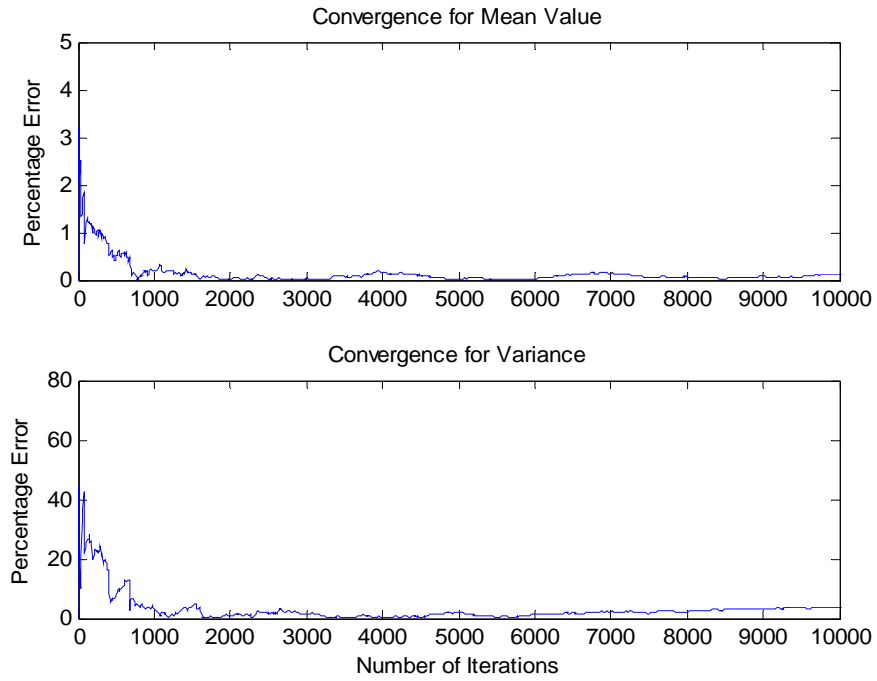


Figure 6.1 - Convergence analysis of the MCS in Case 1, when $COV_E=COV_\rho=20\%$ and $t=0.5s$

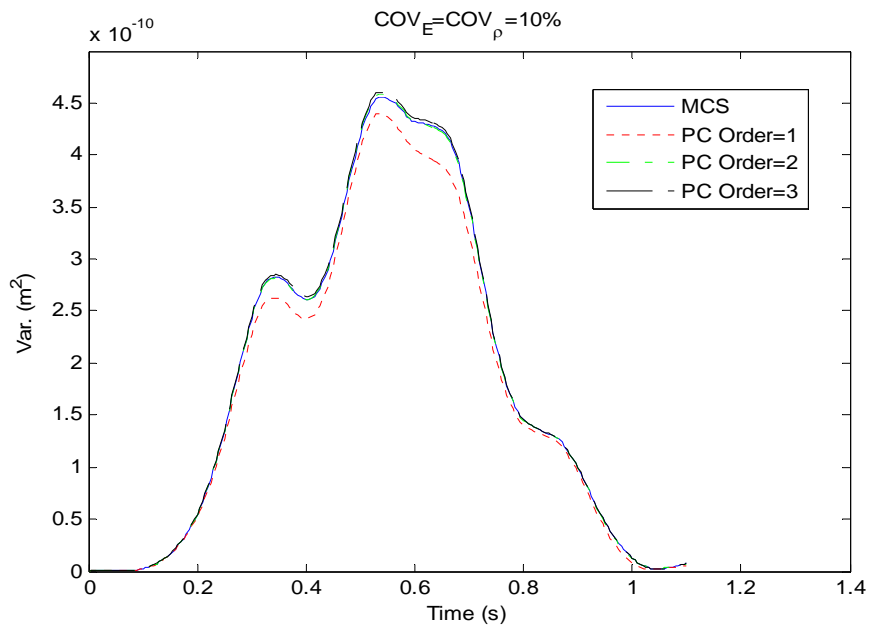


Figure 6.2 - Comparison of calculated variance from SSFEM and MCS in Case 1 when $COV_E=COV_\rho=10\%$

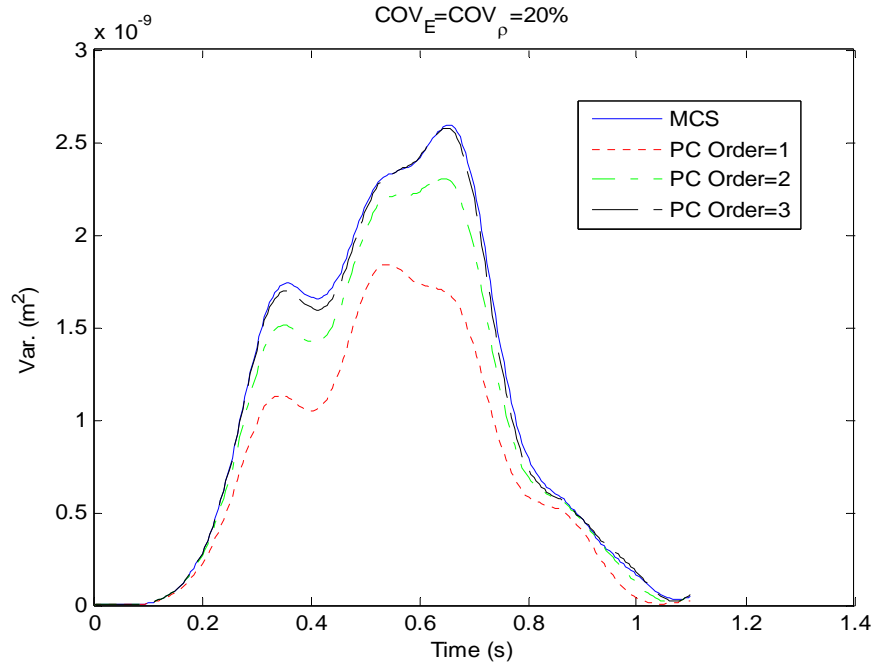


Figure 6.3 - Comparison of calculated variance from SSFEM and MCS in Case 1 when $COV_E=COV_\rho=20\%$

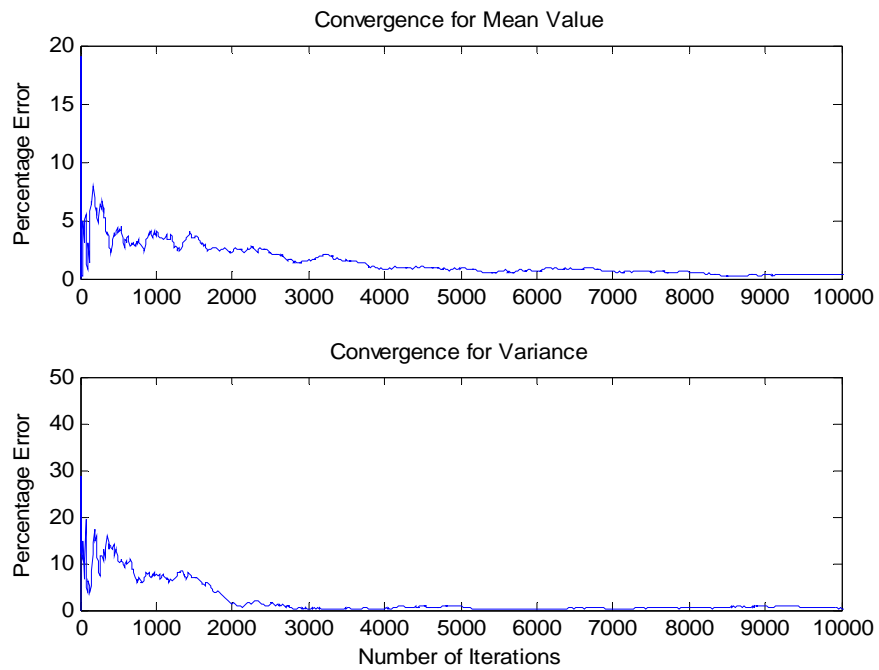


Figure 6.4 - Convergence analysis of the MCS in Case 2, when $COV_E=COV_\rho=10\%$, $COV_F=62.56\%$ and $t=0.5s$

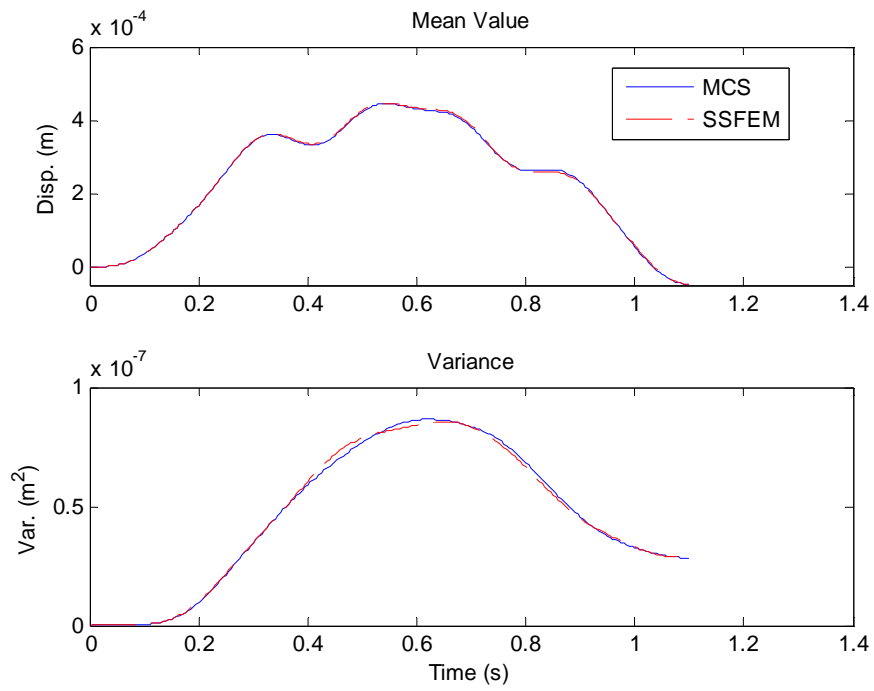


Figure 6.5 - Comparison of calculated statistics from SSFEM and MCS in Case 2, when $COV_E=COV_\rho=10\%$ and $COV_F=62.56\%$

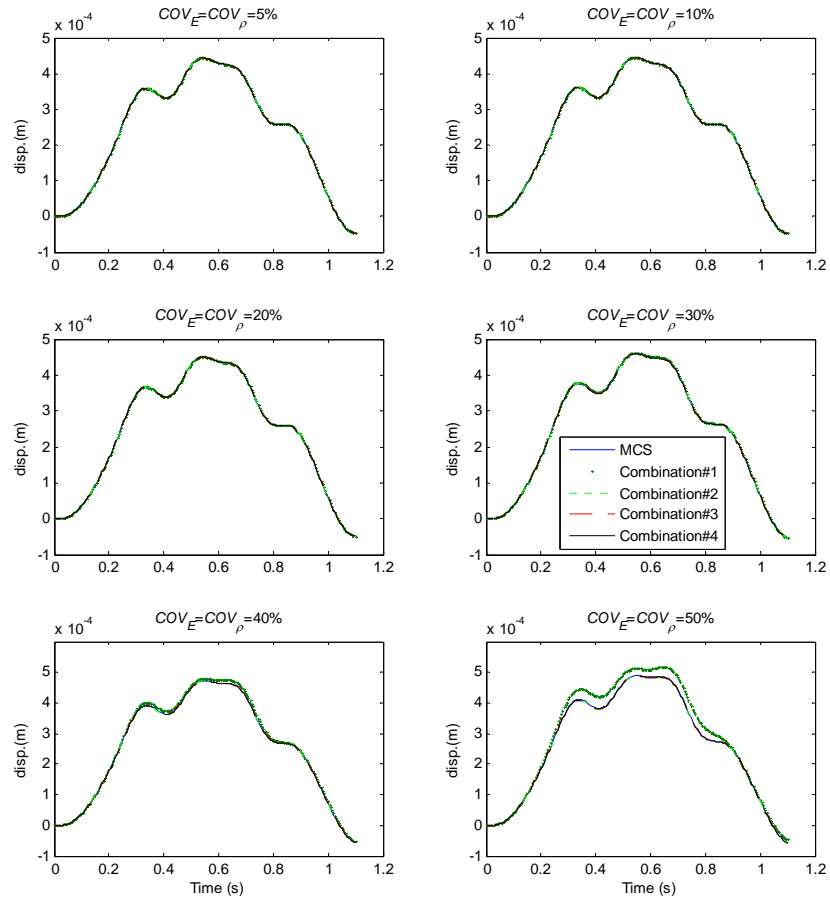


Figure 6.6 - Comparison of mean value of mid-span displacement with different order of PC used

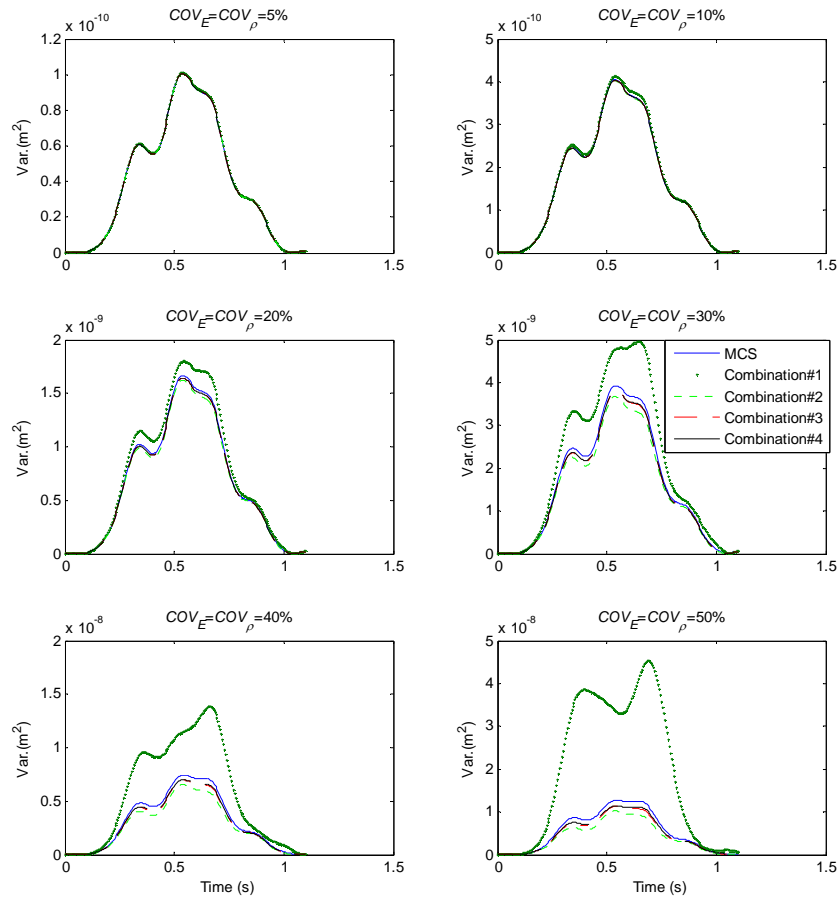


Figure 6.7 - Comparison of variance of mid-span displacement with different order of PC used

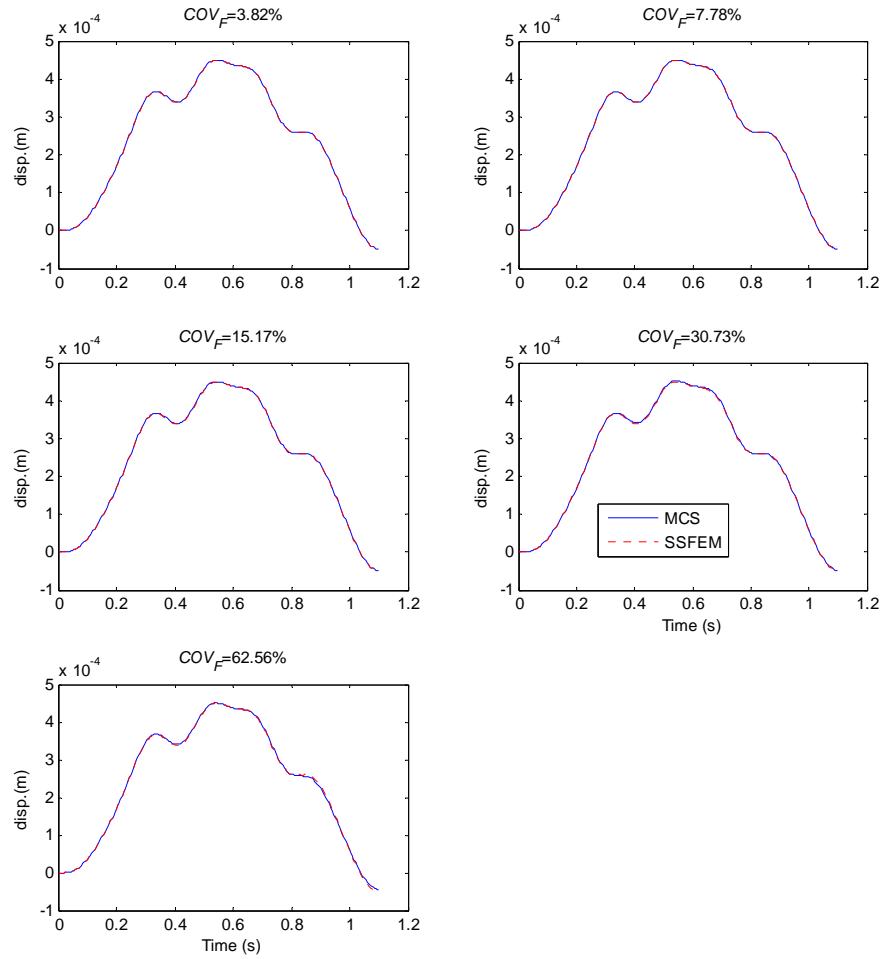


Figure 6.8 - Comparison of mean value of mid-span displacement with different level of randomness in excitation when $COV_E=COV_\rho=20\%$

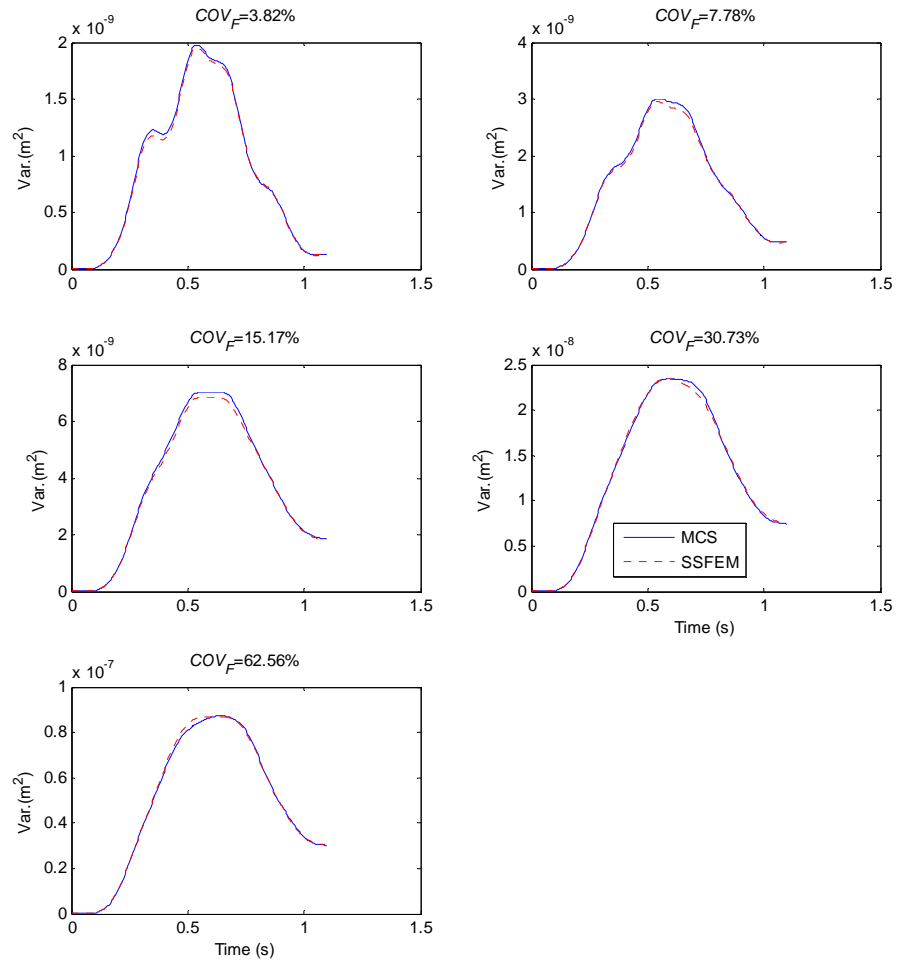


Figure 6.9 - Comparison of variance of mid-span displacement with different level of randomness in excitation when $\text{COV}_E = \text{COV}_\rho = 20\%$

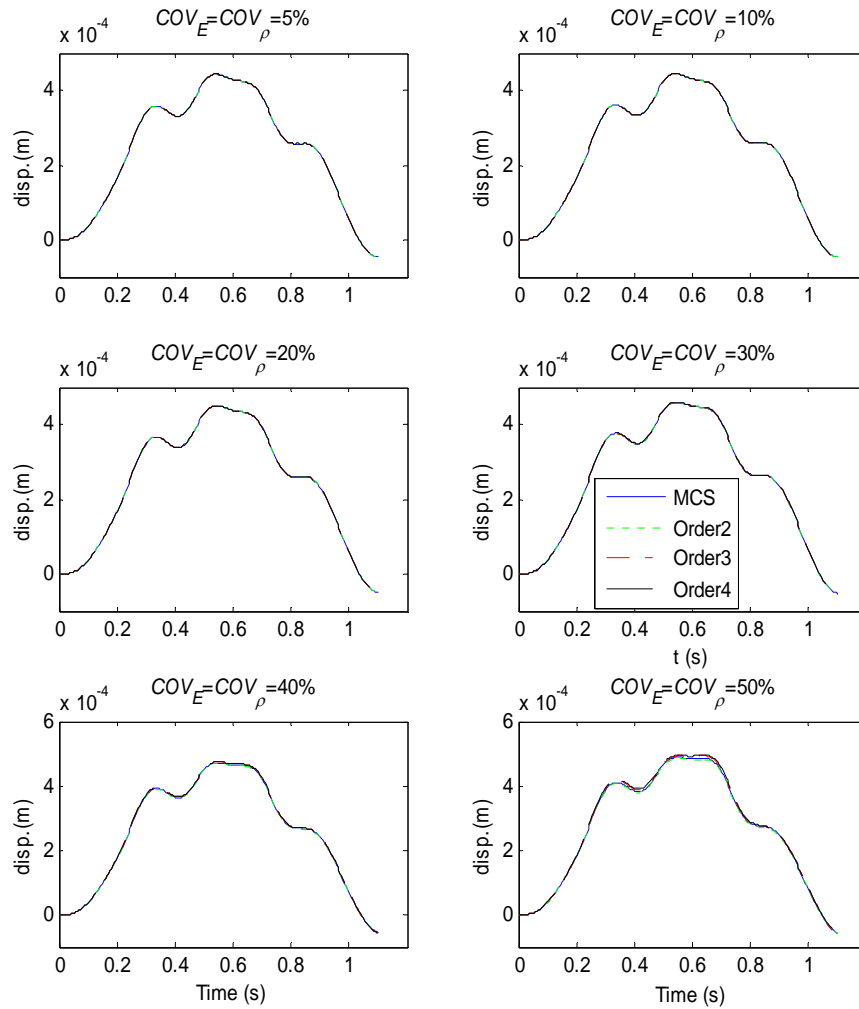


Figure 6.10 - Comparison of mean value of mid-span displacement when $COV_F=0\%$ and different order of PC Used

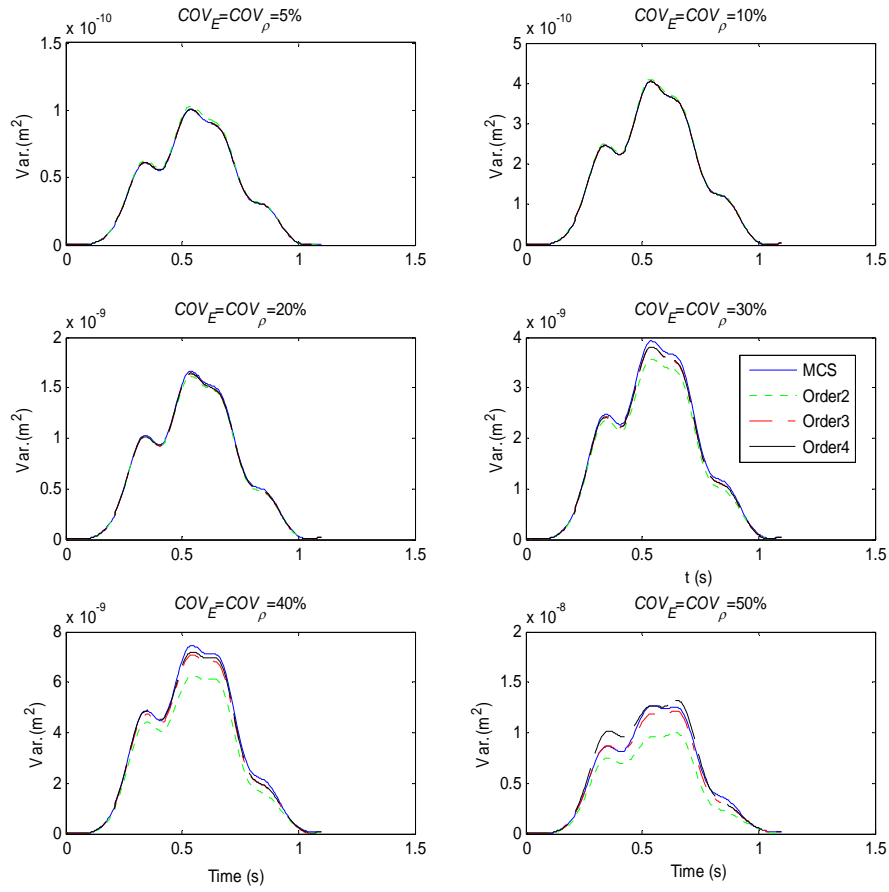


Figure 6.11 - Comparison of variance of mid-span displacement when $COV_F=0\%$ and different order of PC Used

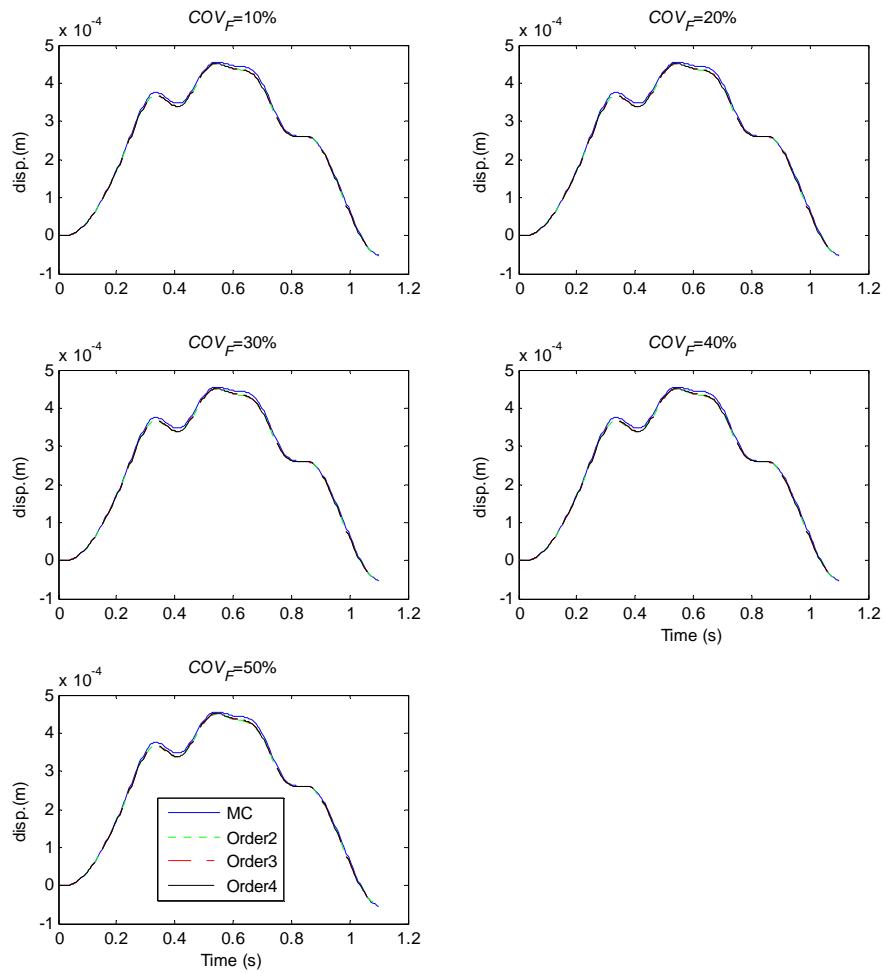


Figure 6.12 - Comparison of mean value of mid-span displacement when $COV_E = COV_\rho = 20\%$ with different level of randomness in excitation

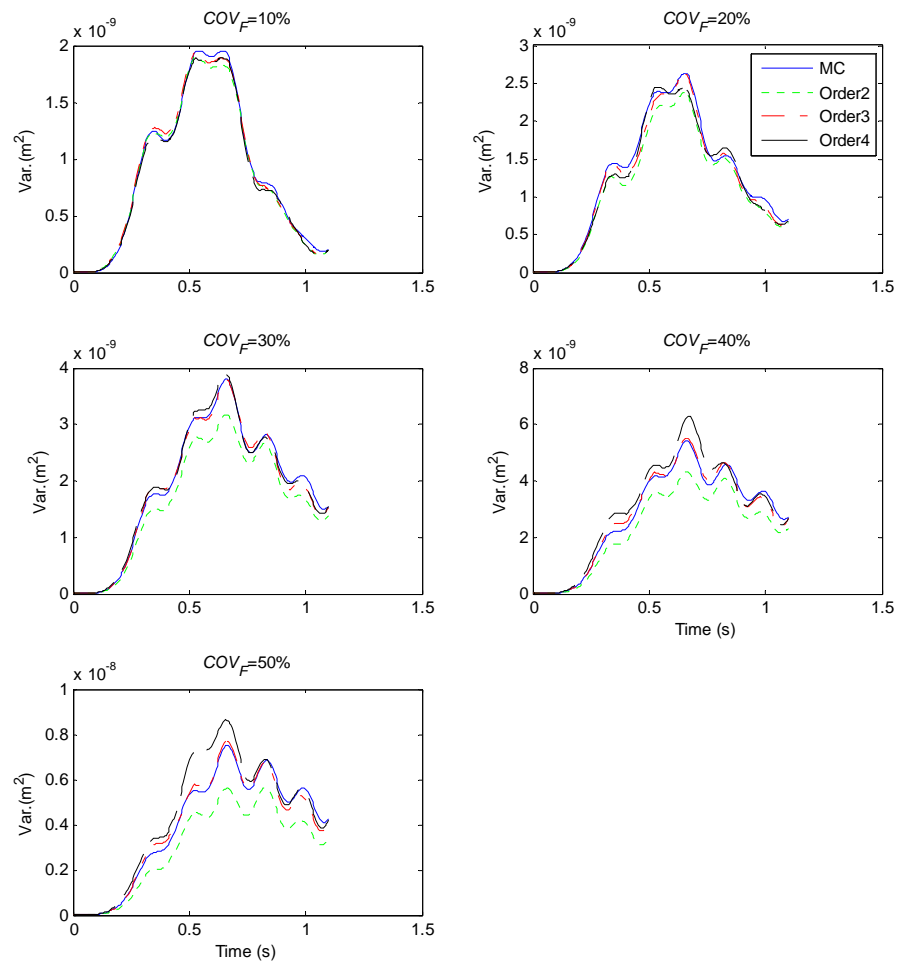


Figure 6.13 - Comparison of variance of mid-span displacement when $COV_E = COV_\rho = 20\%$ with different level of randomness in excitation

CHAPTER 7

STOCHASTIC BRIDGE-VEHICLE

INTERACTION: THE SSFEM MODEL

7.1 Introduction

In this Chapter, an extension of the theory developed on the beam-load model in Chapter SIX is presented for the bridge-vehicle interaction problem in which the Spectral Stochastic Finite Element Method (SSFEM) is adopted to model the bridge structure with Gaussian distributed material property. The road surface roughness is assumed as Gaussian random process with Power Spectrum Density (PSD) function defined according to the ISO standard (ISO 8606:1995(E) 1995). It will be represented by the Karhunen-Loève Expansion. The bridge-vehicle system is modeled by a simply supported planar beam with a four degrees-of-freedom moving mass-spring system on top. It should be noted that since the finite element method is adopted to model the bridge-vehicle system, theoretically, an extension to a more complex structure can be achieved.

The outline of this Chapter is: the modeling of the bridge-vehicle system with uncertainties is introduced in Section 7.2 in which the material properties of the bridge are assumed as Gaussian random processes and they will further be assumed with non-Gaussian property and modeled by the PCE. Numerical

simulations are conducted in Section 7.3 with verifications on the proposed algorithm with the Monte Carlo Simulation. Discussions on the computational aspects of the SSFEM on the bridge-vehicle interaction problem with uncertainties will be addressed in Section 7.4. A summary will be given in Section 7.5 at the end of the Chapter.

7.2 The Coupled Model with Uncertainty in System Parameters

7.2.1 Gaussian System Parameters

The coupled equation of motion of the bridge-vehicle interaction system has already been formulated in Equation (4.3). In this Chapter, the uncertainty in the system parameters is considered and the system matrices are stochastic. The Young's modulus, mass density and damping, which are assumed as Gaussian random processes, are represented by the KLE. Following the procedure introduced in Section 5.2.1, the stochastic stiffness, mass and damping matrix can be derived as shown in Equations (5.8) to (5.10), respectively. The road surface roughness which is assumed as a Gaussian random process is represented by KLE according to Equation (4.7). The random excitation forces $\mathbf{f}(t,\theta)$ due to road surface roughness acting on the bridge-vehicle system can be obtained as shown in Equation (4.9).

Since the covariance matrix of the response is not known *a-priori*, the nodal displacement vector of the bridge-vehicle system $\mathbf{R}(t,\theta)$ and $\mathbf{Y}(t,\theta)$ in Equation

(4.3) which may have non-Gaussian property due to the existence of the Gaussian uncertainties in the system parameters, will be expanded by the Polynomial Chaos according to Equation (6.2) after truncation as

$$\mathbf{R}(t, \theta) = \sum_{j=0}^{K_Z} \Psi_j(\theta) \mathbf{R}^{(j)}(t) \quad (7.1)$$

$$\mathbf{Y}(t, \theta) = \sum_{j=0}^{K_Z} \Psi_j(\theta) \mathbf{Y}^{(j)}(t) \quad (7.2)$$

Combining Equations (7.1) and (7.2), we have

$$\mathbf{Z}(t, \theta) = \sum_{j=0}^{K_Z} \Psi_j(\theta) \mathbf{Z}^{(j)}(t) \quad (7.3)$$

where $\mathbf{Z}^{(j)}(t) = \{\mathbf{R}^{(j)}(t) \mathbf{Y}^{(j)}(t)\}^T$ and K_Z is the dimension of the PCE for the response vector of the bridge-vehicle system which can be calculated as

$$K_Z + 1 = \frac{(k_s + p)!}{k_s! p!} \quad (7.4)$$

where k_s represents the number of K-L components of the response which depends on the number of K-L components in representing both the road surface roughness and system parameters, e.g. if the randomness in Young's modulus, mass density and the road surface roughness are independent, then $k_s = k_E + k_\rho + k_r$. p is the order of the Polynomial Chaos. It is noted that the PCE of the responses of the bridge-vehicle system contains the zeroth component ($j=0$) which represents the responses due to the deterministic moving vehicular axle loads.

Then the random velocity vector and acceleration vector will take the following form as

$$\dot{\mathbf{Z}}(t, \theta) = \sum_{j=0}^{K_Z} \Psi_j(\theta) \dot{\mathbf{Z}}^{(j)}(t) \quad (7.5)$$

$$\ddot{\mathbf{Z}}(t, \theta) = \sum_{j=0}^{K_Z} \Psi_j(\theta) \ddot{\mathbf{Z}}^{(j)}(t) \quad (7.6)$$

where $\dot{\mathbf{Z}}^{(j)}$ and $\ddot{\mathbf{Z}}^{(j)}$ are the first and second derivatives of coefficients $\mathbf{Z}^{(j)}$ with respect to time, respectively.

The KLE of the excitation force vector due to road surface roughness in Equation (4.9) can be rewritten on the basis of the Polynomial Chaos as

$$\mathbf{P}(t, \theta) = \sum_{j=0}^{K_Z} \Psi_j(\theta) \mathbf{P}^{(j)}(t) \quad (7.7)$$

where $\{\overbrace{\mathbf{P}^{(0)}(t) \dots \mathbf{P}^{(K_Z)}(t)}^{K_Z}\}^T = \{\mathbf{f}^{(0)}(t) \overbrace{0 \dots 0}^{(k_E+k_\rho)} \mathbf{f}^{(1)}(t) \dots \mathbf{f}^{(k_r)}(t) \overbrace{0 \dots 0}^{(K_Z-k_s-1)}\}^T$,

Substituting Equations (5.8) to (5.10), (7.3), and (7.5) to (7.7) into Equation (4.3), taking the inner product on both sides of the equation with $\Psi_k(\theta)$ and employing the orthogonal property in Equation (6.3), we have

$$\begin{aligned} \sum_{j=0}^{K_Z} \sum_{i_2=0}^{k_\rho} \langle \xi_{i_2}(\theta) \Psi_j(\theta) \Psi_k(\theta) \rangle \mathbf{M}_{i_2} \ddot{\mathbf{Z}}^{(j)}(t) + \sum_{j=0}^{K_Z} \sum_{i_3=0}^{k_c} \langle \xi_{i_3}(\theta) \Psi_j(\theta) \Psi_k(\theta) \rangle \mathbf{C}_{i_3} \dot{\mathbf{Z}}^{(j)}(t) \\ + \sum_{j=0}^{K_Z} \sum_{i_1=0}^{k_E} \langle \xi_{i_1}(\theta) \Psi_j(\theta) \Psi_k(\theta) \rangle \mathbf{K}_{i_1} \mathbf{Z}^{(j)}(t) = \mathbf{H}_b \langle \Psi_k^2 \rangle \mathbf{P}^{(k)}(t) \end{aligned} \quad (7.8)$$

$$\text{Let } \mathbf{M}^{(k,j)} = \sum_{i_2=0}^{k_\rho} \frac{\langle \xi_{i_2}(\theta) \Psi_j(\theta) \Psi_k(\theta) \rangle}{\langle \Psi_k^2 \rangle} \mathbf{M}_{i_2},$$

$$\mathbf{C}^{(k,j)} = \sum_{i_3=0}^{k_c} \frac{\langle \xi_{i_3}(\theta) \Psi_j(\theta) \Psi_k(\theta) \rangle}{\langle \Psi_k^2 \rangle} \mathbf{C}_{i_3}, \text{ and } \mathbf{K}^{(k,j)} = \sum_{i_1=0}^{k_E} \frac{\langle \xi_{i_1}(\theta) \Psi_j(\theta) \Psi_k(\theta) \rangle}{\langle \Psi_k^2 \rangle} \mathbf{K}_{i_1}.$$

Rewrite Equation (7.8) in matrix form, we have

$$\begin{bmatrix} \mathbf{M}^{(0,0)} & \mathbf{M}^{(0,1)} & \dots & \mathbf{M}^{(0,K_Z)} \\ \mathbf{M}^{(1,0)} & \mathbf{M}^{(1,1)} & \dots & \mathbf{M}^{(1,K_Z)} \\ \vdots & \vdots & \ddots & \vdots \\ \mathbf{M}^{(K_Z,0)} & \mathbf{M}^{(K_Z,1)} & \dots & \mathbf{M}^{(K_Z,K_Z)} \end{bmatrix} \begin{bmatrix} \ddot{\mathbf{Z}}^{(0)}(t) \\ \ddot{\mathbf{Z}}^{(1)}(t) \\ \vdots \\ \ddot{\mathbf{Z}}^{(K_Z)}(t) \end{bmatrix} + \begin{bmatrix} \mathbf{C}^{(0,0)} & \mathbf{C}^{(0,1)} & \dots & \mathbf{C}^{(0,K_Z)} \\ \mathbf{C}^{(1,0)} & \mathbf{C}^{(1,1)} & \dots & \mathbf{C}^{(1,K_Z)} \\ \vdots & \vdots & \ddots & \vdots \\ \mathbf{C}^{(K_Z,0)} & \mathbf{C}^{(K_Z,1)} & \dots & \mathbf{C}^{(K_Z,K_Z)} \end{bmatrix} \begin{bmatrix} \dot{\mathbf{Z}}^{(0)}(t) \\ \dot{\mathbf{Z}}^{(1)}(t) \\ \vdots \\ \dot{\mathbf{Z}}^{(K_Z)}(t) \end{bmatrix}$$

$$+ \begin{bmatrix} \mathbf{K}^{(0,0)} & \mathbf{K}^{(0,1)} & \dots & \mathbf{K}^{(0,K_Z)} \\ \mathbf{K}^{(1,0)} & \mathbf{K}^{(1,1)} & \dots & \mathbf{K}^{(1,K_Z)} \\ \vdots & \vdots & \ddots & \vdots \\ \mathbf{K}^{(K_Z,0)} & \mathbf{K}^{(K_Z,1)} & \dots & \mathbf{K}^{(K_Z,K_Z)} \end{bmatrix} \begin{Bmatrix} \mathbf{Z}^{(0)}(t) \\ \mathbf{Z}^{(1)}(t) \\ \vdots \\ \mathbf{Z}^{(K_Z)}(t) \end{Bmatrix} = \begin{bmatrix} \mathbf{H}_b & \mathbf{0} & \dots & \mathbf{0} \\ \mathbf{0} & \mathbf{H}_b & \dots & \mathbf{0} \\ \vdots & \vdots & \ddots & \vdots \\ \mathbf{0} & \mathbf{0} & \dots & \mathbf{H}_b \end{bmatrix} \begin{Bmatrix} \mathbf{P}^{(0)}(t) \\ \mathbf{P}^{(1)}(t) \\ \vdots \\ \mathbf{P}^{(K_Z)}(t) \end{Bmatrix} \quad (7.9)$$

where the values of inner product of polynomial chaos $\langle \bullet \rangle$ are constants and they can be obtained analytically (Ghanem and Spanos 1991) or numerically (Field et al. 2002).

7.2.2 Non-Gaussian System Parameters

When the material properties of the bridge structure are assumed to have non-Gaussian property, which is more appropriate for engineering applications, the PCE will be adopted to represent these non-Gaussian random processes in the SSFEM model. The stochastic system matrices with non-Gaussian property are represented by PCE according Equations (6.16) to (6.18). Substituting these equations together with Equations (7.3), and (7.5) to (7.7) into Equation (4.3) and taking the inner product on both sides of the equation with $\Psi_k(\theta)$ and employing the orthogonal property in Equation (6.3), we have

$$\begin{aligned} & \sum_{j=0}^{K_Z} \sum_{i=0}^{K_p} \langle \Psi_i(\theta) \Psi_j(\theta) \Psi_k(\theta) \rangle \mathbf{M}_i \ddot{\mathbf{Z}}^{(j)}(t) + \sum_{j=0}^{K_Z} \sum_{i=0}^{K_c} \langle \Psi_i(\theta) \Psi_j(\theta) \Psi_k(\theta) \rangle \mathbf{C}_i \dot{\mathbf{Z}}^{(j)}(t) \\ & + \sum_{j=0}^{K_Z} \sum_{i=0}^{K_E} \langle \Psi_i(\theta) \Psi_j(\theta) \Psi_k(\theta) \rangle \mathbf{K}_i \mathbf{Z}^{(j)}(t) = \mathbf{H}_b \langle \Psi_k^2 \rangle \mathbf{P}^{(k)}(t) \end{aligned} \quad (7.10)$$

$$\text{Let } \mathbf{M}^{(k,j)} = \sum_{i=0}^{K_p} \frac{\langle \Psi_i(\theta) \Psi_j(\theta) \Psi_k(\theta) \rangle}{\langle \Psi_k^2 \rangle} \mathbf{M}_i,$$

$$\mathbf{C}^{(k,j)} = \sum_{i=0}^{K_c} \frac{\langle \Psi_i(\theta) \Psi_j(\theta) \Psi_k(\theta) \rangle}{\langle \Psi_k^2 \rangle} \mathbf{C}_i, \text{ and } \mathbf{K}^{(k,j)} = \sum_{i=0}^{K_E} \frac{\langle \Psi_i(\theta) \Psi_j(\theta) \Psi_k(\theta) \rangle}{\langle \Psi_k^2 \rangle} \mathbf{K}_i. \text{ The}$$

matrix form of Equation (7.10) is the same as Equation (7.9).

7.2.3 Response Statistics

Equations (7.8) and (7.10) can be solved by employing the Newmark- β method. The coefficients in the Polynomial Chaos Expansion for the responses of the bridge-vehicle system can be obtained, and the first two statistics of the nodal displacements for both the bridge and vehicle model can be evaluated as

$$MEAN_{\mathbf{Z}}(t) = \mathbf{Z}^{(0)}(t), \quad VAR_{\mathbf{Z}}(t) = \sum_{j=1}^{K_Z} (\mathbf{Z}^{(j)}(t))^2 \langle \Psi_j^2 \rangle \quad (7.11)$$

where the subscript “Z” notes the nodal displacement vector for the bridge-vehicle system.

The random displacement of the bridge at position x and time t can be derived according to Equations (4.4) and (7.11) as

$$w(x, t, \theta) = \mathbf{H}(x) \sum_{j=0}^{K_Z} \Psi_j(\theta) \mathbf{R}^{(j)}(t) = \sum_{j=0}^{K_Z} \Psi_j(\theta) (\mathbf{H}(x) \mathbf{R}^{(j)}(t)) \quad (7.12)$$

The mean and variance of displacement at position x and time t can be obtained as

$$MEAN_w(x, t) = \mathbf{H}(x) \mathbf{R}^{(0)}(t), \quad VAR_w(x, t) = \sum_{j=1}^{K_Z} (\mathbf{H}(x) \mathbf{R}^{(j)}(t))^2 \langle \Psi_j^2 \rangle \quad (7.13)$$

Samples of the bridge displacements can be easily generated by using any sampling techniques e.g. LHS, to simulate the standard Gaussian random variables $\Psi_j(\theta)$ in Equation (7.12). These samples are useful for further numerical simulation for moving force identification and reliability analysis for bridge safety assessment, etc. The probabilistic density function of the bridge

displacement at position x and time t can also be obtained according to Equation (7.12) when the coefficients $\mathbf{R}^{(j)}$ are calculated. By replacing the coefficients $\mathbf{R}^{(j)}$ with $\dot{\mathbf{R}}^{(j)}$ and $\ddot{\mathbf{R}}^{(j)}$ in Equation (7.13), the mean and variance of random velocity and acceleration at position x and time t can also be obtained.

7.3 Numerical Simulation

7.3.1 Gaussian System Parameters

When the system parameters such as the Young's modulus, mass density and damping of the bridge structure are assumed as Gaussian random processes, the exponential auto-covariance function can be defined as in Equation (5.34) with a and $|x_1 - x_2|$ which are the correlation length and the positive dislocation of two points in a spatial domain of interest. They are set to 1.0 and 3.75m, respectively, for all the parameters. The sampling rate in all the numerical simulation is 200 Hz. The bridge structure is divided into eight beam elements with uncertain system parameters. The velocity of the moving vehicle is 20 m/s

To select the appropriate order of PC in the representation of response for different level of randomness in system parameters, an investigation is carried out without considering the road surface roughness, i.e. let $S_d(f_0)$ in Equation (4.6) equal to zero. Performing the eigenvalue analysis on the defined kernel for the system parameters, the nine K-L components for each system parameter can be obtained. Following the procedure introduced in Section 5.2.1, the stochastic stiffness, mass and damping matrix can be derived according to Equations (5.8)

to (5.10), respectively. In this case, only the $\mathbf{P}^{(0)}(t)$ in the force vector in Equation (7.7) is non-zero. By solving Equation (7.9), the statistics of the nodal response of bridge model can be obtained according to Equation (7.13). The first two statistics of the mid-span displacement of the bridge from the proposed method and the MCS with 10000 runs in the cases when $COV_E=COV_\rho=10\%$ and $COV_E=COV_\rho=20\%$ are compared in Figure 7.1 and 7.2, respectively. For both cases, either the 2nd-order or the 3rd-order PCE are adopted to represent the bridge response. The relative errors between the first two statistics of the mid-span displacement calculated from the two methods are shown in Table 7.1.

Results show that the calculated response statistics of the mid-span displacement agree well with those from MCS. Using higher order of PCE for the response can improve the accuracy in the calculated variance and this improvement may not significant when the randomness in system parameters is small, e.g. COV_E and COV_ρ are smaller than 10%.

It is noted in Table 7.1 that the 2nd-order PC is capable of representing the randomness in system parameters equals to 10% with good accuracy. In the following study, the 2nd-order PC is adopted to represent the response of bridge with $COV_E=COV_\rho=10\%$ under a moving vehicle with different road surface conditions. The criterion for truncation in the KLE of the road surface roughness is $\sum_{j=1}^{k_F} \lambda_j / \sum \lambda_j \geq 0.99$. A comparison of the mean value and variance of the mid-span displacement of the bridge deck from the SSFEM and MCS with 10000 runs under different road surface conditions is given in Figure 7.3 and 7.4,

respectively. The corresponding percentage errors calculated according to Equation (3.39) are shown in Table 7.2.

Results show that the calculated response statistics are very accurate with all road surface conditions. The errors in the calculated mean value increase slightly with the deterioration of the road surface condition while the errors in calculated variance decrease slightly with the deterioration of the road surface condition. The reason for this phenomenon has been explained at the end of Section 6.4.2.3.

7.3.2 Non-Gaussian System Parameters

7.3.2.1 Dynamic Analysis Procedure

The dynamic analysis of the bridge-vehicle system with uncertainties is performed with the proposed algorithm implemented in MATLAB software. 10000 samples of the irregular road profile are generated according to Equation (4.6) in Section 4.3 in which uniformly distributed random angle θ_k is expressed by a random number between 0 to 1 using the command '*rand*'. The corresponding samples of random excitation forces $\mathbf{P}(t,\theta)$ are calculated according to the Equations in Section 4.2.2. These samples of excitation forces will be adopted either to calculate samples of the response in the MCS or to obtain the covariance kernel of the excitation forces in SSFEM.

The procedure of calculating the covariance kernel from samples according to Section 3.3.2 is: (a) the mean value and random component of the samples for the vector of the Gaussian processes are calculated according to Equations (3.13)

and (3.14) respectively; (b) Then the random component of the vector can be reshaped according Equation (3.15). (c) Finally, the covariance kernel for the samples can be calculated according to Equation (3.16).

Eigenvalue analysis is then performed on the kernel to give the corresponding K-L components. The first k_F K-L components with eigenvalue λ_j larger than a threshold value B are retained according to the criterion of $\sum_{j=1}^{k_F} \lambda_j / \sum \lambda_j \geq B$. For the system parameters with log-normal property, the KLE is performed on the prescribed auto-covariance function of the corresponding Gaussian random process as shown in Equation (6.40) to obtain the K-L components $g_i(x)$ for the corresponding Gaussian processes $g(x, \theta)$. In this study, a and $|x_1 - x_2|$ are set to unity and $3.75m$ respectively for both parameters, and nine K-L components are adopted to represent the fluctuation of the corresponding Gaussian random process in the structural model with eight beam elements. The corresponding coefficients in the PCE for the system parameters with log-normal properties can be calculated according Equation (6.36) to form the system matrices in Equation (7.10). The Newmark- β method is employed to solve the formulated Equation (7.10) and the response statistics can be obtained. In the MCS, samples for the log-normal distributed system parameters can be obtained according to Equation (6.36) in which the deterministic coefficients $g_i(x)$ are calculated from the covariance kernel defined in Equation (6.40) and samples for the standard Gaussian random variables $\xi_i(\theta)$ are generated by the command “*randn*” in MATLAB software.

According to the procedure introduced above, the response statistics of the mid-span displacement of the bridge for the case when $S_d(f_0) = 64 \times 10^{-6} \text{ m}^3/\text{cycles}$ and $COV_E = COV_\rho = 20\%$ with the threshold value $B = 0.99$ is calculated and compared with those from 10000 Monte Carlo Simulations in Figure 7.5. The order of PC for representing both the log-normal distributed system parameters and the response are equal to two to facilitate further study on the effect of the order of PC on the accuracy of the proposed method in Section 7.3.2.2. Results show that the mean values and variances of the mid-span displacement from the two methods are in good agreement. The percentage errors defined in Equation (3.39) for the mean value and variance are 0.22% and 1.36%, respectively.

To further study the effectiveness of the SSFEM on bridge-vehicle interaction problem with non-Gaussian uncertainties, different factors including the level of randomness, the order of PC used in SSFEM, the threshold for truncation in the K-L expansion of the excitation forces and the level of the randomness in excitation will be investigated in the following sub-Sections.

7.3.2.2 Level of Randomness in System Parameters

In the study of the level of randomness in system parameters on the accuracy of the proposed method, the randomness in the excitation forces due to the road surface roughness will not be considered, i.e. $S_d(f_0) = 0$. As different order of PC for representing both the system parameters and responses is required at different level of randomness in system parameters to maintain a good accuracy of the SSFEM algorithm, a study is carried out in this sub-Section to examine the

features observed for an appropriate selection.

The cases with different level of randomness in system parameters when $COV_E=COV_\rho=5\%$, 10%, 20%, 30%, 40% and 50% are chosen. Four combinations on the order of PC are adopted including: (1) $OD_S=1$, $OD_R=3$; (2) $OD_S=2$, $OD_R=2$; (3) $OD_S=2$, $OD_R=3$; (4) $OD_S=3$, $OD_R=3$, where OD_S and OD_R are the order of PC for representing the system parameters and the response, respectively. In MCS, 10000 samples of the log-normal distributed system parameters are generated to calculate samples of the bridge response according to Equation (6.36) in which $k_l=9$, $OD_S=3$. The deterministic coefficients $g_i(x)$ are calculated from the covariance kernel defined in Equation (6.40) and samples of the standard Gaussian random variables $\zeta_i(\theta)$ are generated with the command “*randn*” in MATLAB software. The first two statistics of the mid-span displacement of the bridge deck are calculated from the SSFEM with different combinations of the order of PC and MCS, and they are compared in Figures 7.6 and 7.7, respectively, and with the percentage error calculated according to Equation (3.39) and shown in Table 7.3.

Results in Table 7.3 show that the order of PC with $OD_S=1$ and $OD_R=3$ can only give accurate results for different level of randomness in system parameters when the COV of the system parameters is small, e.g. smaller than 20% in calculating the mean value and smaller than 10% in calculating the variance. Large errors in the results occur with larger COV_E and COV_ρ . It is noted that when the order of PC is equal to unity, the PCE is identical to the KLE and the

non-Gaussian random processes, e.g. the log-normal distributed system parameters in this study, are approximated by the corresponding Gaussian random processes with the same mean and variance. It may be concluded that when the COV of the system parameters is small, the non-Gaussian distributed system parameters can be well approximated with the Gaussian distributions which can be represented properly with the KLE. For calculating the mean value of the mid-span displacement, the combinations with order of PC where $OD_S > 1$ and $OD_R > 1$ give accurate results as shown in Table 7.3. The relative errors increase with the level of randomness in system parameters and decrease with the order of PC used. The adoption of a higher order PC larger than two for both the system parameters and response will slightly improve the accuracy of the proposed algorithm but with a dramatic increase of the computational efforts due to a significant increase in both the size of the system matrices and the number of non-zero sub-matrices in Equation (7.9).

The relative error in calculating the variance of the mid-span displacement also increases with the level of randomness in system parameters and it decreases with the order of PC used. When the randomness in system parameters is not very large, e.g. smaller than 30%, the order of PC with $OD_S=2$ and $OD_R=2$ can give acceptable results on the variance. Results from Table 7.3 show that the accuracy of the proposed algorithm is significantly improved by adopting the second order PC instead of the first order PC in representing the non-Gaussian randomness in the system parameters.

In the following sub-Sections, the randomness in excitation due to road surface roughness will be included into the bridge-vehicle interaction problem with the level of randomness in system parameters assumed as $COV_E=COV_\rho=20\%$. Results in Table 7.3 shows that the order of PC with $OD_S=2$ and $OD_R=2$ can be selected to maintain a good representation of the randomness in system parameters. This combination of the order of PC will be adopted for further study in this Chapter on the effect of randomness in the excitation forces on the proposed algorithm for the bridge-vehicle interaction with non-Gaussian uncertainty in system parameters.

7.3.2.3 Truncation in Karhunen-Loève Expansion

Since the number of terms retained in the KLE of the excitation forces will affect both the number of terms in the PCE for the response and the accuracy of the calculated response statistics from the proposed algorithm, the threshold value B defined in the criterion in Section 7.3.2.1 for the truncation in KLE is investigated in this sub-Section.

Different classes of road profile are included in this study. A comparison of statistics of the mid-span displacement with different threshold values in truncation from both MCS and SSFEM is given in Figure 7.8 when $COV_E=COV_\rho=20\%$ and $S_d(f_0)=64\times 10^{-6}$. Only results for the case with $S_d(f_0)=64\times 10^{-6} \text{ m}^3/\text{cycles}$ are shown in Table 7.4 and both the number of K-L components retained after truncation and the percentage errors in the calculated statistics of the mid-span displacement with different value of the threshold B

adopted are listed. For other classes of road profile defined by $S_d(f_0)$, the number of K-L components retained after truncation for each value of B is found identical with the results shown in Table 7.4 due to the linear relationship between $S_d(f_0)$ and $r(x)$ as noted in Equation (4.6). The errors in the calculated mean values are not sensitive to the value of B while the errors in the calculated variances falls sharply at $B=0.95$ to $B=0.96$ and it decreases slightly with further increase of B . Similar trend has also been shown in Figure 7.8. Large error in the calculated variance of the mid-span displacement when $B=0.95$ is mainly due to the truncation of two K-L components from 14 to 12 for the excitation forces which have been included in the case when $B=0.96$. When the threshold value B is close to unity, more K-L components are retained and the proposed algorithm is more accurate but at the expense of a dramatic increase of the computational effort as noted in Equation (7.4) where an increase of k_r may lead to a significant increase of K_z . To maintain the accuracy of the proposed method and yet a reasonable computation effort, a threshold with $B=0.97$ will be adopted in the following sub-Section.

7.3.2.4 Level of the Randomness in Excitation

Investigations on the effect of the level of randomness in excitation due to different road surface roughness are conducted in this sub-Section. The mean value and variance of the mid-span displacement of the bridge deck calculated with the SSFEM and the MCS are compared in Figure 7.9 and Figure 7.10, respectively. The percentage errors according to Equation (3.39) in the results

from SSFEM compared with those from the MCS are listed in Table 7.5.

Results show that the first two statistics of the mid-span displacement calculated from the proposed method and the MCS at a specific level of randomness in excitation, are very close to each other. The percentage error in the mean value increases slightly with an increase in the level of randomness in excitation and the errors in the calculated variance in the response are not sensitive to randomness in excitation as noted in Table 7.5. It may be concluded that the proposed algorithm has good performance in the response statistics prediction in solving the bridge-vehicle interaction problem with large uncertainties in both system parameters and the excitation forces.

7.4 Discussions on Computational Aspects

Computational aspects in numerical simulations related to the application of the proposed algorithms on the bridge-vehicle interaction problem with uncertainties are discussed in this sub-Section.

To solve the formulated mathematical models in forward analysis as shown in Equations (5.16), (6.11) and (6.22), one of the key points is to form the system matrices denoted as \mathbf{M} , \mathbf{K} and \mathbf{C} in which numerous sub-matrices denoted as $\mathbf{M}^{(j,k)}$, $\mathbf{K}^{(j,k)}$ and $\mathbf{C}^{(j,k)}$, respectively are included. These sub-matrices have the same sizes as the corresponding deterministic system matrices noted as \mathbf{M}_d , \mathbf{K}_d and \mathbf{C}_d , respectively, therefore, the sizes of the system matrices for the random system can be extremely large when either the bridge contains numerous

degrees-of-freedom or a high order of Polynomial Chaos is required in representing the non-Gaussian random processes involved. For static analysis of a random structure, system equation based on the SSFEM is a set of linear equations where methods for solving large-scale linear equations can be adopted to solve. A hierarchical approach (Ghanem and Kruger 1996) was also developed for the numerical solution of the static analysis on a random structure according to the symmetric nature of the system matrices. For dynamic analysis of random structures, the system equations of a random structure based on stochastic finite element model are ordinary differential equations and numerical methods such as the Newmark- β method is employed to solve. Due to the large-scale of the system matrices especially for the case of non-Gaussian system parameters, only the sub-matrices $\mathbf{M}^{(j,k)}$, $\mathbf{K}^{(j,k)}$, $\mathbf{C}^{(j,k)}$ with non-zero values are stored and this strategy is achieved with the command “sparse” in the MATLAB programme, and it can dramatically save the storage required and improve the computational efficiency.

The sparsity patterns of the system matrices \mathbf{M} , \mathbf{C} and \mathbf{K} respectively are determined by the value of inner product of polynomial chaos $\langle \cdot \rangle$ in $\mathbf{M}^{(j,k)}$, $\mathbf{K}^{(j,k)}$ and $\mathbf{C}^{(j,k)}$, respectively. Typical sparsity patterns when the number of K-L components is equal to nine with different order of Polynomial Chaos adopted are shown in Figure 7.11. In the four figures, each dot represents a sub-matrix with non-zero values and the ‘nz’ denotes the number of non-zero sub-matrices.

Figure 7.11(a) shows the sparsity pattern for $OD_s=OD_R=1$ which represents

the case introduced in Chapter 5 with the Gaussian assumption for both random system parameters and the random response. Noted from Figure 7.11(a) that the system matrices have small sizes and contain a small number of non-zero sub-matrices which is the reason why the model is regarded as “economic”.

Figure 7.11(b) shows the sparsity pattern for $OD_s=1$ and $OD_R=3$ which represents the case introduced in Section 6.3.1 with the Gaussian assumption for the random system parameters and the non-Gaussian assumption for the random responses represented by a 3rd-order Polynomial Chaos. It is noted from Figure 7.11(b) that the size of the system matrices is much larger than that in Figure 7.11(a). Since the Gaussian assumption is made for system parameters, the number of non-zero sub-matrices is relatively small comparing with the total number of sub-matrices in the system matrices. Only a small storage is required if these system matrices are sparsely stored in the procedure of numerical computing.

Figure 7.11(c) shows the sparsity pattern for $OD_s=2$ and $OD_R=2$ which represents the case introduced in Section 6.3.2 with the non-Gaussian assumption for both the random system parameters and the random response are adopted with a 2nd-order Polynomial Chaos in the representation. Since the maximum order of PCE is 2, the size of the system matrices is much smaller than that in Figure 7.11(b). When an order of Polynomial Chaos larger than one is adopted in the representation of the non-Gaussian system parameters, the number of the non-zeros sub-matrices will increase dramatically. In case of large non-Gaussian

uncertainties exist in the system parameters for an engineering structure, a high order of PC is required to calculate the response statistic with SSFEM which may be very time consuming. The sparsity pattern for $OD_s=2$ and $OD_R=3$ is also shown in Figure 7.11(d).

When the randomness in system parameters is small, the accuracy of the algorithm may not be improved by increasing the order of Polynomial Chaos adopted as shown in the numerical simulation in Chapters 6 and 7, which however may require much more computational efforts. Therefore, appropriate selections on both the algorithm and the order of PC adopted are very important and they should be carefully examined.

7.5 Summary

The dynamic analysis of the bridge-vehicle interaction problem with Gaussian/non-Gaussian uncertainties is presented in this Chapter. The bridge is modeled as a simply supported Euler-Bernoulli beam with Gaussian/non-Gaussian material parameters. A vehicle moves on top of the beam is modeled by a deterministic four degrees-of-freedom mass-spring system, and the road surface roughness is assumed as a Gaussian random process with a power spectrum density function defined according to ISO standard. The mathematic model of the bridge is formulated based on the Spectral Stochastic Finite Element Method coupling with the equation of motion of the vehicle system. Numerical simulations with the proposed method and the Monte Carlo

simulation show good agreement in the results for cases with different level of uncertainties in the system parameters and different road conditions. The following conclusions on the proposed method are drawn:

- (1) The proposed algorithm by employing the SSFEM on the dynamic analysis of the bridge-vehicle interaction problem with Gaussian/non-Gaussian uncertainty in system parameters is effective and with good performance in the response statistics prediction even when large variation exists in both the system parameters and the excitations.
- (2) Appropriate order of PC adopted for representing the non-Gaussian system parameters and the response should be selected to improve the computational efficiency while maintaining the accuracy of the proposed algorithm. When the COV of the system parameters is smaller than 10%, the non-Gaussian system parameters may be approximated with a Gaussian distribution with the same mean value and variance. Higher order PC must be adopted to represent the non-Gaussian randomness when the COV of system parameters increases.
- (3) The randomness in the Gaussian excitation forces on the bridge-vehicle system can be well represented by the KLE. An appropriate threshold for truncation in the KLE should be chosen to minimize the number of K-L components retained while maintaining the accuracy. The percentage error in the mean value increases slightly with an increase in the level of randomness in the excitation and the errors in the calculated variance on

response are not sensitive to randomness in the excitations.

Table 7.1 - Percentage error in mid-span displacement statistics due to different level of Gaussian randomness in system parameters

$RE(\%)$	$COV_E=COV_\rho=10\%$		$COV_E=COV_\rho=20\%$	
$S_d(f_0)=0$	2 nd -Order PC	3 rd -Order PC	2 nd -Order PC	3 rd -Order PC
Mean Value	0.11	0.11	0.25	0.19
Variance	2.75	3.03	11.64	5.12

Table 7.2 - Percentage error in mid-span displacement statistics due to different level of randomness in excitation with Gaussian system parameters

$B=0.99$	$COV_E=COV_\rho=10\%$					
$S_d(f_0)$	0	6×10^{-6}	16×10^{-6}	64×10^{-6}	256×10^{-6}	1024×10^{-6}
Mean Value	0.11	0.12	0.14	0.33	0.48	1.28
Variance	2.75	2.45	1.89	2.19	1.14	0.78

Table 7.3 - Percentage error in mid-span displacement statistics due to different level of non-Gaussian randomness in system parameters

$COV_F=0\%$		Order of PC							
		Combination#1		Combination#2		Combination#3		Combination#4	
	$COV_E=COV_\rho$	OD _S	OD _R						
		1	3	2	2	2	3	3	3
Mean Value	5%	0.01		0.01		0.01		0.01	
	10%	0.02		0.01		0.01		0.01	
	20%	0.12		0.03		0.03		0.03	
	30%	0.68		0.09		0.05		0.05	
	40%	2.79		0.29		0.18		0.15	
	50%	11.48		0.74		0.61		0.23	
Variance	5%	0.17		0.02		0.02		0.02	
	10%	2.60		0.18		0.07		0.07	
	20%	11.64		1.09		0.15		0.15	
	30%	34.51		2.79		0.49		0.38	
	40%	98.91		5.30		2.27		1.68	
	50%	358.11		9.19		7.72		5.43	

Table 7.4 - Percentage error in the calculated responses using different threshold for truncation in KLE of road surface roughness

$COV_E = COV_\rho = 20\%$ $S_d(f_0) = 64 \times 10^{-6}$	Threshold B for truncation					
	0.95	0.96	0.97	0.98	0.99	
Number of K-L Components k_F Retained	12	14	18	24	39	
RE (%)	Mean Value	0.22	0.22	0.22	0.22	0.22
	Variance	18.99	3.21	1.77	1.82	1.68

Table 7.5 - Percentage error in mid-span displacement statistics due to different level of randomness in excitation with non-Gaussian system parameters

$B = 0.97$	$COV_E = COV_\rho = 20\%$					
$S_d(f_0)$	0	6×10^{-6}	16×10^{-6}	64×10^{-6}	256×10^{-6}	1024×10^{-6}
Mean Value	0.03	0.07	0.11	0.22	0.28	0.54
Variance	1.09	1.19	2.32	1.77	1.62	1.62

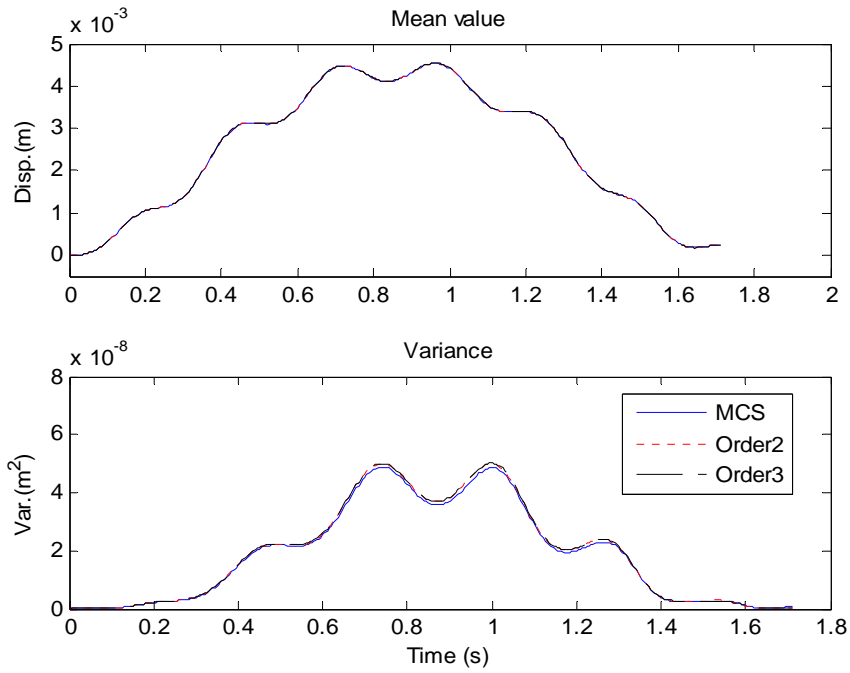


Figure 7.1 - Comparison of statistics of mid-span displacement from SSFEM and MCS with different order of PC when $COV_E=COV_\rho=10\%$

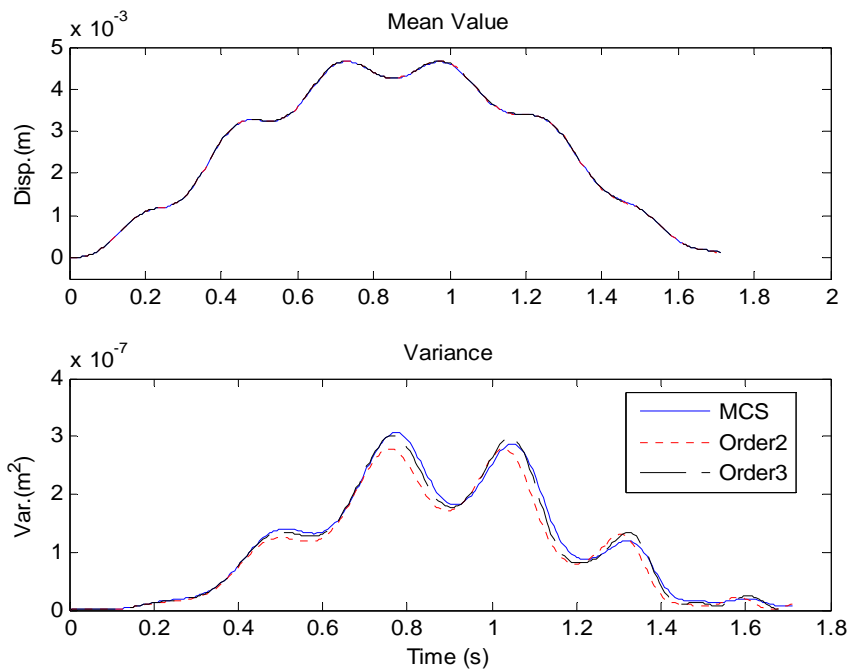


Figure 7.2 - Comparison of statistics of mid-span displacement from SSFEM and MCS with different order of PC when $COV_E=COV_\rho=20\%$

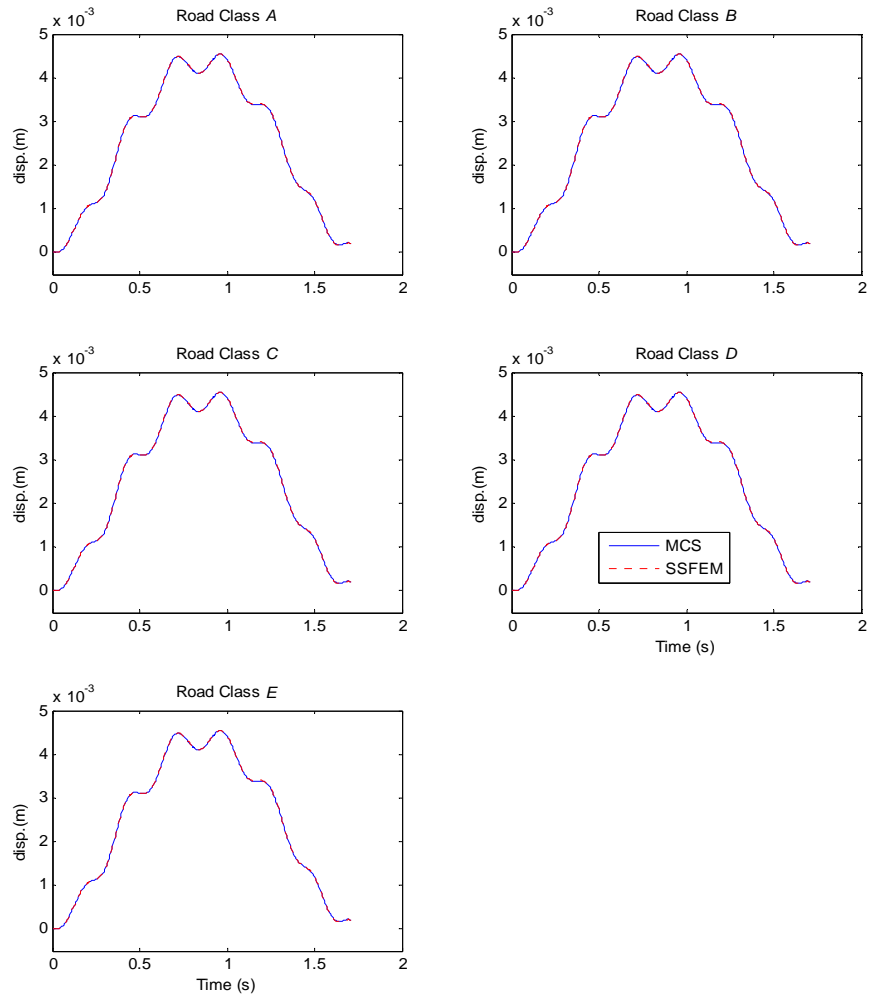


Figure 7.3 - Comparison of mean values of mid-span displacement from SSFEM and MCS, when $COV_E=COV_\rho=10\%$

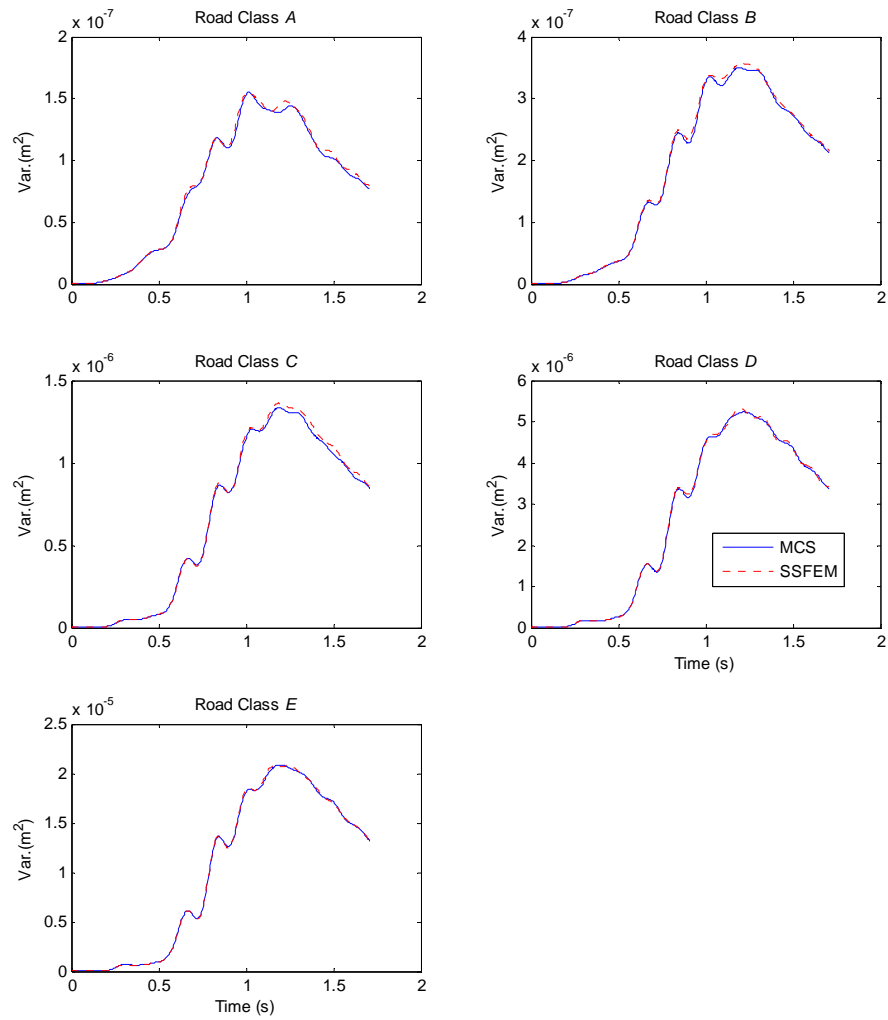


Figure 7.4 - Comparison of variances of mid-span displacement from SSFEM and MCS, when $COV_E=COV_\rho=10\%$

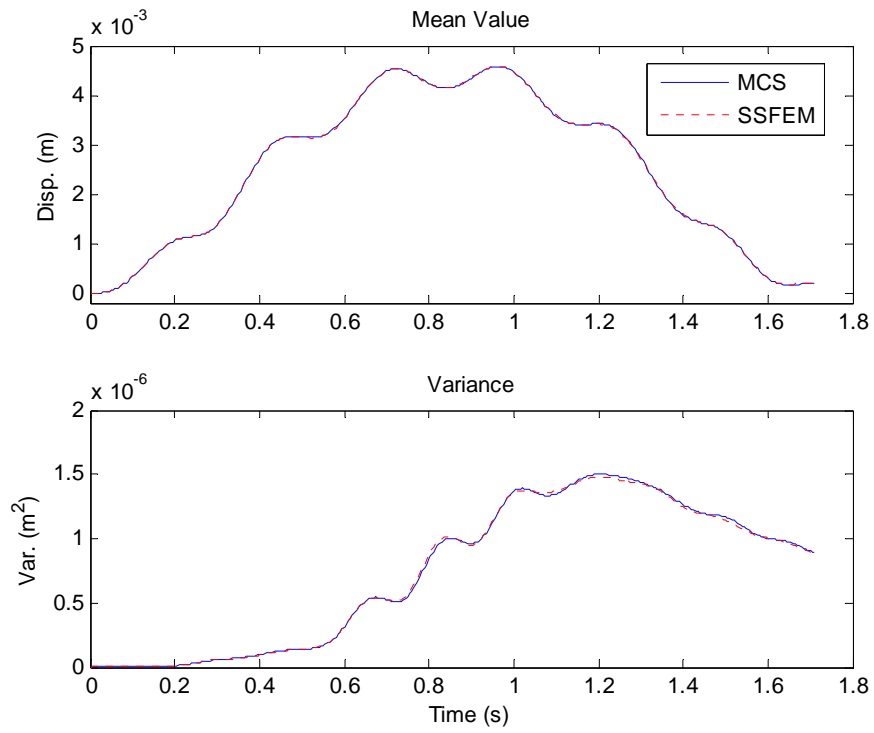


Figure 7.5 - Comparison of response statistics from SSFEM and MCS, when $COV_E=COV_p=20\%$, Road C and $B=0.99$

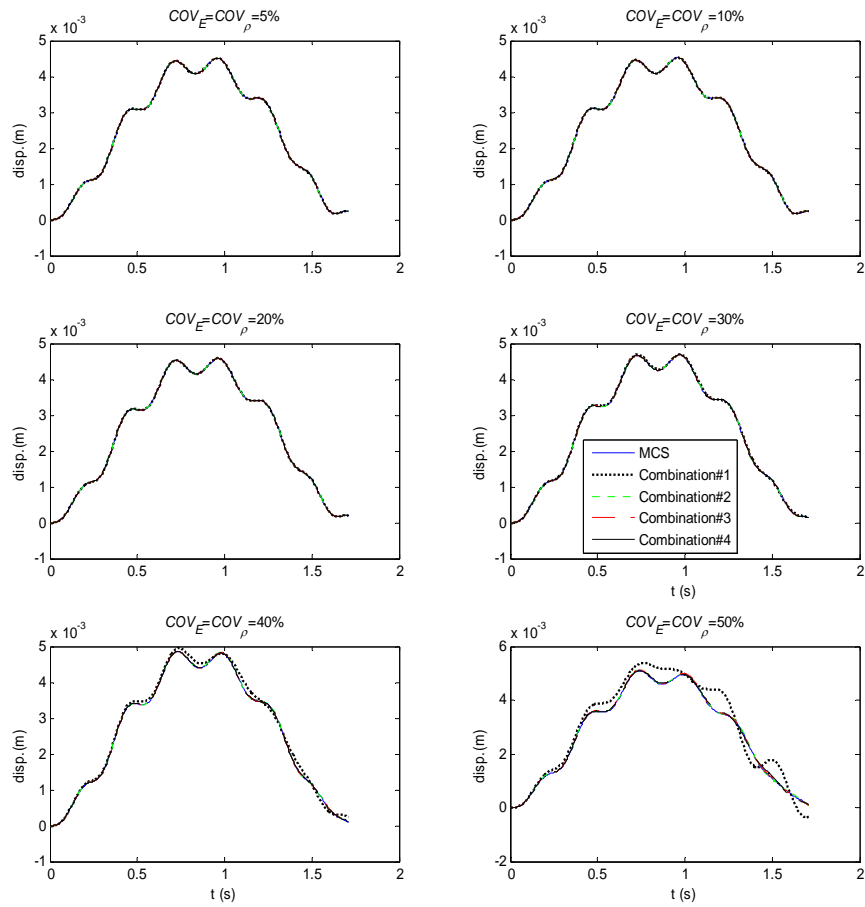


Figure 7.6 - Comparison of mean values of mid-span displacement with different order of PC used

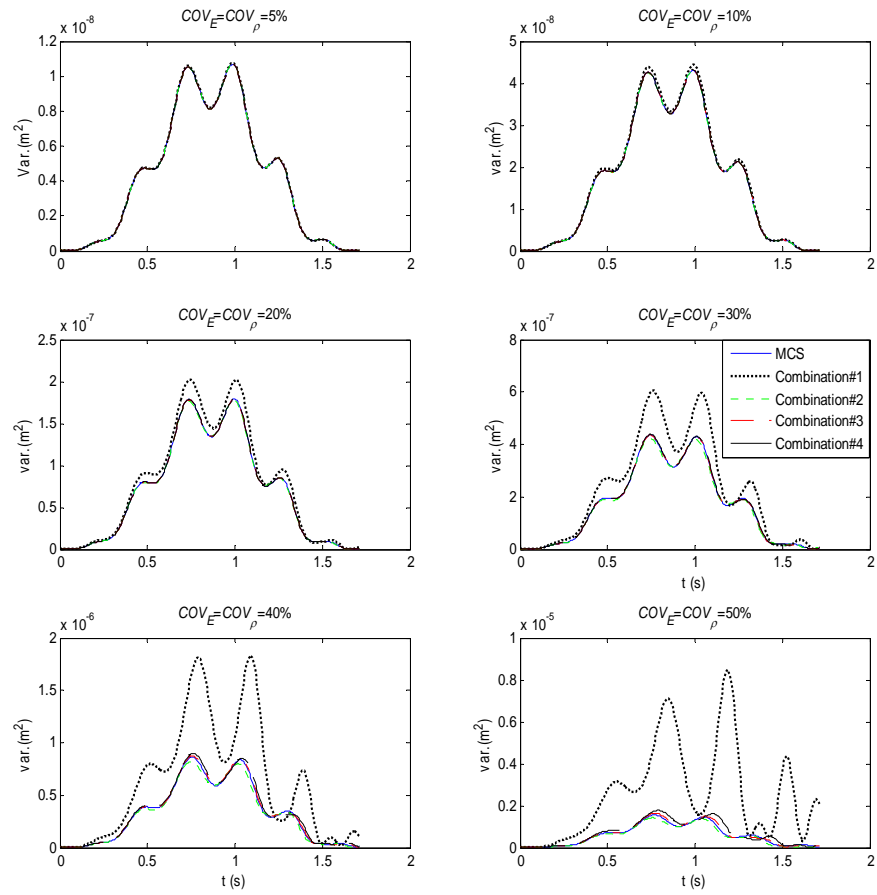


Figure 7.7 - Comparison of variances of mid-span displacement with different order of PC used

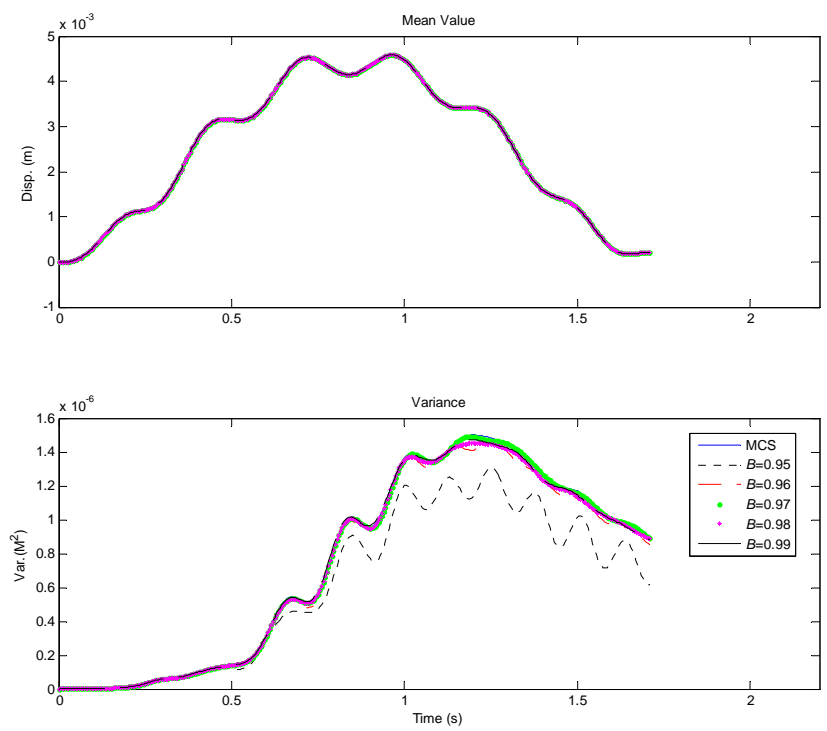


Figure 7.8 - Comparison of statistics of mid-span displacement with different threshold for truncation when $COV_E=COV_\rho=20\%$ and $S_d(f_0)=64 \times 10^{-6}$

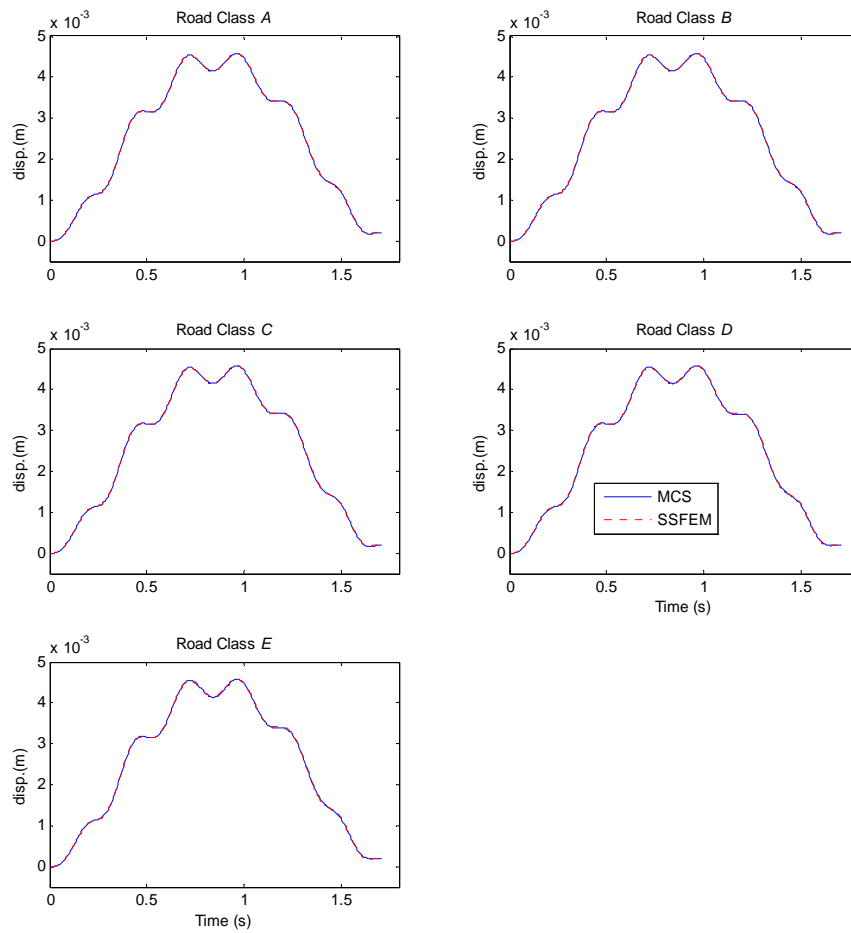


Figure 7.9 - Comparison of mean values of mid-span displacement under different road surface conditions when $COV_E=COV_\rho=20\%$, $B=0.97$ and $OD_s=OD_R=2$

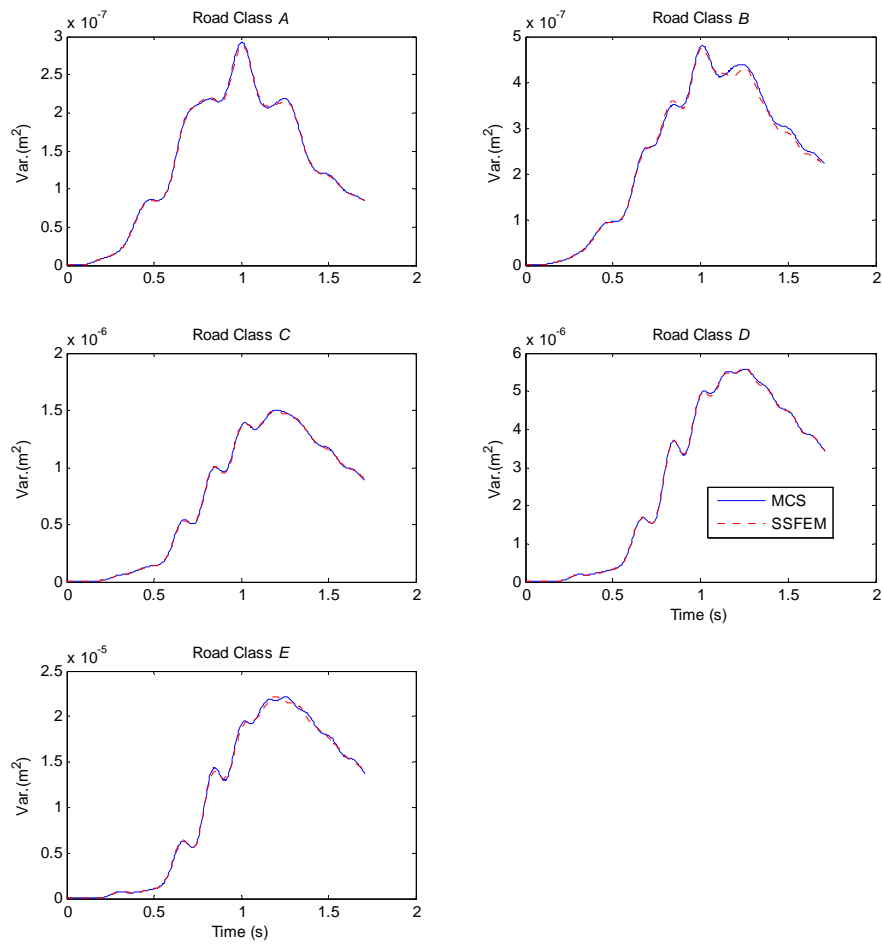


Figure 7.10 - Comparison of variances of mid-span displacement under different road surface conditions when $COV_E=COV_\rho=20\%$, $B=0.97$ and $OD_s=OD_R=2$

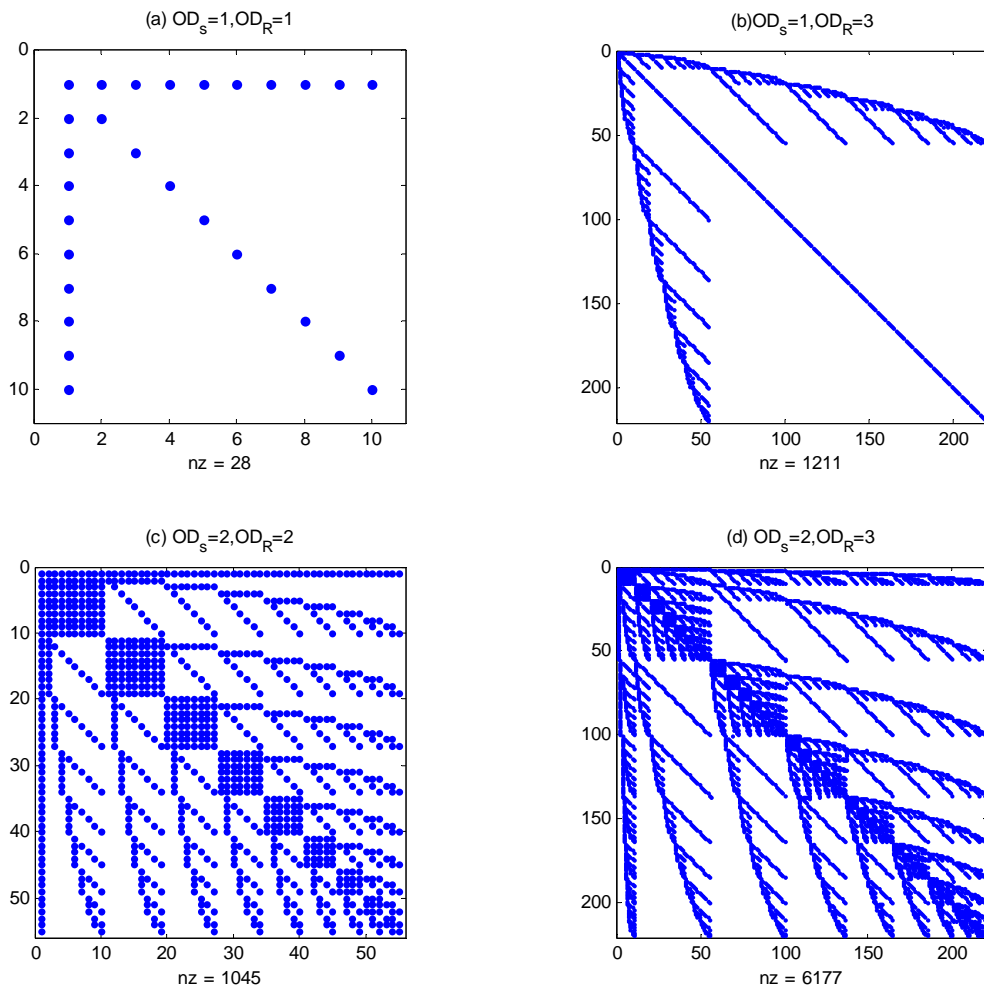


Figure 7.11 - Typical sparsity patterns of the system matrices in SSFEM with different order of PCE when $k_s=9$

CHAPTER 8

SUMMARY, CONCLUSIONS AND RECOMMENDATIONS

8.1 Summary

The work in this Thesis aims to provide a theoretical study of bridge-vehicle interaction problem with uncertainties in both the interaction forces due to road surface roughness and the material properties in the bridge structure. The uncertainties in this system are modeled as Gaussian/non-Gaussian random processes which are represented by the Karhunen-Loève Expansion and/or Polynomial Chaos Expansion. The research work is conducted the following steps:

- (1) Only the randomness due to road surface roughness is considered in the bridge-vehicle interaction problem in Chapters THREE and FOUR. The bridge-vehicle system is assumed to have deterministic parameters and the road surface roughness is assumed as a Gaussian random process with a Power Spectrum Density function defined according to the ISO standard (ISO 8606:1995(E) 1995). The system modeling is conducted with the Gaussian random processes represented by the Karhunen-Loève Expansion. Based on the model developed, a moving force identification technique is

proposed to identify the statistics of the interaction forces (or moving forces) on the bridge deck from samples of “measured” bridge response. The algorithm is first developed on a beam-load model and then extended to a bridge-vehicle interaction model with the vehicle modeled as a four degrees-of-freedom mass-spring system. Since the finite element method is adopted for the system modeling, the proposed method can be applied to cases with more complex bridge and vehicle configurations.

- (2) To carry out the research work one step further, small uncertainty in the material properties of the bridge structure is included in the study of the bridge-vehicle interaction problem in Chapter FIVE. According to the fact that when the randomness in the system parameters is small, the random responses of bridge which may have non-Gaussian properties can be approximated by Gaussian random processes. The moving excitation forces applied on the bridge deck are also assumed as Gaussian random processes. All these Gaussian random processes are represented by the Karhunen-Loève Expansion based on which an “economic” stochastic finite element model is formulated. The proposed model in this Chapter can accurately simulate the bridge-vehicle interaction problem with small uncertainties in the system parameters and large uncertainties in the excitation forces. Based on the model developed, a general Stochastic Moving Force Identification (SMFI) algorithm is proposed to identify the statistics of the moving forces on the bridge deck from samples of the

random bridge response considering randomness in the system parameters.

- (3) Since the algorithm developed in Step two may tend to be inaccurate with increasing randomness in system parameters, the Spectral Stochastic Finite Element Method is adopted in Chapter SIX and SEVEN to modeling the uncertainties. The stochastic bridge response, which may have non-Gaussian property, is represented by the Polynomial Chaos Expansion. The material properties of the bridge structure are firstly assumed as Gaussian random processes which are represented by the Karhunen-Loève Expansion. With increasing uncertainty in system parameters, the Gaussian assumption for the system parameters which has a small probability of taking negative values, is impractical in engineering problems, and these negative system parameters will cause divergence in MCS. Therefore, the non-Gaussian assumption is further adopted for the system parameters to have an algorithm to be effective in case of large uncertainties in both the system parameters and excitation forces. The theory is first applied on a beam-load model and then to a bridge-vehicle interaction problem.

8.2 Conclusions

With all the research work conducted, the following conclusions are drawn:

- (1) When the material properties of a bridge structure are assumed to be deterministic and the randomness in the excitations on the bridge due to road surface roughness is considered in the bridge-vehicle interaction

problem.

- The modeling of Gaussian uncertainties in the excitations and the responses with the Karhunen-Loève Expansion is very accurate. Moreover, the accuracy is not sensitive to the level of randomness.
 - The proposed stochastic moving force identification algorithm based on this model for the identification of the statistics of excitation forces from the “measured” response samples is found to be effective even when the randomness in excitation forces is very large, e.g. when COV_F is larger than 0.8. The relative error in the variance of the identified forces is also not sensitive to the level of randomness.
 - The accuracy of identified interaction forces (or moving forces) is significantly improved with a small number of measured responses samples in the stochastic force identification approach when compared to that obtained from an existing deterministic method (Law et al. 2004) of using one sample of measured response.
 - The uncertainty in the measured responses can be largely removed from the mean values of the identified moving forces in the identification process when a relative large number of response samples are used. It is recommended that 50 response samples may be suitable for a satisfactory identification of the variance of the moving vehicle axle forces.
- (2) When the material properties of bridge structure are assumed to have small Gaussian uncertainties, e.g. the coefficient of variation is not larger than

5%, the response of the bridge under Gaussian random moving forces can be approximated by Gaussian random processes and is represented by the Karhunen-Loève Expansion.

- This “economic” stochastic finite element model proposed based on the KLE has high computational efficiency, insensitive to the velocity of the moving forces and good accuracy in the prediction of response statistics for the practical case with relatively small uncertainty in system parameters but large randomness in excitation.
- A general stochastic moving force identification algorithm which includes both the Gaussian system parameters and excitations in the inverse problem is developed based on this stochastic finite element model for the bridge-vehicle interaction problem. The relative error in the mean value of the identified force increases slightly with a decrease in the number of sample of “measured” responses. Whether or not the samples used can truly represent the statistics of its population will be the most important requirement for an accurate identification on the variance of the moving force.
- The effect of level of randomness depends on the relationship between the covariance kernel for the case of a deterministic system under random excitation and the third term in Equation (5.32) which is the key to good accuracy on the statistics, particularly the variance of the identified force. When the covariance kernel is relatively large compared

with the error term (the third term in Equation (5.32)), all the statistics including the mean value and variance of the moving force can be accurately identified.

- It should be declared that by eliminating the location matrix in this SMFI algorithm, it is also applicable for other force identification procedure in a stochastic dynamic system as long as the assumption of small uncertainties in the system parameters is valid.
- (3) The proposed algorithm by employing the SSFEM in the dynamic analysis of the bridge-vehicle interaction problem with Gaussian/non-Gaussian uncertainty in system parameters is effective and with good performance in the response statistics prediction even when large variation exists in both the system parameters and the excitations.
- For the case with Gaussian system parameters, when the uncertainty in system parameters is very small, e.g. smaller than 5%, the Gaussian assumption for the response of bridge structure is appropriate. An assumption of non-Gaussian uncertainties for the solution cannot improve the accuracy in the variance prediction.
 - When the level of randomness in the system parameters increases, the Gaussian assumption for the solution, i.e. the use of first order PC in response representation, will result in large error in the variance prediction. Hence the non-Gaussian assumption with higher order PC must be adopted for the random response of the bridge structure to

achieve accurate results especially in the variance.

- At a high level of randomness in system parameters, e.g. COV larger than 0.3, the Gaussian assumption for the system parameter which may result in negative values, will cause divergence in the response statistics calculation in MCS. Therefore, a non-Gaussian assumption should be adopted.
- In case of non-Gaussian system parameters, appropriate orders of PC adopted for representing both the non-Gaussian system parameters and the response should be selected to improve the computational efficiency while maintaining the accuracy of the proposed algorithm. When the COV of the system parameters is smaller than 10%, the non-Gaussian system parameters may be approximated with a Gaussian distribution with the same mean value and variance. Higher order of PC larger than one must be adopted to represent the non-Gaussian randomness when the COV of system parameters increases.
- In cases when the excitation forces require a large number of K-L components to represent, an extremely large number of Polynomial Chaos may be required in the PCE of the non-Gaussian random responses which makes the problem unsolvable due to the limit capability of computer. A reduce PCE model is proposed as an alternative in which the uncorrelated non-Gaussian random variables in PCE are assumed to be independent with a larger number of K-L

components as a compensation. This model can effectively reduce the computational efforts with a trade off in the accuracy of prediction. When the coefficients of variation of both the system parameters and excitation forces is smaller than 0.2, a 2nd-order representation of the polynomial chaos is sufficient to obtain accurate response statistics of a beam structure. In other cases with larger coefficients of variations, a 3rd-order representation of polynomial chaos is recommended.

8.3 Recommendations

The proposed algorithms in this Thesis can successfully solve the bridge-vehicle interaction problem with uncertainties to some extent. Nevertheless, there are still flaws in these algorithms to note. Moreover, some further research which is regarded to be important by the author within the scope of the bridge-vehicle interaction problem with uncertainties will be addressed. Recommendations on the improvements of the existing algorithms and on further research directions of this interesting topic are:

- (1) The Spectral Stochastic Finite Element Method adopted in modeling the uncertainties in the bridge-vehicle interaction problem has good accuracy even when the randomness in both system parameters and excitation forces are large. However, the dimension of Polynomial Chaos is noted to be dependent on the number of K-L components and the order of Polynomial Chaos adopted. The covariance kernel which requires minimum number of

K-L components to represent the uncertain system parameters should be selected. The covariance matrix for the random excitation forces tends to become very large with an increasing number of the forces and the number of time instances. This will lead to long computation time in the eigenvalue analysis. A high sampling rate of data is therefore not recommended. A Galerkin type procedure (Ghanem and Spanos 1991) can also be employed for solving the Fredholm equation to improve the computational efficiency for the eigenvalue problem. Since the size of the system matrices in SSFEM equals to the dimension of Polynomial Chaos multiplied by the number of degrees-of-freedom of the random system, in the dynamic analysis of a stochastic finite element model with a large number of degrees-of-freedom, the stochastic model reduction technique (Doostan et al. 2007) is recommended to reduce the computation. Other methods such as the modal superposition technique in which the stochastic shape functions obtained from random eigenvalue analysis (Ghosh et al. 2005, Ghanem and Ghosh 2007) are adopted, the Stochastic Reduced Basis Method (SRBM) (Nair and Keane 2002; Mohan et al. 2008), etc. can also be employed as alternatives to solve this problem.

- (2) The stochastic moving force identification algorithm proposed in this Thesis is based on the stochastic finite element model with the assumption of small uncertainty in system parameters. Since the algorithm in this thesis tends to loss accuracy with increasing level of randomness in system

parameters, a more general force identification algorithm based on the Spectral Stochastic Finite Element Model with Gaussian/non-Gaussian uncertainty in system parameters would be a new task to be accomplished to fill the gap of the lack of force identification algorithm on stochastic finite element model. Once this force identification algorithm is proposed, the response data from either experiments or field tests can be utilized to identify the statistics of the excitation forces based on the representation of experimental data with Polynomial Chaos (Desceliers et al. 2006; 2007).

- (3) The randomness in the velocity of vehicles, the physical parameters of the vehicle system especially for the stiffness and damping of tires, should be further included in the uncertain bridge-vehicle interaction model. It should be noted that the inclusion of the randomness in the parameters of tires will introduce the inner product of Polynomial Chaos with four terms which can be calculated according to the method provided by Debusschere et al. (2004).
- (4) Further research work may also be extended to develop a stochastic bridge-vehicle interaction model with a stream of vehicles moving on the bridge with Poisson arrivals in which only the randomness in the arrival of vehicle is considered. The Poisson distribution can be represented by Charlier Polynomial Chaos and the stochastic analysis of this bridge-vehicle interaction model may give an overall estimation on the vehicle loading of the bridge structure.

REFERENCES

- Abdel Wahab, M. M., Roeck, G. D. and Peeters, B. (1999) "Parameterization of damage in reinforced concrete structures using model updating." *Journal of Sound and Vibration*, 228(4), 717-730.
- Abu-Hilal, M. and Mohsen, M. (2000) "Vibration of beams with general boundary conditions due to a moving harmonic load." *Journal of Sound and Vibration*, 232(4), 703-717.
- Abu-Hilal, M. (2003) "Vibration of beams with general boundary conditions due to a moving random load." *Archive of Applied Mechanics*, 72(7), 637-650.
- Asnachinda, P., Pinkaew T. and Laman, J. A. (2008) "Multiple vehicle axle load identification from continuous bridge bending moment response." *Engineering Structures*, 30, 2800-2817.
- Asokan, B. V. and Zabaras, N. (2006) "A stochastic variational multiscale method for diffusion in heterogeneous random media." *Journal of Computational Physics*, 218 (2), 654-676.
- Azeez, M. F. A. and Vakakis, A. F. (2001) "Proper orthogonal decomposition (POD) of a class of vibroimpact oscillations." *Journal of Sound and Vibration*, 240(5), 859-889.
- Bilello, C. and Bergman, L. A. (2004) "Vibration of damaged beams under a moving mass: theory and experimental validation." *Journal of Sound and Vibration*, 274(3-5), 567-582.

- Blair, M. A., Camino, T. S. and Dickens, J. M. (1991) "An iterative approach to a reduced mass matrix." *Proceedings of the 8th International Modal Analysis Conference*, Florence, Italy, April, 510-515.
- Borrelli, R. L. and Coleman, C. S. (1987) *Differential Equations A Modeling Approach*, Prentice-Hall, Inc., Englewood Cliffs, New Jersey 07632.
- Cameron, R. H. and Martin, W. T. (1947) "The orthogonal development of non-linear functionals in series of Fourier-Hermite functionals." *Annals of Mathematics*, 48, 385-392.
- Cantieni, R. (1983) "Dynamic load tests on highway bridges in Switzerland – 60 years of experience." *Report 211, Federal Laboratories for Testing of Materials*, Dubendorf, Switzerland.
- Cantieni, R. (1992) "Dynamic behaviour of highway bridges under the passage of heavy vehicles." *Report No.220, Swiss Federal Laboratories for Materials Testing and Research (EMPA)*.
- Cebon, D. (1987) "Assessment of the dynamic wheel forces generated by heavy road vehicles." *Symposium on Heavy vehicle Suspension and Characteristics, Australian Road Research Board*.
- Chakraborty, S. and Dey, S.S. (1998) "A stochastic finite element dynamic analysis of structures with uncertain parameters." *International Journal of Mechanical Science*, 40(11), 1071-1087.
- Chakraborty, S. and Sarkar, S. K. (2000) "Analysis of a curved beam on uncertain elastic foundation." *Finite Elements in Analysis and Design*, 36, 73-82.

- Chan, T. H. T. and O' Connor, C. (1990) "Wheel loads from highway bridge strains." *Journal of Structural Engineering Division-ASCE*, 116, 1751-1771.
- Chan, T. H. T., Law, S. S. and Yung, T. H. (1999) "An interpretive method for moving force identification." *Journal of Sound and Vibration*, 219(3), 503-524.
- Chan, T. H. T., Yu, L., Law, S. S. and Yung, T. H. (2001a) "Moving force identification studies, I: Theory." *Journal of Sound and Vibration*, 247(1), 59-76.
- Chan, T. H. T., Yu, L., Law, S. S. and Yung, T. H. (2001b) "Moving force identification studies, II: Comparative studies." *Journal of Sound and Vibration*, 247(1), 77-95.
- Chang, T. P., Lin, G. L. and Chang, E. (2006) "Vibration analysis of a beam with an internal hinge subject to a random moving oscillator." *International Journal of Solids and Structures*, 43, 6398-6412.
- Chang, T. P., Liu, M. F. and O, H. W. (2009) "Vibration analysis of a uniform beam traversed by a moving vehicle with random mass and random velocity." *Structural Engineering Mechanics*, 31(6), 737-749.
- Chaudhuri, A. and Chakraborty, S. (2006) "Reliability of linear structures with parameter uncertainty under non-stationary earthquake." *Structural Safety*, 28, 231-246.
- Chatterjee, P. K., Datta, T. K. and Surana, C. S. (1994) "Vibration of continuous bridge under moving vehicles." *Journal of Sound and Vibration*, 169,

619-632.

- Chen, Y. B., Feng, M. Q. and Tan, C. A. (2009) "Bridge structural condition assessment based on vibration and traffic monitoring." *Journal of Engineering Mechanics*, 135(8), 747-758.
- Cho, T., Song, M. K. and Lee, D. H (2010) "Reliability analysis for the uncertainties in vehicle and high-speed railway bridge system based on an improved response surface method for nonlinear limit states." *Nonlinear Dynamics*, 59, 1-17.
- Choi, S. K., Grandhi, R. V., Canfield, R. A. and Pettit, C. L. (2004) "Polynomial chaos expansion with Latin Hypercube Sampling for estimating response variability." *AIAA Journal*, 42(6), 1191-1198.
- Das, S., Ghanem, R. and Finette, S. (2009) "Polynomial chaos representation of spatio-temporal random fields from experimental measurements." *Journal of Computational Physics*, 228, 8726-8751.
- Da Silva, J. G. S. (2004) "Dynamical performance of highway bridge decks with irregular pavement surface." *Computers and Structures*, 82(11-12), 871-881.
- Davis, P. and Sommerville, F. (1987) "Calibration and accuracy testing of weigh-in-motion systems." *Transportation Research Record*, 1123, 122-126.
- Debusschere, B. J., Najm, H. N., Pebay, P. P., Knio, O. M., Ghanem, R. G. and Le Maiter, O. P. (2004) "Numerical challenges in the use of polynomial chaos representations for stochastic processes." *SIAM-Journal on Scientific Computing*, 26(2), 698-719.

- Deodatis, G. (1990) "Bounds on response variability of stochastic finite element systems." *Journal of Engineering Mechanics-ASCE*, 116(3), 565-585.
- Deodatis, G. and Micaletti, R. C. (2001) "Simulation of highly skewed non-Gaussian stochastic processes." *Journal of Engineering Mechanics-ASCE*, 114(7), 1183-1197.
- Desceliers, C., Ghanem, R. and Soize, C. (2006) "Maximum likelihood estimation of stochastic chaos representations from experimental data." *International Journal for Numerical Methods in Engineering*, 66, 978-1001.
- Desceliers, C., Soize, C. and Ghanem, R. (2007) "Identification of chaos representation of elastic properties of random media using experimental vibration tests." *Computational Mechanics*, 39, 831-838.
- Der Kiureghian, A. and Ke, J. B. (1988) "The stochastic finite-element method in structural reliability." *Probabilistic Engineering Mechanics*, 3(2), 83-91.
- Dijkerman, R. W. and Mazumdar, R. R. (1994) "Wavelet representations of stochastic Processs and Multiresolution stochastic models." *IEEE Transactions on Signal Processing*, 42(7), 1640-1652.
- Doostan, A., Ghanem, R. G. and Red-Horse, J. (2007) "Stochastic model reduction for chaos representations." *Computer Methods in Applied Mechanics and Engineering*, 196 (37-40), 3951-3966.
- Eiermann, M., Ernst, O. G. and Ullmann, E. (2007) "Computational aspects of the stochastic finite element method." *Computing and Visualization in Science archive*, 10(1), 3-15.

- Elishakoff, I. and Ren, Y. J. (2003) *Finite Element Methods for Structures with Large Stochastic Variations*, Oxford University Press, New York.
- Faravelli, L. (1989) "Response surface approach for reliability analysis." *Journal of Engineering Mechanics-ASCE*, 115 (12), 2763-2781.
- Faravelli, L. (1990) "Stochastic finite elements for crash problems." *Structural Safety*, 9 (1-4), 113-130.
- Field, R. V. (2002) "Numerical methods to estimate the coefficients of the polynomial chaos expansion." *15th ACSE Engineering Mechanics Conference*, June 2-5, Columbia University, New York, NY.
- Field, R. V. and Grigoriu, M. (2004) "On the accuracy of the polynomial chaos approximation." *Probabilistic Engineering Mechanics*, 19, 65-80.
- Florian, A. (1992) "An efficient sampling scheme: Updated Latin Hypercube Sampling." *Probabilistic Engineering Mechanics*, 7, 123-130.
- Foo, J., Yosibash, Z. and Karniadakis, G. E. (2007) "Stochastic simulation of riser-sections with uncertain measured pressure loads and/or uncertain material properties." *Computer Methods in Applied Mechanics and Engineering*, 196, 4250-4271.
- Freund, D. M. and Bonaquist, R. F. (1989) "Evaluation of a weigh-in-motion device at the pavement testing facility." *Public Roads*, 52, 97-106.
- Friswell, M. I., Garvey, S. D. and Penny, J. E. T. (1995) "Model reduction using dynamic and iterated IRS techniques." *Journal of Sound and Vibration*, 186(2), 311-323.

- Fryba, L., Nakagiri, S. and Yoshikawa, N. (1993) "Stochastic finite elements for beam on a random foundation with uncertain damping under a moving force." *Journal of Sound and Vibration*, 163(1), 31-45.
- Fryba, L. (1999) *Vibration of solids and structures under moving loads*. London: Thomas Telford , 3rd Ed.
- Galal, O. H., EI-Tahan, W., EI-Tawil, M. A. and Mahmoud, A. A. (2008) "Spectral SFEM analysis of structures with stochastic parameters under stochastic excitation." *Structural Engineering and Mechanics*, 28(3), 281-294.
- Gersch, W. and Yonemoto, J. (1977) "Synthesis of multi-variant random vibration systems: a two-stage least squares ARMA model approach." *Journal of Sound and Vibration*, 52(4), 553-565.
- Ghanem, R. G. and Spanos, P. D. (1991) *Stochastic finite elements: A spectral approach*, New York, Springer.
- Ghanem, R. G. and Kruger R. M. (1996) "Numerical solution of spectral stochastic finite element systems." *Computer Methods in Applied Mechanics and Engineering*, 129 (3), 289-303.
- Ghanem, R. G. (1999a) "Ingredients for a general purpose stochastic finite elements implementation." *Computer Methods in Applied Mechanics and Engineering*, 168 (1-4), 19-34.
- Ghanem, R. G. (1999b) "Stochastic finite elements with multiple random non-Gaussian properties." *Journal of Engineering Mechanics-ASCE*, 125(1), 26-40.

- Ghanem, R. G. (1999c) "The nonlinear Gaussian spectrum of log-normal stochastic processes and variables." *Journal of Applied Mechanics-ASCE*, 66, 964-973.
- Ghanem, R. and Ghosh, D (2007) "Efficient characterization of the random eigenvalue problem in a polynomial chaos decomposition." *International Journal for Numerical Methods in Engineering*, 72, 486-504.
- Ghanem, R. G., Saad, G. and Doostan, A. (2007) "Efficient solution of stochastic systems: Application to the embankment dam problem." *Structural Safety*, 29 (3), 238-251.
- Ghosh, D. and Ghanem, R. (2007) "Analysis of eigenvalues and modal interaction of stochastic systems." *AIAA Journal*, 43 (10), 2196-2201.
- González, A., Rowley, C. and O'Brien, E. J. (2008) "A general solution to the identification of moving vehicle forces on a bridge." *International Journal for Numerical Methods in Engineering*, 75, 335-354.
- Gordis, J. H. (1992) "An analysis of the improved reduced system (IRS) model reduction procedure." *Proceedings of the 7th International Modal Analysis Conference*, San Diego, California, February, 471-479.
- Green, M. F. and Cebon, D. (1994) "Dynamic response of highway bridges to heavy vehicle loads: theory and experimental validation." *Journal of Sound and Vibration*, 170(1), 51-78.
- Grigoriu, M. (1996) "Response of dynamic systems to Poisson white noise." *Journal of Sound and Vibration*, 195(3), 375-389.

- Grigoriu, M. (1998) "Simulation of stationary non-Gaussian translation processes". *Journal of Engineering Mechanics-ASCE*, 124(2), 121-126.
- Gutierrez, R. H. and Laura, P. A. A. (1997) "Vibration of a beam of non-uniform cross-section traversed by a time varying concentrated force." *Journal of Sound and Vibration*, 207 (3), 419-425.
- Guyan, R. J. (1965) "Reduction of stiffness and mass matrices." *AIAA Journal*, 3(2), 380.
- Haldar, A. and Mahadevan, S. (2000) *Reliability Assessment using Stochastic Finite Element Analysis*, John Wiley and Sons, New York.
- Hall, P., Müller, H. G. and Wang, J. L. (2006) "Properties of principal component methods for functional and longitudinal data analysis." *The Annals of Statistics*, 34(3), 1493-1517.
- Hamed, E. and Frostig, Y. (2006) "Natural frequencies of bouded and unbouded prestressed beams-prestress force effects." *Journal of Sound and Vibration*, 295, 28-39.
- Henchi, K., Fafard, M., Talbot, M. and Dhatt, G. (1998) "An efficient algorithm for dynamic analysis of bridges under moving vehicles using a coupled modal and physical components approach." *Journal of Sound and Vibration*, 212(4), 663-683.
- Hien, T. D. and Kleiber, M. (1997) "Stochastic finite element modelling in linear transient heat transfer." *Computer Methods in Applied Mechanics and Engineering*, 144(1-2), 111-124.

- Hisada, T. and Nakagiri, S. (1981) "Stochastic finite element method developed for structural safety and reliability." *Proceedings of the 3rd International Conference on Structural Safety and Reliability*, Trondheim, Norway, 395-408.
- Hosseini, S. A. A. and Khadem, S. E. (2005) "Free vibration analysis of rotating beams with random properties." *Structural Engineering and Mechanics*, 20(3), 293-312.
- Hosseini, S. A. A. and Khadem, S. E. (2007) "Vibration and reliability of a rotating beam with random properties under random excitation." *International Journal of Mechanical Sciences*, 49, 1377-1388.
- Hua, X. G., Ni, Y. Q., Chen, Z. Q. and Ko, J. M. (2008) "An improved perturbation method for stochastic finite element model updating." *International Journal for Numerical Methods in Engineering*, 73, 1845-1864.
- Huang, D. Z., Wang, T. L. and Shahawy, M. (1998) "Vibration of horizontally curved box girder bridges due to vehicles." *Computers and Structures*, 68, 513-528.
- Huang, D. Z. and Wang, T. L. (1998) "Vibration of highway steel bridge with longitudinal grades." *Computers and Structures*, 69, 235-245.
- Huang, S. P. and Kou, X. J. (2007) "An extended stochastic response surface method for random field problems." *Acta Mechanica Sinica*, 23, 445-450.
- Huang, S. P., Mahadevan, S. and Rebba, R. (2007) "Collocation-based stochastic finite element analysis for random field problems." *Probabilistic*

Engineering Mechanics, 22(2), 194-205.

Huntington, D. E. and Lyrintzis, C. S. (1998) "Improvements to and limitations of Latin hypercube sampling." *Probabilistic Engineering Mechanics*, 13(4), 245-253.

Hussein, A., EI-Tawil, M., EI-Tahan, W. and Mahmoud, A. A. (2008) "Solution of randomly excited stochastic differential equations with stochastic operator using spectral stochastic finite element method (SSFEM)." *Structural Engineering and Mechanics*, 28(2), 129-152.

Irons, B. (1965) "Structural eigenvalue problems elimination of unwanted variables." *AIAA Journal*, 3(5), 961-962.

Isukapalli, S. S., Roy, A. and Georgopoulos, P. G. (1998) "Stochastic response surface methods (SRSMs) for uncertainty propagation: Application to environmental and biological systems." *Risk Analysis*, 18(3), 351-363.

ISO 8606:1995(E). (1995) *Mechanical vibration—road surface profiles—reporting of measured data*.

Jacob, B. A. (1994) "European research activity COST 323—weigh-in-motion of road vehicles." *Proceedings of NATDAC '94*.

Jacob, B. A. and O'Brien, E. J. (1996) "WAVE—a European research project on weigh-in-motion." *National Traffic Acquisition Conference (NATDAQ '96)*, 659-668.

Jiang, R. J., Au, F. T. K. and Cheung, Y. K. (2003) "Identification of masses moving on multi-span beams based on a genetic algorithm." *Computers and*

Structures, 81(22-23), 2137-2148.

Jiang, R. J., Au, F. T. K. and Cheung, Y. K. (2004) "Identification of vehicles moving on continuous bridges with rough surface." *Journal of Sound and Vibration*, 274(3-5), 1045-1063.

Ju, S. H. and Lin, H. T. (2006) "A finite element model of vehicle-bridge interaction considering braking and acceleration." *Journal of Sound and Vibration*, 303(1-2), 46-57.

Kac, M. and Siegert, J. F. (1947) "An explicit representation of a stationary Gaussian process." *The Annals of Mathematical Statistics*, 18(3), 438-442.

Kerschen, G., Golinval, J. C., Vakakis, A. F. and Bergman, L. A. (2005) "The method of proper orthogonal decomposition for dynamic characterization and order reduction of mechanical systems: An overview." *Nonlinear Dynamics*, 41, 147-169.

Khiem, N. T. and Lien, T. V. (2002) "The dynamic stiffness matrix method in forced vibration analysis of multiple-cracked beam". *Journal of Sound and Vibration*, 254(3), 541-555.

Kim, C. W., Kawatani, M. and Kim, K. B. (2005) "Three-dimensional dynamic analysis for bridge-vehicle interaction with roadway roughness." *Computers and Structures*, 83(19-20), 1627-1645.

Kim, H. M. and Inoue, J. (2004) "A spectral stochastic element free Galerkin method for the problems with random material parameter." *International Journal of Numerical Methods in Engineering*, 61, 1957-1975.

- Kim, S. M. (2004) "Vibration and stability of axial loaded beams on elastic foundation under moving harmonic loads." *Engineering Structures*, 26(1), 95-105.
- Kleiber, M. and Hien, T. D. (1993) *Stochastic Finite Element Method*, John Wiley and Sons, New York.
- Knio, O. M. and Le Maitre, O. P. (2006) "Uncertainty propagation in CFD using polynomial chaos decomposition." *Fluid Dynamic Research*, 38, 616-640.
- Kocaturk, T. and Simsek, M. (2006) "Dynamic analysis of eccentrically prestressed viscoelastic Timoshenko beams under a moving harmonic load." *Computers and Structures*, 84(31-32), 2113-2127.
- Koh, C. G., Ong, J. S. Y., Chua, D. K. H. and Feng, J. (2003) "Moving element method for train-track dynamic." *International Journal for Numerical Methods in Engineering*, 56(11), 1549-1567.
- Kuhar, E. J. and Stahle, C. V. (1974) "Dynamic transformation method for model synthesis." *AIAA Journal*, 12(5), 672-678.
- Law, S. S., Chan, T. H. T. and Zeng, Q. H. (1997) "Moving force identification: A time domain method." *Journal of Sound and Vibration*, 201(1), 1-22.
- Law, S. S., Chan, T. H. T. and Zeng, Q. H. (1999) "Moving force identification: A frequency and time domains analysis." *Journal of Dynamic Systems, Measurement, and Control-ASME*, 12(3), 394-401.
- Law, S. S., Chan, T. H. T., Zhu, X. Q. and Zeng, H. Q. (2001) "Moving loads identification through regularization." *Journal of Engineering Mechanics*,

127(2), 136-148.

Law, S. S. and Fang, Y. L. (2001) "Moving force identification: optimal state estimation approach." *Journal of Sound and Vibration*, 239(2), 233-254.

Law, S. S., Bu, J. Q., Zhu, X. Q. and Chan, S. L. (2004) "Vehicle axle loads identification using finite element method." *Engineering Structures*, 26(8), 1143-1153.

Law, S. S. and Zhu, X. Q. (2004) "Dynamic behavior of damaged concrete bridge structures under moving vehicular loads." *Engineering Structures*, 26(9), 1279-1293.

Law, S. S. and Lu, Z. R. (2005) "Time domain responses of a prestressed beam and prestress identification." *Journal of Sound and Vibration*, 288(4-5), 1011-1025.

Law, S. S. and Zhu, X. Q. (2005) "Bridge dynamic responses due to road surface roughness and braking of vehicle." *Journal of Sound and Vibration*, 282(3-5), 805-830.

Law, S. S., Bu, J. Q., Zhu, X. Q. and Chan, S. L. (2007) "Moving load identification on a simply supported orthotropic plate." *International Journal of Mechanical Sciences*, 49, 1262-1275.

Law, S. S., Wu, S. Q. and Shi, Z. Y. (2008) "Moving load and prestress identification using wavelet-based method." *Journal of Applied Mechanics-ASME*, 75(2), Article Number: 021014.

Lawrence, M. (1987) "Basis random variables in finite element analysis."

- International Journal for Numerical Methods in Engineering*, 24(10), 1849-1863.
- Lee, S.Y. and Yhim, S.S. (2004) "Dynamic analysis of composite plates subject to multi-moving loads based on a third order theory." *International Journal of Solids and Structures*, 41(16-17), 4457-4472.
- Lee, S.Y. and Yhim, S.S. (2005) "Dynamic behavior of long-span box girder bridges subject to moving loads: Numerical analysis and experimental verification." *International Journal of Solids and Structures*, 42(18-19), 5021-5035.
- Lei, X. and Noda, N. A. (2002) "Analysis of dynamic response of vehicle and track coupling system with random irregularity of track vertical profile." *Journal of Sound and Vibration*, 258(1), 147-165.
- Lei, Z. and Qiu, C. (2000) "Neumann dynamic stochastic finite element method of vibration for structures with stochastic parameters to random excitation." *Computers and Structures*, 77, 651-657.
- Lei, Z. and Qiu, C. (2000) "A stochastic variational formulation for non-linear dynamic analysis of structure." *Computer Methods in Applied Mechanics and Engineering*, 190, 597-608.
- Le Maitre, O. P., Knio, O. K., Najm, H. N. and Ghanem, R. G. (2001a) "A stochastic projection method for fluid flow I. basic formulation." *Journal of Computational Physics*, 173 (2), 481-511.
- Le Maitre, O. P., Reagan, M. T., Najm, H. N., Ghanem, R. G. and Knio, O. K.

- (2001b) "A stochastic projection method for fluid flow II. random process."
Journal of Computational Physics, 181 (1), 9-44.
- Li, C. C. and Der Kiureghian, A. (1993) "Optimal discretization of random fields."
Journal of Engineering Mechanics-ASCE, 119(6), 1136-1154.
- Li, H., Wekezer, J. and Kwasniewski, L. (2008) "Dynamic response of a highway bridge subject to moving vehicles." *Journal of Bridge Engineering*, 13(5), 439-448.
- Li, J. Q., Leng, X. L. and Fang, T. (2002) "Evolutionary random response problem of a coupled vehicle-bridge system." *Archive of Applied Mechanics*, 72, 536-544.
- Liang, Y. C., Lee, H. P., Lim, S. P., Lin, W. Z., Lee, K. H. and Wu, C. G. (2002) "Proper Orthogonal decomposition and its applications-Part I: Theory."
Journal of Sound and Vibration, 252 (3), 527-544.
- Lin, J. H. (2006) "Response of a bridge to moving vehicle load." *Canadian Journal of Civil Engineering*, 33(1), 49-57.
- Liu, C., Huang, D. and Wang T. L. (2002) "Analytical dynamic impact study based on correlated road roughness." *Computers and Structures*, 80, 1639-1650.
- Liu, P. L. and Liu, K. D. D. (1993) "Selection of random field mesh in finite element reliability analysis." *Journal of Engineering Mechanics-ASCE*, 119(4), 667-680.
- Liu, W. K., Belytschko, T. and Mani, A. (1986) "Random field finite elements."
International Journal for Numerical Methods in Engineering, 23(10),

1831-1845.

- Liu, Y. and Shepard, W. S. (2005) "Dynamic force identification based on enhanced least squares and total least-squares schemes in the frequency domain." *Journal of Sound and Vibration*, 282(1-2), 37-60.
- Lu, F., Lin, J. H., Kennedy, D. and Williams, F. W. (2009) "An algorithm to study non-stationary random vibrations of vehicle-bridge systems." *Computers and Structures*, 87, 177-185.
- Lu, Z. R. and Law, S. S. (2006) "Force identification based on sensitivity in time domain." *Journal of Engineering Mechanics*, 195(44-47), 1050-1056.
- Ma, X. Z., Vakakis, A. F. and Bergman, L. A. (2008) "Karhunen-Loeve analysis and order reduction of the transient dynamics of linear coupled oscillators with strongly nonlinear end attachments." *Journal of Sound and Vibration*, 309, 569-587.
- Mahadevan, S. and Haldar, A. (1991) "Practical random field discretization in stochastic finite element analysis." *Structural Safety*, 9(4), 283-304.
- Mahnoud, M. A. and Abou Zaid, M. A. (2002) "Dynamic response of a beam with a crack subject to a moving mass." *Journal of Sound and Vibration*, 256(4), 591-603.
- Marchesiello, S., Fasana, A., Garibaldi, L. and Piombo B. A. D. (1999) "Dynamic of multi-span continuous straight bridges subject to multi-degrees of freedom moving vehicle excitation." *Journal of Sound and Vibration*, 224(3), 541-561.

- Matta, K. W. (1987) "Selection of degrees of freedom for dynamic analysis." *Journal of Pressure Vessel Technology-ASME*, 109(1), 65-69.
- Mckay, M. D., Beckman, R. J. and Conover, W. J. (1979) "A comparison of three methods for selecting values of input variables in the analysis of output from a computer code." *Techniques*, 2, 239-245.
- Mikhlin, S. G. (1957) *Integral Equations*, Pergamon Press, Oxford.
- Miller, C. A. (1980) "Dynamic reduction of structural models." *Journal of the Structural Division*, 106(10), 2079-2108.
- Mohan, P., Nair, P. B. and Keane, A. J. (2008) "Multi-element stochastic reduced basis methods." *Computer Methods in Applied Mechanics and Engineering*, 197, 1495-1506.
- Moon, B. Y., Kang, G. J. Kang, B. J. and Cho, D. S. (2004) "Dynamic and reliability analysis of stochastic structure system using probabilistic finite element method." *Structural Engineering and Mechanics*, 18(1), 125-135.
- Moses, F. (1979) "Weigh-in-motion system using instrumented bridges." *Transportation Engineering Journal of ASCE*, 105(3), 233-249.
- Mulcahy, N. L. (1983) "Bridge response with tractor-trailer vehicle loading." *Earthquake Engineering and Structural Dynamics*, 11, 649-665.
- Muscolino, G., Benfratello, S. and Sidoti, A. (2002) "Dynamics analysis of distributed parameter system subject to a moving oscillator with random mass, velocity and acceleration." *Probabilistic Engineering Mechanics*, 17, 63-72.

- Nair, P. B. and Keane, A. (2002) "Stochastic reduced basis methos" *AIAA Journal*, 40(8), 1653-1664.
- Nakagiri, S. and Hisada, T. (1985) *An Introduction to Stochastic Finite Element Method: Analysis of Uncertain Structures*, BaiFuKan, Tokyo (in Japanese)
- Nallasivam, K., Dutta, A. and Talukdar, S. (2007) "Dynamic analysis of horizontally curved thin-walled box-girder bridge due to moving vehicle." *Shock and Vibration*, 14(3), 229-248.
- Newman, A. J. (1996a) "Model reduction via the Karhunen-Loeve expansion Part I: An exposition." *A Technical Report for Institute for Systems Research*, T.R. 96-32., 1-19.
- Newman, A. J. (1996b) "Model reduction via the Karhunen-Loeve expansion Part II: Some Elementary Examples." *A Technical Report for Institute for Systems Research*, T.R. 96-32., 1-15.
- Ngah, M. F. and Young, A. (2007) "Application of the spectral stochastic finite element method for performance prediction of composite structures." *Computers and Structures*, 78, 447-456.
- Nordberg, T. P. and Gustafsson, I. (2006a) "Dynamic regularization of input estimation problems by explicit block inversion." *Computer Methods in Applied Mechanics and Engineering*, 168(44-47), 5877-5890.
- Nordberg, T. P. and Gustafsson, I. (2006b) "Using QR factorization and SVD to solve input estimation problems in structural dynamics." *Computer Methods in Applied Mechanics and Engineering*, 195(44-47), 5891-5908.

- Nordstrom, L. J. L. and Nordberg, T. P. (2004) "A time delay method to solve non-located input estimation problems." *Mechanical Systems and Signal Processing*, 18(6), 1469-1483.
- O'Brien, E., Li, Y. Y. and Gonzalez, A. (2006) "Bridge roughness index as an indicator of bridge dynamic amplification." *Computers and Structures*, 84(12), 759-769.
- O'Callahan, J. C. (1989) "A procedure for an improved reduced system (IRS) model." *Proceedings of the 7th International Modal Analysis Conference*, LasVegas, 17-21.
- O'Connor, C. and Chan, T. H. T. (1988) "Dynamic loads from bridge strains." *Journal of Structural Engineering-ASCE*, 114(8), 1703-1723.
- Onkar, A. K., Upadhyay, C. S. and Yadav, D. (2006) "Generalized buckling analysis of laminated plates with random material properties using stochastic finite elements." *International Journal of Mechanical Sciences*, 48(7), 780-798.
- Pan, T. C. and Li, J. (2002) "Dynamic vehicle element method for transient response of coupled vehicle-structure systems". *Journal of Structural Engineering*, 128(2), 214-223.
- Pandit, M. K., Singh, B. N. and Sheikh, A. H. (2009) "Stochastic perturbation-based finite element for deflection statistics of soft core sandwich plate with random material properties". *International Journal of Mechanical Sciences*, 51, 363-371.

- Pellisetti, M. F. and Ghanem, R. G. (2000) "Iterative solution of systems of linear equations arising in context of stochastic finite elements". *Advances in Engineering Software*, 31, 607-616.
- Phoon, K. K., Huang, S. P. and Quek, S. T. (2002) "Simulation of second-order processes using Karhunen-Loeve expansion". *Computers and Structures*, 80(12), 1049-1060.
- Phoon, K. K., Huang, S. P. and Quek, S. T. (2005) "Simulation of strongly non-Gaussian processes using Karhunen-Loeve expansion". *Probabilistic Engineering Mechanics*, 20(2), 188-198.
- Pinkaew, T. and Akarawittayapoom, T. "Determination of truck weight from response of bridges." *16th ASCE Engineering Mechanics Conference*, July 16-18, 2003, University of Washington.
- Pinkaew, T. (2006) "Identification of vehicle axle loads from bridge responses using updated static component technique." *Engineering Structures*, 28(11), 1599-1608.
- Pinkaew, T. and Asnachinda, P. (2007) "Experimental study on the identification of dynamic axle loads of moving vehicles from the bending moments of bridges." *Engineering Structures*, 29(9), 2282-2293.
- Pradlwarter, H. J., Schuëller, G. I. and Schenk, C. A. (2003) "A computational procedure to estimate the stochastic dynamic response of large non-linear FE-models." *Computer Methods in Applied Mechanics and Engineering*, 192, 777-801.

- Qin, Q., Lin, D. J. and Mei, G. (2006) *Reliability Stochastic Finite Element Methods: Theory and Application*, Tsinghua University Press, Beijing (in Chinese).
- Qiu, C. and Liu, X. B. (1993) *Stochastic Finite Element Method and Its Engineering Applications*, South Jiaotong University Press, Chengdu (in Chinese).
- Reagan, M. T., Najm, H. N., Ghanem, R. G. and Knio, O. M. (2005) “Uncertainty quantification in reacting-flow simulations through non-intrusive spectral projection.” *Combustion and Flame*, 132, 545-555.
- Ren, Y. J., Elishakoff, I. and Shinozuka, M. (1997) “Finite element method for stochastic beams based on variational principles.” *Journal of Applied Mechanics-ASME*, 64, 664-669.
- Reusch, F. and Estrin, Y. (1998) “FE-analysis of mechanical response of simple structures with random non-uniformity of material properties.” *Computational Materials Science*, 11, 294-308.
- Saiidi, M., Douglas, B. and Feng, S. (1994) “Prestress force effect on vibration frequency of concrete bridges.” *Journal of Structural Engineering*, 120(7), 2233-2241.
- Sakamoto, S. and Ghanem, R. (2002a) “Polynomial chaos decomposition for the simulation of non-Gaussian nonstationary stochastic processes.” *Journal of Engineering Mechanics*, 128(2), 190-201.
- Sakamoto, S. and Ghanem, R. (2002b) “Simulation of multi-dimensional

- non-Gaussian non-stationary random fields.” *Probabilistic Engineering Mechanics*, 17, 167-176.
- Samaras, E., Shinozuka, M. and Tsurui, A. (1985) “ARMA representation of random processes.” *Journal of Engineering Mechanics-ASCE*, 111(3), 449-461.
- Sarkar, A. and Ghanem, R. G. (2003) “A substructure approach for the midfrequency vibration of stochastic systems.” *Journal of the Acoustical Society of America*, 113 (4), 1922-1934.
- Sasidhar, M. N. V. and Talukdar, S. (2003) “Nonstationary response of bridge due to eccentrically moving vehicle at variable velocity.” *Advances in Structure Engineering*, 6(4), 309-324.
- Schenk, C. A. and Bergman, L. A. (2003) “Response of continuous system with stochastically varying surface roughness to moving load.” *Journal of Engineering Mechanics-ASCE*, 129(7), 759-768.
- Schenk, C. A., Pradlwarter, H. J. and Schuëller, G. I. (2004) “On the dynamic stochastic response of FE models.” *Probabilistic Engineering Mechanics*, 19, 161-170.
- Schenk, C. A., Pradlwarter, H. J. and Schuëller, G. I. (2005) “Non-stationary response of large, non-linear finite element systems under stochastic loading.” *Computers and Structures*, 83, 1086-1102.
- Schenk, C. A. and Schuëller, G. I. (2005) *Uncertainty Assessment of Large Finite Element Systems*, Springer-Verlag , Berlin Heidelberg.
- Schuëller, G. I. and Brenner, C. E. (1996) “Stochastic finite elements-a challenge for material science.” *Advances in Building Material Science*, Festschrift

- Professor F Wittmann A. Gerdes, Aedificioed., Freiburg, Germany, 1996, 259-273.
- Schuëller, G. I. (1997) "A state-of art report on computational stochastic mechanics." *Probabilistic Engineering Mechanics*, 12(4), 197-321.
- Schuëller, G. I. (2006) "Developments in stochastic structural mechanics". *Archive of Applied Mechanics*, 75(10-12), 755-773.
- Seetapan, P. and Chucheepsakul, S. (2006) "Dynamic responses of a two-span beam subject to high speed 2DOF sprung vehicles." *International Journal of Structural Stability and Dynamics*, 6(3), 413-430.
- Shan, V. N. and Raymund, M. (1982) "Analytical selection of masters for the reduced eigenvalue problem." *International Journal for Numerical Methods in Engineering*, 18(1), 89-98.
- Shinnozuka, M. and Jan, C. M. (1972) "Digital simulation of random process and its applications." *Journal of Sound and Vibration*, 25(1), 111-128.
- Shinnozuka, M. (1972) "Monte Carlo solution of structural dynamics." *Computer and Structures*, 2(5-6), 855-874.
- Shinnozuka, M. and Jan, C.M. (1972) "Digital simulation of random processes and its applications." *Journal of Sound and Vibration*, 25(1), 111-128.
- Shinnozuka, M. and Nomoto, T. (1980) *Response Variability Due to Spatial Randomness of Material Properties*, Technical Report, Dept. of Civil Engineering, Columbia University, New York.
- Shinnozuka, M. and Deodatis, G. (1988) "Response variability of stochastic finite element systems." *Journal of Engineering Mechanics-ASCE*, 114(3),

499-519.

Shinozuka, M. and Deodatis, G. (1991) "Simulation of stochastic processes by spectral representation." *Applied Mechanics Reviews*, 44(4), 191-204.

Simsek, M. and Kocaturk, T. (2006) "Dynamic analysis of eccentrically prestressed damped beam moving harmonic force using higher order shear deformation theory." *Journal of Structural Engineering*, 133(12), 1733-1741.

Sniady, P. (2008) "Dynamic response of a Timoshenko beam to a moving force" *Journal of Applied Mechanics*, 75, Paper No. 024503.

Spanos, P. D. and Hansen, J. (1981) "Linear prediction theory for digital simulations of sea waves." *Journal of Energy Resources Technology*, 103(3), 243-249.

Spanos, P. D. and Ghanem, R. G. (1989) "Stochastic finite element expansion for random media." *Journal of Engineering Mechanics-ASCE*, 115(5), 1035-1053.

Spanos, P. D. and Failla, G. (2004) "Evolutionary spectra estimation using wavelets." *Journal of Engineering Mechanics-ASCE*, 130(8), 952-960.

Spanos, P. D., Tezcan, J. and Tratskas, P. (2005) "Stochastic processes evolutionary spectrum estimation via harmonic wavelets." *Computer Methods in Applied Mechanics and Engineering*, 194(12-16), 1367-1383.

Standard Specification for Highway Bridges (1989) *American Association of State Highway and Transportation Officials*, 14th Edn, Washington, DC.

Stefanou, G. (2009) "The stochastic finite element method: past, present and future." *Computer Methods in Applied Mechanics and Engineering*, 198,

1031-1051.

Takada, T. (1990) "Weighted integral method in stochastic finite element analysis." *Probabilistic Engineering Mechanics*, 5(3), 146-156.

Thite, A. N. and Thompson, D. J. (2003a) "The quantification of structure-borne transmission paths by inverse methods. Part 1: Improved singular value rejection methods." *Journal of Sound and Vibration*, 264(2), 411-431.

Thite, A. N. and Thompson, D. J. (2003b) "The quantification of structure-borne transmission paths by inverse methods. Part 2: Use of regularization techniques." *Journal of Sound and Vibration*, 264(2), 433-451.

Vanmarcke, E. H. and Grigoriu, M. (1983) "Stochastic finite element analysis of simple beams." *Journal of Engineering Mechanics-ASCE*, 109(5), 1203-1214.

Vanmarcke, E. H. (1983) *Random Field: Analysis and Synthesis*, The MIT Press, Cambridge, MA.

Wang, T. L., Huang, D. Z. and Shahawy, M. (1992) "Dynamic response of multigirder bridges." *Journal of Structural Engineering*, 118(8), 2222-2238.

Wang, T. L., Huang, D. Z., Shahawy, M. and Huang, K. Z. (1996) "Dynamic response of highway girder bridge." *Computers and Structures*, 60(6), 1020-1027.

Wang, R. T. (1997) "Vibration of multi-span Timoshenko beams to a moving forces." *Journal of Sound and Vibration*, 207(5), 731-742.

Wang, R. T. and Chou, T. H. (1998) "Non-linear vibration of Timoshenko beam

- due to a moving force and the weight of beam.” *Journal of Sound and Vibration*, 218(1), 117-131.
- Whittemore, A. P., Wiley, J. R., Schultz, P. C. and Pollock, D. E. (1970) “Dynamic pavement loads of heavy highway vehicles.” *Highway Research Board, National Cooperative Highway Research Program Report No.105*.
- Wiener, N. (1938) “The Homogeneous Chaos”. *American Journal of Mathematics*, 60(4), 897-936.
- Wu, C. G., Liang, Y. C., Lin, W. Z., Lee, H.P. and Lim, S. P. (2003) “A note on equivalence of proper orthogonal decomposition methods.” *Journal of Sound and Vibration*, 265, 1103-1110.
- Wu, J. J. (2005a) “Dynamic analysis of an inclined beam due to moving loads.” *Journal of Sound and Vibration*, 288, 107-131.
- Wu, J. J. (2005b) “Vibration analysis of a portal under the action of a moving distributed mass using moving mass element.” *International Journal for Numerical Methods in Engineering*, 62(14), 2028-2052.
- Wu, J. J. (2007) “Use of moving distributed mass element for the dynamic analysis of a flat plate undergoing a moving distributed load.” *International Journal for Numerical Methods in Engineering*, 71(3), 347-362.
- Wu, S. Q. and Shi, Z. Y. (2006) “Identification of vehicle axle loads based on FEM-Wavelet- Galerkin method.” *Journal of Vibration Engineering*, 19(4), 494-498. (in Chinese)
- Xia, Y. and Hao, H. (2003) “Statistical damage identification of structures with

- frequency changes.” *Journal of Sound and Vibration*, 263, 853-870.
- Xiang, T., Zhao, R. and Xu, T. (2007) “Reliability evaluation of vehicle-bridge dynamic interaction.” *Journal of Structural Engineering-ASCE*, 133(8), 1092-1099.
- Xiu, D. and Karniadakis, G. E. (2002) “The Wiener-Askey polynomial chaos for stochastic differential equations.” *SIAM Journal on Scientific Computing*, 24, 619-644.
- Yamazaki, F., Shinozuka, M. and Dasgupta, G. (1988) “Neumann expansion for stochastic finite element analysis.” *Journal of Engineering Mechanics-ASCE*, 114 (8), 1335-1354.
- Yamazaki, F. and Shinozuka, M. (1988) “Digital generation of non-Gaussian stochastic fields”. *Journal of Engineering Mechanics-ASCE*, 127(12), 1284-1295.
- Yang, J., Chen, Y., Xiang, Y. and Jia, X. L. (2008) “Free and forced vibration of cracked inhomogeneous beams under an axial force and a moving load.” *Journal of Sound Vibration*, 312(1-2), 166-181.
- Yang, Y. B. and Lin, B. H. (1995) “Vehicle-bridge interaction by dynamic condensation method.” *Journal of Structural Engineering-ASCE*, 121(11), 1636-1643.
- Yang, Y. B., Liao, S. S. and Lin, B. H. (1995) “Impact formulas for vehicles moving over simple and continuous beams.” *Journal of Structural Engineering-ASCE*, 121(11), 1644-1650.

- Yang, Y. B. and Yau, J. D. (1997) "Vehicle-bridge interaction element for dynamic analysis." *Journal of Structural Engineering-ASCE*, 123(11), 1512-1518.
- Yang, Y. B. and Wu, Y. S. (2001) "A versatile element for analyzing vehicle-bridge interaction response." *Engineering Structure*, 23(5), 452-469.
- Yu, L. and Chan, T. H. T. (2002) "Moving force identification from bending moment responses of bridge." *Structural Engineering and Mechanics*, 14(2), 151-170.
- Yu, L. and Chan, T. H. T. (2003) "Moving force identification based on the frequency-time domain method." *Journal of Sound and Vibration*, 261(2), 329-349.
- Yu, L. and Chan, T. H. T. (2007) "Recent research on identification of moving loads on bridges." *Journal of Sound and Vibration*, 305, 3-21.
- Yu, L., Chan, T. H. T. and Zhu, J. H. (2008a) "A MOM-based algorithm for moving force identification: Part I- Theory and numerical simulation." *Structural Engineering and Mechanics*, 29(2), 135-154.
- Yu, L., Chan, T. H. T. and Zhu, J. H. (2008b) "A MOM-based algorithm for moving force identification: Part II- Experiment and comparative studies." *Structural Engineering and Mechanics*, 29(2), 155-169.
- Zeldin, B. A. and Spanos, P. D. (1996) "Random field representation and synthesis using wavelet bases". *Journal of Applied Mechanics-ASME*, 63(4), 946-952.
- Zhi, X., Shalaby, A. and Middleton, D. (1999) "Evaluation of Weigh-in-motion in Manitoba." *Canadian Journal of Civil Engineering*, 26(5), 655-666.

- Zibdeh, H. S. (1995) "Stochastic vibration of an elastic beam due to random moving loads and deterministic axial forces." *Engineering Structures*, 17(7), 530-535.
- Zibdeh, H. S. and Abu-Hilal, M. (2003) "Stochastic vibration of laminated composite coated beam traversed by a random moving load." *Engineering Structures*, 25, 397-404.
- Zibdeh, H. S. and Juma, H. S. (2004) "Dynamic response of a rotating beam subject to a random moving load." *Journal of Sound and Vibration*, 223(5), 741-758.
- Zhu, X. Q. and Law, S. S. (1999) "Moving forces identification on a multi-span continuous bridge." *Journal of Sound and Vibration*, 228(2), 377-396.
- Zhu, X. Q. and Law, S. S. (2000) "Identification of vehicle axle loads from bridge dynamic response." *Journal of Sound and Vibration*, 236(4), 705-724.
- Zhu, X. Q. and Law, S. S. (2001a) "Identification of moving loads on an orthotropic plate." *Journal of Vibration and Acoustics-ASME*, 123(2), 238-244.
- Zhu, X. Q. and Law, S. S. (2001b) "Orthogonal function in moving loads identification on a multi-span bridge." *Journal of Sound and Vibration*, 245(2), 329-345.
- Zhu, X. Q. and Law, S. S. (2001c) "Precise time-step integration for the dynamic response of a continuous beam under moving loads." *Journal of Sound and Vibration*, 240(5), 962-972.

- Zhu, X. Q., Law, S. S. and Bu, J. Q. (2006) "A state space formulation for moving loads identification." *Journal of Vibration and Acoustics-ASME*, 128(4), 509-520.
- Zhu, X. Q. and Law, S. S. (2002a) "Dynamic load on continuous multi-lane bridge deck from moving vehicles." *Journal of Sound and Vibration*, 251(4), 697-716.
- Zhu, X. Q. and Law, S. S. (2002b) "Moving loads identification through regularization." *Journal of Engineering Mechanics*, 128(9), 989-1000.
- Zhu, X. Q. and Law, S. S. (2002c) "Practical aspects in moving load identification." *Journal of Sound and Vibration*, 258(1), 123-146.
- Zhu, X. Q. and Law, S. S. (2003a) "Dynamic behavior of orthotropic rectangular plates under moving loads." *Journal of Engineering Mechanics*, 129(1), 79-87.
- Zhu, X. Q. and Law, S. S. (2003b) "Moving loads on bridge deck." *Journal of Vibration and Acoustics-ASME*, 125(2), 187-198.
- Zhu, X. Q. and Law, S. S. (2003c) "Identification of moving interaction forces with incomplete velocity information." *Mechanical Systems and Signal Processing*, 17(6), 1349-1366.
- Zhu, X. Q. and Law, S. S. (2006) "Moving load identification on multi-span continuous bridges with elastic bearings." *Mechanical Systems and Signal Processing*, 20(7), 1758-1782.
- Zhu, X. Q., Law, S. S. and Bu, J. Q. (2006) "A state space formulation for moving

loads identification.” *Journal of Vibration and Acoustics*, 128, 509-520.